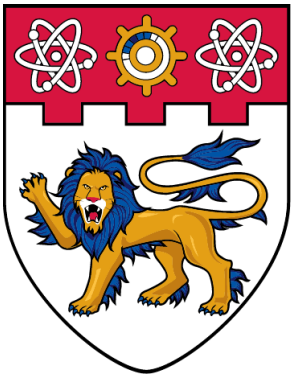

NANYANG TECHNOLOGICAL UNIVERSITY
SINGAPORE

# UNDERSTANDING THE MOLECULAR BASIS OF FLAVIVIRUS REPLICATION PROCESS FOR ANTIVIRAL THERAPEUTICS DEVELOPMENT

QUEK JUN PING

LEE KONG CHIAN SCHOOL OF MEDICINE

2021

# UNDERSTANDING THE MOLECULAR BASIS OF FLAVIVIRUS REPLICATION PROCESS FOR ANTIVIRAL THERAPEUTICS DEVELOPMENT

**QUEK JUN PING**

**Lee Kong Chian School of Medicine**

**The thesis is submitted to the Nanyang Technological University in partial fulfilment of the requirement for the degree of Doctor of philosophy**

**2021**

## Statement of Originality

I hereby certify that the work embodied in this thesis is the result of original research, is free of plagiarised materials, and has not been submitted for a higher degree to any other University or Institution.

2 March 2022

. . . . . .

Date

. . . . . .

Quek Jun Ping

## Supervisor Declaration Statement

I have reviewed the content and presentation style of this thesis and declare it is free of plagiarism and of sufficient grammatical clarity to be examined. To the best of my knowledge, the research and writing are those of the candidate except as acknowledged in the Author Attribution Statement. I confirm that the investigations were conducted in accord with the ethics policies and integrity standards of Nanyang Technological University and that the research data are presented honestly and without prejudice.

Mar 07 2022

. . . . . .

Date

. . . . . .

Assoc Prof Luo Dahai

## Authorship Attribution Statement

This thesis contains material from 5 papers published in the following peer-reviewed journals where I was the first and/or corresponding author.

1. Part of Chapter 1 is published as Van den Elsen, K.[*], **Quek, J.P.[*]**, and Luo, D.* (2021). **Molecular Insights into the Flavivirus Replication Complex.** Viruses 13. doi:10.3390/v13060956.
   [*] These authors contributed equally.
   The contributions of the co-authors are as follows:
   All authors contribute to the writing and review of the manuscript.

2. Part of Chapter 3.1 is published as **Quek, J.P.[*]**, Liu, S.[*], Zhang, Z., Li, Y., Ng, E.Y., Loh, Y.R., Hung, A.W., Luo, D., and Kang, C. (2020). **Identification and structural characterization of small molecule fragments targeting Zika virus NS2B-NS3 protease.** Antiviral Res 175, 104707. doi:10.1016/j.antiviral.2020.104707.
   [*] These authors contributed equally.
   The contributions of the co-authors are as follows:
   The experiments were designed by Dr Alvin W Hung, Assoc Prof Dahai Luo and Dr Congbao Kang. The inhibitors are synthesized by EDDC, A*STAR. The fragment screening and thermal shift assays were performed by Dr Shuang Liu and Dr Alvin W Hung at EDDC, A*STAR. The NMR experiments are conducted and analysed by Dr Yan Li and Dr Congbao Kang at EDDC, A*STAR. The protein purification, protein crystallization, data collection, and structure determination of the co-crystal structures were performed by me, Ms Zhenzhen Zhang and Assoc Prof Dahai Luo. All authors contribute to the writing and review of the manuscript.

3. Part of Chapter 3.2.1 is published as Nitsche, C., Onagi, H., **Quek, J.P.**, Otting, G., Luo, D., and Huber, T. (2019). **Biocompatible Macrocyclization between Cysteine and 2-Cyanopyridine Generates Stable Peptide Inhibitors.** Org Lett 21, 4709-4712. doi:10.1021/acs.orglett.9b01545.
   The contributions of the co-authors are as follows:
   The experiments were designed by Dr Thomas Huber and Dr Christoph Nitsche. The inhibitors are synthesized by the Research School of Chemistry, Australian National University. The enzyme kinetics assay, inhibition assay and NMR experiments are conducted and analysed by Dr Christoph Nitsche, Dr Hideki Onagi, Dr Gottfried Otting and Dr Thomas Huber. The protein purification, protein crystallization, data collection, and structure determination of the co-crystal structures were performed by me and Assoc Prof Dahai Luo. All authors contribute to the writing and review of the manuscript.

4. Part of Chapter 3.2.1 is published as Patil, N.A., **Quek, J.P.**, Schroeder, B., Morewood, R., Rademann, J., Luo, D., and Nitsche, C. (2021). **2-Cyanoisonicotinamide Conjugation: A Facile Approach to Generate Potent Peptide Inhibitors of the Zika Virus Protease.** ACS Med Chem Lett 12, 732-737. doi:10.1021/acsmedchemlett.0c00657.
   The contributions of the co-authors are as follows:
   The experiments were designed by Dr Nitin A. Patil and Dr Christoph Nitsche. The inhibitors are synthesized by the Research School of Chemistry, Australian National University. The enzyme kinetics assay, inhibition assay and mass spectrometry experiments are conducted and analysed by Dr Christoph Nitsche, Ms Barbara Schroeder, Mr Richard Morewood, Dr Jörg Rademann and Dr Nitin A. Patil. The protein purification, protein crystallization, data collection, and structure determination of the co-crystal structures were performed by me and Assoc Prof Dahai Luo. All authors contribute to the writing and review of the manuscript.

5. Part of Chapter 3.2.2 is published as Braun, N.J.[*], **Quek, J.P.[*]**, Huber, S.[*], Kouretova, J., Rogge, D., Lang-Henkel, H., Cheong, E.Z.K., Chew, B.L.A., Heine, A., Luo, D., et al. (2020). **Structure-Based Macrocyclization of Substrate Analogue NS2B-NS3 Protease Inhibitors of Zika, West Nile and Dengue viruses.** ChemMedChem 15, 1439-1452. doi:10.1002/cmdc.202000237.

   [*] These authors contributed equally.

   The contributions of the co-authors are as follows:

   The experiments were designed by Assoc Prof Dahai Luo and Prof Torsten Steinmetzer. The inhibitors are synthesized by the Institute of Pharmaceutical Chemistry, Philipps University. The enzyme kinetics assay and inhibition assay of West Nile Virus Protease and bZiPro are conducted and analysed by Mr Niklas J. Braun, Mr Simon Huber, Ms Jenny Kouretova, Ms Dorothee Rogge and Mr Heike Lang-Henkel. The enzyme kinetics assay and inhibition assay of bD4Pro and bZiPro are conducted and analysed by Mr Ezekiel Z. K. Cheong and me. The mass spectrometry was conducted by Mr Bing L. A. Chew. The protein purification, protein crystallization, data collection, and structure determination of the co-crystal structures were performed by me and Assoc Prof Dahai Luo. All authors contribute to the writing and review of the manuscript.

2 March 2022

. . . . . .

Date

. . . . . .

Quek Jun Ping

## Acknowledgements

Firstly, I would like to express my sincere gratitude to my supervisor, Assoc Prof Luo Dahai, for his continuous guidance in conducting scientific research, his 'happy reading' emails to keep me updated on the latest research development, and his patience and understanding throughout my graduate education. I would also like to thank my co-supervisor, Assoc Prof Yeo Tsin Wen, for his suggestion and clinical insights to value add to my research. I would also like to thank my thesis advisory committee, Assoc Prof Kevin Pethe, Asst Prof Zhao Wenting and Assoc Prof Wang Xiaomeng for their suggestions and discussions during my PhD.

Next, I would like to thank all the members in the DL lab for their suggestions and help in areas ranging from procurement to housekeeping. I would like to thank Dr Melissa Wirawan for her sweet treats, advice and guidance throughout the PhD, Dr Zhang Kuo for his help with membrane protein purification and EM imaging. Mai Trinh for rendering assistance and administrative support. I also thank my fellow PhD peers Alvin Chew, Tan Yaw Bia, Dr Michelle Law and Dr Law Yee Song for their moral support and lunch buddies during the PhD journey. I would also like to express my thanks to my FYP student, Ezekiel, and all the other attachment students that have contributed to my PhD journey in one way or another.

I thank the funding support from NTU and Lee Kong Chain School of Medicine. I also thank Prof Philip Ingham, Mr Edwin Lim, Ms Zarifah and the LKCMedicine graduate programme for their support throughout my PhD candidature.

Lastly, I would also like to thank my family for their moral support.

## Table of Contents

## List of figures

## List of tables

## Table of abbreviations

| Abbreviations | Full Name |
|---|---|
| ADE | Antibody-dependent Enhancement |
| ANU | Australian National University |
| bD4Pro | Bivalent Dengue 4 Protease |
| BPTI | Bovine Pancreatic Trypsin Inhibitor |
| bZiPro | Bivalent Zika Protease |
| C | Capsid |
| cHP | Capsid-coding region Hairpin |
| CINA | 2-cyanoisonicotinamide |
| CM | Convoluted Membrane |
| Cpa | 3-(2-cyano-4-pyridyl)-alanine |
| CS | Cyclisation Sequence |
| CV | Column volume |
| DAA | Direct Antiviral Agents |
| DAR | Downstream AUG Region |
| DB | Dumbbell |
| DC-SIGN | Dendritic cell-specific ICAM grabbing nonintegrin |
| DENV | Dengue Virus |
| dsRNA | Double-stranded RNA |
| E | Envelope |
| EDDC | Experimental Drug Development Centre |
| eIF4G | eukaryotic Initiation Factor 4G |
| EM | Electron Microscope |
| FAS | Fatty Acid Synthase |
| FBS-X | Fragment-Based Screening by X-ray crystallography |
| GABA | g-aminobutyric acid |
| GTase | Guanylyltransferase |
| HCV | Hepatitis C Virus |
| HIV | Human Immunodeficiency Virus |
| HSP90 | Heat Shock Protein 90 |
| HTS | High-throughput Screening |
| IC | Infectious Clone |
| IFN-I | Type I Interferon |
| IPTG | Isopropyl β-D-1-thiogalactopyranoside |
| IRF9 | Interferon Regulatory Factor 9 |
| ISRE | Interferon Stimulating Response Element |
| JAK | Janus kinase |
| JEV | Japanese Encephalitis Virus |
| LAV | Live-attenuated Virus |
| LB | Luria Broth |
| M | Membrane |
| MTase | Methyltransferase |
| MW | Molecular Weight |

| | |
|---|---|
| NI | Nucleotide analog Inhibitors |
| NIH | National Institutes of Health |
| NMR | Nuclear magnetic resonance |
| NNI | Non-nucleoside Inhibitors |
| NS | Non-Structural |
| NTP | Nucleoside triphosphate |
| NTU | Nanyang Technological University |
| PABP | poly(A) binding protein |
| PBS | Phosphate buffered saline |
| PEG | Polyethene glycol |
| Phac | Phenylacetyl |
| PK | Pseudoknot |
| PPP | Protein Production Platform |
| pr | Precursor |
| prM | Precursor Membrane |
| PRRs | Pathogen Recognition Receptors |
| PU | Philipps University |
| RBS | Ribosome Binding Site |
| RC | Replication Complex |
| RdRp | RNA-dependent RNA polymerase |
| RRM | RNA Recognition Motif |
| RTN3.1A | Reticulon 3.1 |
| SAM | S-adenosylmethionine |
| SAR | Structure-activity Relationship |
| SF2 | Superfamily 2 |
| sfRNAs | Sub-genomic flaviviral RNAs |
| sHP | small hairpin |
| SL | Stem Loop |
| STAT | Signal Transducer and Activator of Transcription |
| TAM | TYRO3, AXL, MER |
| TBEV | Tick-Borne Encephalitis Virus |
| TBK1 | TANK-binding kinase |
| TEV | Tobacco Etch Virus |
| TIM | T-cell immunoglobulin and mucin domain |
| U1A | U1 small nuclear ribonucleoprotein A |
| UAR | Upstream AUG Region |
| URB4 | Ubiquitin ligase E3 N-recognin 4 |
| UTR | Untranslated region |
| VP | Vesicle Packet |
| WNV | West Nile Virus |
| YFV | Yellow Fever Virus |
| ZIKV | Zika Virus |
| β-ME | β-Mercaptoethanol |

## Summary

Flavivirus is a genus of viruses belonging to the family, Flaviviridae. They are single-stranded, positive-sense RNA viruses with a genome size of about 11-kilo bases long. During the last decade, there were increased frequency and larger magnitude of *flaviviruses'* outbreaks. However, to date, there are still no antiviral treatments for these infections.

The viral polyprotein consists of three structural and seven non-structural (NS) proteins. These viral NS proteins are involved in numerous processes from viral polyprotein synthesis, viral RNA synthesis to viral RNA capping. While numerous studies have characterised the respective NS proteins using both structural and functional approaches, the details of viral RNA replication and the dynamics of these proteins in the replication complex during the replication process have yet to be fully identified. Moreover, even though many antiviral inhibitors were identified to target these individual NS proteins in the lab, none of these inhibitors has yet been approved to combat the disease. Hence, this project aims to gain a better understanding of the function of these viral proteins and the viral RNA replication process to guide and accelerate drug discovery.

This thesis consists of six chapters as described below. Chapter **1** describes the literature on epidemiology and pathogenesis of the various flavivirus. The chapter will elaborate on the molecular biology of flavivirus, from the viral life cycle to the features and functions of the viral genome and proteins. Next, the current status of vaccines and antiviral research efforts against flavivirus will also be discussed. The specific objective and hypotheses are also stated towards

the end of chapter **1**. Chapter **2** details the various experimental design and materials used in the study. A structure-based drug discovery approach was employed to study the interaction between NS2B-NS3 protease and various inhibitors in chapter **3**. Different x-ray crystallography structures of Zika NS2B-NS3 protease bound to different inhibitors were reported. Biochemical assays were also conducted to characterise the inhibitory effects of these compounds on NS2B-NS3 protease activity. In chapter **4**, structural studies using both x-ray crystallography and electron microscopy were used to examine viral RNA recognition by NS5 polymerase. Using a bottom-up approach, biochemical characterisation was carried out on the viral replication complex in Chapter **5**. The protein components responsible for negative-sense RNA synthesis were identified and *in-vitro* reconstitution of the replication complex was performed for the structural study. Lastly, chapter **6** summarises the finding as well as proposes future research directions.

Overall, these findings provide valuable information on the functions of the viral non-structural proteins. By understanding their molecular interactions with the substrates and inhibitors, it will aid in the development of antiviral drugs by targeting the different stages of the flavivirus' lifecycle.

# Chapter 1: Literature Review

## 1.1 Flavivirus

*Flavivirus* is a genus of viruses belonging to the family, *Flaviviridae*. The flaviviruses are single-stranded, positive-strand RNA viruses. The genome is about 11-kilo bases long with a type I cap at the 5' end of the genome, a unique feature not found in other genera of the *Flaviviridae* family (Simmonds et al., 2017). The 3' ends lack a terminal poly(A) tail. The viral genome encodes for 3 structural proteins as well as 7 non-structural (NS) proteins.

The majority of the flaviviruses are arthropod-borne viruses with about 50% of them being mosquito-borne, 28% are spread by ticks and the rest are without any known arthropod vectors (Simmonds et al., 2017). A few members of the genus with clinical relevance are Dengue Virus (DENV), Japanese Encephalitis Virus (JEV), West Nile Virus (WNV), Yellow Fever Virus (YFV), and Zika Virus (ZIKV) (Barrows et al., 2018; Daep et al., 2014; Holbrook, 2017; Simmonds et al., 2017). Flaviviruses can be found worldwide but individual species are usually only found in specific regions (**Figure 1.1**) (Holbrook, 2017; Pierson and Diamond, 2020; Simmonds et al., 2017). The thesis will be mainly focused on the Aedes-transmitted flaviviruses, DENV and ZIKV, given that *Aedes aegypti* and *Aedes albopictus* are widely prevalent in Singapore (Ong et al., 2019; Rajarethinam et al., 2020).

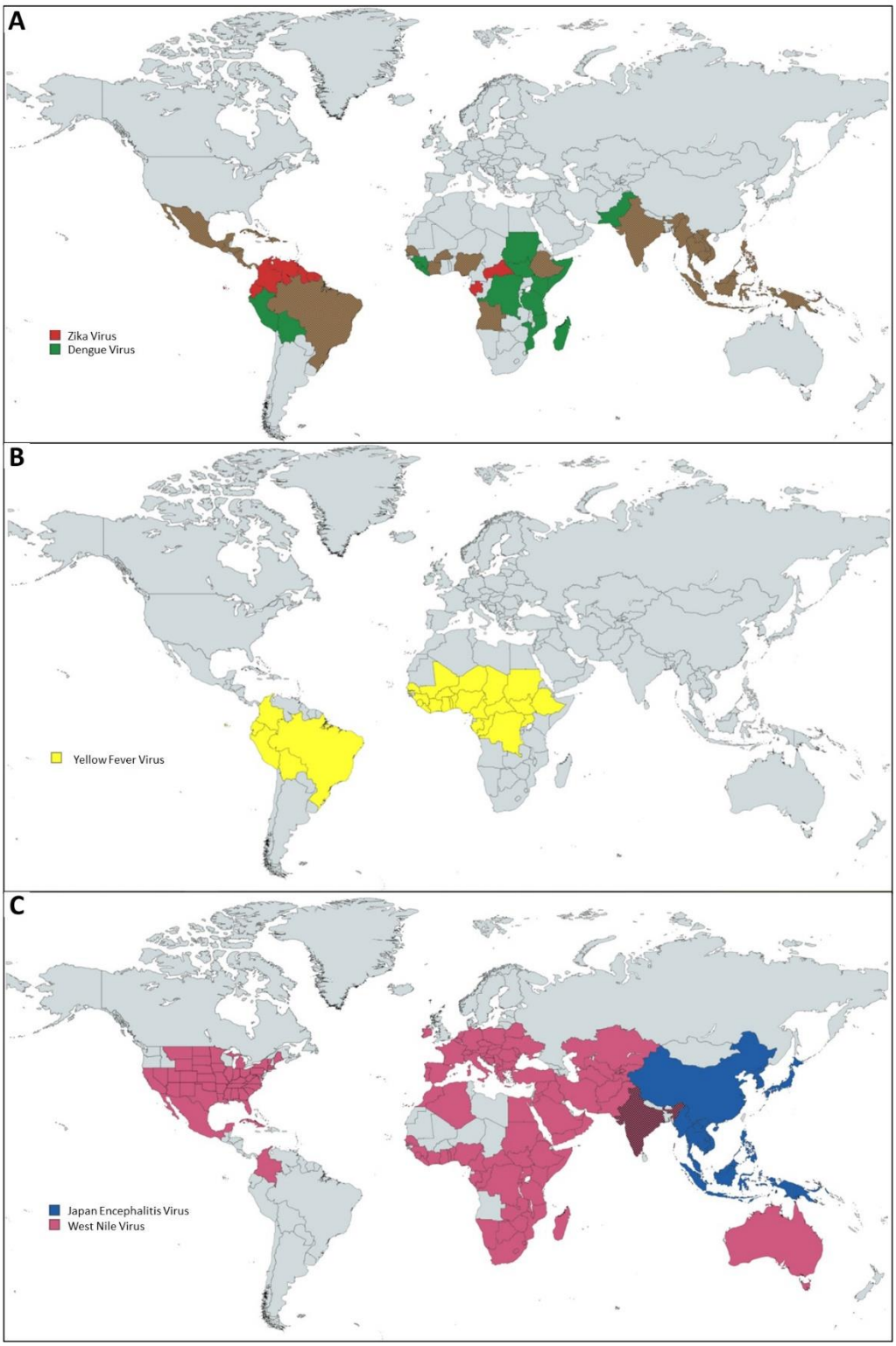


**Figure 1.1. Worldwide Distribution of the Flavivirus.** (A) Global distribution of Dengue and Zika virus. (B) Global distribution of Yellow Fever Virus. (C) Global distribution of Japan Encephalitis and West Nile Virus. The figure is produced using information from (Holbrook, 2017; Pierson and Diamond, 2020; Simmonds et al., 2017).

### 1.1.1 Yellow Fever Virus Epidemiology and Pathogenesis

Yellow fever virus (YFV) is one of the earliest known *flaviviruses*. In 1647, Barbados reported the earliest yellow fever outbreak. The largest outbreak was recorded in 1878, along the southern Mississippi River, with 120000 cases and at least 20000 deaths (Holbrook, 2017). Today, yellow fever remains to be endemic in the areas of Africa and South America (**Figure 1.1**) (Holbrook, 2017; Pierson and Diamond, 2020). Modelling based on African data suggests up to 130000 severe cases with 78000 deaths (Garske et al., 2014). In 2016, outbreaks occurred in Angola, Congo and Uganda with a death rate of approximately 14% (Barrows et al., 2018).

The 'Eliminate Yellow Fever Epidemics' strategy was initiated by the World Health Organisation (WHO) and launched in 2017 (WHO, 2017). The project aims to protect vulnerable populations, prevent worldwide spread, and contain outbreaks rapidly. The program aims to protect more than 1 billion people against YFV infection by 2026.

Patients with symptomatic yellow fever are usually presented with symptoms such as fever, chills, and headache during the 'infection' phase. Most patients will recover as they progress through the 'remission' phase. However, a portion of the patients will enter 'intoxication phase, whereby they will be presented with more severe clinical manifestations such as jaundice, nausea, vomiting, haemorrhagic disease, and multi-organ dysfunction (Barrows et al., 2018; Holbrook, 2017).

### 1.1.2 Dengue Virus Epidemiology and Pathogenesis

There are four Dengue virus (DENV) serotypes, sharing 60-75% similarities at the amino acid level. Then, the serotype is further grouped into genetically distinct classes based on genetic similarity (Vasilakis et al., 2008).

Before the 1970s, dengue is only endemic in 9 countries. However currently, the disease is prevalent in more than 120 countries putting 3.9 billion people at risk (Brady et al., 2012; Messina et al., 2014; WHO, 2019). The numbers of reported dengue cases have increased 8-fold during the past 2 decades with increased frequency and bigger magnitude of outbreaks (WHO, 2020). But WHO reported that the number of cases were severely under-reported and based on modelling, the global annual incidence could be about 50 – 100 million symptomatic cases with 1% of the cases being severe dengue, resulting in about 25,000 deaths (WHO, 2019).

Dengue has a wide range of clinical manifestations. Thus, in 2009, the WHO proposed a new classification system to help standardise the clinical description of dengue (Holbrook, 2017; WHO, 2009). The new system classified dengue into 3 main categories, dengue with or without warning signs towards severe dengue and severe dengue (**Figure 1.2A**) (WHO, 2009).

Locally, Singapore typically undergoes periodic dengue epidemics every five- to six-year cycle (Rajarethinam et al., 2018). The 2004-2005 outbreak resulted in 23668 indigenous cases, followed by 2013-2016 and 2019-2020 outbreaks with 64875 and 51322 cases respectively (NEA, 2020; Rajarethinam et al., 2018). These epidemics were attributed to the switch in the predominant dengue

serotypes as well as low herd immunity among the younger generation (Rajarethinam et al., 2018; Sim et al., 2020). To avoid straining the healthcare services from over-admission, the Singapore Ministry of Health reviewed their hospital admission criteria for dengue cases (**Figure 1.2B**) (Ang et al., 2019). The streamlined guidelines lead to a three-fold reduction in hospitalisation rate without any increase in adverse outcomes (Ang et al., 2019). The average economic cost of dengue disease in Singapore ranged between US$ $0.85 to $1.15 billion from 2000 to 2009. While the average disease burden of dengue was estimated to be 9–14 disability-adjusted life-years per 100,000 population (Carrasco et al., 2011).

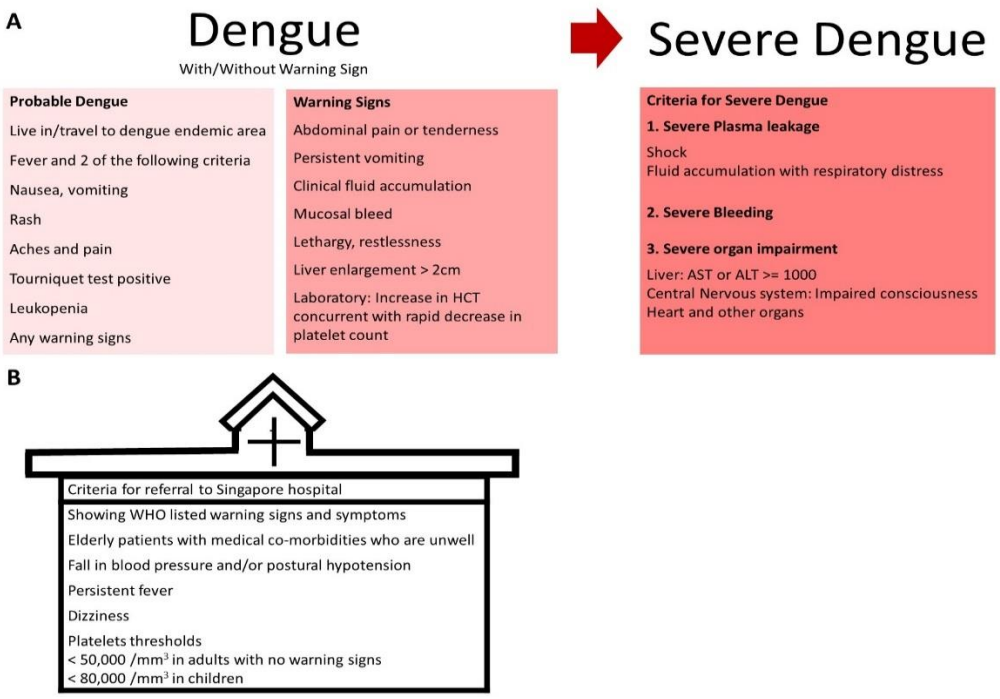


**Figure 1.2. Suggested treatments for dengue patients. (A)** Classification of dengue cases and their level of severity. Based on the clinical manifestations, patients are classified into 3 main categories, dengue with or without warning signs and severe dengue The figure is adapted from (WHO, 2009). **(B)** Criteria for referral to Singapore hospitals. A new guideline was drafted to manage hospital admission (Ang et al., 2019).

### 1.1.3 Zika Virus Epidemiology and Pathogenesis

Zika virus (ZIKV) was named after the Zika forest in Uganda after it was first isolated in 1947. Over the years, there are only rare sporadic cases of human infection in Africa and Asia. But in 2007, a Zika virus outbreak occurred on Yap island, followed by French Polynesia in 2013. Then in 2015, a large epidemic occurred in Brazil that spread throughout the Americas. Finally, in 2016, there have been reported outbreaks in the continental USA and Asia (Baud et al., 2017; Wikan and Smith, 2016; Yun and Lee, 2017). In February 2018, WHO listed Zika as one of the diseases prioritized under the Research & Development Blueprint (WHO, 2018a).

Individuals infected with the Zika virus are usually non-symptomatic or only display slight symptoms from fever, rash, to muscle and joint pain. Due to the mild severity, Zika infections were likely underreported but only recently resurfaced as serious complications were found to be linked to Zika virus infection. Zika infection during pregnancy can result in pregnancy complications such as miscarriage and premature birth. They can also lead to microcephaly and other congenital abnormalities in the foetus and newborn. In adults and older children, the infection can also trigger Guillain-Barré syndrome, myelitis, and neuropathy (Baud et al., 2017; WHO, 2018b; Wikan and Smith, 2016; Yun and Lee, 2017).

Since 2014, the National Environment Agency of Singapore has already started lab testing and routine surveillance for ZIKV (Fisher and Cutter, 2016; Li et al., 2012). Singapore experienced its first Zika outbreak in the third quarter of 2016 with 455 cases (Singapore Zika Study, 2017). Interestingly, the circulating strain in Singapore was a Southeast Asian Zika virus strain that was already present in the region, distinct from the strains that caused the large outbreaks in the Americas (Maurer-Stroh et al., 2016). Since then, no large Zika outbreaks were detected from the national surveillance programme.

## 1.2. Molecular Biology of Flavivirus

### 1.2.1 Life Cycle

The life cycle of flavivirus is illustrated in **Figure 1.3** (Guzman and Harris, 2015; Pierson and Diamond, 2020; Suthar et al., 2013). The viral life cycle commences when the virion binds to the host cell cognate receptors and undergoes clathrin-dependent endocytosis into susceptible target cells. Upon acidification of the endosomal vesicles, it induces the fusion of the cell and viral membranes. Then, the virus particle disassembles and release the viral RNA into the cytoplasm. The viral RNA genome can act as messenger RNA for viral protein synthesis. Upon viral polyprotein processing, the membrane-bound viral proteins and co-opted cellular factors induce membrane rearrangements forming viral replication organelles. Within the viral replicating organelles, all seven of the viral non-structural proteins, viral RNA and host factors aggregate and form the viral replication complex (RC). The positive-strand RNA will be used to synthesise a negative-strand intermediate that serves as a template to produce new positive-strand RNA molecules. The newly synthesised positive-strand RNA will be processed and subsequently be used as mRNA for translation of viral proteins, templates to synthesise more negative-strand RNA or be packaged as the viral genome for progeny virus. The immature viral particles, consisting of the structural proteins and the viral RNA, will travel from the endoplasmic reticulum to the Golgi apparatus, undergo modification and maturation before exiting the cell via exocytosis. The molecular details of the lifecycle will be further elaborated in the subsequent sub-section.

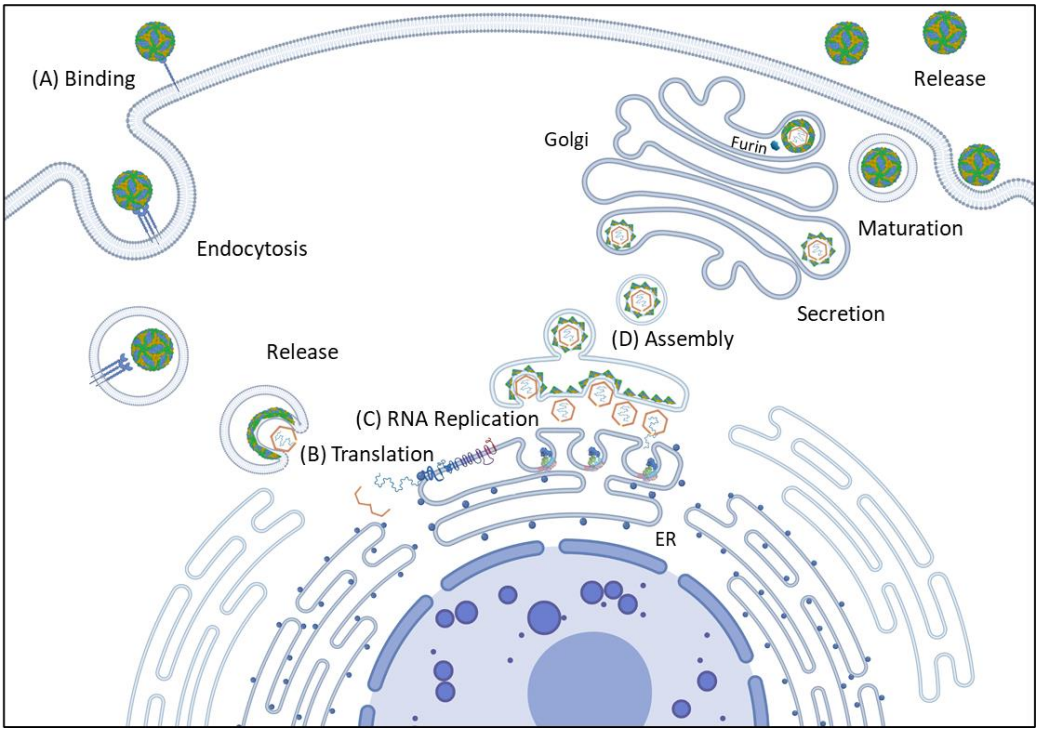


**Figure 1.3. Life Cycle of Flavivirus.** The main stages are (A) Flavivirus binding and entry, (B) Viral Polyprotein Translation, (C) Viral genome synthesis and replication and (D) Virion assembly and maturation. The

### 1.2.1.1 Flavivirus binding and entry

Flaviviruses can bind to multiple cell types using different cell surface attachment factors such as C-type lectins, glycosaminoglycans, T-cell immunoglobulin and mucin domain (TIM) receptors and TYRO3, AXL, MER (TAM) family receptors. C-type lectins such as dendritic cell-specific ICAM grabbing nonintegrin (DC-SIGN) recognised the asparagine-linked sugars on the viral envelope protein (Davis et al., 2006; Tassaneetrithep et al., 2003). Negatively charged glycosaminoglycan such as heparan sulphate binds the envelope protein via charge-charge interactions (Chen et al., 1997b; Kim et al., 2017). TIM interact directly with the viral lipid envelope while TAM binds indirectly via bridging molecules such as Gas6 (Meertens et al., 2012).

Upon attachment to the cells, the virus enters via the cell clathrin-dependent endocytosis. Host molecules are shown to aid in the endocytosis process (Hackett and Cherry, 2018; Hackett et al., 2015). Nevertheless, the clathrin-independent entry pathway was also recorded (Acosta et al., 2009). Upon entering the cell, the viral particles are transported via the early endosomes, which will subsequently mature into late endosomes (van der Schaar et al., 2008). Membrane fusion of the viral and cell membranes was proposed to follow the class II membrane fusion process (Modis et al., 2004; Mukhopadhyay et al., 2005). Upon acidification of the late endosome, the envelope protein dimer will dissociate, enabling domain II of the envelope protein to insert its fusion loop into the endosomal membrane. Then outwardly projected monomers will be rearranged and clustered forming a trimer. Domain III of the envelope protein will fold back onto itself. Free energy generated from the folding will bend the viral membrane and the endosomal membrane towards each other resulting in membrane fusion.

#### 1.2.1.2 Viral Polyprotein Translation

After the viral RNA is released into the cytoplasm, the viral RNA genome can directly serve as messenger RNA for viral protein synthesis. The viral genome having a 5' cap structure will undergo cap-dependent translation initiation (Garcia-Blanco et al., 2016). Furthermore, despite lacking a poly(A) tail, the 3' end of the viral genome can associate with poly(A) binding protein (PABP), which together with the eukaryotic initiation factor 4G (eIF4G) can mediate the circularisation of the viral genome to facilitate translation (Polacek et al., 2009).

Other functional elements in the viral genome also help to initiate translation. The capsid-coding region hairpin helps to signal and initiate translation from the correct AUG start codon (Clyde and Harris, 2006). Mutagenesis study reveals that the top loops of pseudoknot motifs of the 3' untranslated region affect the translation efficiency (Manzano et al., 2011). In response to the cellular condition, flavivirus can also switch to cap-independent translation (Edgil et al., 2006). Recently, an internal ribosomal entry site function was identified in the 5' untranslated region of DENV and ZIKV, which is responsible for cap-independent translation (Song et al., 2019). After translation, these newly synthesised viral polyproteins will be processed by cellular and viral proteases.

#### 1.2.1.3 Viral genome synthesis and replication

After translation, the membrane-bound viral proteins and co-opted host factors will induce membrane rearrangements of the ER membrane forming viral replication organelles (Paul and Bartenschlager, 2015). Within these organelles, all seven of the viral non-structural proteins, viral RNA and host factors aggregate and form the viral RC (Paul and Bartenschlager, 2015). More details of the RC will be discussed in **Section 1.2.5**.

The proposed mechanism is illustrated in **Figure 1.4**. After sufficient viral NS5 proteins are being synthesised, they will bind to the 5' untranslated regions (UTRs) of the viral genome and prevent ribosome binding (Fajardo et al., 2020). Afterwards, promoted by viral and cellular factors, the viral genome will undergo conformation change and cyclised.

Genome cyclisation helps to decrease ribosome occupancy (Sanford et al., 2019). Furthermore, the cyclisation process also destabilized the interaction between the 5'UTR and the viral NS5 (Liu et al., 2016). Then, the viral NS5 will translocate to the 3' UTR and synthesise the negative-strand RNA, producing a double-stranded RNA intermediate. The replication intermediate will undergo a semi-conservative RNA synthesis, using the negative-strand RNA as a template to produce new positive-strand RNA molecules. The newly synthesised positive-strand RNA will be capped by viral enzymes. Subsequently, it will be used as mRNA for translation of viral proteins, templates to synthesise more negative-strand RNA or be packaged as the viral genome for progeny virus.

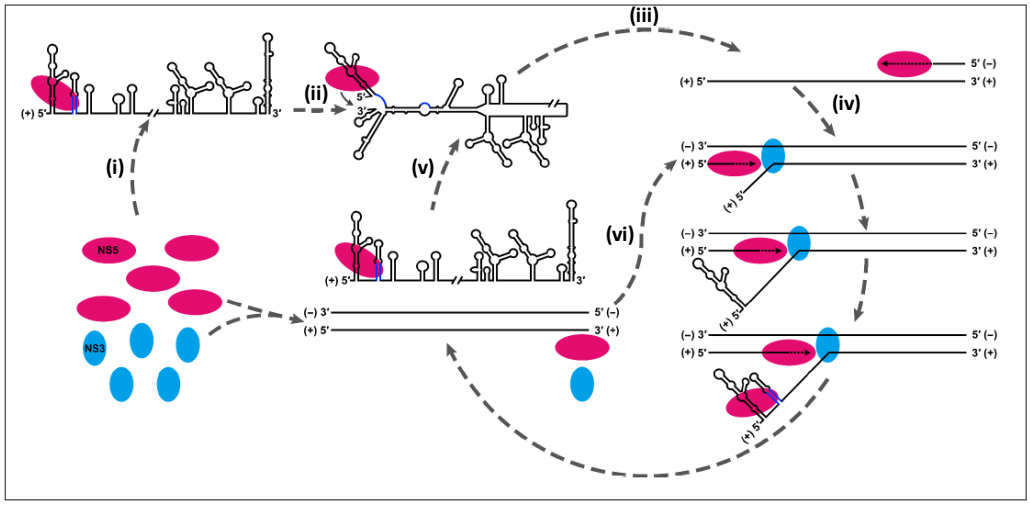


**Figure 1.4. Proposed mechanism for viral RNA replication.** (**i**) Viral NS5 will bind to the 5' UTR and (**ii**) translocate to the 3' UTR upon genome cyclisation. (**iii**) NS5 will synthesis the negative-strand RNA producing a double-stranded intermediate. (**iv**) The replication intermediate will undergo a semi-conservative RNA synthesis to produce new positive-strand RNA molecules. (**v**) The newly synthesised positive-strand RNA can be used as the template for more negative-strand RNA synthesis. (**vi**) The replication intermediate will continue to produce new positive-strand RNA molecules. The figure is adapted from (Liu et al., 2016).

#### 1.2.1.4 Virion assembly and maturation

An NS2A mediated virion assembly model was proposed by Shi's group (Xie et al., 2019; Zhang et al., 2019a). The proposed virion assembly process is illustrated in **Figure 1.5.** In this model, NS2A binds to the newly synthesised viral genome via the 3'UTR region. NS2A also recruits C-prM-E and NS2B/NS3 to the virion assembly site (Xie et al., 2019; Zhang et al., 2019a). The oligomerisation of NS2A helps to promote interaction between its interacting partners. Subsequently, the viral protease together with host signalase will process C-prM-E into the capsid, prM and envelope protein. Next, the capsid proteins, which is previously stored in the lipid droplets, will bind to the viral genome to form the nucleocapsid core.

On the cytoplasmic side of the ER, the capsid proteins form homodimers arranged in an antiparallel fashion. While on the luminal side, the precursor membrane protein and the envelope assemble to form a heterodimer, and three copies of the heterodimer will associate to form an inverted tripod conformation. Subsequently, the capsid homodimer will interact with the transmembrane regions of the heterodimers forming an assembly unit. Three of the assembly unit will form a triangular network generating a unique intertwined conformation. The assembly process will continue to form the immature virion, consisting of 180 copies of precursor membrane/envelope heterodimers which will assemble into 60 spikes (Tan et al., 2020b).

The assembled virions will bud into the ER lumen and will be transported along the Trans Golgi Network (TGN). Several host factors such as Src kinase c-Yes, KDEL receptors, Alastin-3 and Class II ADP-ribosylation factors; were also identified to facilitate the movement of the immature virion through the TGN (Neufeldt et al., 2019; Rothan and Kumar, 2019). Due to the changes in pH, a large conformational change is induced, exposing the furin cleavage site on the precursor membrane. Subsequently, the precursor membrane will be cleaved by host furin endoprotease into pr peptide and membrane protein. Next, the pr peptide is released and precursor membrane/envelope heterodimers dissociate to form the envelope protein homodimers (Yu et al., 2008). Subsequently, upon the fusion TGN vesicle with the plasma membrane, the virion will be released into the extracellular space and ready to infect other cells.

Other than viral exit via exocytosis, Studies have also highlighted virus spread via the secretory autophagy pathway (Li et al., 2020; Mateo et al., 2013; Zhang et al., 2016). Instead of fusing with the lysosome for degradation, the autophagosomes containing the viral protein and genomes fused with multivesicular bodies to form amphisomes. Subsequently, these amphisomes will fuse with the plasma membrane and release the exosome containing the viral particles (Wu et al., 2021). These exosomes enable the virus to evade circulating antibodies and promote virus spread. Lyn, a Src family kinase, was found to be responsible for virus transport using autophagosomes (Li et al., 2020). To promote the formation of autophagosome, in the presence of NS4B, NS4A also interacts with native lipid droplet protein AUP1 to induce lipophagy and supply phospholipids required for the formation of the autophagosomal

membrane (Cloherty et al., 2020; Zhang et al., 2018). Cell-to-cell transmissions were also observed in mosquito and neural progenitor cells (Clark et al., 2020; Yang et al., 2015).

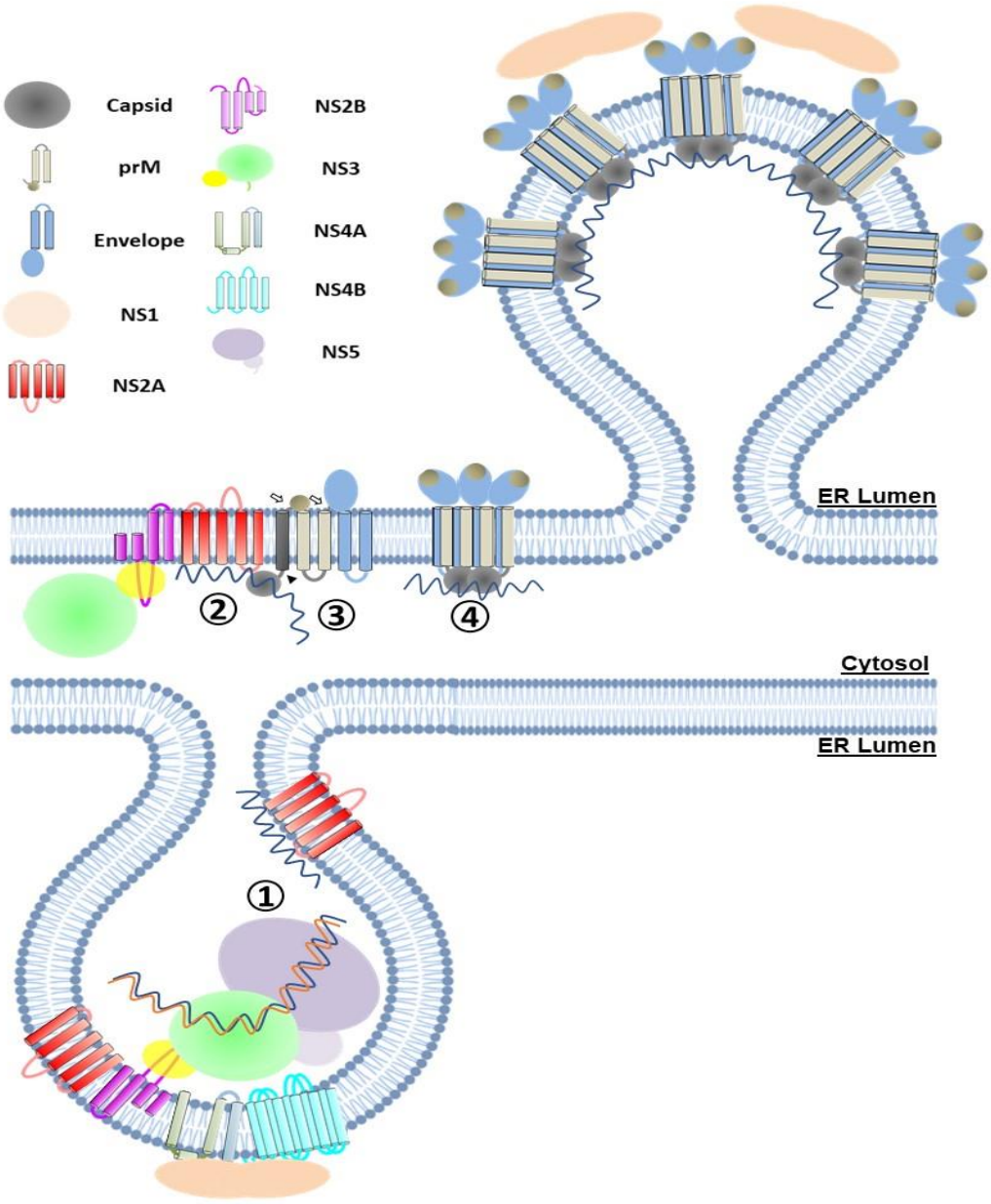


**Figure 1.5. Proposed model of NS2A mediated virion assembly.** (1) After viral RNA replication, the newly synthesised positive-sense genomic RNA will be transferred to NS2A. (2) NS2A binds to prM-E complexes, NS2B-NS3 and the viral RNA via the interactions with the 3' UTR. By associating with the NS2B protein, host signalase is also recruited to the complex. (3) The C-prM-E will be processed into the capsid, prM and envelope protein by host signalase and NS2B-NS3 protease. (4) The capsid homodimer will interact with the trimers of prM-E heterodimers forming an assembly unit of the flavivirus virion. The figure is adapted from (Barnard et al., 2021).

### 1.2.2 Virion Structure

Cryo-electron microscopy (cryo-EM) indicate that the mature viral particle of DENV, ZIKV and WNV have a similar overall structure to each other (Kostyuchenko et al., 2016; Kuhn et al., 2002; Sirohi et al., 2016). The mature flavivirus particles are around 50 nm in diameter and have a smooth surface with icosahedral symmetry. On the surface of the virus, there are 180 copies of the envelope proteins with the associated membrane proteins hidden below the envelope layer. The envelope proteins exist as dimers, three sets of parallel dimers formed a raft with thirty envelope rafts covering the entire viral surface. Beneath the surface, the capsid proteins bind the viral genome forming the nucleocapsid core of the particle.

On the other hand, the immature viral particles are slightly larger in diameter and have a spiky icosahedral shape (Tan et al., 2020b; Zhang et al., 2003). Sixty spikes can be found on the surface, with each spike is being formed by three copies of the precursor membrane/envelope heterodimer which associate together to form an inverted tripod conformation.

### 1.2.3 Viral RNA Genome

The flavivirus has a single-stranded, positive-sense RNA genome that is approximately 11,000 nucleotides long. The genome has a type 1 cap structure at its 5'end with no poly(A) tail at its 3'end. The cap structure is essential for protection against 5'-3' exonucleases as well as cap-dependent translation of the flavivirus genome. The RNA genome is made up of a single open reading frame that flanked by 5' and 3' untranslated regions (UTRs) (**Figure 1.6**). The UTRs are known to be important regulators of viral replication as well as acting as immune modulators (Gebhard et al., 2011; Iglesias and Gamarnik, 2011; Ng et al., 2017).

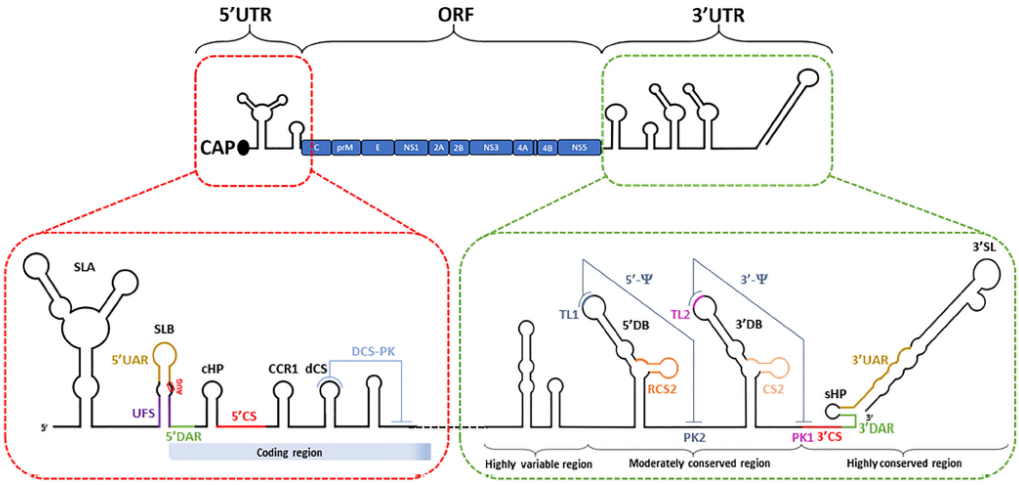


**Figure 1.6. Schematic representation of flavivirus' genome.**The figure is adapted from (Mazeaud et al., 2018). The viral genome is capped with a single open reading frame that is flanked by both 5' and 3' UTRs. Functional RNA elements in the 5' UTR include stem-loop (SL) A, SLB, the upstream AUG region (UAR), UAR-flanking stem (UFS) and the capsid-coding region hairpin (cHP). The 3' UTR can be classified into three regions based on sequence conservation and includes functional elements such as DB and 3'SL. These secondary structures and functional RNA elements are shown and annotated.

The 5'UTR is around 100 nucleotides long, with different lengths for the different flaviviruses. It has two conserved stem-loops domains, stem-loop (SL) A and SLB, which are separated by an oligo(U) spacer for the proper functioning of the two stem-loops. The SLA is around 70 nucleotides long and acts as a promoter for NS5 protein to initiate RNA synthesis at the 3' end of the cyclised genome (Filomatori et al., 2011). SLA binding also serves as an RNA selectivity mechanism to recognise the viral positive sense genome and avoid cellular mRNAs for negative-sense RNA synthesis (Saeedi and Geiss, 2013). Recently, the crystal structures for DENV and ZV SLA were also solved (**Figure 1.7**) (Zhang, 2021). They were observed to have different folding (Zhang, 2021). Some key elements of the SLA were well described. They include the base pairing in the bottom stem for structural stability (Filomatori et al., 2006). Next, the CAG nucleotides in the top stem-loop for interaction with NS5 protein (Bujalowski et al., 2020; Filomatori et al., 2011; Filomatori et al., 2006; Hodge et al., 2016; Lee et al., 2021). Then, the side loop contributes to the conformation and folding of SLA (Lee et al., 2021). Lastly, the self-complementarity element in the side loop also helps to maintain interaction with neighbouring SLA which is shown to be essential for viral replication (Lee et al., 2021). The SLB is around 30 nucleotides long and has 5'UAR (upstream AUG Region) sequences to form the cyclised RNA structure via long-range RNA-RNA interaction with 3'UAR.

Next, 5'DAR (downstream AUG Region) sequences for long-range RNA-RNA interaction for genome cyclisation was also identified (Friebe and Harris, 2010). Additionally, 5'-UAR-flanking stem, a highly-conserved RNA duplex region, was observed to bind to NS5 (Liu et al., 2016). This structure is destabilised upon genome cyclisation, which is suggested to promote the translocation of NS5 from the 5'UTR to 3'UTR for viral RNA synthesis (Liu et al., 2016). Other RNA elements within the 5' ends include the 5' cyclisation sequence (CS), which is located within the capsid protein-coding region and interacts with 3'CS for genome RNA circularization. A capsid-coding region hairpin (cHP), also help in viral RNA replication and recognition of the start codon (Clyde and Harris, 2006).

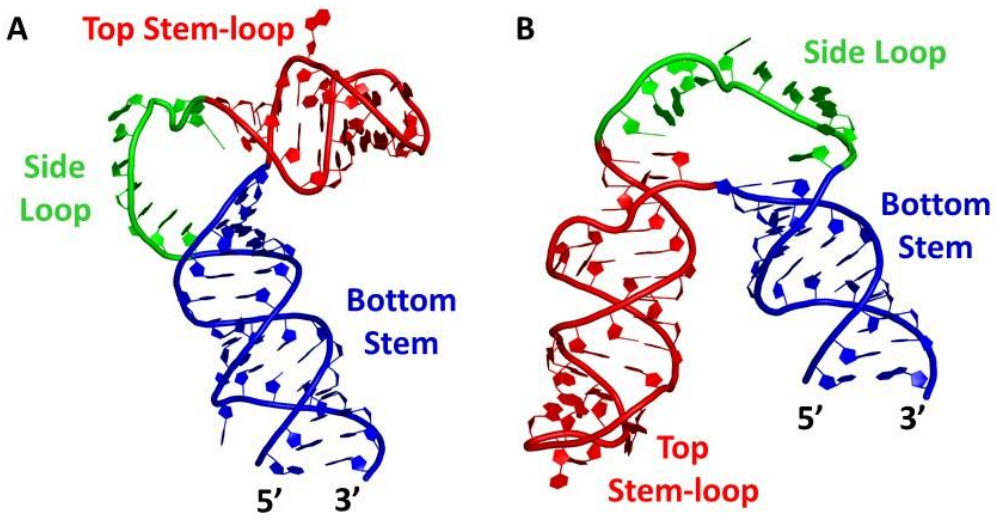


**Figure 1.7. The crystal structures of *Flaviviruses'* SLA.** (**A**) The DENV SLA (PDB: 7LYF) and (**B**) ZIKV SLA (PDB: 7LYG) structures were shown in cartoon models with bottom stem coloured in blue, side loop in green and top stem-loop in red.

The length of the 3'UTR varies for different flavivirus and ranges from 400 to 600 nucleotides long. It is grouped into three distinct domains. Domain 1 is located immediately after the stop codon and has the most variable nucleotides sequence within the 3'UTR. Although the functionality of the variable region is currently unknown, the variable region contributes to the formation of stem-loop (SL) structures, which helps to play different functions in different hosts. Studies have also shown that these stem-loop structures are resistant to degradation to host exonuclease Xrn-1 and are referred to as xrRNA-1 and/or xrRNA-2 (Akiyama et al., 2016; Chapman et al., 2014; Slonchak and Khromykh, 2018). Next, domain 2 is moderately conserved with a tandem-duplicated dumbbell structure (DB1 and DB2. The DB structure is further stabilised by the pseudoknot (PK), which play a functional role during viral RNA synthesis, translation and sub-genomic flaviviral RNAs (sfRNAs) formation (Chapman et al., 2014; Manzano et al., 2011). Lastly, domain 3 is highly conserved and is characterised by CS1, small hairpin (sHP) and large 3'SL. The 3'SL interacts with both host and viral proteins to regulate viral polyprotein and RNA synthesis (Gebhard et al., 2011; Iglesias and Gamarnik, 2011; Ng et al., 2017). Recently, it was also reported that 3'SL contribute to vesicle packets formation (Cerikan et al., 2020).

Other than at the UTRs, defined secondary and tertiary RNA structures can also be found in coding regions in the viral genome (Dethoff et al., 2018; Huber et al., 2019; Li et al., 2018b). Different studies have identified different sets of secondary structures in the coding regions of the genome, from sixteen to

twenty-four for DENV and twelve to twenty-four for ZIKV, due to the differences in methodology and analysis criteria (Dethoff et al., 2018; Huber et al., 2019; Li et al., 2018b). However, all studies indicated that the RNA is more structured in virion as compared to the more extended forms in infected cells. These structures are also capable of forming both short- and long-range RNA interactions which could influence viral fitness. Depending on the lifecycle of the virus, RNA structural heterogeneity can also be observed due to transient long-range RNA interactions (Huber et al., 2019). Different modes of long-range RNA interactions were observed for different viruses (Huber et al., 2019). While short-range interactions were found to be more conserved than long-range ones between the virus' strains (Li et al., 2018b). Furthermore, strain-specific structures were also observed and proposed to influence viral infectivity. For example, 5'UTR and envelope protein-coding region was found in an only pandemic strain of Zika virus (Li et al., 2018b).

Another feature of the viral genome includes well-conserved dinucleotide sequences 5' AG…CU 3' at the 5' and 3' ends (Khromykh et al., 2003; Markoff, 2003). The conservation of the dinucleotide sequences can be attributed to the ATP-specific priming site by the NS5 RNA-dependent RNA polymerase domain (Selisko et al., 2012).

It has also been reported that the viral genome can also be methylated at the internal adenosine site (Goertz et al., 2018). G4 RNA structures were also observed, of which 7 putative G4 structures are conserved across flavivirus (Goertz et al., 2018).

### 1.2.3.1 Genome Cyclisation

The flavivirus RNA genome exists as two conformations, linear and cyclised forms, the balance between the two conformations is essential for viral replication (**Figure 1.8**) (Villordo et al., 2010). Genome cyclisation occurs via the base pairing of sets of inverted complementary sequences at the terminal ends of the flavivirus genome. The sets of inverted complementary sequences are 5'UAR-3'UAR, 5'DAR-3'DAR, 5'CS-3'CS and 5' C1 of Capsid region-3' DB1 (De Borba et al., 2015; Friebe and Harris, 2010; Iglesias and Gamarnik, 2011; Villordo and Gamarnik, 2009).

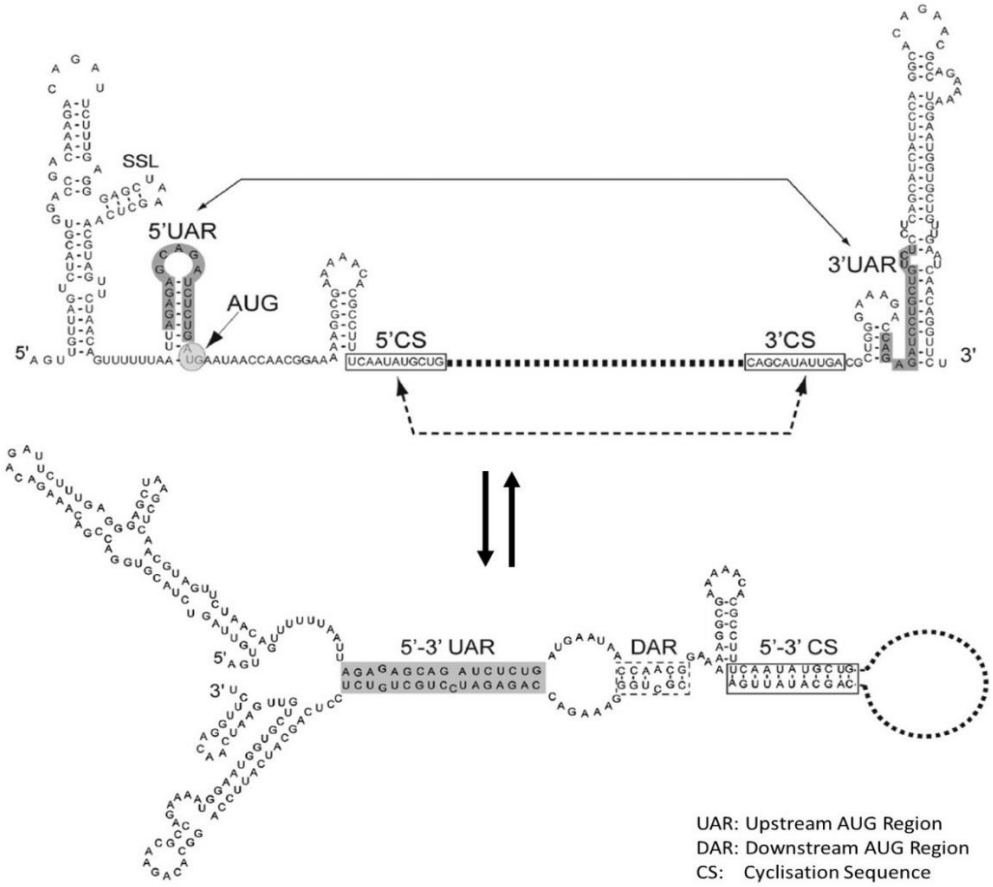


**Figure 1.8. Genome cyclisation of the viral genome.** Base pairing between the sets of inverted complementary sequences brings about genome cyclisation of the viral genome. The sets of inverted complementary sequences 5'UAR-3'UAR, 5'DAR-3'DAR and 5'CS-3'CS are shown and annotated. The figure is adapted from (Iglesias and Gamarnik, 2011).

Numerous host chaperones were found to interact with the UTR regions of the viral genome and are suggested to help in genome cyclisation (De Nova-Ocampo et al., 2002; Friedrich et al., 2018; Friedrich et al., 2014; Vashist et al., 2011).

Through numerous functional studies of the elements in the flavivirus genome, genome cyclisation was proposed to be essential for negative-sense viral RNA replication (Iglesias and Gamarnik, 2011). During genome cyclisation, the 5' polymerase-promoter complex is brought near the 3' transcription initiation site. It also promotes the correct folding of the 3' end for initiation (Iglesias and Gamarnik, 2011; Villordo and Gamarnik, 2009). Genome cyclisation also inhibits *de novo* translation initiation of viral proteins via inhibition of ribosome scanning (Sanford et al., 2019). These findings suggest that flavivirus used genome cyclisation as a molecular switch to regulate viral polyprotein translation and viral RNA replication, switching between linear translation-competent RNA form to a circular replication-competent RNA.

#### 1.2.3.2 Sub-genomic flaviviral RNA (sfRNA)

Following a flavivirus infection, small sub-genomic flaviviral RNAs (sfRNAs) were also found to be accumulated in patients along with the genomic viral RNA. These sfRNAs are formed from the incomplete cleavage of the viral genomic RNA by host 5'-3' exoribonuclease Xrn-1 (Akiyama et al., 2016; Chapman et al., 2014; Slonchak and Khromykh, 2018).

Through biochemical and structural studies, it was revealed that complex secondary and tertiary structures of the 3’ UTR at xrRNA-1 and xrRNA-2 confer resistance to degradation by Xrn-1 (Akiyama et al., 2016; Chapman et al., 2014; Slonchak and Khromykh, 2018). Both xrRNA-1 and xrRNA-2 form a ring-like conformation with the 5’ end of the RNA passing through the centre of the ring (Akiyama et al., 2016; Chapman et al., 2014). Numerous base-pair interactions like a base triple interaction, involving U4, A24, U38/42 at the 5’ end, were observed to be essential for the structure formation (Akiyama et al., 2016; Chapman et al., 2014). This ring-like structure blocks the Xrn-1 from accessing the next nucleotide in the 5' to 3' direction, enabling the RNA to resist degradation. Although Xrn-1 contain helicase activity, it is unable to bypass the block as it is unable to go through the ring and unwind the structure inside out. However, the ring structure does not inhibit viral RNA-dependent RNA polymerase, which is acting from the 3’ to 5’ direction, as they can move through the ring structure from the outside of the ring.

Furthermore, an L3-S4 pseudoknot, observed in the ZIKV xrRNA-1 structure, was shown to form a continuous stack with the P4 helix (Akiyama et al., 2016). Modelling of Xrn-1 and the xrRNA-1 showed that the P4 helix formed close contacts with the conserved winged-helix region of Xrn-1. This contact may prevent conformational changes in the enzyme which is important for enzyme activity.

The sfRNAs were suggested to play numerous roles in viral pathogenicity. Firstly, it was found that the sfRNAs can repress Xrn-1 leading to the accumulation of uncapped mRNAs and viral genomic RNA while increasing the half-life of host transcript (Michalski et al., 2019; Moon et al., 2012). However, future studies are required to determine the dysregulation effect of host mRNA turnover. Another role that the sfRNAs play is by acting as protein sponges and sequester multiple host RNA-binding proteins, ranging from proteins involved in RNA splicing, type I interferon response to apoptosis pathways (Michalski et al., 2019; Slonchak and Khromykh, 2018). Due to the secondary structure of the sfRNAs, there are numerous stem-loops and double-stranded regions which could serve as a binding site for the RNA silencing protein. Co-precipitation studies have shown that dicer and argonaute proteins are found together with the sfRNAs (Moon et al., 2015; Schnettler et al., 2012).

### 1.2.4 Viral Proteins

The viral genome will be translated into a single polyprotein which will be cleaved by host and viral protease into three structural proteins; capsid (C), precursor membrane (prM) and envelope (E) and seven NS proteins; NS1, NS2A, NS2B, NS3, NS4A, NS4B and NS5. The viral polyprotein is represented in **Figure 1.9**.

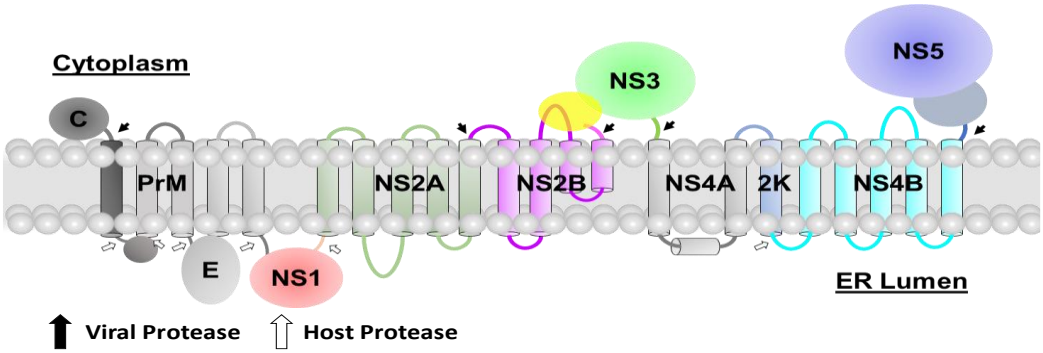


**Figure 1.9. Representation of the flavivirus' polyprotein.** The cleavage site of viral protease is represented by a solid arrow while the cleavage site by host protease is represented by an open arrow.

### 1.2.4.1 Capsid

The capsid protein is a small protein comprising around 104 to 114 amino acids. Structural studies of the mature capsid proteins reveal that they exist as a homodimer, mediated by antiparallel pairing between $\alpha1-\alpha1'$, $\alpha2-\alpha2'$ and $\alpha4-\alpha4'$ helices. Each monomer consists of an N-terminal loop followed by 4 helices. The capsid dimer has an asymmetric charge distribution, having a hydrophobic pocket that is responsible for binding to membrane, as well as having a positively charged surface to mediate binding to viral RNA (Dokland et al., 2004; Ma et al., 2004; Poonsiri et al., 2019; Shang et al., 2018). A study by Tan and colleagues also shows that there are 60 copies of the capsid dimer in the immature ZIKV particles. They also reveal that the capsid dimers formed a triangular network which is mediated helix $\alpha5$, previously thought to be absent in the mature capsid proteins (Tan et al., 2020b).

Based on the interaction with the prM-E proteins, the capsid proteins were proposed to play a vital role in the virus assembly process (Tan et al., 2020b). Other than binding to the viral RNA, DENV capsid proteins also act as RNA chaperones and assist in viral RNA folding (Pong et al., 2011). Capsid protein from various flaviviruses was also found to localise into the nucleus (Mori et al., 2005; Netsawang et al., 2010). Although they interact with host nucleus proteins, the exact function of the capsid protein in the nucleus is not known (Balinsky et al., 2013; Colpitts et al., 2011; Netsawang et al., 2010).

#### 1.2.4.2 Membrane Protein

The flavivirus membrane protein is translated as a prM protein, consisting of an N-terminal (pr) peptide and C-terminal membrane-associated (M) protein. On ER lumen, the newly synthesised prM forms heterodimers with E and three copies of the heterodimer associate together to form a 'spike'. In a crystal structure, prM consists of seven antiparallel β-strands that is stabilized by three disulfide bonds (Li et al., 2008). The pr peptide also enclosed the hydrophobic loops of the E protein, to prevent the E protein from premature fusion with the host membranes (Li et al., 2008). During the virus maturation process, a large conformational change is induced when the environment is acidified. Following the conformational change, the prM will be accessible for cleavage by host furin endoprotease into pr peptide and M protein. Subsequently, the pr peptide is released and prM-E heterodimers dissociate to form the E-homodimers (Yu et al., 2008). Mutations that affect the formation of prM-E heterodimer prevent membrane curvature and budding from the ER (Yoshii et al., 2012).

### 1.2.4.3 Envelope Protein

The envelope protein is a membrane-associated glycoprotein. It is also glycosylated at N154 for most flaviviruses and an additional unique glycosylation site at N67 for DENV. It is responsible for the membrane fusion between the virus and the host cell as well as the viral antigenicity and pathogenesis (Zhang et al., 2017). The envelope proteins exist as homodimers that are arranged antiparallel to each other on the virion surface.

The E protein can be subdivided into domain I, domain II, domain III, and a C-terminal transmembrane domain (Modis et al., 2004; Nybakken et al., 2006; Rey et al., 1995). Domain I have an eight-stranded β-barrel structure and acts as a hinge to control the overall conformation of the protein. At the tip of Domain II, it contains a highly conserved hydrophobic fusion loop that is involved in membrane fusion. Furthermore, it is also responsible for the formation of E homodimer. Lastly, domain III has β-barrel structure. It contains epitopes for receptors binding but could also be recognised by host neutralising antibodies (Chavez et al., 2010). The C-terminal transmembrane regions participate in E protein rearrangements, where the homodimer E protein will undergo conformation changes and transform into a trimer under low pH conditions (Blazevic et al., 2016). Histidine residues are also proposed to regulate E protein dimer to trimer rearrangements.

#### 1.2.4.4 NS1

NS1 is a glycosylated protein with a molecular weight of around 48 kDa. It exists as a homodimer after post-translational modification in the ER lumen. Upon secretion into the extracellular space, it exists as hexameric lipoprotein particles. Each NS1 monomer is characterised by twelve conserved cysteines and two glycosylation sites at N130 and N207, with a third glycosylation site at N175 for DENV and WNV (Akey et al., 2014; Xu et al., 2016). NS1 was also found to be poly-ubiquitinated (Giraldo et al., 2018).

Each monomer is made up of three domains, core β-ladder domain, β-roll dimerization domain, and wing domain (Akey et al., 2014; Brown et al., 2016; Xu et al., 2016). In the β-roll dimerization domain, a β-hairpin will intertwine with the β-hairpin of the adjacent monomer to form a four-stranded β-sheet 'roll-like' structure. The wing domain protrudes from the core β-ladder domain and consists of two subdomains, an α/β subdomain and a discontinuous connector domain which connect the wing domain to the core β-ladder domain. The core β-ladder domain is the most distinctive feature of NS1. It folds into a series of antiparallel β-strands with each monomer contributing half of the ladder. Most of the antiparallel β-strands are short except a long 'spaghetti' loop, which is stabilised by extensive hydrogen bonding.

The dimer adopts an overall structure with the core β-ladder domain acting as a plane, separating the hydrophobic protrusion (β-roll domain, connector subdomain and part of the wing domain) from the rest of the protein. The

conserved aromatic residues in the hydrophobic protrusion can provide additional anchor points for membrane association (Brown et al., 2016; Ci et al., 2020). Three copies of the NS1 dimers assemble and form a symmetric barrel structure, with their hydrophobic protrusion concealed inside and the glycosylation sites, wing and spaghetti loop facing outward. In the centre of the barrel, a hydrophobic hole is present to accommodate host lipids, forming the secreted NS1 lipoprotein complex.

Comparative analysis of NS1 from different flaviviruses reveals that although the NS1 dimers are structurally similar, they are distinct in their electrostatic surface potential which may contribute to the differences in viral pathogenicity (Song et al., 2016; Xu et al., 2016).

Biochemical and genetic studies revealed that NS1 is essential for viral RNA replication and the formation of the RC (Ci et al., 2020; Lindenbach and Rice, 1997; Youn et al., 2013). NS1 was also observed to colocalise with dsRNA (Mackenzie et al., 1996). A recent study revealed that NS1 involvement in viral RNA replication could be due to its role in ER modelling and the formation of vesicle packets (Ci et al., 2020; Ci et al., 2021; Plaszczyca et al., 2019). NS1 was also proposed to regulate the formation and activity of the RC via the interaction with NS4A, NS4B and NS4A-2K-NS4B intermediate (Lindenbach and Rice, 1999; Plaszczyca et al., 2019; Tan et al., 2020a; Youn et al., 2012). Other than being involved in RNA replication, NS1 also interact with the structural proteins and modulate infectious particle production (Scaturro et al., 2015).

#### 1.2.4.5 NS2A

NS2A is a transmembrane protein with a molecular weight of around 22 kDa. The N-terminal of the protein is cleaved by unknown host protease and localised on the endoplasmic reticulum (ER) lumen, while the C-terminal is found in the cytoplasm and cleaved by viral NS2B-3 protease. Numerous biochemical studies have revealed that the NS2A proteins from different flaviviruses adopt different membrane topologies, with YFV having three integral transmembrane regions, DENV with five integral transmembrane regions and ZIKV having only a single integral transmembrane region (Vossmann et al., 2015; Xie et al., 2013; Zhang et al., 2019b). This could be due to the low sequence conservation in the coding region of NS2A proteins between flaviviruses.

Recent biochemical and mutagenesis studies identified NS2A as a key player in virion assembly (Kummerer and Rice, 2002; Leung et al., 2008; Xie et al., 2019; Zhang et al., 2019a). During virion assembly, NS2A is involved in recruiting C-prM-E, NS2B/NS3, and viral RNA through interacting with 3'UTR to the virion assembly site (Xie et al., 2019; Zhang et al., 2019a). Additionally, in DENV-2, it also coordinated C-prM-E cleavage in a sequential manner (Xie et al., 2019).

Biochemical and mutagenesis studies identified NS2A to be involved in RNA replication (Xie et al., 2015; Zhang et al., 2019b). Furthermore, NS2A was shown to be co-localised with double-stranded RNA (Mackenzie et al., 1998). Although NS2A is involved in both RNA replication and virion assembly, further complementary assay recovers virion production activity but not RNA replication, this suggests that two different sets of NS2A at a different cellular location are involved in each process (Xie et al., 2015; Zhang et al., 2019b).

NS2A also modulate the immune response by the down-regulation of IFN-β-stimulated gene expression (Liu et al., 2004; Liu et al., 2006; Munoz-Jordan et al., 2003). The N-terminal region of DENV NS2A is also responsible for the virus-induced cytopathic effect (Wu et al., 2017).

#### 1.2.4.6 NS2B

NS2B is a 14 kDa protein consisting of 130 amino acid residues. It consists of the central hydrophilic region at the cytoplasmic side of the ER, which is flanked by two transmembrane helices at both the N and C terminals of the proteins (Kang et al., 2017; Li et al., 2015c; Ng et al., 2019a). The residues involved in membrane association were also revealed by nuclear magnetic resonance (NMR) spectroscopy study( **Figure 1.10**) (Li et al., 2015c; Ng et al., 2019a). The central hydrophilic region alone is sufficient and act as the co-factor for the folding and enzymatic activity of NS3 protease (Kang et al., 2017). The NS2B cofactor was also shown to contribute to the substrate selectivity of NS3 protease (Hill et al., 2018).

Other than acting as the co-factor for NS3, NS2B also helps to anchor NS3 onto the ER membrane (Clum et al., 1997). Through the interactions with other membrane-bound NS proteins, NS2B was also part of the RC, suggesting a role in viral replication (Uchil and Satchidanandam, 2003; Welsch et al., 2009). Further study reveals that the correct topology of the α4 helix in NS2B is essential for NS2B-NS2A interaction (Li et al., 2016a). Mutagenesis study also revealed that the transmembrane domain could affect viral RNA replication and virion assembly (Li et al., 2016a). DENV NS2B was also shown to inhibit the type-I interferon pathway by targeting cyclic GMP-AMP synthase for degradation via the autophagy-lysosomal-dependent pathway, prevent the detection of mitochondrial DNA that were released during DENV infection (Aguirre et al., 2017).

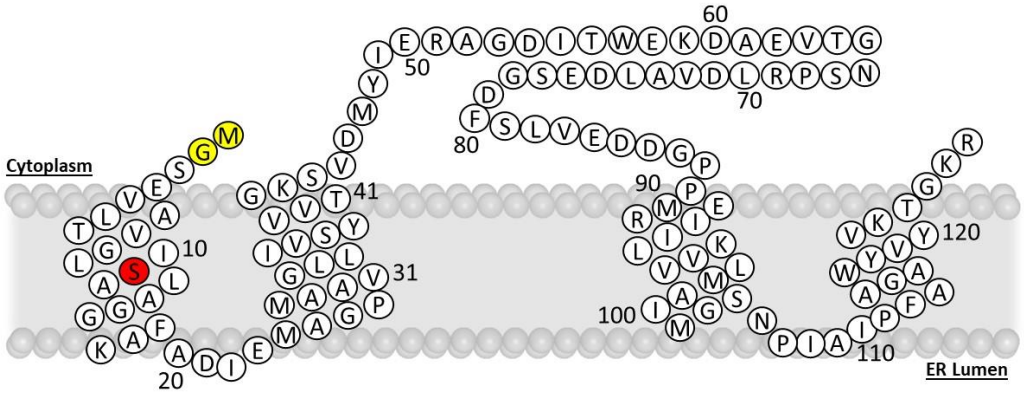


**Figure 1.40. Predicted membrane topology of ZIKV NS2B C11S mutant revealed by NMR studies.** The residues in NS2B are numbered. The first two amino acids do not belong to NS2B and are highlighted in yellow. The mutated residue is highlighted in red. The figure is adapted from (Ng et al., 2019a).

### 1.2.4.7 NS3

NS3 is a 68kDa multifunctional protein. It consists of 2 main domains, N-terminal protease and C-terminal helicase.

#### N-terminal Protease Domain

Together with the NS2B cofactor, NS3 N-terminal protease formed a functional viral protease critical for the processing of the viral polyproteins. The polyprotein cleavage junctions are at Capsid, NS2A|2B, NS2B|3, NS3|4A, NS4A|2K and NS4B|5 junctions (**Table 1.1**). In-vitro characterisation using synthetic peptides representing polyprotein cleavage junctions reveals that viral protease has the highest affinity to NS2A/2B followed by NS3/4A, NS4B/5 and NS2B/3 junction sequences (Chanprapaph et al., 2005; Leung et al., 2001).

**Table 1.1. The protein sequence of viral polyprotein cleavage junctions.**

| Virus | Entry ID | Capsid | 2A\|2B | 2B\|3 | 3\|4A | 4A\|2K | 4B\|5 |
|---|---|---|---|---|---|---|---|
| **ZIKV** | Q32ZE1 | RKRR\|GA | SGKR\|SW | TGKR\|SG | AGKR\|GA | EKQR\|SP | VKRR\|GG |
| **DENV1** | P33478 | RRKR\|SV | WGRK\|SW | KKQR\|SG | AGRR\|SV | DRQR\|TP | GGRR\|GT |
| **DENV2** | P29990 | RRRR\|SA | SKKR\|SW | KKQR\|AG | AGRK\|SL | EKQR\|TP | NARR\|GT |
| **DENV3** | Q5UB51 | KRKK\|TS | LKRR\|SW | QTQR\|SG | AGRK\|SI | EKQR\|TP | TGKR\|GT |
| **DENV4** | Q5UCB8 | GRKR\|ST | ASRR\|SW | KTQR\|SG | SGRK\|SI | EKQR\|TP | TPRR\|GT |
| **WNV** | Q9Q6P4 | QKKR\|GG | NRKR\|GW | YTKR\|GG | SGKR\|SQ | EKQR\|SQ | GLKR\|GG |
| **JEV** | P27395 | QNKR\|GG | NKKR\|GW | TTKR\|GG | AGKR\|SA | EKQR\|SQ | SLKR\|GR |
| **YFV** | Q6DV88 | RKRR\|SH | FGRR\|SI | GARR\|SG | EGRR\|GA | GQQR\|SI | TGRR\|GS |

The viral protease typically recognised basic residues at the P1 to P3 position followed by small residues at the P1' position (Ang et al., 2014; Gruba et al., 2016; Li et al., 2005; Rut et al., 2020; Rut et al., 2017). In-vitro characterisation

also revealed that the S4 pocket can accommodate a wide range of residues for DENV, WNV and ZIKV proteases (Gruba et al., 2016; Li et al., 2005; Rut et al., 2020; Rut et al., 2017). Additionally, preferences for unnatural, basic residues as P1-P3 residues were also observed for DENV, WNV and ZIKV proteases (Rut et al., 2020; Rut et al., 2017). In contrast, the viral protease shows different preferences for the residues at the P1' to P3' position (Li et al., 2005; Shiryaev et al., 2007a). Further study on the influence of prime side specificity by Prusis and co-workers, revealed that only P1' and P2' prime side residues were critical in affecting the $k_{cat}$ value of DENV protease, while all four prime side residues, P1'–P4', were important determinants for $K_m$ value (Prusis et al., 2008). Furthermore, by mutating conserved residues at the active site, it is possible to switch substrate specificity between flavivirus, highlighting the co-evolution between the protease and the cleavage sequence (Shiryaev et al., 2007b).

The viral protease adopts a chymotrypsin-like fold with the catalytic triad (H51, D75, S135) located at the cleft between the two β-barrels (**Figure 1.11**) (Erbel et al., 2006; Zhang et al., 2016). The N-terminus residues (49 to 67) of NS2B helps to stabilise the folding of NS3 protease through the insertion of a beta-sheet into the N-terminal β-barrel (Erbel et al., 2006; Zhang et al., 2016). While the C-terminus residues (68 to 98) of NS2B helps to form the catalytic site (Erbel et al., 2006; Zhang et al., 2016).

The NS2B-3 protease was also found to be in two predominant conformations, 'open' and 'closed' (**Figure 1.11**). In the 'open' conformation, the C-terminal residues NS2B catalytic cofactor region is disordered and does not participate

in the formation of the active site. In the 'closed conformation', the NS2B cofactor interacts with NS3 protease and contribute to the formation of the S2 and S3 pocket of the active site. From a FRET study, the two conformations were found to be in equilibrium (Gotz et al., 2021).

Studies have shown that depending on the protein construct used, the protease can preferentially adopt a particular conformation (Hill et al., 2019). For the 'linked' protease construct, the NS2B co-factor is linked to the NS3 protease via $Gly_4SerGly_4$ linker and expressed as a single polypeptide chain. Crystallography studies revealed that this construct was typically captured in the 'open' conformation in the apo protein, while the 'closed' conformation was only observed when a ligand is bound to the active site (Erbel et al., 2006; Lee et al., 2017; Lei et al., 2016; Noble et al., 2012). However, in a recent publication of the full-length DENV-3 NS3 structures, it was revealed that the linked construct could also exist in the closed conformation without a ligand (Phoo et al., 2020). These findings were also supported by NMR studies, whereby in the absence of a ligand, closed conformation could also be found (Chen et al., 2014; de la Cruz et al., 2011; Su et al., 2009).

In the 'unlinked' protease construct, two separate polypeptide fragments NS2B co-factor and NS3 protease are co-expressed and assembled in bacteria. This construct exists mainly as the closed conformation as shown by both X-ray crystallography and NMR studies (de la Cruz et al., 2014; Hill et al., 2019; Kim et al., 2013; Zhang et al., 2016).

In terms of their enzymatic activity, the unlinked ZIKV protease was also found to be more enzymatically active and has a greater affinity to the substrate than linked ZIKV protease. (Kuiper et al., 2017; Phoo et al., 2016). The differences in catalytic efficiency can be attributed to the artificial linker blocking access to the active site. Nevertheless, most studies agreed that the 'closed' conformation is the active state for NS2B-3 protease (Hill et al., 2019; Lei et al., 2016; Zhang et al., 2016).

Other than being involved in viral polyprotein processing, the NS2B-3 protease also cleaved host proteins and plays a role in immune evasion. DENV NS2B-3 protease cleaves human stimulator of the interferon gene (STING) and inhibits type I interferon pathway (Aguirre et al., 2012; Rodriguez-Madoz et al., 2010; Yu et al., 2012). Furthermore, DENV NS2B-3 protease also cleaves two mitofusins which are responsible for mitochondrial fusions, the disruption of the mitochondrial dynamics leads to an attenuated mitochondrial antiviral signalling (MAVS) and its downstream pathways (Yu et al., 2015). In addition to inhibiting immune response, flaviviral protease also cleaves FAM134B, a receptor that is involved in reticulophagy, this promotes ER expansion required in the formation of viral replication vesicles and genome replication (Lennemann and Coyne, 2017). Recent studies also identified the nuclear pore complex as a target of Dengue and Zika protease, although, their exact role in viral pathogenesis and replication remains unknown (De Jesus-Gonzalez et al., 2020; Hill et al., 2018).

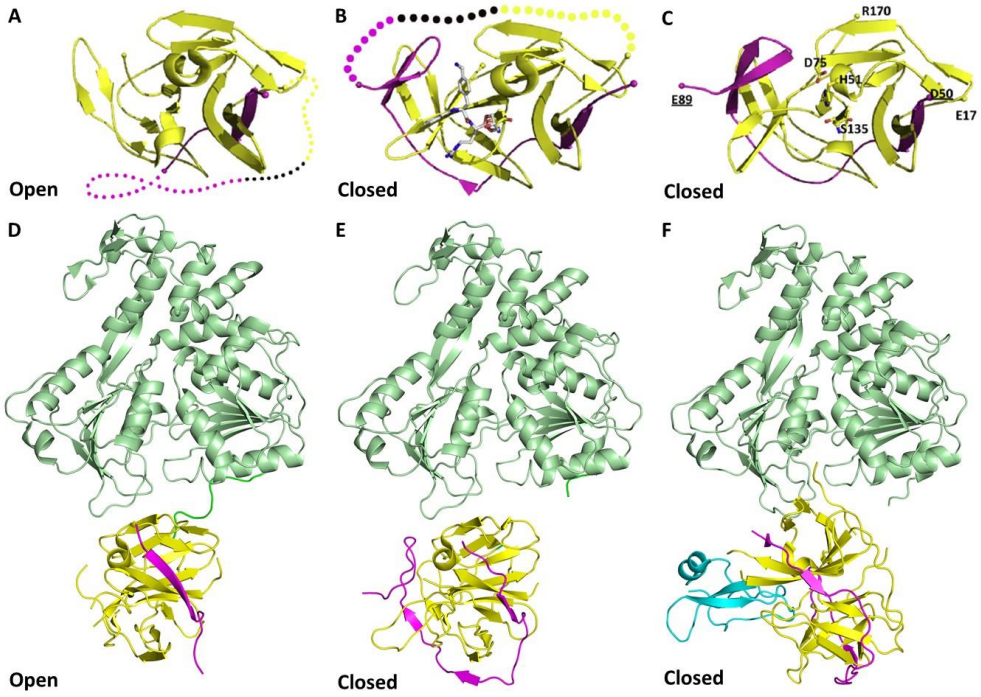


**Figure 1.11. Crystal structures of NS2B-NS3 constructs in various conformation.** (**A**) Apo 'linked' protease construct in the open conformation (PDB: 5T1V). (**B**) 'Linked' protease-inhibitor complex in the closed conformation (PDB: 5LC0). (**C**) Apo 'unlinked' protease construct in the closed conformation (PDB: 5GPI). Apo 'linked' NS2B-NS3 construct in the (**D**) open conformation (PDB: 5YVJ) and (**E**) closed conformation (PDB: 5YVV). (**F**) 'Linked' NS2B-NS3-BPTI complex in the closed conformation (PDB: 5YVU). The figure is adapted from (Kang et al., 2017; Phoo et al., 2020). Ribbon representation shows the arrangement of the NS2B cofactor and NS3 protein. The NS2B cofactor is coloured in magenta, the protease domain is in yellow, the helicase domain in green and the BPTI inhibitor in turquoise.

### C-terminal Helicase Domain

NS3 C-terminal helicase belongs to superfamily 2 (SF2) helicases. The helicase is essential for unwinding the duplex RNA into single-stranded RNA for NS5 polymerase activity. It also possesses NTPase and RTPase activity. The helicase is composed of 3 domains. With domain 1 and 2 having an α/β RecA-like folds, demonstrating characteristic feature of the SF2 helicases (Jain et al., 2016; Tian et al., 2016a; Xu et al., 2005). RNA binding tunnel separates domains 1 and 2 from domain 3 while ATP binding site is located between domain 1 and 2 (Jain

et al., 2016; Tian et al., 2016a; Xu et al., 2005). A P-loop region also exists in domain 1 for NTP binding and catalysis.

Upon RNA binding, subdomain 3 rotate about $10^{o}$ away from the RNA binding tunnel, enlarging the groove to accommodate the ssRNA (Luo et al., 2008b; Tian et al., 2016b). Furthermore, RNA binding is also sufficient to bring inwards movement of the P-loop in the absence of ATP (Luo et al., 2008b). Despite the slight differences in the conformation of the P-loop of the various flavivirus helicase under apo condition (Jain et al., 2016; Tian et al., 2016a), upon RNA and ATP binding, they undergo different local rearrangements to adopt similar binding mode and structures (Tian et al., 2016b).

Crystal structures of full-length NS3 protein reveal that it adopts an elongated structure (Assenberg et al., 2009; Luo et al., 2010; Luo et al., 2008a). Two different conformations with different relative orientations between the protease and helicase domains were captured for the apo protein, while a third conformation was captured when the protease was bound to bovine pancreatic trypsin inhibitor (BPTI) (**Figure 1.12**). Due to the flexibility of the interdomain linker region, the protease domain can rotate from about $50^{o}$ to $180^{o}$ relative to the helicase domain depending on the flavivirus. (Assenberg et al., 2009; Luo et al., 2010; Phoo et al., 2020) The length of the linker between the 2 domains is shown to play a regulatory role (Luo et al., 2010).

Most studies are in consensus and revealed that the helicase domain has no effects on the protease's activity (Assenberg et al., 2009; Chernov et al., 2008; Luo et al., 2010). However, there are conflicting findings concerning the

influence of protease on the helicase domain. This could be due to the intrinsic viral differences, protein construct design or methodology. Some studies revealed that in the absence of the protease, helicase unwinding activity for both dsRNA and dsDNA were decreased (Luo et al., 2008a; Xu et al., 2019b; Xu et al., 2005). While other studies suggested partial or no influence by the protease on the helicase domain (Assenberg et al., 2009; Mastrangelo et al., 2007). Other findings include protease regulating and restricting NS3 helicase unwinding activity to double-stranded RNA (Chernov et al., 2008).

A dimeric model for NS3 protein was also proposed (Lei et al., 2016). The dimerization may also be facilitated by the membrane association of full-length trans-membrane NS2B, where it has been shown to dimerizes in a cell-based assay (Leon-Juarez et al., 2016).

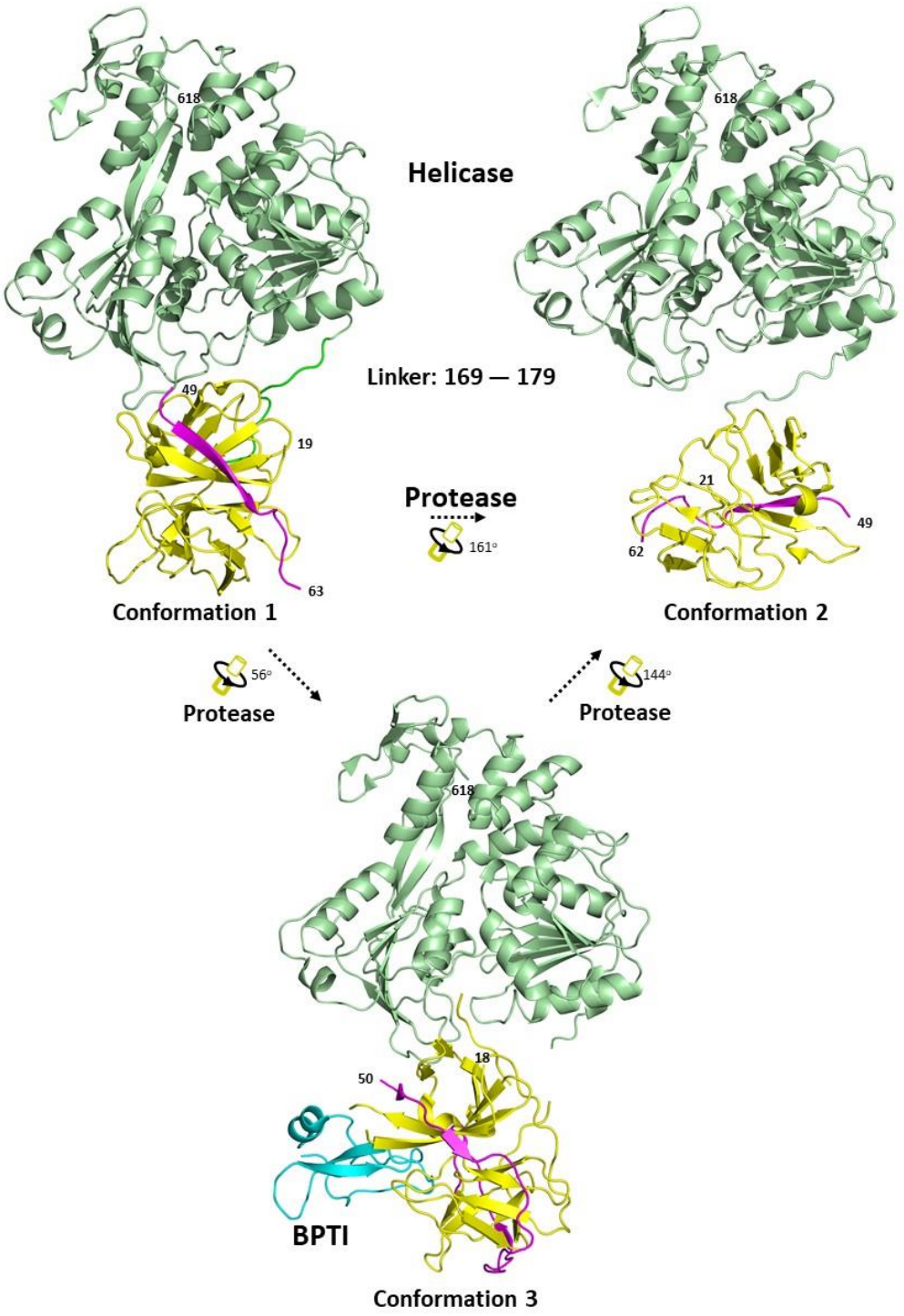


**Figure 1.12. Relationship between different conformational states of the Dengue 4 full-length NS3 structures.** The protein structures were obtained from PDB. Conformation 1 (PDB: 2VBC), conformation 2 (PDB: 2WHX) and conformation 3 (PDB: 5yvu) are shown. Ribbon representation shows the arrangement of the protease and helicase domains of NS3. The NS2B cofactor is coloured in magenta, the protease domain is in yellow, the helicase domain in green and the BPTI inhibitor in turquoise. The conformational changes between the protein structures were analysed using the DynDom database (Lee et al., 2003).

#### 1.2.4.8 NS4A

NS4A is a membrane protein with three N-terminal amphipathic helices and four C-terminal membrane helices (Li et al., 2018c; Miller et al., 2007). The last transmembrane helix, 2K, acted as a signal sequence to direct NS4B into the lumen of the ER. The 2k peptide will be cleaved by the viral protease at the N-terminal while the C-terminal is processed by the host signalase. Mutagenesis study reveals that the first transmembrane region is responsible for the oligomerisation of NS4A. In DENV, E50A and G67A mutation decreased NS4A oligomerization and NS4A protein stability, leading to attenuated viral replication (Lee et al., 2015).

Dengue and Kunjin NS4A were also found to be co-localised with dsRNA, suggesting a role in viral RNA replication (Mackenzie et al., 1998; Miller et al., 2007). Studies have found out that NS4A is sufficient to induce cytoplasmic membrane rearrangement, DENV uses fully processed NS4A while KUNV requires the full-length NS4A (Miller et al., 2007; Roosendaal et al., 2006). Also, WNV NS4A was observed to influence the ATPase activity of the NS3 helicase (Shiryaev et al., 2009). NS4A was also shown to induce autophagy during viral infection, although the mechanism for inducing autophagy might be different among flaviviruses. In DENV infection, the expression of NS4A is sufficient to induce autophagy in renal epithelial cells (McLean et al., 2011). While for ZIKV infection in fetal neural stem cells, NS4A inhibit the Akt-mTOR signalling pathway to promote autophagy and inhibit neurogenesis (Liang et al., 2016).

#### 1.2.4.9 NS4B

NS4B is the largest membrane protein found in the flavivirus' genome. It consists of nine helixes with helix 2, 3, 5, 7, 9 forming transmembrane domains 1 – 5 respectively (Li et al., 2015b; Li et al., 2016b; Miller et al., 2006). DENV accumulate at ER-derived membranes mediated by transmembrane domain 3 - 5 (Miller et al., 2006). Transmembrane domain 5 was also proposed to undergo conformation changes and flip from the cytoplasmic side to the ER lumen upon NS4B-NS5 junction cleavage (Li et al., 2016b; Miller et al., 2006). The cytoplasmic loop, transmembrane domain 4 and 5 were found to be responsible for NS4B dimerization (Zou et al., 2014). Recently, ER membrane protein complex was also identified to act as ER chaperone to facilitate correct insertion and topology of the transmembrane region of NS4B (Barrows et al., 2019; Lin et al., 2019a; Ngo et al., 2019).

NS4B was suggested to play a role in viral RNA replication as it is found localised with the other NS proteins that are involved in viral replication (Miller et al., 2006). NS4B promote the dissociation of ssRNA from NS3, enhancing the unwinding activity of the NS3 helicase domain (Umareddy et al., 2006). Different regions of NS4B were also found to play different immune-modulatory functions. DENV (specifically the first 125 amino acids of DENV NS4B), WNV and YFV disrupts the phosphorylation of Signal Transducer And Activator Of Transcription 1 (STAT1) and impedes the IFN-$\alpha$/$\beta$-induced signal transduction cascade (Munoz-Jordan et al., 2005). Transmembrane domain 3 and 5 also suppress host RNA interference response (Kakumani et al., 2013)

### 1.2.4.10 NS5

NS5 protein carries 2 enzymatic domains, an N-terminal methyltransferase (MTase) domain and a C-terminal RNA-dependent RNA polymerase (RdRp) domain.

**N-terminal Methyltransferase Domain**

The crystal structures of the Mtase domain of various flaviviruses had been determined, they adopt similar globular folds, that can be divided into three sub-domains (Zhou et al., 2007). The first subdomain is characterised by a helix-turn-helix motif followed by a β-strand and an α-helix. The GTP-binding pocket can be found in this subdomain and was proposed to coordinate the GTP moiety of RNA substrate during the 2'-O-ribose methylation (Dong et al., 2008; Zhao et al., 2015b). The second subdomain is the core domain with Rossmann fold, consisting of seven β–sheets and 4 α-helix. Both the active site for methyltransferase activity as well as the SAM and RNA binding sites can be found in the core domain. The conserved catalytic tetrad (KDKE) is also located near the SAM-binding site (Coloma et al., 2016). The last subdomain consists of an α-helix and two β-strands.

The MTase domain methylates both N7 atom of guanosine and 2'O of the initiating adenosine of the nascent viral transcript to form the type I cap structure using S-adenosylmethionine (SAM) as the methyl donor (Dong et al., 2014). The MTase was also proposed to have guanylyltransferase (GTase) activity, to transfer GTP to a 5' di-phosphorylated RNA (Issur et al., 2009). The

type I RNA capping occurs when NS5 bind to GTP and form an NS5-GMP intermediate. Concurrently, NS3 RTPase will remove the γ-phosphate from the viral genome 5’ end, producing a diphosphorylated RNA intermediate product. NS5 will subsequently transfer the GMP to the di-phosphorylated RNA upon RNA binding. Then, the RNA will reposition the guanosine near the SAM binding site to methylate the N7 atom of guanosine. The RNA will then undergo another repositioning, to accommodate the m7-capped RNA in the GTP-binding site, to allow the initiating adenosine to be positioned near the SAM binding site for 2’O methylation. (ppA-RNA > GpppA-RNA > $^{N7M}$GpppA-RNA > $^{N7M}$GpppA$_{2'OM}$-RNA). The RNA capping mechanism is illustrated in **Figure 1.13**.

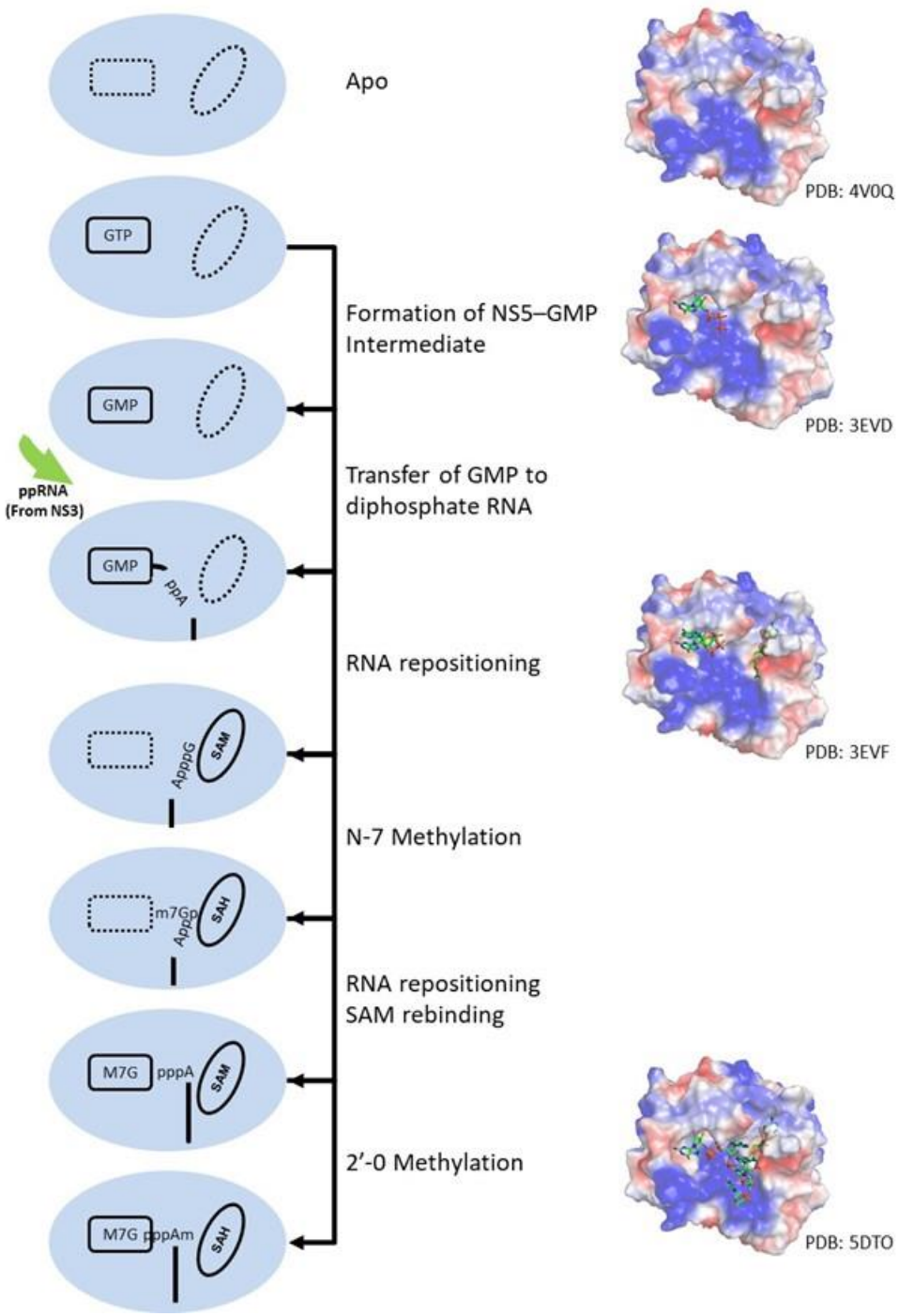


**Figure 1.13. Cartoon representation of the flavivirus capping process.** During the RNA capping process, GTP binds to the GTP binding pocket of NS5 and forms an NS5-GMP intermediate. Concurrently, NS3 RTPase removes phosphate from the viral genome to form a diphosphorylated RNA product. The NS5-GMP intermediate subsequently transfers the GMP to the diphosphorylated RNA upon RNA binding. Then, GpppA-RNA repositions the guanosine near the SAM binding site for N7-methylation. The SAH molecule is replenished by SAM molecule while the $^{N7M}$GpppA-RNA undergoes another repositioning to allow the initiating adenosine to be positioned near the SAM binding site for 2'O methylation to generate $^{N7M}GpppA_{2'OM}$-RNA. Representative protein structures at the different stages with their PDB codes are also shown.

**C-terminal RNA-dependent RNA polymerase Domain**

The crystal structure of the RdRp domain revealed a right-hand architecture consisting of a palm, a thumb and a fingers subdomain (**Figure 1.14**) (El Sahili and Lescar, 2017; Wang et al., 2017; Yap et al., 2007; Zhao et al., 2017; Zhao et al., 2015c). The active site is located on the palm subdomain, the most structurally conserved region of NS5. The active site with two catalytic aspartic acid residues is required for chelating two $Mg^{2+}$ metal ions and the formation of the phosphodiester bond. The crystal structures also reveal a unique region known as the priming loop protruding from the thumb subdomain. It is a unique feature of RdRp and acts as a platform to stabilise the RNA initiation complex and to catalyse *de novo* RNA initiation (El Sahili and Lescar, 2017; Wang et al., 2017; Yap et al., 2007; Zhao et al., 2017; Zhao et al., 2015c). Three tunnels were observed and are responsible for the entry of ssRNA template, the exit of dsRNA and serving as nucleoside triphosphates (NTPs) entry tunnel. In the absence of RNA-bound structures, all solved structures depict a closed conformation, whereby the RNA binding tunnel is too narrow to accommodate a double-stranded RNA. Thus, the structure was proposed to be a preinitiation state, and a retraction of the priming loop will occur following the transition from the initiation to the elongation state.

The RdRp domain is involved in RNA synthesis in both de novo initiation and elongation step. While the RNA synthesis mechanism remains elusive due to the lack of both structural and biochemical information, it can be postulated based on the RdRp-RNA complex structures from other viruses (Appleby et al., 2015;

Wu and Gong, 2018). During the initiation step, upon the binding of the 3' end of the RNA template with sequence 5' … CU 3', ATP and GTP form base pairing with the CU at the 3' end. The residues H798 in the priming loop act as an initiation platform and stabilise the priming ATP through stacking interactions (Selisko et al., 2012). Subsequently, the two catalytic aspartic acid residues and their coordinated $Mg^{2+}$ metal ions catalysed the phosphodiester bond formation between ATP and GTP to form the initial dinucleotide primer. Afterwards, the priming loop was proposed to position away from the active site to accommodate growing dsRNA. Subsequently, the RdRp transit into the elongation phase with an open conformation to allow rapid and processive polymerisation.

Numerous X-ray crystallography studies revealed a series of different global conformations and different modes of interaction between the Mtase domain and the RdRp domain for full-length NS5 proteins from different flavivirus (**Figure 1**.**14**) (El Sahili et al., 2019; Lu and Gong, 2013; Wang et al., 2017; Wu et al., 2020; Zhao et al., 2017; Zhao et al., 2015c). In solution, NS5 from different DENV serotypes were also found to display multiple conformations (Saw et al., 2015). The first conformation is observed in JEV, ZIKV and DENV-2 (El Sahili et al., 2019; Lu and Gong, 2013; Wang et al., 2017; Zhao et al., 2017). In this conformation, the MTase and the RdRP has an interacting interface consisting of mostly hydrophobic residues. In DENV-3, a more compact conformation is observed (Zhao et al., 2015c). In this alternative conformation, the MTase also rotates by approximately 110° and establishes mainly polar contacts instead.

Recently, two additional conformations were observed in DENV-2 (Wu et al., 2020) and an additional conformation in YFV (Dubankova and Boura, 2019). Conformation 1 – 3 are related to each other via the rotation along an axis of the highly conserved GTR residues, which was previously suggested to pivot the MTase movement relative to RdRP (Lu and Gong, 2013). While conformation 4 and 5 are related via a 14° rotation along an axis near the MTase-RdRp interface.

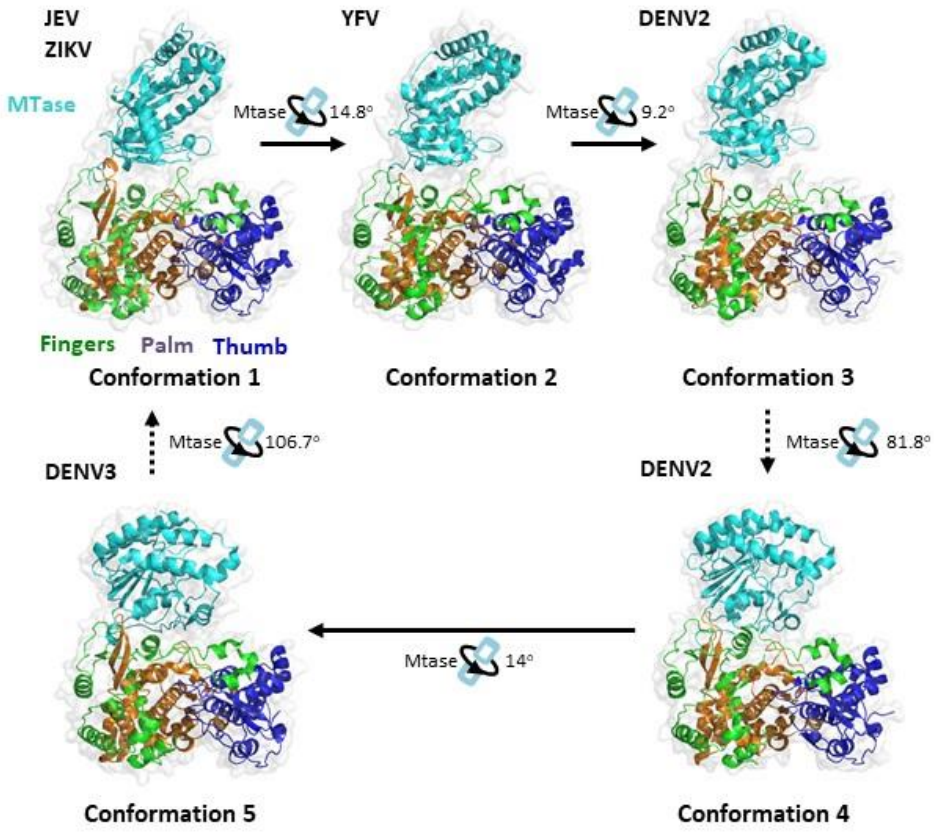


**Figure 1.14. Relationship between the different conformational states of the *Flavivirus* full-length NS5 structures.** The protein structures were obtained from PDB. JEV (PDB: 4K6M), YFV (PDB: 6QSN), DENV2 (PDB: 6KR2), DENV2 (PDB: 6KR3), and DENV3 (PDB:4V0Q). Ribbon representations show the arrangement of the MT and RdRp domains of NS5. The MTase is coloured in cyan, the RdRp fingers in green, the RdRp palm in brown and the RdRp thumb in blue. The conformational changes between the protein structures were analysed using the DynDom database (Lee et al., 2003).

The ability of NS5 to adopt different global conformations was proposed to be facilitated by the linker domain. Comparison between the full-length crystal structures reveals that the first 4 residues of the linker undergo a swinging motion to adopt a short $3_{10}$ helix structure when switching conformation from the JEV-mode conformation to the DENV-3 compact conformation. (Wu et al., 2020; Zhao et al., 2015c). Mutations to the linker region, disrupt the crosstalk between the Mtase and the RdRp, is detrimental to virus replication (El Sahili et al., 2019; Zhao et al., 2015a).

Biochemical studies suggest that the Mtase domain plays different roles in the regulation of the polymerase activity of DENV RdRp (Lim et al., 2013a; Potisopon et al., 2014; Zhao et al., 2015c). These findings are also observed on JEV and Zika, where MTase might differentially regulate both the de novo initiation and elongation phase during viral RNA synthesis (Wu et al., 2015b). Disrupting the hydrophobic interaction of JEV-mode conformation impairs de novo initiation but not the elongation phase, suggesting that assistance by MTase is required in the unstable initiation phase (Wu et al., 2020). Another study suggests that Mtase enhance the stability of the NS5-RNA elongation complex (Rusanov et al., 2018). The interaction between methyltransferase and the RdRp domain in the Zika virus is shown to be necessary for virus replication (Rusanov et al., 2018; Zhao et al., 2017).

Immunofluorescence assay reveals that the majority of the NS5 proteins of various flaviviruses can be found in the nucleus of infected cells (Buckley et al., 1992; Kumar et al., 2013; Lopez-Denman et al., 2018; Ng et al., 2019b). NS5 proteins from some DENV serotypes are incapable of entering the nucleus (Kumar et al., 2013; Tay et al., 2013). Further studies reveal that the nuclear localisation sequence for DENV and ZIKV NS5 lie in 18 amino acids C-terminal NLS and αβNLS region respectively (Ng et al., 2019b; Tay et al., 2016). Distinctively, ZIKV NS5 also forms spherical shell-like structures in the nucleus, which has been proposed to modulate host immune response (Ng et al., 2019b).

It was also observed that NS5 from various flaviviruses antagonizes the type I interferon (IFN-I) pathway in infected cells, suggesting that suppression of this pathway is a critical determinant of pathogenesis (Best, 2017). However, the mechanisms of inhibition by NS5 differ among flaviviruses and host species (Best, 2017; Grant et al., 2016). In DENV, the RdRp domain can interact and bind to STAT2 and prevent its phosphorylation (Mazzon et al., 2009). Furthermore, mature NS5 interact with ubiquitin ligase E3 N-recognin 4 (UBR4) and STAT2. DENV NS5 serves as a bridge and promote the ubiquitination and degradation of STAT2 via ubiquitin-dependent proteasomal degradation pathway (Ashour et al., 2009; Morrison et al., 2013). However, in ZIKV infection, the degradation of STAT2 is independent of UBR4 (Grant et al., 2016). Furthermore, ZIKV NS5 also block the phosphorylation of STAT1 and inhibit the activation of TANK-binding kinase 1 (TBK1) (Hertzog et al., 2018; Lin et al., 2019b). In contrast, for YFV infection, NS5 does not induce the degradation of STAT2, instead, it binds to the

STAT1-STAT2 heterodimer and prevent interferon regulatory factor 9 (IRF9) binding and subsequently to the interferon stimulating response element (ISRE) promoter element (Laurent-Rolle et al., 2014). Host-specific ubiquitination of YFV NS5 is also a prerequisite for the binding to STAT2 of the STAT1-STAT2 heterodimer (Laurent-Rolle et al., 2014; Miorin et al., 2019). Recently, using ZIKV, WNV and JEV infected cells, NS5 interacts with heat shock protein 90 (HSP-90) and prevent HSP-90 from interacting with Janus kinase (JAKs). This targets JAK for degradation and blocks JAK/STAT2 signalling cascade (Roby et al., 2020). Recently, the Zika NS5-STAT2 Cryo-Electron microscope (EM) complex structure was also solved (Wang et al., 2020). The findings reveal that NS5 interacts with STAT2 via both the MTase and RdRp domains.

In contrast to suppressing type I interferon, during ZIKV infection, the degradation of STAT2 promotes the formation of STAT1 homodimer formation and type II interferon signalling response (Chaudhary et al., 2017). This produces proinflammatory cytokines, which facilitate the viral spread and exacerbate the infection.

Recently, NS5 proteins were also found to regulate the translation of viral genomic RNA by decreasing ribosome occupancy (Fajardo et al., 2020).

### 1.2.5 Replication Complex

Flavivirus genome replication takes place in virus-induced organelle-like membrane structures (**Figure 1.15**). Cryo-EM study of DENV-infected cells revealed invaginations into the ER with a diameter of 90 nm as well as an unstructured convoluted membranes (CMs) structure (Welsch et al., 2009). The lumen of the vesicle packets (VPs) is connected to the cytoplasm via a 10 nm pore-like opening. These VPs contain both the viral NS proteins as well as dsRNA, thus it was suggested to be the viral RNA replication site. On the other hand, CMs are only enriched with viral proteins with an undefined role in the viral replication cycle, proposed to be the site for viral polyprotein translation.

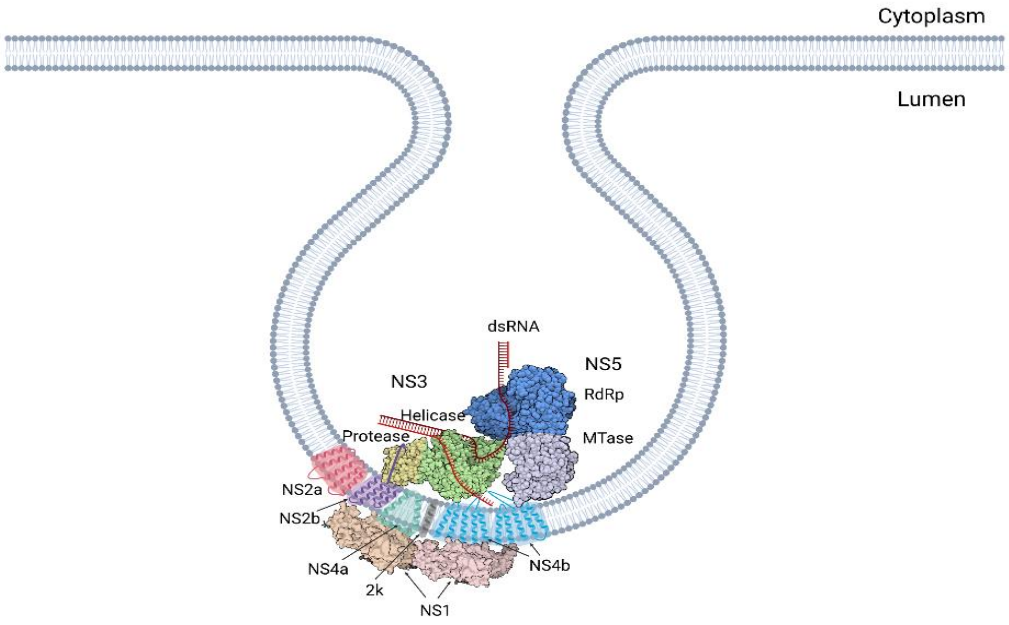


**Figure 1.15. A cartoon representation of the Flavivirus' replication organelle.** A possible configuration of the replication complex based on current understanding. The complex is situated on the ER membrane with all seven non-structural proteins forming the replication complex.

These VPs play multiple roles in the viral replication cycle (Paul and Bartenschlager, 2015). Firstly, they can help to separate the different stages of the viral replication cycle. Next, they help to localise the viral proteins and required metabolites in close proximity. Lastly, they also shield viral products from the host innate immune system.

Viral transmembrane proteins NS4A and NS4B are proposed to be primarily involved in the formation of the vesicle packets (Miller et al., 2007; Miller et al., 2006; Roosendaal et al., 2006). NS1 is also involved in the formation of the VPs through the remodelling of the ER (Ci et al., 2020; Plaszczyca et al., 2019). Positively charged residues of NS1, R31 in ZIKV, binds to a series of negatively charged lipids, such as PI4P, on the ER membrane (Ci et al., 2021). Subsequently, it induces ER invaginations via the conserved aromatic residues in the hydrophobic protrusion (Brown et al., 2016; Ci et al., 2020).

3'SL also contribute to the formation of VPs (Cerikan et al., 2020).

Host factors such as Reticulon 3.1 (RTN3.1A), a member of the reticulon family involved in ER membrane curvature, was also found to be recruited to the VPs. RTN3.1A promote the remodelling of the ER membrane and stability of NS4A (Aktepe et al., 2017). Through its interaction with DENV NS4A, Vimentin acts as a scaffold and help organise ER membrane into VPs (Teo and Chu, 2014). Alastin-2, a member of the ER membrane-bound GTPases of the dynamin family, were also required for the production of VPs (Neufeldt et al., 2019). DNAJC14, a chaperone molecule within the Hsp40 family, was found to modulate the protein-protein interaction network and promote the formation of a protein

scaffold that maintains the VPs in YFV (Yi et al., 2012). Although viral and host components required for the formation of VPs were identified, the exact mechanism for the formation of the VPs and the involvement of other host proteins remains to be elucidated.

To enhance viral replication, flaviviruses also promote lipogenesis in infected cells for membrane formation. Fatty acid synthase (FAS) was observed to be recruited to the site of the replication.(Martin-Acebes et al., 2011; Tang et al., 2014). At the replication site, DENV NS3 interact with FAS and stimulate fatty acid biosynthesis (Heaton et al., 2010). Other than promoting lipogenesis, flavivirus infection also alters the host membrane lipid composition. By varying the lipid composition, it can help to promote VPs formation through the enrichment of negative or positive curvature inducing lipid groups (Aktepe and Mackenzie, 2018)

#### 1.2.5.1 Interactions between the NS proteins within the replication complex

Many studies have shown that all seven non-structural proteins can be found at the RC (Mackenzie et al., 1996; Mackenzie et al., 1998; Miller et al., 2007; Miller et al., 2006; Uchil and Satchidanandam, 2003; Welsch et al., 2009). NS3 and NS5 are the only two viral proteins that have enzymatic functions, thus they are proposed to form the core of the RC. The rest of the NS proteins are proposed to play a regulatory role to support viral replication. The interactions between the NS proteins are summarised in **Table 1.2**.

NS1, which resides in the ER lumen, was also proposed to transmit signals across the ER membrane to regulate viral RNA replication via the interaction with NS4A and NS4B for YFV and WNV respectively (Lindenbach and Rice, 1999; Youn et al., 2012). However, the mechanism for signal transduction remains to be further studied. Recently, DENV NS1 (residue G161 and W168) was also found to interact with the NS4A-2K-NS4B intermediate (Plaszczyca et al., 2019). While domain II of DENV NS1 was found to interact with NS4A (residue Y41) (Tan et al., 2020a). Further studies are required to understand the role of these interactions. The former interaction was proposed to regulate NS4A-2K-NS4B cleavage for proper membrane association and maturation of NS4A and NS4B. While the latter interaction was proposed to help in the formation of the RC.

The transmembrane proteins were also observed to interact with each other. NS4A (residues 40 – 76) and NS4B (residues 84 – 146) were also found to interact with one another. Furthermore, compensatory mutations were also found in NS4B when NS4A were mutated for both DENV and JEV, supporting NS4A-NS4B interaction (Chatel-Chaix et al., 2015; Li et al., 2015a; Tajima et al., 2011). A study conducted using FRET and BiFC assay further revealed additional interaction partners NS2A and NS4A, NS2A and NS2B and between NS4A and NS4B for WNV (Yu et al., 2013). Taken together, NS4A could be a key driver in organising the luminal, transmembrane and cytoplasmic components of the RCs.

Extensive interactions were found between the NS proteins to regulate NS3 enzymatic activity. Firstly, the central hydrophilic region of NS2B interact with the NS3 protease domain and act as the co-factor for enzymatic activity and stability of NS3 protease (Kang et al., 2017). Secondly, WNV NS4A modulates the ATPase activity of the NS3 helicase (Shiryaev et al., 2009). Next, the cytoplasmic loop of NS4B (residue Q134) was found to interact with domain II and III of NS3 helicase (Chatel-Chaix et al., 2015; Umareddy et al., 2006; Zou et al., 2015b). This interaction allows NS4B dimer to promote the dissociation of ssRNA from NS3 and enhance the helicase unwinding activity (Umareddy et al., 2006). Lastly, NS3 helicase activity is also stimulated and upregulated by NS5 mediated by NS3-NS5 interaction (Cui et al., 1998; Xu et al., 2019b; Yon et al., 2005).

N570 of NS3 and K330 of NS5 were shown to be key residues involved in NS3-NS5 interaction (Tay et al., 2015; Zou et al., 2011). Further electrostatic potential analysis of NS3 (residues 566-585) and NS5 (residues 320-341) shows negatively charged and positively charged surfaces respectively, supporting the hypothesis that the two regions interact via charge interaction (Tay et al., 2015). Optimal NS3-NS5 interaction affinity is proposed to be essential in coordinating RNA unwinding by NS3 Helicase and RNA synthesis by NS5 RdRp (Tay et al., 2015; Zou et al., 2011).

**Table 1.2. Interactions between the NS proteins within the replication complex.**

| Virus | Protein: Residues | Protein: Residues | References |
|---|---|---|---|
| DENV | NS1 (G161, W168) | NS4A-2K-NS4B | (Plaszczyca et al., 2019) |
| | NS1: 30 – 180 | NS4A-2K-NS4B: 35 – 61 (Y41) | (Tan et al., 2020a) |
| | NS2B | NS3 | |
| | NS3: Helicase Domain II and III | NS4B: 129 – 165 (Q134) | (Chatel-Chaix et al., 2015; Umareddy et al., 2006; Zou et al., 2015b) |
| | NS3: 566 – 585 (N570) | NS5: 320 – 341 (K330) | (Tay et al., 2015; Zou et al., 2011) |
| | NS4A: 40 – 76 (L48, T54, L60) | NS4B: 84 – 146 | (Zou et al., 2015c) |
| | NS4B | NS4B | (Zou et al., 2014) |
| WNV | NS1 | NS4B | (Youn et al., 2012) |
| | NS2A | NS2B | (Yu et al., 2013) |
| | NS2A | NS4A | (Yu et al., 2013) |
| | NS2B | NS3 | (Yu et al., 2013) |
| | NS2B | NS4A | (Yu et al., 2013) |
| | NS2B | NS4B | (Yu et al., 2013) |
| | NS3 | NS5 | (Yu et al., 2013) |
| | NS4A | NS4B | (Yu et al., 2013) |
| JEV | NS2A | NS2B | (Li et al., 2016a) |
| | NS3 | NS5 | (Chen et al., 1997a) |
| YFV | NS1 | NS4A | (Lindenbach and Rice, 1999) |

### 1.3. Vaccines

To date, there are only licensed vaccines against DENV, JEV, TBEV and YFV (Li et al., 2018a; Pierson and Diamond, 2020).

#### 1.3.1 Yellow fever vaccine

The yellow fever vaccine is based on live-attenuated virus (LAV) strain YFV-17D, which was developed by Max Theiler in the 1930s through repetitive passages in chicken embryos (Collins and Barrett, 2017). Three sub-strains are used in vaccine production, 17DD, 17D-204 and 17D-213 (Collins and Barrett, 2017). The vaccine is highly protective and elicits a robust adaptive immune response, as such, YFV-17D was used as the backbone to develop chimeric vaccines against other flaviviruses such as DENV, JEV, WNV and ZIKV (Arroyo et al., 2004; Giel-Moloney et al., 2018; Monath et al., 2003; Thomas and Yoon, 2019).

#### 1.3.2 Dengue vaccine

The development of the DENV vaccine is challenging as DENV is composed of 4 genetically distinct but closely related serotypes (DENV1-4). These serotypes share a mosaic of conserved and distinct structural antigens (Heinz and Stiasny, 2012). Therefore, upon DENV infection, it will induce serotype-specific antibodies, which can also moderately cross-neutralize other serotypes. These cross-reacting antibodies do not effectively neutralise a different DENV serotype, increasing the risk of severe dengue upon secondary infection with a heterologous virus, a phenomenon known as antibody-dependent enhancement (ADE) (Shukla et al., 2020; Wilder-Smith et al., 2019). ADE is mainly mediated via 2 different modes of actions, extrinsic and intrinsic ADE.

Extrinsic ADE occurs when the non-neutralising antibodies form a virus-antibody complex, binds to the Fcγ receptor and promote virus uptake into cells (Morrone and Lok, 2019; Shukla et al., 2020). A study revealed that the types of antibodies produced in the body play a role in the manifestation of ADE. About 60% of the human antibody response recognised the prM protein, 20-30% target the envelope protein fusion loop epitope while 10% target the host cell receptor binding domain (EDIII) (Beltramello et al., 2010). Unfortunately, the anti-prM and anti-fusion loop antibodies are poor neutralisers but bind well to the immature virus. In doing so, it allows the otherwise non-infectious particles to enter the cell via the Fcγ receptor pathway (Morrone and Lok, 2019; Shukla et al., 2020). Upon entering the cell, the low pH of the endosome promotes massive rearrangements of the surface proteins of the immature virus, resulting in steric clashes and antibody:pr complex dissociation. Subsequently, virus-endosome fusion occurs, completing virus entry into the cell (Wirawan et al., 2019). Structural studies on the antibody-virus complex also reveal that the orientation of the antibody binding onto the surface of the mature virus also influence ADE (Lok, 2018; Renner et al., 2018). Antibodies that bind perpendicularly to the virus surface have their Fc region of the antibody fully exposed, enabling Fcγ receptor binding. While antibodies that lay flat on the virus surface, do not allow the exposure of their Fc region for Fcγ receptor binding (Lok, 2018; Renner et al., 2018).

During intrinsic ADE, the innate immune response and intracellular cytokine signalling are down-regulated, leading to enhanced virus replication and release (Narayan and Tripathi, 2020; Shukla et al., 2020). Transcriptomics studies reveal that in canonical DENV infection, genes responsible for host protein translation were downregulated (Chan et al., 2019; Viktorovskaya et al., 2016). However, for ADE, these genes were activated to facilitate the translation of viral protein. Furthermore, genes in the RNA processing pathway, which are known to interact with viral RNA, are upregulated. In ADE, there is also a shift from a pro-inflammatory Th-1 response to an anti-inflammatory antibody-mediated Th-2 response (Narayan and Tripathi, 2020). The skewed Th-2 immune response further worsens the condition by promoting the production of sub-neutralizing antibodies that promote DENV entry (Narayan and Tripathi, 2020; Ubol and Halstead, 2010).

To prevent the ADE phenomenon, DENV vaccines must provide immunological protection against all serotypes. Hence, they are usually developed as tetravalent formulations, with each component having different monotypic immune responses to target each serotype (Wilder-Smith, 2020). The manufacturers will need to prevent the problem of viral interference, where one component of the tetravalent vaccine replicates better at the expense of the others, leading to a situation whereby even though the formulation is a physically tetravalent mixture but is immunologically monovalent (Shukla et al., 2020).

Other challenges include the lack of a reliable animal model as well as a lack of in-vitro assay to measure immune correlates of protection and disease enhancement (Wilder-Smith, 2020).

#### 1.3.2.1 Vaccine Candidates

Currently, Dengvaxia® is the only approved vaccine against DENV. It is a tetravalent virus cocktail consisting of live-attenuated chimeric monovalent viruses with non-structural genes from YFV-17D and prM and envelope proteins from DENV1-4 (Thomas and Yoon, 2019). Although, it is approved for use, due to the varying vaccine efficacy across the four serotypes and rising concern about the increased risk of severe dengue for vaccinating seronegative individuals, WHO revised their guideline to only recommend persons with evidence of past dengue infection for vaccination (WHO, 2019; Wilder-Smith, 2020).

Two other leading vaccines are also in phase III clinical trial, TAK-003 by Takeda Vaccine Inc and TV003/005 by US NIH. TAK-003 also follow a chimeric vaccine design with DENV-2 as the backbone with prM and envelope proteins from DENV1, 3 & 4. Due to the presence of DENV NS protein, it induces cross-reactive T cell-mediated responses to provide broad coverage against DENV (Osorio et al., 2016). It has an overall vaccine efficacy of 66% for seronegative individuals after 18-months post-vaccination (White et al., 2021). Next, TV003/005 is a LAV cocktail with a varied dosage for each serotype. The LAV was designed with 30 nucleotide deletions in the 3'UTR region coupled with a chimeric vaccine design (Durbin, 2020). In contrast to the other two LAVs, TV003/TV005 can induce a

high neutralizing antibody response with a single dose (Durbin et al., 2016). To date, the phase 3 results have yet to be published.

Other vaccine types, such as subunit vaccine (Manoff et al., 2015); DNA vaccine (Danko et al., 2018) are still in Phase I clinical trial. With many other next-generation vaccines designs, virus-like particles and viral vector vaccines, in preclinical studies (Deng et al., 2020; Redoni et al., 2020).

### 1.3.3 Zika vaccine

There are currently no licensed vaccines against ZIKV. One DNA subunit vaccine is currently in phase II clinical trial. The plasmid DNA encodes wild-type ZIKV prM-E sequence, it elicits the highest neutralizing titre when administered using needle-free injection (Gaudinski et al., 2018; Shan et al., 2018).

Given that DENV and ZIKV co-circulate in many regions, there are also concerns that the ZIKV vaccine could also potentially lead to ADE as observed between DENV serotypes. A study conducted on non-human primates demonstrated that prior exposure to ZIKV can significantly enhance DENV-2 infections (George et al., 2017).

### 1.4. Antiviral Inhibitors

With the limited success in vaccine development for disease prevention, the development of antiviral therapeutics is essential to manage the disease's severity and prevent deaths.

One of the successful antiviral approaches is using direct antiviral agents (DAA) to inhibit the viral enzyme, as demonstrated by many successful drugs used to treat viral diseases caused by the human immunodeficiency virus (HIV), hepatitis B virus and hepatitis C virus (HCV) (Lim et al., 2013b). An online repository, DenvInD, was also recently launched to consolidate the information for experimentally validated inhibitors against DENV viral enzymes (Dwivedi et al., 2020).

#### 1.4.1 NS2B-NS3 Protease Inhibitors

Flavivirus NS2B-NS3 protease is an attractive antiviral target due to its' essential role in viral polyproteins processing and maturation. Furthermore, the NS2B-3 protease also cleaved and inactivate host proteins that are involved in host immunity. However, the progress towards successful drug candidates has been slowed, mainly due to the hydrophilicity and the depth of the protease active site (Lim et al., 2013b; Poulsen et al., 2014).

The viral protease typically recognised basic residues at the P1 to P3 position followed by small residues at the P1' position. In-vitro characterisation has revealed that the most optimal substrate at P3 to P1 position for WNV and ZIKV is KKR and for DENV is KRR (Ang et al., 2014; Gruba et al., 2016; Li et al., 2005;

Rut et al., 2017). Furthermore, DENV has a distinct preference for arginine and homologs at the P2 position (Rut et al., 2020; Rut et al., 2017). While more distinctive differences can be observed for the P1' to P3' position, with the optimal residues for WNV and DENV being GGX and SXS respectively, where X is any natural amino acid residues (Li et al., 2005; Shiryaev et al., 2007a). Thus, by targeting the S1 to S3 pockets, broad-spectrum inhibitors against flaviviral infections can be developed. Alternatively, by targeting the S2, S1' to S3' pockets, it could be possible to improve potency and specificity to a flavivirus.

To develop an antiviral for NS2B-NS3 protease, common strategies include high-throughput screening (HTS), substrate mimicking and drug repurposing (Lim, 2019; Lim et al., 2013b; Poulsen et al., 2014). HTS consisting of both biochemical assay and *in silico* compound docking, are carried out to identify new potential leads for drug design and optimisation. The substrate mimicking approach involves making modifications to the substrate that are already known to bind to the active site. While drug repurposing is employed as a riskless and efficient strategy. Structure-activity relationship studies (SAR) are also often used to allow researchers to gain a deeper understanding of the binding mode of the inhibitor, complementing and guiding modifications to the lead compounds identified by the previously mentioned strategies to improve the potency for antiviral developments. Some examples of viruses, with successful and licensed viral protease inhibitors, which benefited from SAR include HIV and HCV (Bassetto et al., 2016; Nalam and Schiffer, 2008; Wlodawer and Erickson, 1993)

#### 1.4.1.1 Compound screening

Numerous screenings were carried out to identify both competitive and allosteric inhibitors against flavivirus protease. The scaffolds of the inhibitors are illustrated in **Figure 1.16**.

Mueller and colleagues performed HTS against WNV protease and identified a potential 8-hydroxyquinoline scaffold (Mueller et al., 2008). The most potent inhibitor, compound B, shows high inhibitory activity in both enzymatic and cell-based assays. Molecular docking of compound B reveals binding to the S2 to S4 pocket. Subsequently, follow up studies were also performed on the 8-hydroxyquinoline and derivatives and shows that they also follow competitive inhibition (Chu et al., 2015; Ezgimen et al., 2012; Lai et al., 2013b). A virtual HTS was conducted by Tomlinson and co-workers, who identified 2 compounds consisting of an anthracene scaffold (Tomlinson et al., 2009). They proceeded to test anthracene-based compounds and show that the inhibitors bind to the S1 pocket via docking study (Tomlinson and Watowich, 2011). Another HTS study conducted by Balasubramanian and colleagues identified a series of compounds consisting of catechol and polyphenolic scaffolds to work against both DENV and WNV proteases (Balasubramanian et al., 2016). Two of the compounds, tolcapone and tannic acid, were already used to treat both viral and non-viral diseases. Next, Lee and colleagues utilised a small molecule inhibitors screen that they have previously tested against HCV protease (Lee et al., 2017). In the study, the top 10 potent compounds against ZIKV protease can be categorised into 2 scaffolds, sulphonamide conjugated with either

benzothiazole or thiazole group. Of which 2 have IC50 value below 10 uM and displayed competitive inhibition.

HTS also identified non-competitive allosteric inhibitors that prevent the interaction between the NS2B cofactor and NS3 protease. Johnston and colleagues screened a library from the National Institutes of Health (NIH) against WNV protease and identified non-competitive inhibitors consisting of a 5-amino-1*H*-pyrazol-3-yl scaffold (Johnston et al., 2007). Another group screened another library from NIH National Cancer Institute and identified an allosteric inhibitor with $EC_{50}$ of 280 nM, 810 nM and 1 μM for YFV, DENV-2 and ZIKV respectively (Brecher et al., 2017). Next, Swaminathan's group identified benzimidazole and quinoline derivatives that bind to the allosteric site of DENV protease (Beesetti et al., 2018; Raut et al., 2015). These inhibitors displayed antiviral effects against all dengue serotypes in a cell-based assay. Wu and colleagues screened an in-house library and identified diaryl thioethers as a potential scaffold (Wu et al., 2015a). The benzothiazole derivative containing inhibitor was found to have low $IC_{50}$ and $EC_{50}$ against DENV-3. To improve on the hydrophobicity, a proline residue was used to substitute an aromatic residue to enhance solubility by Millies et al (Millies et al., 2019). The series of allosteric inhibitors containing benzothiazole and proline residues scaffold have sub-micromolar $IC_{50}$ against both DENV and ZIKV. A library targeting histone-modifying enzymes were screened against DENV, WNV and ZIKV protease (Yao et al., 2019). The inhibitors have $IC_{50}$ values within the nanomolar range against all three flaviviruses. Furthermore, the inhibitory exhibited significant antiviral activities in cells and mouse models of Zika virus infection.

HTS was also employed for drug repurposing. Li group screened NIH Chemical Genomic Center Pharmaceutical Collection library and identified compounds that can prevent interaction between NS2B cofactor and NS3 protease (Li et al., 2017b). Three approved drugs, temoporfin, niclosamide, and nitazoxanide, were found to have nanomolar potency against ZIKV. A follow-up study also identified Erythrosin B, an FDA-approved food additive, inhibiting numerous flaviviruses with $EC_{50}$ within the low micromolar range (Li et al., 2018e).

Other than HTS, a small compound library also identified competitive inhibitors against the viral protease. Lai and colleagues designed a series of hybrid derivatives of 1,2-Benzisothiazol-3(2H)-one and 1,3,4-oxadiazole and tested them against DENV and WNV protease (Lai et al., 2013a). Nine compounds were able to inhibit 50% of both DENV and WNV proteases activity at 10 μM. Another study was conducted by Weng et al to modify a methionine–proline dipeptides into fused-bicyclic derivatives, with the most potent inhibitor having an $EC_{50}$ value of around 39 μM (Weng et al., 2017). Inhibitors against DENV protease was developed using thiadiazoloacrylamide as a scaffold by Li and colleagues (Liu et al., 2014). Six of the inhibitors were found to have an $IC_{50}$ of less than 5 μM.

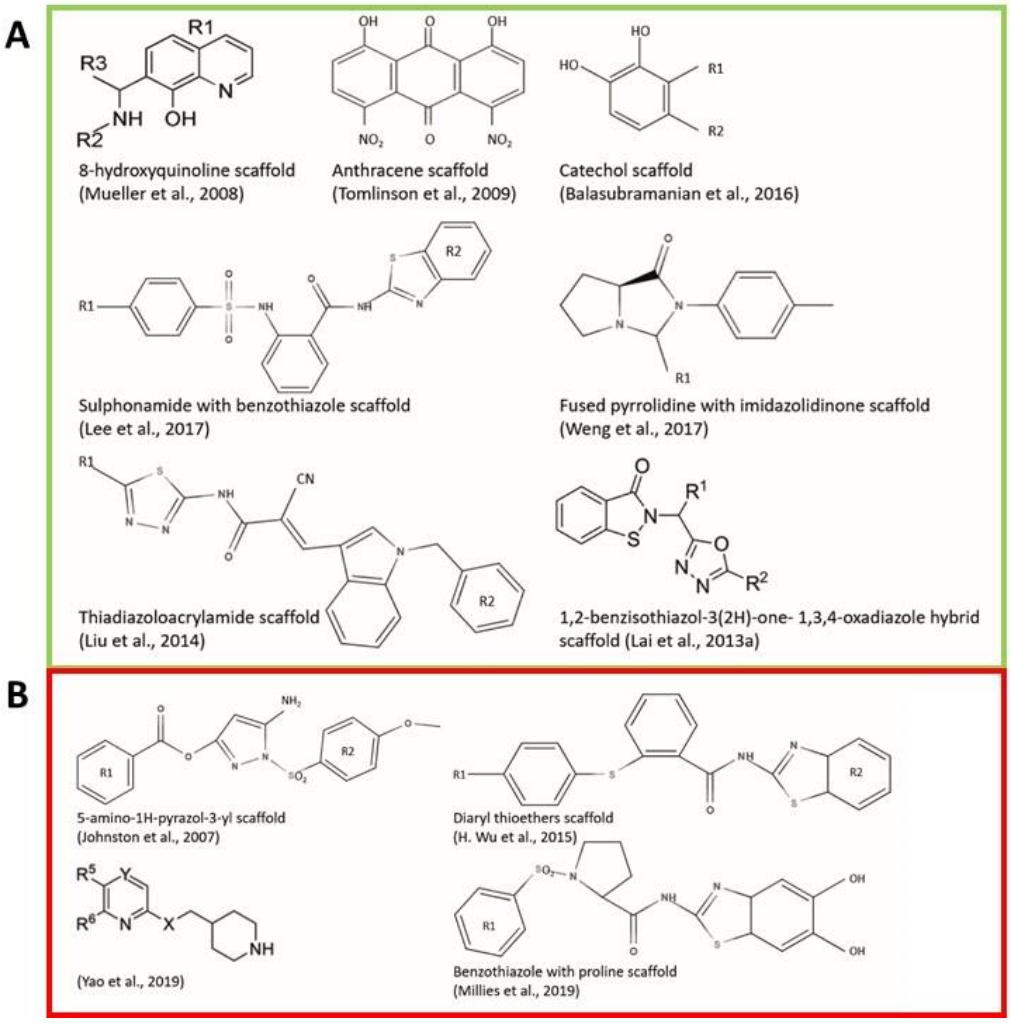


**Figure 1.16. Chemical scaffolds of the inhibitors from the compound screening library.** (A) Competitive and (B) allosteric inhibitors.

### 1.4.1.2 Peptidomimetics

Peptidomimetics inhibitors are substrate mimicking compounds that bind to the active site of viral protease. The first series of peptidomimetics inhibitors were designed by Leung and colleagues (Leung et al., 2001). The inhibitors were designed based on the substrate recognition sites of the viral polyprotein. They contain peptide sequence from P6 to P2' residues of NS3/4A and NS4B/5 cleavage site with a non-cleavable $\alpha$-keto amide bond at the P1-P1' junction.

They also improved the inhibition efficiency by replacing the P1'-P2' residues with an aldehyde warhead.

Subsequent studies aim to identify new chemical groups by the modification of the N- and C-terminal of peptidomimetic inhibitors, to improve membrane permeability and inhibition efficiency for future drug development.

Yin and co-workers investigated the effect of C-terminal modifications, they discovered those peptide inhibitors with electrophilic warheads can improve the inhibitory effect on viral protease (Yin et al., 2006b). A follow-up study by the same group further analysed a series of tetra-peptidyl aldehyde inhibitors against dengue NS3 protease (Yin et al., 2006a). They observed that the $P_2$ side-chain interaction with the protease is the most important followed by $P_1$, $P_3$ and $P_4$. At the same time, they also show that the C-terminal aldehyde warhead, dipeptide, tripeptide, as well as uncharged P1 residue, could also be potent inhibitors. The same set of tetra-peptidyl aldehyde inhibitors was also tested on WNV protease (Knox et al., 2006). SAR analysis reveals that a residue capable of both π-stacking and hydrogen bonding is favoured in the S1 pocket, while a positively charged residue is preferred in the S2 pocket. In another study, Stoermer and colleagues synthesised and tested a series of tripeptidyl inhibitors with C-terminal aldehyde group and different N-terminal cap against WNV protease (Stoermer et al., 2008). Phenylacetyl-Lys-Lys-Arg-aldehyde is stable in serum, cell-permeable and displays antiviral activity $EC_{50}$ value of 1.6 μM. Motivated by the previous finding, Schuller and co-workers, tested another series of tripeptidyl inhibitors with C-terminal aldehyde group and different N-

terminal cap (Schuller et al., 2011). In contrast, Phenylacetyl-Lys-Arg-Arg-aldehyde was found to be the most potent against DENV, supporting previous findings that P2-arginine and P2 lysine are favoured for DENV2 and WNV respectively. Kang and colleagues also illustrated that while P3 residues can improve inhibition activity, acetyl-Lys-Arg-aldehyde is sufficient for high potency against WNV and ZIKV protease (Kang et al., 2013; Li et al., 2017a). The crystal structures of ZIKV in complex with acetyl-Lys-Arg-aldehyde was also solved (Li et al., 2017a).

Instead of using a C-terminal aldehyde warhead, studies were also carried out using boronic acid at the C-terminal (Lei et al., 2016; Nitsche et al., 2017). The crystal structures of both ZIKV and WNV protease in complex with the dipeptidyl boronic acid inhibitors had been solved (Lei et al., 2016; Nitsche et al., 2017). However, although there are high inhibitory effects in a biochemical assay, the inhibitors lack activity in a cell-based assay. This could be attributed to the high polarity of both the P1-P2 residues as well as the boronic acid moiety.

With regards to N-terminal modification, Steuer and colleagues tested a series of inhibitors with N-terminal styryl derivatives coupled to an $\alpha$-ketoamide (Steuer et al., 2011). However, this series of inhibitors only displayed modest inhibition to DENV protease. Another study conducted by Klein group explored a series of retro-peptides coupled with different N-terminal caps, Cap-Arg-Lys-Nle (Nitsche et al., 2012). Retro tripeptide hybrids were found to display stronger inhibitory activity. Subsequently, the group retained the tripeptide sequence and explore rhodanines or thiazolidinediones derivatives as N-

terminal capping group (Nitsche et al., 2013). Thiazolidinedione-based peptide hybrids have the highest inhibitory effects against DENV protease while rhodanine-capped peptide hybrids are more potent in cell-based assay due to their high cellular permeability ability. Subsequently, the group optimised C-terminal residues and identified phenylglycine as having improved potency as compared to norleucine (Behnam et al., 2014). Afterwards, Cap-Arg-Lys-Phg was used as a backbone for other independent optimisation experiments. Next, the group further tested and optimised other thiazolidinedione-based peptide hybrids, Thiazolidinedione-cap-Arg-Lys-Phg, and identified numerous inhibitors with high potency against both DENV and WNV proteases (Bastos Lima et al., 2015). The group also tried using and optimising benzoyl derivatives instead of thiazolidinediones derivatives as the N-terminal capping group. One study replaced the arginine residues in Cap-Arg-Lys-Phg with phenylalanine analogues coupled with different benzoyl derivatives as N-terminal capping group (Weigel et al., 2015). Another study optimised phenylglycine residues of cap-Arg-Lys-Phg with phenylglycine derivatives coupled with different N-terminal benzoyl derivatives (Behnam et al., 2015). Several of the protease inhibitors in the series reduced DENV and WNV replication in cell-based assays, with compound 104 having the lowest $EC_{50}$ value of 3.4 µM against DENV infection. Recently, to enhance the cellular permeability, the group developed a new series of non-peptidic inhibitors while retaining the phenylglycine element (Kuhl et al., 2020). The compounds have high potency and selectivity with low cytotoxicity. Kouretova and colleagues also investigate the inhibitory effects of P1' residues in the presence of the N-terminal capping group (Kouretova et al., 2017).

Although some of the inhibitors displayed high inhibitory effects for both WNV and DENV in biochemical assays, the inhibitors lack activity in cell-based assays. Using the same inhibitors, Phoo and co-authors reported three co-crystal structures using ZIKV protease (Phoo et al., 2018). The structures revealed that the residues in S1-S3 pockets involved in the interaction with the basic residues appears to be relatively conserved. On the other hand, the N terminal cap moieties can adopt different conformations, highlighting the possibility of introducing modification to improve the inhibitors' functionality. Furthermore, uncleavable P1' residues can contribute to improved inhibition.

Other than modifying the two termini, cyclization of the peptide inhibitors was also explored. The optimisation of conotoxin, MrIA, generated a cyclic peptide inhibitor with a $K_i$ value of 2.2 μM against DENV protease (Xu et al., 2012). HTS of organic macrocyclic peptidomimetic compounds was carried out by Takagi and colleagues (Takagi et al., 2017). Their findings show that optimising the position of arginine and aromatic residues, can lead to an improvement in inhibition in cell-based assays. Furthermore, by replacing the amide bond at the P1-P1' site with an amino methylene moiety, it stabilized the cyclic peptides against hydrolysis by NS2B-NS3 protease. Allosteric, unnatural macrocyclic peptides were also identified using display screening and were shown to display sub-micromolar inhibition efficiency against ZIKV (Nitsche et al., 2019).

#### 1.4.1.3 Structure-activity relationship (SAR) studies

Although, both molecular docking and X-ray crystallography are used in SAR studies. This section will only be focused on SAR studies by X-ray crystallography. The first NS3 protease-inhibitor co-crystal structure was solved by Erbel and colleagues using a peptidomimetics inhibitor, Benzoyl-Nle-Lys-Arg-Arg-H (Erbel et al., 2006). Since then, other co-crystal structures were also solved (**Table 1.3**). By comparing the published protease-inhibitor co-crystal structures, some key findings can be observed. Firstly, the peptidomimetics inhibitors typically adopt the horseshoe-like conformation. Secondly, there is a low RMSDs value between the various co-crystal structures of the same virus, highlighting that the protease conformation remains the same regardless of the types of inhibitors bound. Next, the residues in S1-S3 pockets involved in the interaction with the inhibitors also appear to be relatively conserved. Furthermore, the S1 pocket can allow different residues to bind, ranging from small fragment inhibitors to bulky aromatic groups. Lastly, different P4 moieties can adopt different conformations, highlighting the possibility of modifying the P4 moieties to improve the inhibitors' functionality.

**Table 1.3. Published Protease-Inhibitor Co-crystal Structure**

| Virus | PBD Code | Ligand | References |
|---|---|---|---|
| WNV | 2FP7 | Benzoyl-Nle-Lys-Arg-Arg-H | (Erbel et al., 2006) |
| | 2IJO | BPTI | (Aleshin et al., 2007) |
| | 3E9O | 2-napthoyl-Lys-Lys-Arg-H | (Robin et al., 2009) |
| | 2YOL | 3,4-dichlorophenylacetyl-Lys-Lys-GCMA | (Hammamy et al., 2013) |
| | 5IDK | Benzoyl-(4-$CH_2NH_2$)-Phe-Arg-H | (Nitsche et al., 2017) |
| DENV | 3U1I | Benzoyl-Nle-Lys-Arg-Arg-H | (Noble et al., 2012) |
| | 3U1J | BPTI | |
| | 4M9T | DTNB | (Yildiz et al., 2013) |
| | 6MO0 | Compound 2 | (Yao et al., 2019) |
| | 6MO1 | Compound 8 | |
| | 6MO2 | Compound 9 | |
| ZIKV | 5LCO | Borate dipeptide inhibitor | (Lei et al., 2016) |
| | 5GPI | KKGE reverse peptide | (Zhang et al., 2016) |
| | 5H4I | Benzimidazole-1-ylmethanol | |
| | 5H6V | Acyl-Lys-Arg-H | (Li et al., 2017a) |
| | 5YOD | 5-amino-1-((4-methoxyphenyl)sulfonyl) -1H-pyrazol-3-yl benzoate | (Li et al., 2018d) |
| | 5YOF | Acyl-Lys-Arg-H | |
| | 5ZMQ | Phenylacetyl-Lys-Lys-Arg-COOH | (Phoo et al., 2018) |
| | 5ZMS | 4-guanidinomethyl-phenylacetyl-Lys-Lys-Arg-H | |
| | 5ZOB | 4-guanidinomethyl-phenylacetyl-Arg-Arg-Arg-4-amidinobenzylamide | |

### 1.4.2 NS3 Helicase Inhibitors

For NS3 helicase, 2 main enzymatic activities can be targeted, ATPase activity and RNA unwinding activity. However, based on the structural study of ATP binding to NS3, it was observed that there is a lack of specific amino acid interaction with the ATP, making it hard to design inhibitors that target the ATPase active site. Furthermore, it was observed that the RNA binding pocket of the NS3 helicase is shallow (Lim et al., 2013b; Luo et al., 2008a). Another challenge of NS3 helicase inhibitors will be to ensure that the specificity of the inhibitors, as many host helicases also belong to the SF2 superfamily (Lim et al., 2013b). To address these challenges, two novel binding sites were identified in ZIKV helicase using direct fragment-based screening by X-ray crystallography (FBS-X) (Munawar et al., 2018). The first site is at the interface between NS3-NS5 interaction while the second interface is at the interdomain hinge region that provides conformational flexibility for enzymatic activity.

Similar strategies such as *in silico* docking and HTS were also employed to identify potential antiviral candidates against NS3 helicase.

From *in silico* docking study, ivermectin was found to inhibit NS3 helicase unwinding activity of Dengue, West Nile and Yellow Fever virus at sub-micromolar range (Lim et al., 2013b; Mastrangelo et al., 2012). Another docking study also identified epigallocatechin-3-gallate, a green tea polyphenol, which interacts with protein residues at both the ATPase and RNA binding site of ZIKV NS3 helicase (Kumar et al., 2020). In vitro ATPase assay also revealed that the inhibitor has an inhibitory potency at the nanomolar range.

HTS using both cell-based assay and biochemical assay also identified small molecules that target NS3 helicase. A novel small compound inhibitor, ST-610, showed marginal activity against Dengue NS3 helicase unwinding activity and only resulted in a lesser than 10-fold decrease in virus load in a mouse model (Byrd et al., 2013; Lim et al., 2013b). Suramin act as a non-competitive inhibitor and inhibit DENV NS3 helicase activity with a $K_i$ value of 0.75 ± 0.03 μM (Basavannacharya and Vasudevan, 2014). While most groups utilised high-throughput unwinding assay to identify potential inhibitors against NS3 helicase, Sweeney and colleagues developed a high-throughput ATPase assay and identified two classes of inhibitors, benzothiazole and pyrrolone derivatives, which target DENV and WNV (Sweeney et al., 2015). The pyrrolone inhibitors are also specific against DENV and not HCV.

### 1.4.4 NS4B Inhibitors

Most NS4B inhibitors are identified via cell-based screening experiments. Using a replicon-based HTS assay, Patkar and colleagues identified two compounds that inhibit YFV replication from a library of 34000 compounds (Patkar et al., 2009). The inhibitors, CCG-4088 and CCG-3394, have $EC_{50}$ of 0.4 μM and 1.48 μM respectively and were suggested to act on Lysine128 of NS4B. Similarly using a replicon system, Shi's group screened 1.8 million compounds library and identified aminothiazole NITD-618 that specifically inhibits only the four dengue serotypes, with an $EC_{50}$ of 1.0 μM, but not other related flaviviruses or positive-sense RNA viruses (Xie et al., 2011). Escape mutants were mapped to have P104L mutation, suggesting that NITD-618 acts via preventing NS3-NS4B

interaction. HTS from numerous groups also identified P104 as a hotspot for escape mutants with their NS4B inhibitors (Hernandez-Morales et al., 2017; van Cleef et al., 2013). Other residues targeted includes F164 by inhibitor SDM25N and T108 by inhibitor JNJ-1A (Hernandez-Morales et al., 2017; van Cleef et al., 2013).

For the first time, using an improved dual replicon screening, Shi's group also identified spiropyrazolopyridone compound-14a that is capable of inhibiting DENV-2 and DENV-3 both in vitro and in vivo (Wang et al., 2015; Zou et al., 2015a). After the success of NS4B inhibitor compound 14a in preclinical testing, the group seeks to improve potency against the other serotypes. Unfortunately, despite guided modifications, the Compound 15 (JMX0254) is still not potent against DENV-4 and exhibited $EC_{50}$ of 0.78, 0.16 and 0.035 μM against DENV-1 to DENV-3 respectively (Xu et al., 2019a). Finally, a pan serotype inhibitor NITD-688 was identified to show high potency against all four dengue serotypes with favourable pharmacokinetics and efficacy in both rats and dogs (Moquin et al., 2021). Similarly, Neyts' group also identified another pan serotype inhibitor, JNJ-A07, that block the interaction between NS3 and NS4B, demonstrating strong potency in the DENV-infected mouse model (Kaptein et al., 2021). A first-in-human phase 1 clinical study was completed, the compound demonstrated antiviral activity and was well-tolerated in humans. Currently, phase 2a clinical trials are ongoing in Singapore and New York (ClinicalTrials.gov, 2020, 2021).

A safe and effective NS4B inhibitor against YFV-infected hamsters were also successfully developed (Guo et al., 2016).

### 1.4.4 NS5 Methyltransferase Inhibitors

Due to the high homology of flavivirus MTase to the host, targeting the S-adenosine-L-methionine binding site will be challenging. However, a flavivirus MTase unique pocket, next to the SAM binding site, was identified from a structural study (Dong et al., 2010). Subsequently, numerous compounds were developed to target this pocket (Chen et al., 2013; Lim et al., 2011; Vernekar et al., 2015). Although there are improvements in selectivity towards flavivirus MTase, no successful lead compound with high potency was identified. Nevertheless, this unique pocket remains a potential target for Mtase inhibitors.

Hence, to identify new target sites as well as potential lead compounds, FBS-X were also conducted against DENV MTase (Coutard et al., 2014). From the study, five fragments exhibited slightly inhibitory activity against DENV Mtase. Three novel binding sites were also revealed. To improve the inhibitory activities of the fragments, the group proceeded to link the fragments together (Benmansour et al., 2017). Despite, the conjugated fragments demonstrating a 10-100-fold improvement in inhibition of the 2'-O MTase, the potency was still not ideal.

Alternatively, Geiss and colleagues seek to target the GTP binding site and the guanylyltransferase activity of NS5 (Geiss et al., 2011). HTS identified numerous hits with three compounds having $IC_{50}$ of less than 10 μM against guanylation activity. Virtual HTS were also performed on 5 million compounds (Podvinec et al., 2010). Of which, only four exhibited $IC_{50}$ values of less than 10 μM in in-vitro assays.

### 1.4.5 NS5 RNA dependent RNA polymerase Inhibitors

The NS5 RdRp is an attractive drug target as the RdRp domain is absent in the host cell, thus enabling the development of antiviral with low toxicity. Furthermore, by comparing the crystal structures of the different flavivirus, it reveals similar architecture among the RdRp, suggesting the possibility of developing compound with board activity against the flavivirus (Lu and Gong, 2013; Malet et al., 2007; Wang et al., 2017; Zhao et al., 2017). There are 2 main classes of RdRp inhibitors, nucleotide analogue inhibitors (NIs) and non-nucleoside inhibitors (NNIs).

NIs, in their corresponding triphosphate state, works by competing with substate NTPs and terminate elongation. (Lim et al., 2013b). There are several advantages to using NIs. Firstly, as the polymerase active site is conserved, there is a high barrier to emerging resistance. Secondly, it can have pan-flaviviral inhibitors. Next, there could be cell type-specific activity, depending on the enzymes present in the cell to convert it into the triphosphate form. However, the toxicity of NIs is unpredictable as evident in the drug NITD-008 (Lim et al., 2013b). Only Balapiravir managed to enter a clinical trial, however, it did not improve the clinical outcomes in patients despite a low EC50 value from the in-vitro study (Lim et al., 2013b; Low et al., 2017; Nguyen et al., 2013).

NNIs works by binding to the polymerase and blocking the conformational changes needed for its activity. One of the major drawbacks of using NNIs, is the potential for mutation near the binding site, giving rise to resistance virus.

Hence, a good understanding of the mechanism and binding interaction of the NNIs to the polymerase is essential (Lim et al., 2013b).

Using the FBS-X approach, Noble and colleagues identified a conserved, novel site that is located between the thumb and palm subdomain of the RdRp and the priming loop (Noble et al., 2016). Subsequently, the group improved the potency of the fragment hits to generate a potent inhibitor with $EC_{50}$ of 1.8 to 2.3 μM against the four DENV serotypes (Yokokawa et al., 2016). This novel site was later termed as the 'N pocket'. Mechanism study shows that the inhibitors targeting the N pocket were shown to primarily act by inhibiting the de novo initiation polymerase activity (Lim et al., 2016). The inhibitors were modified and improved to target ZIKV RdRp (Gharbi-Ayachi et al., 2020). Structural comparison between DENV and Zika RdRp revealed that the N pocket of ZIKV RdRp has a smaller volume, thus only the core scaffold, consisting of the thiophene and phenyl rings, from the DENV inhibitor were retained (Gharbi-Ayachi et al., 2020).

From the HTS screening of 16,240 fragments, Shimizu and colleagues identified a potent compound, RK-0404678, having $EC_{50}$ of around 6.0 μM (Shimizu et al., 2019). A further structural study revealed that the compound binds to two unique conserved binding sites, within the thumb domain and the RNA tunnel (Shimizu et al., 2019). Another class of inhibitor, pyridobenzothiazole inhibitor, was also shown to bind to two unique sites, RNA tunnel and cavity B (Cannalire et al., 2020; Tarantino et al., 2016).

**Table 1.4. Published RdRp-Inhibitor Co-crystal Structure**

| Virus | PBD Code | Ligand | References |
|---|---|---|---|
| DENV | 5F3T | JF-31-MG46 | (Noble et al., 2016) |
| | 5F3Z | PC-79-SH52 | |
| | 5F41 | FD-83-KI26 | |
| | 5HMW | Compound 5 | (Yokokawa et al., 2016) |
| | 5HMX | Compound 10 | |
| | 5HMY | Compound 15 | |
| | 5hMZ | Compound 23 | |
| | 5HN0 | Compound 4 | |
| | 5I3P | Compound 27 | (Lim et al., 2016) |
| | 5I3Q | Compound 23 | |
| | 5K5M | Compound 27 | |
| | 5JJS | Compound 27 | |
| | 5JJR | Compound 29 | |
| | 5IQ6 | HeE1-2Tyr | (Tarantino et al., 2016) |
| | 6IZX | RK-0404678 | (Shimizu et al., 2019) |
| | 6IZZ | RK-0404678 | |
| ZIKV | 6LD2 | Compound 7 | (Gharbi-Ayachi et al., 2020) |
| | 6LD3 | Compound 13 | |
| | 6LD4 | Compound 14 | |
| | 6LD5 | Compound 15 | |

### 1.4.6 Drug Repurposing Clinical Studies

Other than the dengue-specific NS4B inhibitor by Johnson & Johnson, clinical studies were also carried out on other antiviral drugs for repurposing (Low et al., 2017; Wilder-Smith et al., 2019). These drugs include Balapiravir, NS5 nucleoside inhibitor for HCV (Nguyen et al., 2013); Chloroquine, an antimalarial drug to prevent virus entry (Tricou et al., 2010); Celgosivir, an inhibitor of host α-glucosidase to induce viral protein misfolding (Low et al., 2014); Lovastatin, cholesterol synthesis inhibitor to prevent the formation of the replication organelles (Whitehorn et al., 2016) and Ivermectin, antiparasitic drugs that can target NS3 helicase activity (Suputtamongkol et al., 2021). While, these drugs were generally well-tolerated, but they do not reduce viraemia.

## 1.5 Scope of the thesis

During the last decade, *flavivirus* has come into the spotlight due to the increasing frequency and larger magnitude of outbreaks. To exacerbate the situation, globalisation and climate change will further accelerate the geographical expansion of Aedes mosquito vectors, exposing more people to *flavivirus* infection (Ebi and Nealon, 2016; Lee et al., 2013; Liu-Helmersson et al., 2016; Liu et al., 2019).

To date, there are only clinically approved vaccines against YFV, JEV and TBEV and a sub-optimally vaccine against DENV (Collins and Metz, 2017; Scherwitzl et al., 2017). Currently, there is a lack of effective antiviral treatment for *flavivirus* infection, patients can only rely on supportive care and symptomatic treatment.

*Flavivirus*' replication occurs on the virus-induced membrane-associated replication complex. The viral replication complex is made up of all seven of the viral NS proteins, viral RNA and host factors (Brand et al., 2017; Lescar et al., 2018). Although many antiviral inhibitors were identified to target these individual NS proteins, with NS4B inhibitors showing promising results in phase 1 clinical trial, none of these inhibitors has yet been approved as a direct-acting antiviral inhibitor against the *flavivirus* (Kaptein et al., 2021; Lim et al., 2013b; Low et al., 2017; Moquin et al., 2021). Hence, in this study, we will employ a variety of techniques to further characterise two of the viral drug-target, NS3 and NS5, as well as the whole replication complex to target the different stages of the flavivirus' lifecycle.

Firstly, there are only limited numbers of NS3 protease-inhibitor complex structures available, with most of them focusing on linear peptidomimetics inhibitors. Hence, we aim to characterise NS3 protease with other novel inhibitor designs, to guide and optimise future inhibitors' design.

Secondly, while there are crystal structures of fragments inhibitors binding to the RdRp, the structural information of inhibitors binding to the RdRp remains limited. Hence, we aim to elucidate catalytically relevant polymerase ternary complexes to facilitate the design of the inhibitors. Furthermore, with the induced conformation changes of the RdRp upon RNA binding, other potential allosteric sites might also be formed and discovered.

Thirdly, although, numerous studies have characterised the respective NS protein components of the RC, using both structural and functional approaches, as well as the protein-protein interactions between different NS proteins (Brand et al., 2017; Lescar et al., 2018; Tay and Vasudevan, 2018). Neither the details of viral RNA replication nor the dynamics of these proteins in the replication complex during the replication process have yet to be fully identified (Brand et al., 2017; Lescar et al., 2018; Tay and Vasudevan, 2018). Thus, we hypothesise that by understanding the whole *flavivirus* replication complex, it can provide unique insights and develop alternative approaches and target sites to manage the diseases caused by the *flavivirus*.

The specific aims of the thesis are:

1. Structural characterisation of NS3 protease in complex with (a) small molecule inhibitors and (b) cyclic peptidomimetics inhibitors to understand the structural basis of NS3 protease in recognising different substrates for optimisation of inhibitors design.
2. Structural characterisation of NS5 in complex with the RNA substrate to understand the mechanism of RNA synthesis.
3. Characterisation of the minimal replication complex to understand the dynamic interaction between the NS proteins and the precise molecular mechanism of various stages of viral replication.

# Chapter 2: Materials and Methods

## 2.1 Plasmids, inhibitors and oligonucleotides

### 2.1.1 Plasmids, molecular cloning and mutagenesis

The ZIKV bivalent protease plasmid, bZiPro, was obtained from Kang Lab, Experimental Drug Development Centre (EDDC), A*STAR. The DENV-4 bivalent protease, bD4Pro construct plasmid was synthesized by Biobasic Asia Pacific Pte Ltd.

The Dengue-4 RdRp, Dengue-3 NS5, U1A and human STAT2 plasmids were subcloned by Nanyang Technological University Protein Production Platform (NTU-PPP).

The priming loop deletion mutants of DENV RdRp were generated in the lab using the NEB Q5 site-directed mutagenesis kit (New England Biolabs, United States) according to the manufacturer's protocol. The transformed colonies were sub-cultured overnight in Luria Broth (LB) with appropriate antibiotics at 37 °C. The plasmids were then purified using AxyPrep Plasmid Miniprep Kit (Axygen) and sent for verification and Sanger sequencing (Bio Basic Asia Pacific Pte Ltd., Singapore).

The NS5-U1A fusion protein was generated using the megaprimer PCR cloning methodology (Barik, 2002). The pair of megaprimers were generated by amplifying the U1A gene with flanking sequence from the NS5 plasmid using the KOD FX NEO PCR kit (Toyobo, Japan) according to the manufacturer's protocol. Subsequently, the megaprimers were purified using the Monarch® PCR & DNA

Cleanup Kit (New England Biolabs, United States) according to the manufacturer's protocol. The megaprimers were used to insert the U1A gene into the NS5 plasmid using the KOD FX NEO PCR kit (Toyobo, Japan). The PCR reaction was subjected to DpnI digestion and transformed into NEB® 5-alpha Competent E. coli (New England Biolabs, United States). Then, the plasmids were purified from transformed bacterial colonies using AxyPrep Plasmid Miniprep Kit (Axygen, United States) and sent for verification and Sanger sequencing (Bio Basic Asia Pacific Pte Ltd., Singapore).

The ZIKV MR766 Infectious Clone (IC) plasmid was received from Evans Lab, Icahn School of Medicine at Mount Sinai, USA. Codon-optimised HisTev-eZiNS3-StrepHisSumo-NS5 plasmid was synthesised by Biobasic Asia Pacific Pte Ltd. The various protein constructs used in the bacterial reporter assay were generated using the megaprimer PCR cloning methodology (Barik, 2002). The pair of megaprimers were generated by using the ZIKV MR766 IC plasmid to amplify the respective NS protein genes with flanking sequence from the HisTev-eZiNS3-StrepHisSumo-NS5 plasmid using the KOD FX NEO PCR kit (Toyobo, Japan) according to the manufacturer's protocol. The primers used were summarized in **Table 2.2**. Subsequently, the megaprimers were purified using the Monarch® PCR & DNA Cleanup Kit (New England Biolabs, United States) according to the manufacturer's protocol. The megaprimers were used to insert the NS genes into the plasmid using the KOD FX NEO PCR kit (Toyobo, Japan). The PCR reaction was subjected to DpnI digestion and transformed into NEB® 5-alpha Competent E. coli (New England Biolabs, United States). Then, the plasmids were purified from transformed bacterial colonies using AxyPrep Plasmid

Miniprep Kit (Axygen, United States) and sent for verification and Sanger sequencing (Bio Basic Asia Pacific Pte Ltd., Singapore).

All the plasmids used in the experiments are summarised in **Table 2.1** and **Figure 2.1**.

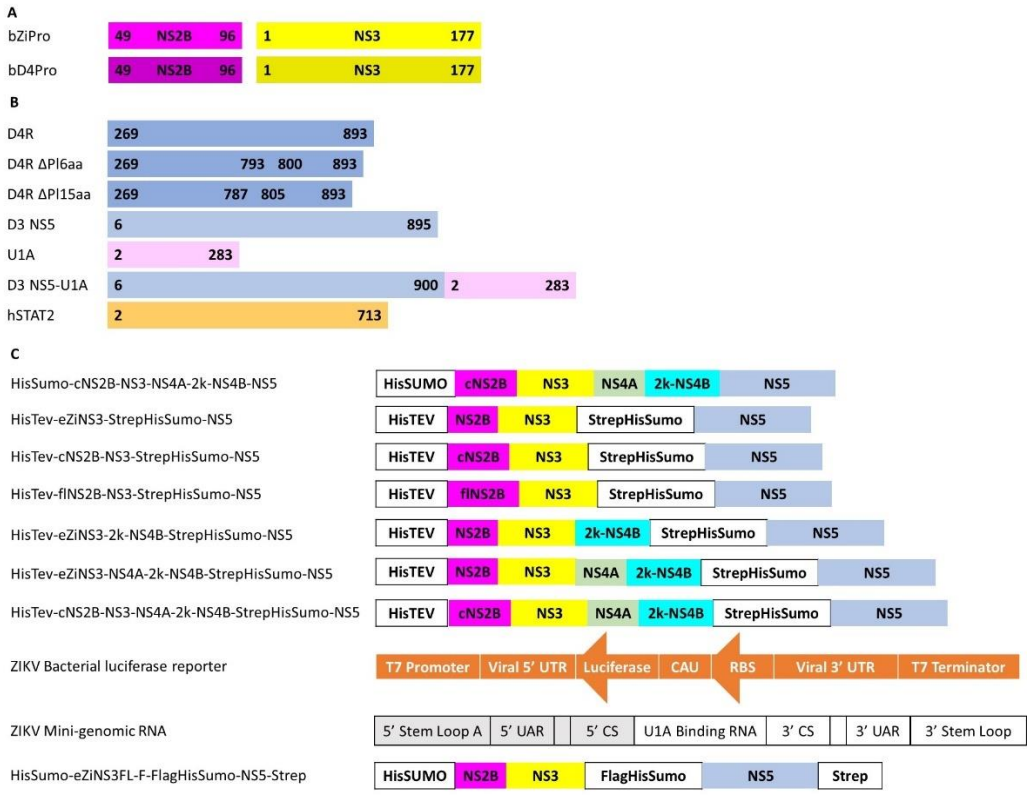


**Figure 2.1. The graphical representation of the protein constructs used in the thesis.** (**A**) The protease construct used in Chapter 3. Both bZiPro and bD4Pro are expressed as bivalent constructs consisting of NS2B (residue 49 – 96) and NS3 (residue 1 – 177). (**B**) The protein constructs used in Chapter 4. The residue numbers are indicted. All the D4R constructs consist of residue 269 to 893. Residue 794 – 799 were removed in ΔPl6aa construct while residue 788 – 804 were replaced by GG in the ΔPl15aa construct. The D3 NS5-U1A construct involved a direct fusion between D3 NS5 (residue 6 – 900) and U1A (residue 2 – 283). (**C**) The protein constructs used in Chapter 5. The various polyprotein designs are shown. The reporter plasmid encodes the ribosome binding site (RBS), start codon and luciferase gene in a reverse complementary direction that is flanked by the viral UTR. The mini-genomic RNA consists of a U1A protein recognition sequence flanked by ZIKV 5' and 3' UTR.

### 2.1.2 Inhibitors

The fragment compound library used in **Chapter 3.1** was received from Dr Congbao Kang Lab, EDDC, A*STAR. Cyclic peptidomimetics inhibitors generated via click reaction used in **Chapter 3.2.1** were received from Dr Christoph Nitsche Lab at Australian National University (ANU). Cyclic peptidomimetics inhibitors used in **Chapter 3.2.2** were received from Prof Torsten Steinmetzer Lab from Philipps University (PU).

### 2.1.3 Oligonucleotides

All the DNA and RNA oligonucleotides are synthesis by IDT (Integrated DNA Technologies). The list of DNA primers and RNA oligonucleotides used were summarized in **Table 2.2** and **Table 2.3** respectively.

**Table 2.1. The plasmids used in experiments.** The residues number of the protein construct are stated in parenthesis.

| No. | Constructs (aa) | Origin | Purpose |
|---|---|---|---|
| 1 | bZiPro<br>NS2B (49 – 96), NS3 (1 – 177) | Kang Lab, EDDC, A*STAR | Protease Inhibition Assay, Co-crystal structure |
| 2 | bD4Pro<br>NS2B (49 – 96), NS3 (1- 177) | Biobasic | Protease Inhibition Assay |
| 3 | D4 RdRp (269 – 893) | NTU PPP | Mutagenesis, Crystallization Screening, Polymerase Assay |
| 4 | D4 RdRp Priming Loop 6aa Mutant | From Cloning | Crystallization Screening, Polymerase Assay |
| 5 | D4 RdRp Priming Loop 15aa Mutant | From Cloning | Crystallization Screening, Polymerase Assay |
| 6 | D3 NS5 (6 – 895) | NTU PPP | Mutagenesis, Polymerase Assay |
| 7 | U1A (2 – 283) | NTU PPP | Mutagenesis |
| 8 | D3 NS5-U1A | From Cloning | Complex Formation, Polymerase Assay |
| 9 | hSTAT2 (2 – 713) | NTU PPP | Complex Formation |
| 10 | ZIKV MR766 Infectious Clone (IC) | Matthew Evans | Mutagenesis |
| 11 | HisSumo-cNS2B-NS3-NS4A-2k-NS4B-NS5 | NTU PPP | Bacterial luciferase reporter assay |
| 12 | HisTev-eZiNS3-StrepHisSumo-NS5 | Biobasic | Mutagenesis, Bacterial luciferase reporter assay |
| 13 | HisTev-cNS2B-NS3-StrepHisSumo-NS5 | From Cloning | Mutagenesis, Bacterial luciferase reporter assay |
| 14 | HisTev-cNS2B-NS3-StrepHisSumo-NS5 GNN Mutant | From Cloning | Bacterial luciferase reporter assay |
| 15 | HisTev-flNS2B-NS3-StrepHisSumo-NS5 | From Cloning | Bacterial luciferase reporter assay |
| 16 | HisTev-eZiNS3-2k-NS4B-StrepHisSumo-NS5 | From Cloning | Bacterial luciferase reporter assay |
| 17 | HisTev-eZiNS3-NS4A-2k-NS4B-StrepHisSumo-NS5 | From Cloning | Bacterial luciferase reporter assay |
| 18 | HisTev-cNS2B-NS3-NS4A-2k-NS4B-StrepHisSumo-NS5 | From Cloning | Bacterial luciferase reporter assay |
| 19 | ZIKV Bacterial luciferase reporter | Biobasic | Bacterial luciferase reporter assay |
| 20 | ZIKV Mini-genomic RNA | Biobasic | Complex Formation |
| 21 | HisSumo-eZiNS3FL-F-FlagHisSumo-NS5-Strep | From Cloning | Complex Formation |

**Table 2.2. The primers used in mutagenesis and cloning**

| Mutation | Target | Orientation | Sequence |
|---|---|---|---|
| Priming Loop 6aa Deletion | D4 RdRp | Forward | CATCACCAGTGGATGACGACCG |
| | | Reverse | CGTGCGGGAGGTCGGGAA |
| Priming Loop 15aa Deletion | D4 RdRp | Forward | GGCACGACCGAAGATATGCTGAAAG |
| | | Reverse | GCCCCATTCCGTCGGCACTGC |
| U1A Megaprimer | U1A | Forward | ATGAAGAGATTCAGGAAGGAAGAGGAGTCGGAGGGAGCCATTTGGATGGCAGTTCCCGAG |
| | | Reverse | GAATTCGGATCCGTATCCACCTTTACTGCTATTTCATCTTGGCAATGATATCTGAGTCGG |
| HisTev-cNS2B-ZiNS3-StrepHisSumo-NS5 GNN Mutant | HisTev-cNS2B-ZiNS3-StrepHisSumo-NS5 | Forward | AGTGTCCGGGAACAACTGCGTGGTGA |
| | | Reverse | GCCATCCTCTTGAGCCGATC |
| C-terminal NS2B Megaprimer | ZIKV MR766 IC | Forward | GTGGAGGAGGATGGCCCACCCATGAGAGAAATCATACTCAAGGTGGTCCTGATGGCCATC |
| | | Reverse | CCACAGGGCCCCAGACCGTTTCCCAGTCTTCACATACACATACCACGCTCCTGCAGCAAA |
| NS2B Megaprimer | ZIKV MR766 IC | Forward | ACAGAGAACCTGTACTTCCAGAGCATGGGC AGCTGGCCCCCTAGTGAAGTTCTCACAGCC |
| | | Reverse | GGGGGCAGGCACATCCCACAGGGCCCCAGACCTTTTCCCAGTCTTCACATACACATACCA |
| 2k-NS4B Megaprimer | ZIKV MR766 IC | Forward | AGCTTCAAGGAGTTTGCCGCCGGCAAGCGGTCTCCCCAAGATAACCAGATGGCAATTATC |
| | | Reverse | GGGGTGGCTCCAAGCGCTGCCGGCTGCGCCACGTCTCTTAACCAGGCCAGCGTTTCTCGT |
| NS4A-2k-NS4B Megaprimer | ZIKV MR766 IC | Forward | AGCTTCAAGGAGTTTGCCGCCGGCAAGCGG GGAGCGGCTTTGGGAGTAATGGAGGCCCTG |
| | | Reverse | GGGGTGGCTCCAAGCGCTGCCGGCTGCGCCACGTCTCTTAACCAGGCCAGCGTTTCTCGT |
| HisSumo-eZiNS3FL-F-FlagHisSumo-NS5 | HisSUMO-eZiNS3-StrepHisSumo-NS5 | Forward | TACAAAGACGATGACGACAAGGGGTCTGGGCTCGTCCCC |
| | | Reverse | GTCAGCGCTGCCGGCTGCGAACCGCTTGCCGGCGGCAAA |

**Table 2.3. The RNA oligonucleotides used in the experiments.**

| RNA | Sequence |
|---|---|
| T2-4 | AUGGCC |
| T4-4 | CGAUGGCC |
| T4-6 | GCAUGGCGCC |
| T4-8 | GCAUGGGCGCCC |
| T31 | GGGAGAUGAAAGUCUCCAGGUCUCUCGGAAA |
| P8 | UGUUCCGA |
| T30-6 | GGGAGAUGAAAGUCUCCAGGUCUCGCUAGC |
| T8-11 Hairpin | UUUUUUUUUUAGGACCGCUC(FAM)GGCGGUCCUAA |
| T8-11 U1A Hairpin | UUUUUUUUUUAGGACCGCAUUGCACUCCGCGGUCCUAA |
| 19-19 Hairpin | UUUUUUUUUUAGGACCGCUC(FAM)GGCGGUCCUAAAAAAAAAAA |

## 2.2 Protein expression and purification

All the protein expression plasmids were transformed into Escherichia coli Rosetta T1R. An overnight starter culture was prepared by growing the transformants in LB medium, supplemented with appropriate antibiotics, at 37 °C for 18 hours. The overnight culture will be used to grow LB medium until $OD_{600}$ of 0.8-1.0 was reached. Subsequently, 1 mM Isopropyl β-D-1-thiogalactopyranoside (IPTG) was added to induce protein overexpression for 18 hours at 18 °C. Cells were harvested via centrifugation at 6000 rpm for 10 minutes at 4°C.

### 2.2.1 Protease expression and purification

The purification protocol for bZiPro was adapted from (Zhang et al., 2016). Cells were resuspended in resuspension buffer (1X phosphate-buffered saline (PBS), supplemented with 160 mM Sodium chloride (NaCl), 5 % glycerol and 5 mM β-Mercaptoethanol (β-ME)). The cells were lysed by sonication at 70 % intensity using a 5-sec on/off cycle for 5 minutes. Subsequently, the cells were subjected to another round of lysis via the homogenizer (GEA) at 900 - 1000 bar for 15 minutes. To remove the unbroken cells and cell debris, centrifugation of the lysate was carried out at 35,000 rpm for 1 hour at 4 °C. The supernatant was collected.

Ni NTA Beads 6FF beads (Bio Basic Asia Pacific Pte Ltd., Singapore) equilibrated with resuspension buffer was incubated with the supernatant for 1.5 hours at 4 °C with slight agitation. The beads were then washed with 10 column volume (CV) of resuspension buffer supplemented with 20 - 40 mM imidazole. Finally,

the protein of interest was eluted with 5 CV of resuspension buffer with 300 mM imidazole. The N-terminal Histidine affinity tag was cleaved by thrombin protease (GE Healthcare) and dialyzed overnight in the 1X PBS dialysis buffer as per manufacturer protocol. The cleaved His-tag was removed by flowing the dialyse through Ni-NTA agarose beads and the flow-through fraction was collected. The fractions were concentrated and purified using HiLoad 16/600 Superdex 75 pg (GE Healthcare) column with SEC150 buffer (25mM HEPES, pH 7.5, 150 mM NaCl, 2mM DTT, 5% glycerol). Fractions were pooled, concentrated using Amicon® Centrifugal Filter Units with 10 kDa molecular weight cut-off via centrifugation at 3500g. The purified proteins were aliquoted and flash-frozen with liquid nitrogen for storage.

The purification protocol for bD4Pro was similar as described above, with changes to using Tobacco Etch Virus (TEV) protease for affinity tag cleavage.

### 2.2.2 NS5, RdRp and hSTAT2 purification

The purification protocol for NS5 and RdRp was adapted from (Zhao et al., 2015c) Cells were resuspended in resuspension buffer, as previously described. The cells were lysed by sonication at 70 % intensity using a 5-sec on/off cycle for 5 minutes. Subsequently, the cells were subjected to another round of lysis via the homogenizer (GEA) at 900 - 1000 bar for 15 minutes. To remove the unbroken cells and cell debris, centrifugation of the lysate was carried out at 35,000 rpm for 1 hour at 4 °C. The supernatant was collected.

Ni NTA Beads 6FF beads (Bio Basic Asia Pacific Pte Ltd., Singapore) equilibrated with resuspension buffer was incubated with the supernatant for 1.5 hours at

4 °C with slight agitation. The beads were then washed with 10 column volume (CV) of resuspension buffer supplemented with 20 - 40 mM imidazole. Finally, the protein of interest was eluted with 5 CV of resuspension buffer with 300 mM imidazole. The Histidine affinity tag was removed by TEV protease and dialyzed overnight in the SEC300 buffer (25mM HEPES, pH 7.5, 300 mM NaCl, 2mM DTT, 5% glycerol) at 4 degrees Celsius. The cleaved His-tag was removed by passing through the dialyse through Ni-NTA agarose beads. Subsequently, the sample was concentrated and purified via using HiLoad 16/600 Superdex 200 pg (GE Healthcare) column with SEC300 buffer. The fractions were concentrated using Amicon® Centrifugal Filter Units with 50 kDa molecular weight cut-off via centrifugation at 3500g. The purified proteins were aliquoted and flash-frozen with liquid nitrogen for storage.

The purification protocol of RdRp priming loop mutants and NS5-U1A fusion protein followed the same approach as that for wild-type proteins. While for hSTAT2, the purification protocol was similar as described above, with changes to using SUMO Protease for affinity tag cleavage.

### 2.2.3 Fusion HisSumo-eZiNS3FL-F-FlagHisSumo-NS5-Strep purification

Cells were resuspended in a resuspension buffer, as previously described. The cells were lysed by sonication at 70 % intensity using a 5-sec on/off cycle for 5 minutes. Subsequently, the cells were subjected to another round of lysis via the homogenizer (GEA) at 900 - 1000 bar for 15 minutes. To remove the unbroken cells and cell debris, centrifugation of the lysate was carried out at 35,000 rpm for 1 hour at 4 °C. The supernatant was collected.

Ni NTA Beads 6FF beads (Bio Basic Asia Pacific Pte Ltd., Singapore) equilibrated with resuspension buffer was incubated with the supernatant for 1.5 hours at 4 °C with slight agitation. The beads were then washed with 10 column volume (CV) of resuspension buffer supplemented with 20 - 40 mM imidazole. Finally, the protein of interest was eluted with 5 CV of resuspension buffer with 300 mM imidazole. Next, the protein sample was subjected to the Strep-Tactin® XT column (IBA lifesciences, Germany) according to the manufacturer protocol. Subsequently, the sample was concentrated and purified via using HiLoad 16/600 Superdex 200 pg (GE Healthcare) column with SEC150 buffer. The fractions were concentrated using Amicon® Centrifugal Filter Units with 100 kDa molecular weight cut-off via centrifugation at 3500g. The purified proteins were aliquoted and flash-frozen with liquid nitrogen for storage.

### 2.3 Crystallization

#### 2.3.1 Protease-inhibitor co-crystallization and structural determination

The bZiPro and inhibitor compound were incubated on ice for 1 h at a molar ratio of 1:3 with a final protein concentration of 40 mg/mL. A hanging-drop vapour diffusion experiment was set up by mixing the protein mixture with an equal volume of the reservoir solution as stated in **Table 2.4** and incubated at 18 °C. The crystals formed after forty-eight hours and were cryoprotected using the reservoir solution supplemented with 20 % glycerol. The crystals were flash-freeze and stored in liquid nitrogen and shipped to various synchrotrons for data collection. The synchrotrons include MXII beamline at Australian Light Source (Melbourne, Australia), PSIII beamline at Swiss Light Source (SLS) Paul Scherrer

Institut, (Villigen Switzerland) and TPS05A beamline at the National Synchrotron Radiation Research Center (Hsinchu, Taiwan). Data processing were carried out using XDS data processing package (Kabsch, 2010; Wojdyla et al., 2018). Molecular replacement using the program PHASER MR, with the model (PDB code 5GPI), were performed to determine the solutions of the complex structures (McCoy, 2007; Vagin and Teplyakov, 2010; Zhang et al., 2016). PHENIX Xtriage was used to calculate the twin laws (k, h, -l) (Adams et al., 2010). The model was subjected to multiple rounds of manual rebuilding using Coot and refinement using the PHENIX refine and the calculated twin law (Afonine et al., 2012; Emsley and Cowtan, 2004). The final data collection and refinement statistics are reported in **Chapter 3**. The structures were deposited in the Protein Data Bank.

**Table 2.4. The crystallization reservoir conditions for bZiPro crystals formation.**

| Inhibitor | Crystallization Reservoir Conditions |
|---|---|
| Compound 6 and 16, Peptide 2C, Inhibitor 3 and 7 | 0.2 M Ammonium sulfate, 0.1 M Sodium acetate trihydrate pH 4.6, 30% Polyethylene glycol (PEG) 2000 |
| Peptide 1C, Inhibitor 1 and 8 | 0.2 M ammonium sulfate, 0.1 M sodium acetate trihydrate pH 4.6, 25% PEG 4000 |
| Inhibitor 9 and 14 | 2 M ammonium sulfate, 0.1 M sodium acetate trihydrate pH 4.6 |
| Inhibitor 15 | 2 M ammonium sulfate, 5 % propanol |

### 2.3.2 Dengue RdRp Pl mutant crystal screenings

The RdRp and RNA were incubated on ice for 1 h, at a molar ratio of 1:1.2 with a final protein concentration of 8 mg/mL. High throughput screenings of the crystallization conditions were set up using sitting drop vapour diffusion method

with crystallization kits, CrystalScreen, Index, GridScreen, Natrix, PEGIon Screen, and PEGRxScreen (Molecular Dimensions, United States). The screenings were set up on INTELLI-PLATE® 96 (Art Robbins Instruments, United States) using the Mosquito nanopipette dispenser (SPT Labtech, United States) to mix the protein-RNA solution with the crystallization conditions at a 1:1 ratio. The plates were incubated in the crystallization hotel (Formulatrix, United States) at 20 °C and the progress was monitored using Rock Imager (Formulatrix, United States).

### 2.4 Biochemical Assay

#### 2.4.1 Protease inhibition assay

The protease inhibition assay was adapted from (Phoo et al., 2016). bD4Pro and bZiPro at a final concentration of 3 nM were incubated with varying concentrations of inhibitor compounds in assay buffer containing 20 mM Tris pH 8.5, 10 % glycerol, 0.01 % Triton X-100 for 1 h at room temperature. The measurements were started by adding the Bz-nKRR-AMC peptide substrate (Peptide Institute Inc, Japan) at 10 μM and 50 μM for bZiPro and bD4Pro reactions respectively. The Synergy H1 Microplate Reader (BioTek) was used to measure the fluorescence readings at 1-minute intervals over 10 minutes with the excitation wavelength (λex) at 380 nm and emission wavelength (λem) at 460 nm. The assays were conducted as triplicates at 37 $^{o}$C. The inhibitors' concentrations were transformed into a logarithmic scale using the Transform function, Graph Pad Prism 8. Initial velocities were calculated from the fluorescent reading and normalized using Normalize function, GraphPad Prism 8. The normalization was performed referencing the initial velocities from the

reactions without enzyme as 0% and the reactions without inhibitors as 100%. IC50 values were calculated by plotting normalized initial velocities against log(concentrations) and non-linear regression curve fitting.

### 2.4.2 Polymerase elongation assay

For the elongation assay, the protein and RNA are mixed at 500 nM in assay buffer (25 mM HEPES pH 7.5, 0.01% Triton X-100, 2.5 mM TCEP, 2.5 mM $MgCl_2$, 2.5 mM $MnCl_2$, 1 mM of NTP and 0.4 unit/µL Murine RNAse Inhibitor (NEB)). The reactions were incubated at 30 °C for 1 hour. The reactions were quenched by mixing 1:1 with RNA loading dye. The RNAs are resolved using a 20% UREA Page, run 2h15min at 200V. The gel was stained with FluroRed Dye ($1^{st}$ Base, Singapore) as per the manufacturer's protocol and imaged using ChemiDoc™ MP Imaging System (Biorad. United States).

### 2.4.3 Bacterial negative-sense RNA synthesis luciferase reporter assay

The Escherichia coli BL21(DE3) Rosetta T1R cells were transformed with the reporter plasmid and/or the protein expression plasmids. An overnight starter culture was prepared by growing the transformants in LB medium supplemented with appropriate antibiotics at 37°C for 18 hours. The overnight culture will be used to grow LB medium until $OD_{600}$ of 0.8-1.0 was reached. The protein was subsequently induced at 37°C for 3 hours by the addition of 1mM IPTG. Next, the $OD_{600}$ were measured and converted to E.coli cell concentration ($OD_{600}$ of 1.0 = 8 x $10^8$ cells/ml). Subsequently, 5*$10^9$ numbers of cells were harvested per condition. Renilla luciferase assay was performed using Pierce® Renilla Luciferase Glow Assay Kit (Thermo Fisher Scientific, USA) with slight

modification to the manufacturer's protocol for cell lysis. The lysis step was modified to use 500 μl of 1X cell lysis buffer, followed by sonication at 30 % intensity using a 2-sec on/off cycle for 1 minute.

### 2.5 Protein-RNA complex screening by size-exclusion chromatography

#### 2.5.1 NS5-U1A fusion protein in complex with T8-11 U1A hairpin RNA and hSTAT2

The protocol was adapted from (Wang et al., 2020). The NS5-U1A, hSTAT2 and U1A hairpin RNA were incubated on ice for 1 hour in a 1:1:1.2 molar ratio. The mixture was then loaded onto Superdex 200 10/300 column (GE Healthcare) pre-equilibrated with buffer containing 25 mM Tris-HCl (pH 7.5), 175 mM NaCl, 2 mM $MgCl_2$, 5 mM DTT. The fractions were collected and analysed by SDS-PAGE. NS5-U1A and hSTAT2 protein samples were also loaded individually onto the column to serve as a reference for the complex formation.

#### 2.5.2 In-vitro protein-RNA complex reconstitution using ZIKV mini-genomic viral RNA.

The protein and ZIKV mini-genomic RNA were incubated on ice for 1 hour in a 1:1.2 molar ratio. The mixture was then loaded onto Superdex 200 10/300 column (GE Healthcare) pre-equilibrated with buffer containing 25mM HEPES (pH 7.4), 150 mM NaCl and 5mM DTT. The fractions containing the eluate were collected and analysed by SDS-PAGE. DENV-4 NS3, DENV-4 NS5 RdRp and ZIKV NS3-5 fusion protein samples as well as the ZIKV mini-genomic RNA were also loaded individually onto the column to serve as a reference for the complex formation.

# Chapter 3: Biochemical and structural characterisation of the substrate-binding site of *Flavivirus*' NS2B-NS3 protease

Flavivirus NS2B-NS3 protease is an attractive antiviral target due to its' essential role in viral polyproteins processing and maturation. Additionally, the NS2B-3 protease also contributes to evading host immune response by cleaving and inactivating host proteins. However, the progress towards successful drug candidates has been slowed, mainly due to the polarity and the depth of the protease active site (Lim et al., 2013b; Poulsen et al., 2014). Structural studies aim to solve these problems by gaining a deeper understanding of how the inhibitors bind to the protease's active site and to promote structure-based optimization of any potential inhibitors.

Recently, using the bivalent Zika protease construct (bZiPro), a reliable crystallization protocol to produce high diffracting crystals was established. Furthermore, the bZiPro have a preformed empty active site making it suitable for soaking as well as co-crystallisation to capture the protease-inhibitor complex structure. Several bZiPro-inhibitor structures were solved in recent years (Li et al., 2018d; Li et al., 2017a; Phoo et al., 2018; Zhang et al., 2016).

In this chapter, we aim to study the interaction between bZiPro with other molecules, it will further our understanding of the substrate-binding site of Zika protease for future drug development via SAR studies. Firstly, we identified twenty-two unique fragments that are capable of binding to ZIKV protease, the co-crystal structures of bZipro in complex with two of the fragments were also reported. Next, two series of cyclic peptidomimetics inhibitors were designed.

For the first series, the inhibitors reached sub-micromolar range inhibitory activity against ZIKV protease while the inhibitors in the second series managed to achieve nanomolar inhibitory activity against ZIKV protease and sub-micromolar range inhibitory activity against DENV and WNV protease. We also managed to capture the first crystal structure of the viral protease with a bound cyclic peptidomimetics inhibitor design.

### 3.1 Fragments screening and structural characterization of fragments molecule targeting Zika virus NS2B-NS3 protease

Although, there are advancements in the development of some small molecule compounds and peptidomimetics inhibitors as mentioned in **Chapter 1.3.1**. Those inhibitors still faced challenges dealing with poor druggability and pharmacokinetics parameters such as oral absorption and membrane permeability. Thus, other small molecules with different scaffolds design can be explored for their suitability in solving those challenges.

In this section, we seek to explore alternative compounds using the fragment-based drug design (FBDD) approach, which starts by finding small molecules that are capable of binding to the protein of interest. These identified fragments will subsequently be expanded or linked to produce leads with improved binding affinity and efficacy. Previously, a small fragment (EN300) was also found in the S1 pocket of the bZiPro as shown by the X-ray crystal structure (Zhang et al., 2016).

Firstly, to identify fragments that bind to the Zika protease, the HTS thermal shift assays were conducted by Kang's Lab. From a fragment library of 1685 fragments, twenty-two fragments were found to improve the stability of the eZiPro, enzymatic self-cleavage construct, by at least 0.6 °C (**Figure 3.1.1**). The identified hits were grouped into four unique clusters based on the type of the aromatic ring cores (**Figure 3.1.1**). The first group is made up of compounds with a 6-membered ring. The next group comprises of a 5-membered heterocyclic compound. And the last two groups comprise of 6-6 and 6-5 fused bicyclic structures respectively.

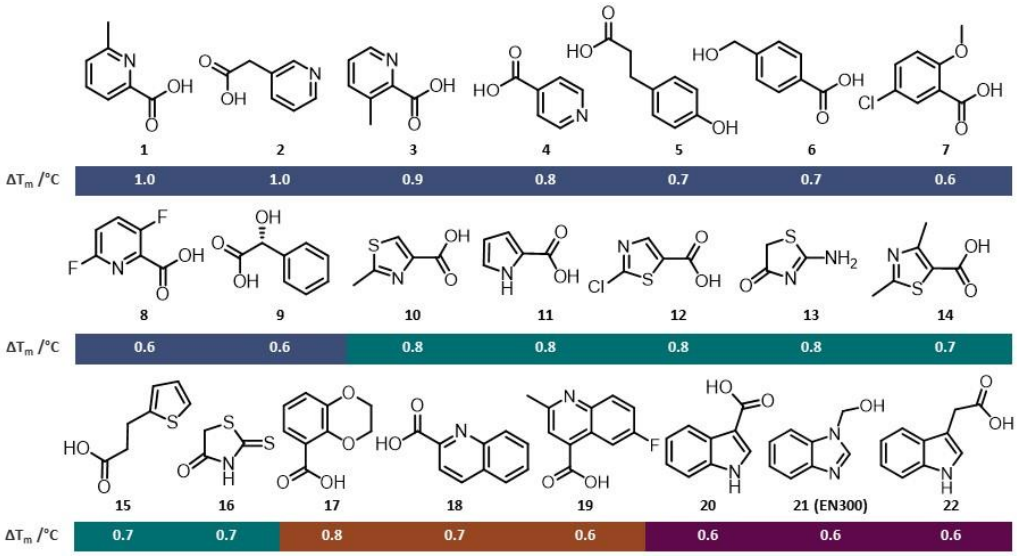


**Figure 3.1.1. Identified fragments against eZiPro using thermal shift assay.** Twenty-two fragments were identified. The structural formulas of the fragments and the temperatures change are illustrated. These compounds are grouped into four clusters (represented in different colours) based on the design of their aromatic core. (The screening experiment is carried out by Kang's Lab, EDDC)

Next, protease inhibition assays were also carried out by Kang's lab on these identified hits. However, all the fragments do not show any measurable IC50 values (< 200 μM). This could be attributed to the fragments being small, thus unable to bind strongly to the protease to cause any significant inhibitory effects.

To understand the molecular interactions between the protease and the fragment hits, co-crystallization studies were carried out using bZiPro. The structures of bZiPro in complexes with compounds **6** and **16** were solved at a resolution of 1.9 Å and 1.95 Å respectively (**Figure 3.1.2 and 3.1.3, and Table 3.1.1**). Similarly to EN300, both of these fragments bind to the S1 pocket of the active site (Zhang et al., 2016). However, the two compounds have different modes of interaction with the protease. The interactions between compound **6** and the protease are mediated by the hydrogen bonding between the hydroxyl group of compound **6** and the side-chain oxygen of D129 as well as between the carboxyl group of compound **6** and S135. π-π interaction was also observed between the benzene ring in compound **6** and Y161. Whereby in compound **16**, hydrogen bonding exists and between the amine hydrogen of compound **16** and the backbone oxygen of Y130 as well as carbonyl oxygen of compound **16** and the hydroxyl group of S135. The binding of the fragments does not induce any conformational or structural changes to NS2B and NS3.

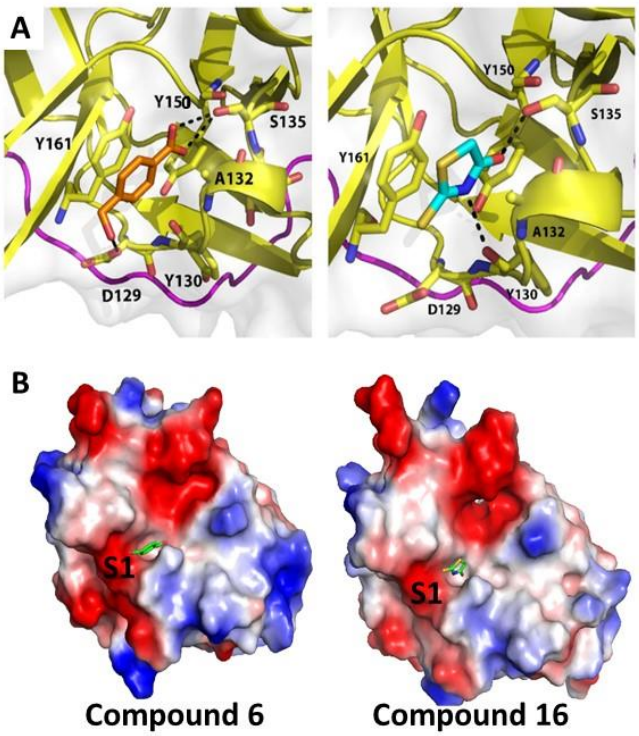


**Figure. 3.1.2. The crystal structures of bZiPro in complex with the identified compound 6 and 16.** (**A**) Zoomed view of the interactions between NS3 and the compounds. NS2B and NS3 are represented as cartoons and coloured in magenta and yellow, while compound 6 and 16 are shown as orange and cyan sticks respectively. The bZiPro residues involved in interactions with the fragments are labelled and shown as sticks. The interactions are shown in black dashed lines. (**B**) Electrostatic potential map of bZiPro in complex with compound **6** and **16**.

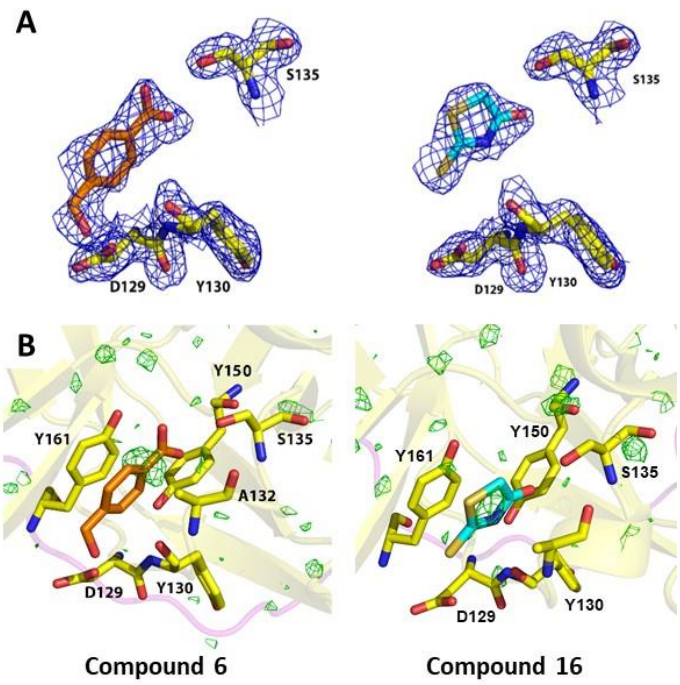


**Figure 3.1.3. Electron density map of crystal structures of bZiPro in complex with the compound 6 and 16** (**A**) The electron density maps (2mFo-Fc) is represented as blue mesh and contoured at 1σ. (**B**) The omit map (mFo-Fc) is represented as green mesh and contoured at 3σ. The neighbouring residues are shown as sticks in yellow.

**Table 3.1.1. X-ray data collection and refinement statistics**

| Data Collection Statistics | bZiPro + Compound **6** (PDB Code: 6L4Z) | bZiPro + Compound **16** (PDB Code: 6L50) |
|---|---|---|
| Wavelength (Å) | 0.9537 | 0.9537 |
| Resolution range (Å) | 45.76 - 1.9 (1.968 - 1.9) | 42.3 - 1.95 (2.02 - 1.95) |
| Space group | P 21 21 21 | P 21 21 21 |
| Unit cell a, b, c | 59.549 59.525 214.556 | 59.744 59.909 214.833 |
| α, β, γ (Å) (°) | 90 90 90 | 90 90 90 |
| Total reflections | 370115 (36242) | 418435 (41495) |
| Unique reflections | 61183 (6015) | 56428 (5506) |
| Multiplicity | 6.0 (6.0) | 7.4 (7.5) |
| Completeness (%) | 99.93 (100.00) | 98.46 (97.62) |
| Mean I/sigma (I) | 14.09 (1.69) | 27.73 (3.20) |
| $R_{merge}$ | 0.5746 (1.109) | 0.2506 (0.647) |
| R-meas | 0.6247 (1.215) | 0.2698 (0.6946) |
| R-pim | 0.2429 (0.4897) | 0.09903 (0.2515) |
| CC1/2 | 0.812 (0.27) | 0.977 (0.586) |
| CC* | 0.947 (0.652) | 0.994 (0.86) |
| Refinement Statistics | | |
| Reflections used in refinement | 61152 (6015) | 56428 (5505) |
| Reflections used for R-free | 3012 (293) | 1999 (194) |
| $R_{work}$ | 0.1785 (0.2701) | 0.2149 (0.3763) |
| $R_{free}$ | 0.2244 (0.2918) | 0.2348 (0.3575) |
| Number of non-hydrogen atoms | 5807 | 5707 |
| macromolecules | 5622 | 5629 |
| ligands | 11 | 7 |
| solvent | 174 | 71 |
| Protein residues | 761 | 760 |
| RMSD (bonds) (Å) | 0.003 | 0.004 |
| RMSD (angles) (°) | 0.58 | 0.67 |
| Ramachandran favored (%) | 95.55 | 96.75 |
| Ramachandran allowed (%) | 4.32 | 3.25 |
| Ramachandran outliers (%) | 0.13 | 0.00 |
| Rotamer outliers (%) | 0.18 | 0.00 |
| Clashscore | 6.32 | 7.86 |
| Average B-factor | 32.29 | 31.63 |
| macromolecules | 32.32 | 31.70 |
| ligands | 34.67 | 35.19 |
| solvent | 31.31 | 26.25 |

Statistics for the highest-resolution shell are shown in parentheses.

To probe the molecular interaction between the proteases and the two compounds, solution NMR was also carried out by Kang's Lab. Superimposition of the $1^{H}$–$15^{N}$-HSQC spectra of 0.6 mM bZiPro with and without 2.4 mM compounds confirmed their molecular interactions in solution (**Figure 3.1.4**).

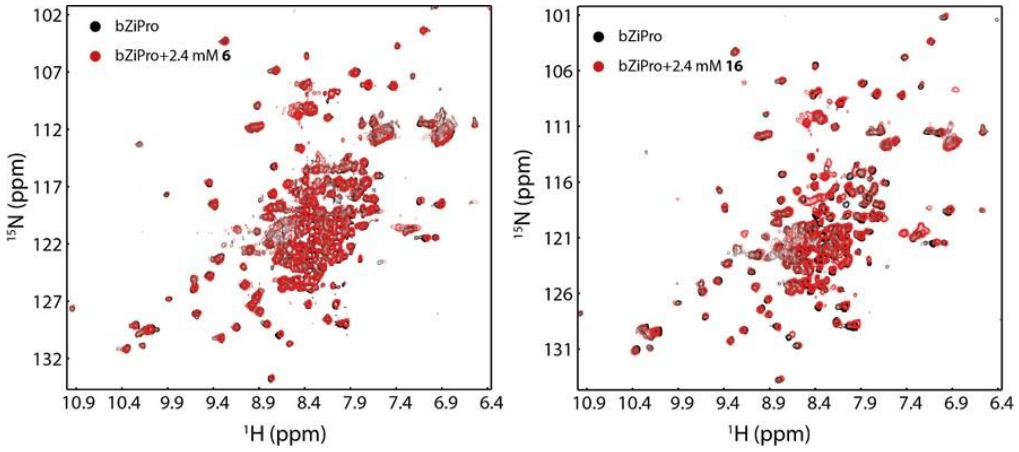


**Figure 3.1.4. NMR studies on the identified compound 6 and 16** (**A**) $^{1}$H–$^{15}$N-HSQC spectra of bZiPro with and without compound **6** and **16**. The $^{1}$H–$^{15}$N-HSQC spectra of bZiPro with and without the compounds are illustrated in red and black respectively. (The experiment is conducted by Kang's Lab, EDDC).

Using the two fragments as starting points, computer-aided fragment optimisations were also conducted using a recently developed browser app, DeepFrag (Green and Durrant, 2021). Optimised fragments with a cosine similarity score of greater than 0.8 were illustrated in **Figure 3.1.5A** and further evaluated using PyMOL. Of particular interest, compound **6-1** established an additional hydrogen bonding with the main chain carbonyl oxygen of Y130 (**Figure 3.15B**).

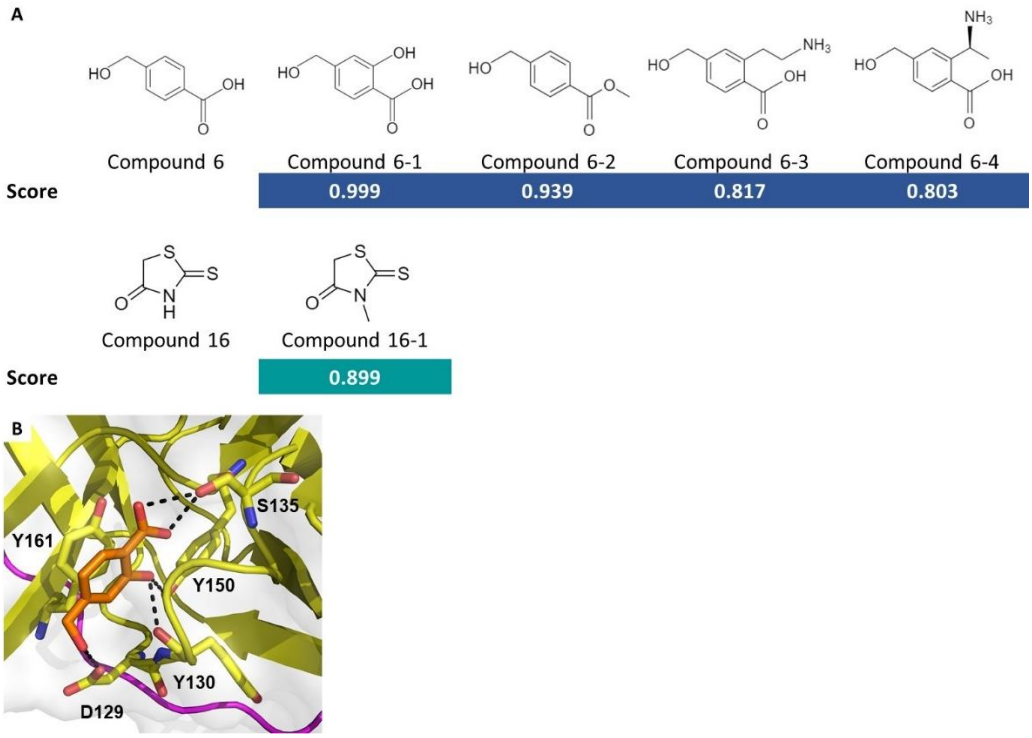


**Figure 3.1.5. Computer-aided lead optimisation of compound 6 and 16.** (**A**) The chemical structures of the predicted fragment optimisation of compound **6** and **16**, with a cosine similarity score of greater than 0.8, are illustrated. (**B**) The molecular representation of bZiPro in complex with compound 6-1. NS2B (magenta) and NS3 (yellow) are shown as cartoon representations, while the fragments are shown as orange. The bZiPro residues involved in interactions with the fragments are labelled and shown as sticks. The interactions are shown in black dashed lines.

### 3.1.1 Discussion

In this section, we reported two crystal structures of ZIKV protease in complex with fragment molecules **6** and **16**. The inhibition potencies of these compounds were also evaluated. While the fragment molecules do not have any measurable IC50 values up to 200 µM. The co-crystal structures do provide suggestions to improve inhibitor design.

The binding sites of these two fragments coincide with the side chain of P1 residues of peptidomimetics inhibitors and substrate. Thus, the positively charged P1 residue of peptidomimetics inhibitors could be replaced by an unnatural amino acid-fragment conjugate. Such modification could help to reduce the peptide characteristics and improve cellular permeability.

Additionally, together with previous studies and our current study, the S1 pocket was shown to be a hotspot for fragment binding (Li et al., 2018d; Zhang et al., 2016). Thus, these fragments can be used as lead compounds for further expansion to improve the binding and potency of the inhibitors. While the S2 pocket is negatively charged and is unsuitable as a potential site for fragment expansion, the S1' site can serve as an alternative. Targeting the S1' site can also be used to target specific flavivirus, given their different preferences for the residues at P1' to P3' position (Shiryaev et al., 2007a). Subsequently, the inhibitory activities of the modified fragments will be confirmed in both enzymatic and cellular antiviral experiments.

### 3.2 Structural characterization of cyclic peptidomimetics inhibitors targeting Zika virus NS2B-NS3 protease

While there are many studies on the development of linear peptidomimetics inhibitors via the various N- and C-terminal modifications, as previously mentioned in **Chapter 1.4.1**, cyclic substrate analogues as potential inhibitors against flavivirus protease are relatively unexplored.

Macrocyclic peptides are a promising modality for drug discovery, having the combination of advantages of both small molecules and antibodies (Morrison, 2018; Vinogradov et al., 2019). Macrocyclization reduces the conformational freedom of peptide derivatives and helps to pre-organise to a favourable orientation for binding, reducing the entropic cost of binding (Buckton et al., 2020; Vinogradov et al., 2019). Furthermore, macrocyclization may also help to improve other pharmacokinetic considerations such as membrane permeability and metabolic stability (Cary et al., 2017; Vinogradov et al., 2019).

Hence, in this section, we seek to understand how does bZiPro interact with two series of macrocyclic peptides and explore their inhibitory potency against the viral protease.

### 3.2.1 Structural characterization of cyclic peptidomimetics inhibitors generated via click reaction involving cysteine and activated nitriles

In the first series, the cyclic inhibitor was generated via a head-to-side chain cyclisation method involving an N-terminal cysteine residue and the unnatural amino acid 3-(2-cyano-4-pyridyl)-alanine (Cpa) (**Table 3.2.1**). The inhibitor is synthesized by Nitsche's Lab, ANU. Protease inhibition assay was carried out and it was revealed that the cyclic peptide **1b** was highly potent with a $K_i$ value of 0.14 μM (**Figure 3.2.1B**). The enzymatic cleavage of the cyclic peptide **1b** is extremely slow, although it resembles the substrate sequence, which could be likely due to the conformational rigidity of the inhibitor. It took around 20 h of incubation for half of cyclic peptide **1b** to be cleaved into the linear peptide **1c** by bZiPro (**Figure 3.2.1D**). The experiments are carried out by Nitsche's Lab, ANU.

**Table 3.2.1. Design and inhibition constant of the peptide inhibitor.** The linear peptide **1a** underwent macrocyclization to produce cyclic peptide **1b** in an aqueous solution (pH 7.5). The cyclic peptide **1b** has a $K_i$ value of 0.14 μM (The experiments were conducted by Nitsche's Lab, ANU.)

| Linear peptide | | Cyclic peptide | | $K_i$ (bZiPro) |
|---|---|---|---|---|
| **1a** | CGKRKSCpa-$NH_2$ | **1b** | 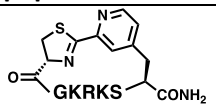 | 0.14 ± 0.30 μM |



Next, to understand the mode of interaction of bZiPro with peptide **1b**, a protein co-crystallisation study was carried out. However, a cleaved product **1c** was observed in the crystal structure (**Figure 3.2.1C, Figure 3.2.2 and Table 3.2.3**). Given that peptide **1b** has a half-life of 20 h, the cleaved product **1c** can be attributed to the high protease concentration and extended incubation period under co-crystallization conditions, favouring enzymatic digestion.

The co-crystal structure reveals hydrogen bonding between the C-terminal carboxyl oxygen atom of the P1 lysine and amide nitrogen of G133 and S135. The other C-terminal carboxyl oxygen atoms interact with the side-chain nitrogen of H51. Furthermore, the P1 amide nitrogen also forms hydrogen bonding with the carbonyl oxygen of G151 and hydroxyl oxygen of S135. The hydrogen on the side chain amine of the P1 lysine residue interacts with the side-chain oxygen of D129 and the carbonyl oxygen of Y130. One of the terminal hydrogens on the side chain of the P2 arginine interacts with the carbonyl oxygens of S81, G82 (both NS2B) and side-chain oxygen of NS2B D83. Another hydrogen on the side chain of the P2 arginine is in close contact with the side-chain oxygen of N152. The P3 lysine carbonyl oxygen and amide NH interact with the G153 amide NH and carbonyl oxygen respectively. Furthermore, the P3 lysine carbonyl oxygen makes close contact with the hydroxyl group of Y161.

Superimpositions of the complex with previously reported co-crystal structures of bZiPro in complex with substrate-derived ligands show similar interaction networks at $P_1$ and $P_2$ position and an overall $P_1$-$P_3$ backbone orientation (**Figure 3.2.3**) (Phoo et al., 2018). However, instead of having a U-shaped conformation as previously observed, the main chain residues are directed towards a nearby hydrophobic groove (**Figure 3.2.2D**) while the $P_3$ lysine side chain of **1c** is reorientated inwards (**Figure 3.2.3**).

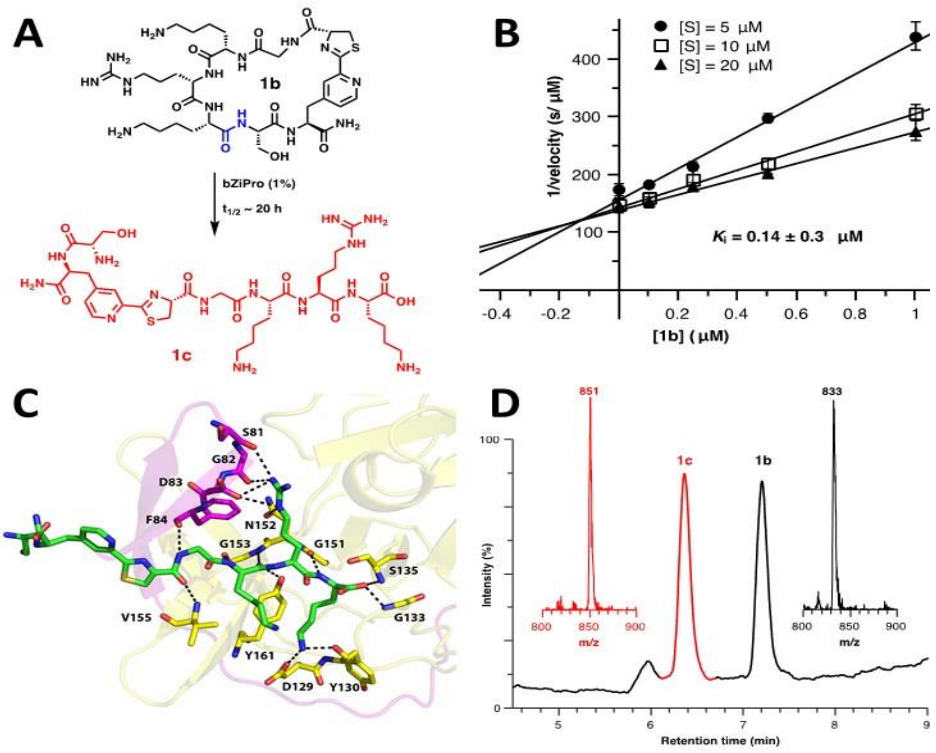


**Figure 3.2.1. Digested derivative 1c interacting with the bZiPro.** (**A**) Schematic representation of the enzymatic cleavage of **1b** to **1c** by bZiPro, with **1b** having a half-life time of around 20 h. The enzymatic cleavage site is coloured in blue. (**B**) Dixon plot for macrocyclic peptide **1b** and bZiPro, showing peptide **1b** as a competitive inhibitor with a $K_i$ value of 0.14 mM. Error bars indicated one standard deviation. (**C**) Zoomed view of the interactions between NS3 and **1c**. NS2B and NS3 are represented as cartoons and coloured in magenta and yellow, while the **1c** is represented as green sticks. The residues involved in interactions with **1c** are also labelled and shown as sticks. (**D**) LC-MS chromatogram and corresponding mass spectra of **1b** after 20 h of incubation with 1% bZiPro. Around 50% of **1b** was enzymatically cleaved into **1c** after 20 h of incubation. (The chemical synthesis, inhibition assay and LC-MS analysis were conducted by Nitsche's Lab, ANU.)

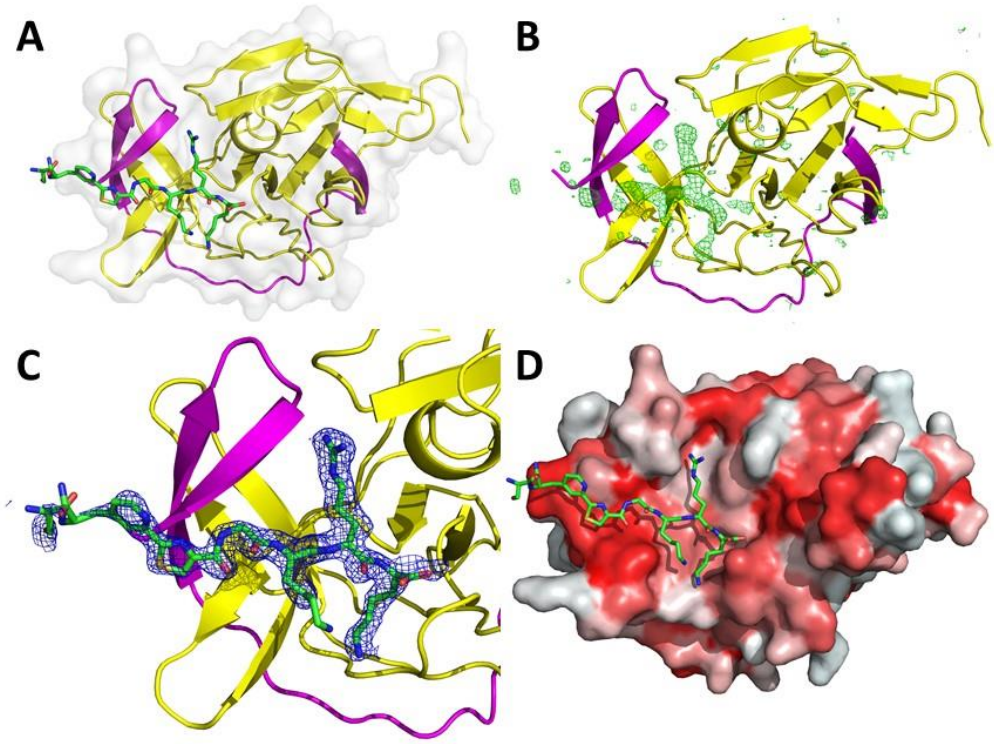


**Figure 3.2.2. Crystal Structure of inhibitor 1c in complex with bZiPro** (**A**) Crystal structure of Zika virus protease NS2B-NS3 (bZiPro) in complex with peptide **1c** (PDB code: 6JPW). NS2B and NS3 are represented as cartoons and coloured in magenta and yellow, while the **1c** is represented as green sticks. (**B**) Omit map (mFo-DFc) of **1c** with bZiPro coloured in green and contoured at 3σ. (**C**) The electron density map (2mFo-Fc) of **1c** is coloured in blue and contoured at 1σ. (**D**) Hydrophobicity map of bZiPro in complex with **1c**. The hydrophobic regions are coloured in red. **1c** is shown as sticks.

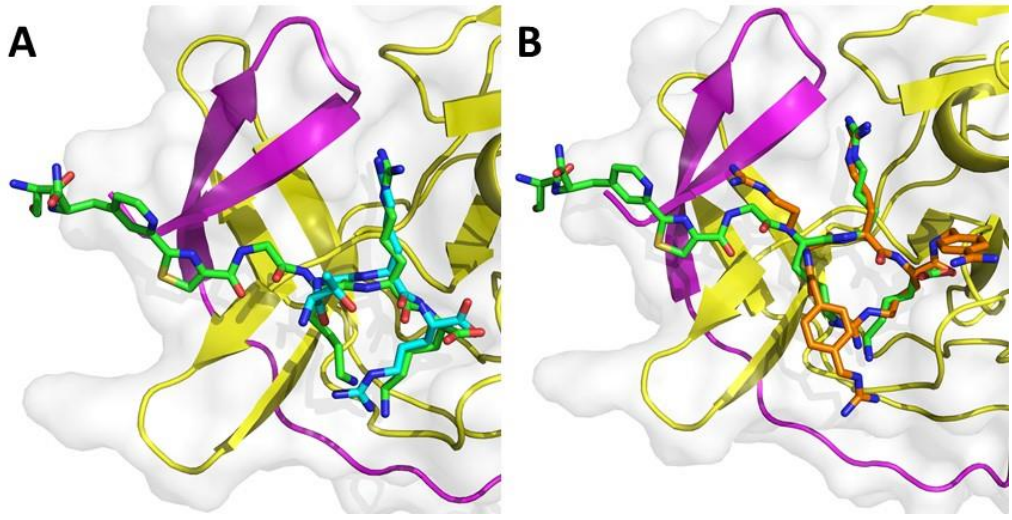


**Figure 3.2.3. Comparison of co-crystal structures of peptide inhibitors in complex with bZiPro.** (**A**) Superimposition of the structure of bound **1c** (PDB code: 6JPW) and the peptide TGKR (carbons in cyan) (PDB code: 5GJ4). (**B**) Superimposition of the structure of bound **1c** (PDB code: 6JPW) and the bound inhibitor 4-guanidinomethyl-phenylacetyl-Arg-Arg-Arg-4-amidinobenzylamide (carbons in orange) (PDB code: 5ZOB).

Enzymatic cleavage product that remains bound to bZiPro was also observed for other linear substrate-derived peptides (Phoo et al., 2018).

The cyclic bZiPro peptide **1b** binds with high affinity to the protease, has a long half-life of 20 h and remains bound with extensive binding interactions with the protease even after cleavage, displaying promising features for lead compounds.

Thus, using peptide **1** as a lead, peptide **2** - **5** with different linkers, containing either Dap, Dab, Orn or Lys, were designed for further SAR study. Additionally, to simplify the chemical synthesis method, the C-terminal Cpa group was replaced with 2-cyanoisonicotinamide (CINA) (**Table 3.2.2**). The chemical modifications are performed by Nitsche's Lab, ANU.

To compare the differences in inhibition potential contributed by the linker, inhibition assays were carried out. All of the cyclic peptides act as competitive inhibitors of bZiPro (**Table 3.2.2**). Derivative **2b** with the shortest linker displays a significantly high affinity with a $K_i$ of 0.64 μM. Interestingly, although peptide **2b** and **3b** only in one methylene group, there is a stark difference in inhibition potential. Peptide **2b** with a Dap-based linker displayed more than 20 times stronger inhibitory activity than analogue **3b** with a Dab-based linker. This result suggests that cyclisation linkers are important in mediating the pre-conformation for binding to maximize affinity. In our study, the most constrained peptide with the shortest linker has the highest inhibitory activity. Although the higher inhibitory activity can also be contributed to the Dap chemical group in 2b, an isostere of serine, facilitates binding to the S1' pocket.

**Table 3.2.2. Sequences and inhibition constant of investigated peptides 2 - 5.** The linear peptide sequence before macrocyclization and chemical structure of the cyclic peptide inhibitors after macrocyclization are shown respectively. The CINA group is highlighted in blue while the P1' groups are highlighted in red. The inhibition constant of the cyclic inhibitors and linear peptide **2c** are also indicated. (The experiments were conducted by Nitsche's Lab, ANU.)

| Linear peptide | | Cyclic peptide | | $K_i$ (bZiPro) |
|---|---|---|---|---|
| **2a** | CGKRK-Dap (CINA)-$NH_2$ | **2b** | 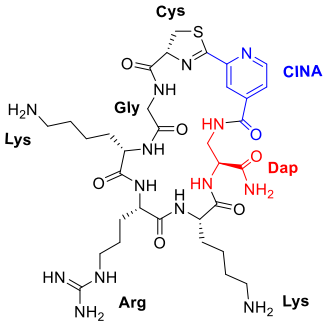 | 0.64 ± 0.01 µM |
| **3a** | CGKRK-Dab (CINA)-$NH_2$ | **3b** | 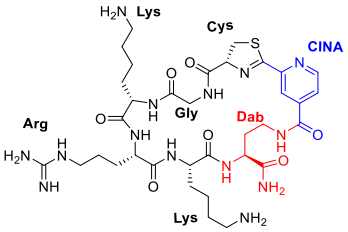 | 14.3 ± 0.70 µM |
| **4a** | CGKRK-Orn (CINA)-$NH_2$ | **4b** | 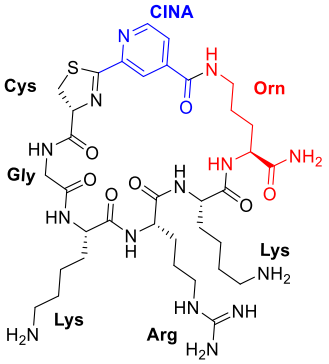 | 1.76 ± 0.31 µM |
| **5a** | CGKRK-Lys (CINA)-$NH_2$ | **5b** | 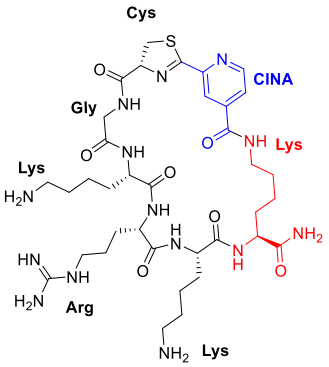 | 7.24 ± 0.34 µM |

| Linear peptide | | $K_i$ (bZiPro) |
|---|---|---|
| **2c** | [H-Dap(CINA)-$NH_2$] Cys-Gly-Lys-Arg-Lys-OH | 50.2 ± 1.20 µM |

Next, a co-crystallization study was carried out to study the SAR. Like **1b**, we observed the enzymatic cleaved linear derivative **2c** in complex with bZiPro instead of **2b** (**Figure 3.2.4 and Figure 3.2.5**). Derivative **2c** resulted from the enzymatic cleavage between $P_1$ Lys and $P_1$' Dap(CINA) of **2b**, which further suggests the Dap-based residue is capable of acting as a serine isostere in $P_1$'.

To verify that the inhibition activity is from the cyclic peptide **2b** not by the hydrolyzed product **2c**, inhibition assay was carried out using the chemically synthesized **2c** and we found a $K_i$ value of 50.2 μM, which is around 78 fold weaker than the cyclic analogue **2b** (**Table 3.2.2**). Furthermore, proteolytic stability of **2b** was also examined with 0.1% bZiPro. After 8 h incubation, only a minor amount of the cleaved product **2c** was observed (**Figure 3.2.4B**), further demonstrating that the $K_i$ value of 0.64 μM arises from the un-cleaved compound **2b**. Thus, as observed with peptide **1b**, the appearance of cleaved product **2c** in the crystal structure can be attributed to the high protease concentration and extended incubation period under co-crystallization conditions, favouring enzymatic digestion.

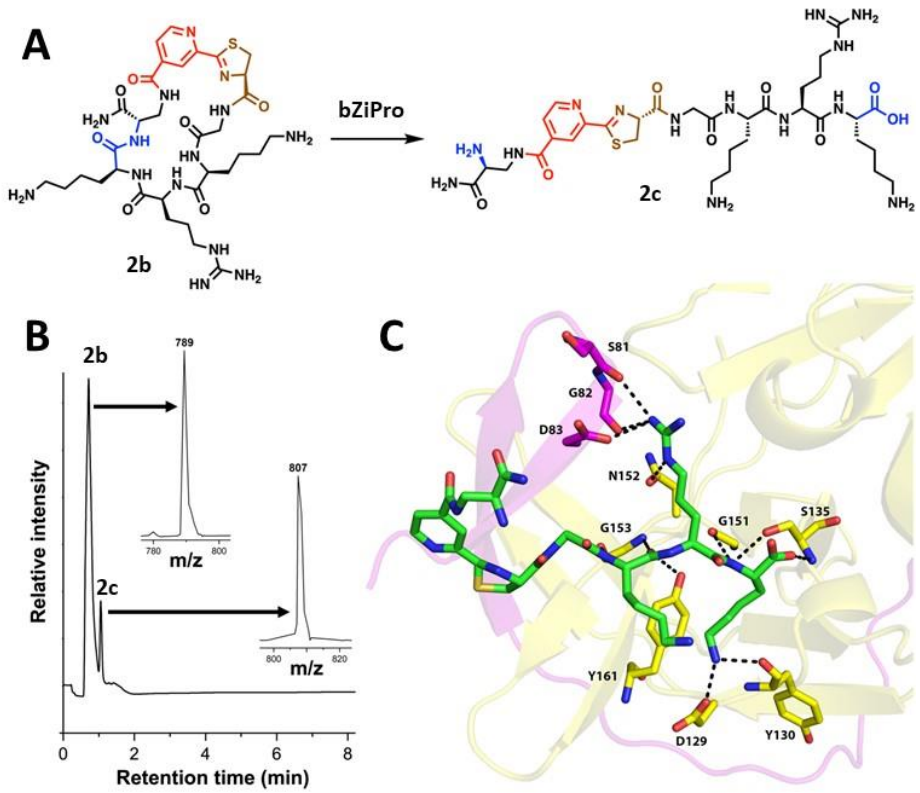


**Figure 3.2.4. Digested derivative 2c interacting with the bZiPro.** (A) Schematic representation of the enzymatic cleavage of **2b** to **2c** by bZiPro. The enzymatic cleavage site is coloured in blue. (B) LC-MS chromatogram and corresponding mass spectra of **2b** after 8 h incubation with 0.1% bZiPro. (C) Zoomed view of the interactions between NS3 and **2c**. NS2B and NS3 are represented as cartoons and coloured in magenta and yellow, while the **2c** is represented as green sticks. The bZiPro residues involved in interactions with **2c** are also labelled and shown as sticks. (The inhibition assay and LC-MS analysis were conducted by Nitsche's Lab, ANU.)

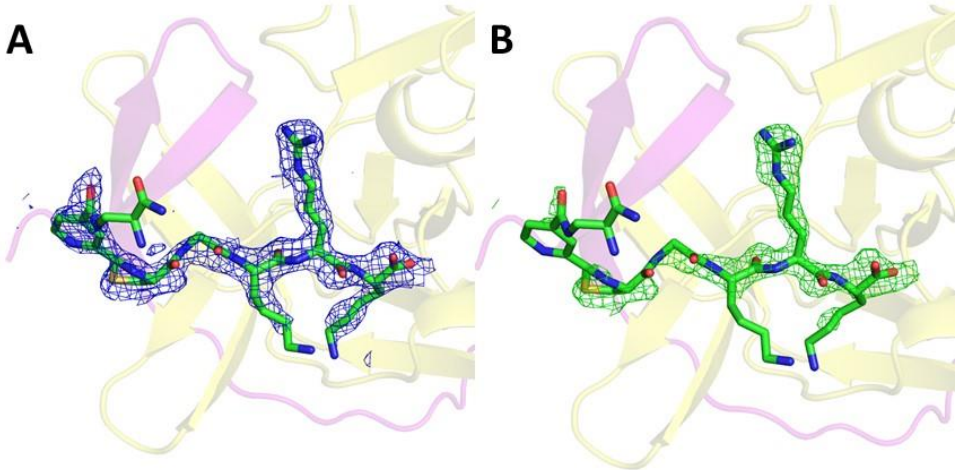


**Figure 3.2.5. Crystal Structure of inhibitor 2c in complex with bZiPro.** (**A**) The electron density maps (2mFo-Fc) of **2c** is represented as blue mesh and contoured at 1 σ. (**B**) The omit map (mFo-DFc) of **2c** is represented as green mesh and contoured at 3 σ.

In a single asymmetric unit of the crystal structure, there were four bZiPro molecules. **2c** was found in one of the molecules while residues K14 to E17 from another molecule was bound to the active site of the neighbouring NS3 molecule in reverse orientation, occupying the $S_4$ to $S_1$ pockets of bZiPro as observed in a previously reported structure (Zhang et al., 2016). The peptide **2c** adopts a similar binding mode as peptide **1c,** showing similar $P_1$ and $P_2$ interactions and $P_1$–$P_3$ backbone conformations with a flipped $P_3$ lysine side chain (**Figure 3.2.6**).

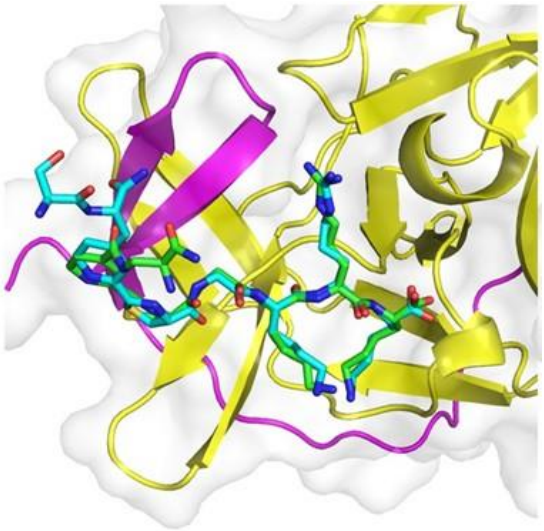

**Figure 3.2.6. Comparison of co-crystal structures of peptide 1c and 2c in complex with the Zika virus NS2B-NS3 protease (bZiPro)**. Superimposition of the structure of bound **2c** (PDB code: 7DOC) (carbons in green) and peptide **1c** (PDB code: 6JPW) (carbons in cyan).

**Table 3.2.3. X-ray data collection and refinement statistics**

| **Data collection statistics** | bZiPro + Peptide 1C (PDB Code: 6JPW) | bZiPro + Peptide 2C (PDB Code: 7DOC) |
|---|---|---|
| Wavelength (Å) | 0.95373 | 0.95372 |
| Resolution range (Å) | 46.1 - 1.951 (2.021 - 1.951) | 45.63 - 1.904 (1.972 - 1.904) |
| Space group | P 21 21 21 | P 21 21 21 |
| Unit cell a, b, c α, β, γ (Å) (°) | 60.107, 60.473, 215.488, 90, 90, 90 | 59.15 59.61 215.07 90 90 90 |
| Total reflections | 779343 (65254) | 798071 (71537) |
| Unique reflections | 57901 (5412) | 60261 (5640) |
| Multiplicity | 13.5 (12.1) | 13.2 (12.7) |
| Completeness (%) | 99.41 (94.30) | 99.39 (94.08) |
| Mean I/sigma (I) | 20.77 (3.73) | 12.20 (2.01) |
| $R_{merge}$ | 0.09683 (0.6722) | 0.1312 (0.8121) |
| R-meas | 0.1007 (0.702) | 0.1365 (0.8459) |
| R-pim | 0.02738 (0.1986) | 0.03716 (0.2344) |
| CC1/2 | 0.999 (0.839) | 0.997 (0.925) |
| CC* | 1 (0.955) | 0.999 (0.98) |
| **Refinement statistics** | | |
| Reflections used in refinement | 57868 (5394) | 60243 (5630) |
| Reflections used for R-free | 1997 (188) | 2981 (281) |
| $R_{work}$ | 0.2068 (0.2755) | 0.2092 (0.2947) |
| $R_{free}$ | 0.2489 (0.3089) | 0.2286 (0.2750) |
| Number of non-hydrogen atoms | 6461 | 5928 |
| macromolecules | 5720 | 5501 |
| ligands | 177 | 56 |
| solvent | 564 | 371 |
| Protein residues | 773 | 765 |
| RMSD (bonds) (Å) | 0.006 | 0.004 |
| RMSD (angles) (°) | 1.18 | 1.06 |
| Ramachandran favored (%) | 97.09 | 96.11 |
| Ramachandran allowed (%) | 2.64 | 3.76 |
| Ramachandran outliers (%) | 0.26 | 0.13 |
| Rotamer outliers (%) | 0.69 | 0.00 |
| Clashscore | 9.88 | 16.95 |
| Average B-factor | 34.59 | 45.77 |
| macromolecules | 33.05 | 45.19 |
| ligands | 48.66 | 69.21 |
| solvent | 45.79 | 50.88 |

Statistics for the highest-resolution shell are shown in parentheses.

### 3.2.2 Structural characterization of cyclic peptidomimetics inhibitors generated via reversely incorporated lysine or ornithine residues

The second series of cyclic inhibitors were designed and synthesised using an alternative method. Macrocyclization occurs via using a lysine or ornithine mimetic compound as the P1 residue. The inhibitor is synthesized by the Steinmetzer's Lab, PU. The compound can be reversely incorporated where the side chain amino group forms a peptide bond with the P2 residue and the $\alpha$-amino group exists as a free guanidine. Such structures would enable the carboxyl group to be available for macrocyclization to a P4 residue via a linker segment.

Firstly, the series of inhibitors were generated using 4-aminomethyl substituted phenylacetyl (Phac) moiety as the P4 residue and $\gamma$-aminobutyric acid (GABA) as the linker segment (**Table 3.3.1**). To determine the binding mode of the inhibitors to the protease, co-crystallization studies were conducted. In this series, the crystal structures of bZiPro in complex with inhibitor **1** and **3** were determined (**Figure 3.3.1**)**.** Based on the structure of inhibitor **1**, only one nitrogen of the P1 guanidino group was interacting with the side chain of Asp129 (**Figure 3.3.1A**).

In contrast, the co-crystal structure of bZiPro-inhibitor **3** showed an improved interaction network between the P1 guanidino group and the side chain of Asp129, the P1 guanidino group also formed additional interaction with Gly159 (**Figure 3.3.1B**). The conformation of the inhibitor was also further stabilized by an intramolecular hydrogen bonding between the P1 guanidine and the P4

carbonyl oxygen. Furthermore, the P4 residue acted as a hydrophobic shield and help to displace competing water molecules from disrupting the electrostatic contacts between the inhibitor and Asp129. The structure also revealed a relatively long linker segment, which prompts the further optimization for a more constrained conformation.

To examine the role of the guanidino group on the binding affinity, amino analogues **5** and **6** were also been prepared as reference compounds. Both amino compounds displayed poor potency, indicating the importance of the P1 guanidino moiety in establishing interaction with the protease (**Table 3.3.1**).

To optimize the linker region, a series of meta-substituted Phac inhibitors were synthesized (**Table 3.3.2**). The direct analogue meta-substituted inhibitor **7** was found to have more than 10 times improvement against bZiPro than inhibitor **3.** Subsequently, the replacement of the GABA linker by shorter linkers such as β-alanine or glycine leads to the improvement of the inhibition potency of inhibitor **8** and **9**. Particularly, inhibitor **9** was the most potent inhibitor displaying $K_i$ values ranging from 1.6 nM to 142 nM against the various tested viral protease.

**Table 3.3.1. Chemical formulas and inhibition constant of the 4-aminomethyl-phac-derived inhibitors.** The chemical structure at the top is the generic chemical structure of the 4-aminomethyl-phac-derived inhibitors series. The different P1 residues are shown as a box and illustrated in the table. The inhibition constants against various viral proteases are also indicated. (The chemical synthesis and inhibition assay against WNV protease were conducted by Steinmetzer's Lab, PU.)

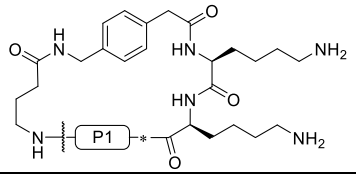


| No. | Ring size | P1 | $K_i$ (μM) bZiPro | $K_i$ (μM) WNV protease | $K_i$ (μM) bD4Pro |
|---|---|---|---|---|---|
| **1** | 26 | 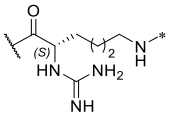 | 0.0918 ± 0.006 | 6.30 ± 0.49 | 11.0 ± 1.0 |
| **2** | 25 | 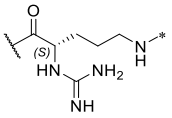 | 0.846 ± 0.111 | 27.8 ± 4.4 | 117 ± 5 |
| **3** | 26 | 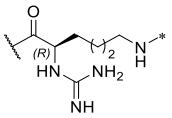 | 0.0701 ± 0.0092 | 4.97 ± 0.50 | 4.73 ± 0.50 |
| **4** | 25 | 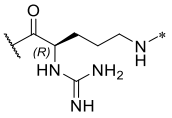 | 3.61 ± 1.33 | 22.0 ± 4.0 | 60.5 ± 5.7 |
| **5** | 26 | 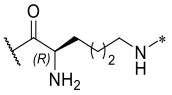 | 24.7 ± 7.2 | 68.1 ± 5.0 | 94.5 ± 11.6 |
| **6** | 25 | 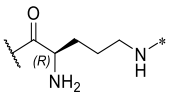 | 13.2 ± 1.7 | 31.7 ± 3.6 | 30.6 ± 3.9 |

However, further shortening of the linker using 3-amino-Phac in combination with glycine, lead to a significant decrease in the inhibitory potency of inhibitor **10.** Subsequent attempts to restore potency by using the longer β-Alanine or GABA instead of glycine to the 3-amino-Phac residue, only resulted in a minor improvement for inhibitors **12** and **13**. This suggests that both the number of linker atoms as well as the proper positioning of the peptide bond can influence the inhibitory potency. Surprisingly, the shortest analogue **11** displays a relatively strong potency.

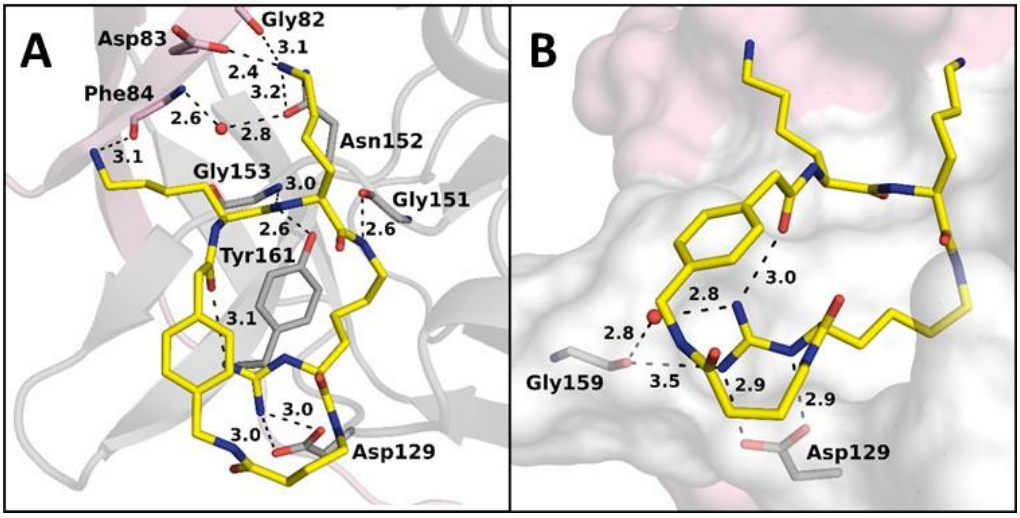


**Figure 3.3.1. Crystal Structure of the 4-aminomethyl-phenylacetyl-derived inhibitors.** (**A**) Zoomed view of the interactions between bZiPro with inhibitor **1**. NS2B and NS3 are represented as cartoon and coloured in magenta and grey, while inhibitor **1** is represented as yellow sticks. Selected bZiPro residues involved in interactions with inhibitor **1** are also labelled and shown as sticks. Water molecules are represented as red spheres. (**B**) Zoomed view of the interactions between bZiPro with inhibitor **3**. With the incorporation of a P1 residue in *R*-configuration, more extensive interactions were observed between the P1 guanidine and Asp129.

A crystal structure was also solved for bZiPro in complex with inhibitor **9** (**Figure 3.3.2**). The mode of interactions of the P1 – P3 residues are similar to the interactions observed for the complex with inhibitor **3**.

**Table 3.3.2. Chemical formulas and inhibition constant P4 meta-substituted Phac-residue inhibitors.** The chemical structure at the top is the generic chemical structure of the P4 meta-substituted Phac-derived inhibitors series. The different P4 linker residues are shown as a box and illustrated in the table. The inhibition constants against various viral proteases are also indicated. (The chemical synthesis and inhibition assay against WNV protease were conducted by Steinmetzer's Lab, PU.)

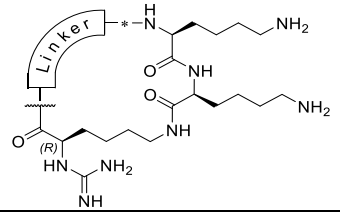


| No. | Ring size | Linker | $K_i$ (nM) bZiPro | $K_i$ (nM) WNV protease | $K_i$ (nM) bD4Pro |
|---|---|---|---|---|---|
| **7** | 25 | 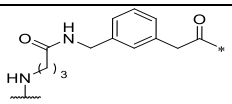 | 4.33 ± 0.35 | 702 ± 83 | 286 ± 9 |
| **8** | 24 | 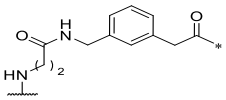 | 3.88 ± 0.81 | 374 ± 44 | 182 ± 5 |
| **9** | 23 | 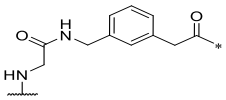 | 1.57 ± 0.32 | 138 ± 31 | 142 ± 10 |
| **10** | 22 | 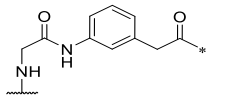 | 1420 ± 270 | 47600 ± 2500 | 60600 ± 5300 |
| **11** | 20 | 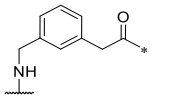 | 37.3 ± 4.7 | 15300 ± 800 | 1280 ± 50 |
| **12** | 23 | 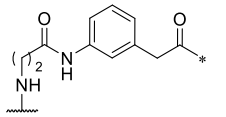 | 80.2 ± 9.7 | 4280 ± 310 | 7960 ± 550 |
| **13** | 24 | 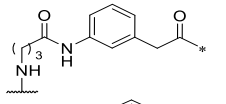 | 106 ± 29 | 16500 ± 4600 | 5800 ± 360 |
| **14** | 23 | 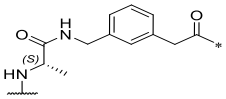 | 18.2 ± 5.1 | 1390 ± 320 | 3600 ± 380 |
| **15** | 23 | 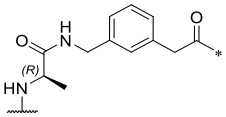 | 3.52 ± 1.09 | 237 ± 21 | 125 ± 4 |
| **16** | 23 | 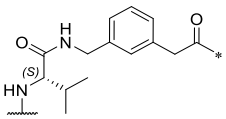 | 42.8 ± 2.2 | 6710 ± 320 | 2810 ± 180 |
| **17** | 23 | 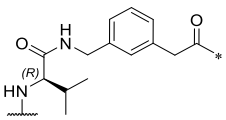 | 7.74 ± 0.66 | 439 ± 28 | 486 ± 27 |
| **18** | 23 | 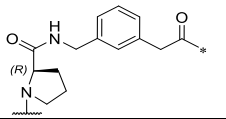 | 17.7 ± 0.5 | 850 ± 68 | 4080 ± 260 |

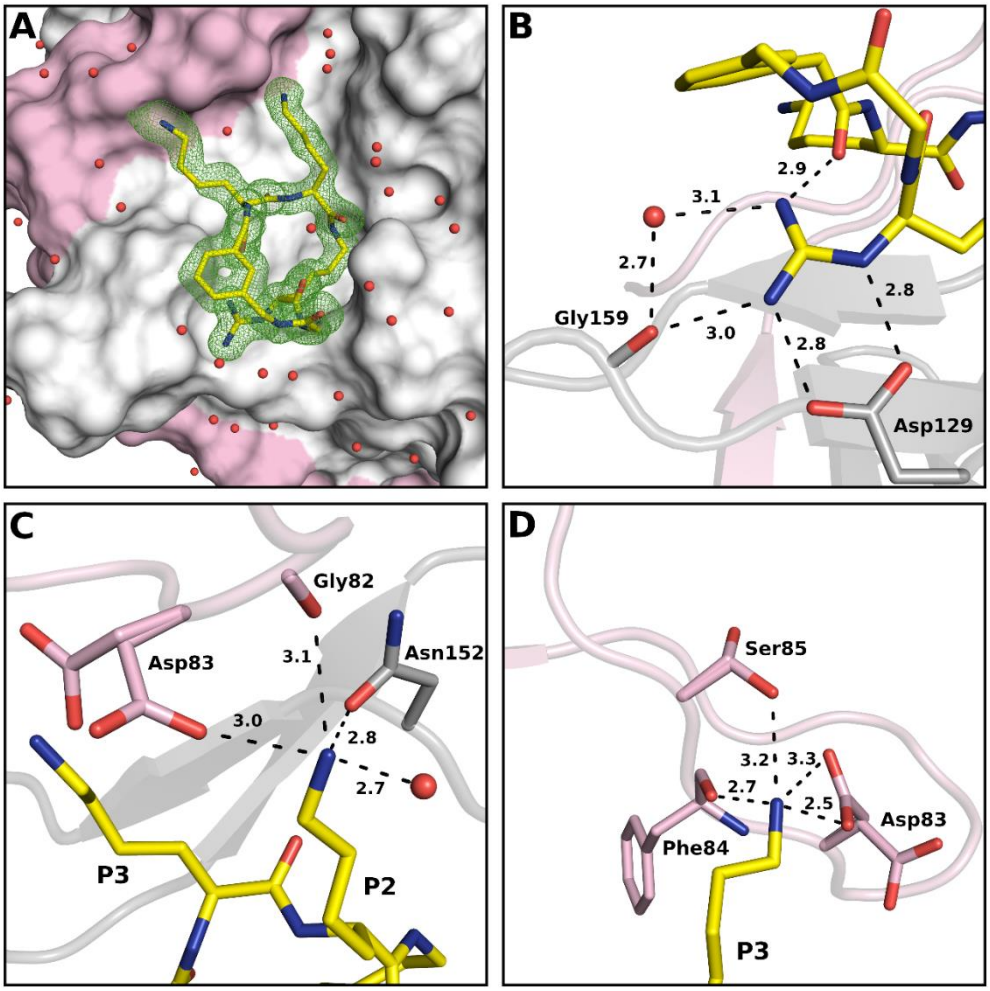


**Figure 3.3.2. Crystal structure of bZiPro in complex with inhibitor 9** Zoomed view of the interactions between bZiPro with inhibitor **9**. NS2B and NS3 are represented as cartoon and coloured in magenta and grey, while inhibitor **9** is represented as yellow sticks. Selected bZiPro residues involved in interactions with inhibitor **9** are also labelled and shown as sticks. Water molecules are represented as red spheres. (**A**) bZiPro in complex with inhibitor **9** is represented in surface with NS2B in pink and NS3 in grey. The omit map (mFo-DFc) is represented as green mesh and contoured at 3 σ. The interaction networks for the P1 guanidine, P2 Lys and P3 Lys are shown in panel **B, C** and **D** respectively. Two conformations were observed for NS2B residues Asp83 and Ser85.

Two other crystal structures were also solved for bZiPro complexes with the inhibitors **7** and **8**. The elongated inhibitors were observed to have a widened backbone conformation. For inhibitor **7**, the P4 phenyl ring was observed to have a significant 1.4 Å displacement from that of analogue **9**. Else, the P1 guanidino groups assume an exact position in all three structures (**Figure 3.3.3A**).

Alanine or D-Alanine as well as Valine and D-Valine (**14**-**17**) were also used to replace glycine in inhibitor **9**. For both pairs, the *R*-configured linker residue displayed a stronger potency. However, inhibitor **9** remains to be the most potent among these analogues and the D-Proline derivative **18**. Based on the structural analysis of bZiPro in complex with the alanine and D-Alanine inhibitors **14** and **15,** the side chains of the linker residue were observed to orientate toward the solvent and does not form any interactions with bZiPro. The binding mode remains the same as compared to inhibitor **9**. However, for inhibitor **14**, there is a shift of the carbonyl group by 1.5 Å (**Figure 3.3.3B**). In turn, the P4 aryl ring was also displaced. These differences may account for the decreased potency of the inhibitor **14** as compared to **9** and **15**.

Two additional analogues based on inhibitor **9** were also designed (**Table 3.3.3**). For inhibitor **19,** the P1 amino group displayed dramatically reduced potency with $K_i$ values of 23 to 282 µM against the tested proteases. Similarly, when a urea moiety (-$NHCONH_2$) was used at the P1 position, inhibitor **20** also showed a reduced potency of 12 to 135 µM.

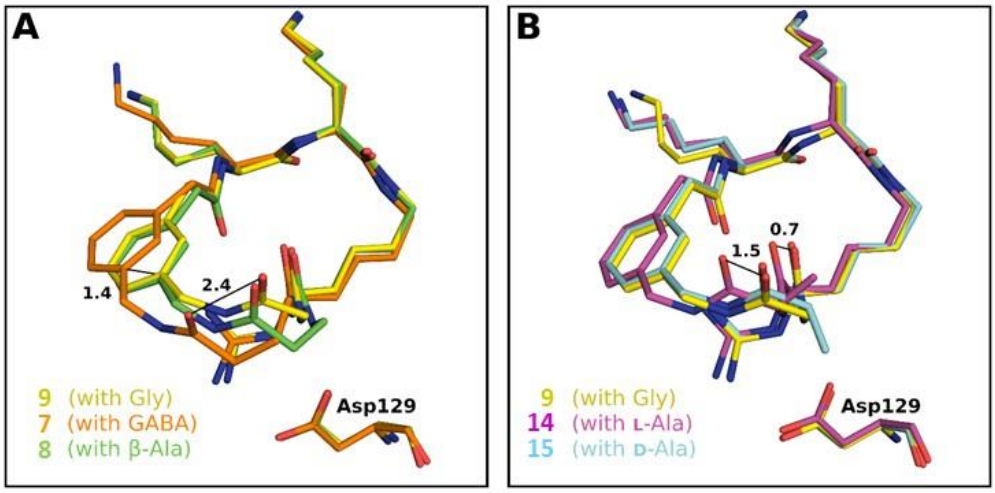


**Figure 3.3.3. Comparison of co-crystal structures of cyclic peptide in complex with the bZiPro** The inhibitors are illustrated as sticks. The differences in distances are represented as lines and given in Å. (**A**) Superimposition of the structure of bound inhibitor ***9*** with analogues ***7*** and **8**. (**B**) Superimposition of the structure of bound inhibitor **9** with inhibitors **14** and **15**.

**Table 3.3.3. Chemical formulas and inhibition constant of compound 9 analogues.** The chemical structures of the compound 9 analogues are illustrated. The inhibition constants against various viral proteases are also indicated. (The chemical synthesis and inhibition assay against WNV protease were conducted by Steinmetzer's Lab, PU.)

| No. | | $K_i$ (μM) bZiPro | $K_i$ (μM) WNV protease | $K_i$ (μM) bD4Pro |
|---|---|---|---|---|
| **19** | 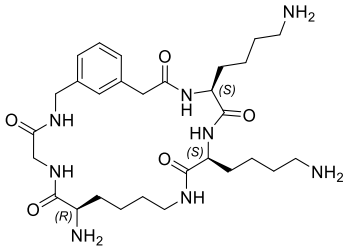 | 23 | 99 | 282 |
| **20** | 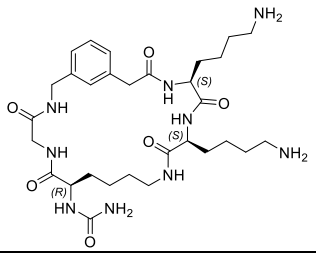 | 12 | 68 | 135 |

The subsequent modification includes using linear amino acids to replace the P4 aryl ring, which contributed seven atoms to the backbone of the inhibitor (**Table 3.3.4**). Inhibitor **21**, which contains five atoms long GABA residue, were found to have the weakest potency. The GABA residue might not be long enough for cyclization. Subsequent stepwise elongation using 5-aminovaleric acid or 6-aminocaproic acid significantly restored potency, however, the potency of the more rigid compound **9** is still approximately 10-fold better than inhibitors **22** and **23** against bZiPro. An additional peptide bond was proposed to stabilize the inhibitor conformation. Hence, various combinations of glycine and β-Alanine residues were used to replace the aliphatic amino acid (**24**-**27**). Interestingly, inhibitor **25** possesses a comparable potency to inhibitor **9** against bZiPro and even a slightly stronger potency against WNV protease.

The crystal structures for the two most potent inhibitors with P4 aliphatic amino acids, inhibitor **24** and **25**, were also determined (**Figure 3.3.4**). As observed with the other inhibitors, the binding mode of P2 and P3 residues remains similar to inhibitor **9**. However, the conformation of the linker segment differs significantly depending on the length of the carbon atoms of the linker. In inhibitor **24**, the shortening of the linker by one atom leads to a rotation of the P3-P4 amide bond by nearly 180°, leading to a loss of the intramolecular hydrogen bond between the P1-guanidine and the P4-carbonyl oxygen (**Figure 3.3.4A**). While for inhibitor **25,** with the same number of carbon atoms as inhibitor **9**, the intramolecular hydrogen bond is maintained (**Figure 3.3.4B**). Interestingly, in inhibitor **25**, all the three carbonyls of the linker point toward the same nitrogen of the P1 guanidino group, forming a chelate-like structure

(**Figure 3.3.4B**). However, in doing so, it results in a slight lengthening of both salt bridges to D129.

**Table 3.3.4. Chemical formulas and inhibition constant of P4 aliphatic amino acids inhibitors.** The chemical structure at the top is the generic chemical structure of the P4 aliphatic inhibitors series. The different P4 linker residues are shown as a box and illustrated in the table. The inhibition constants against various viral proteases are also indicated. (The chemical synthesis and inhibition assay against WNV protease were conducted by Steinmetzer's Lab, PU.)

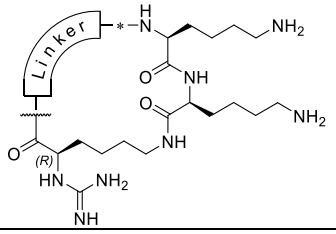


| No. | Ring size | Linker | $K_i$ (nM) bZiPro | $K_i$ (nM) WNV protease | $K_i$ (nM) bD4Pro |
|---|---|---|---|---|---|
| **21** | 21 | 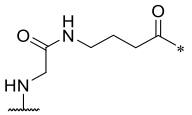 | 124 ± 8 | 6700 ± 520 | 6090 ± 470 |
| **22** | 22 | 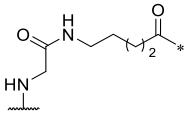 | 16.7 ± 3.4 | 1220 ± 20 | 1120 ± 50 |
| **23** | 23 | 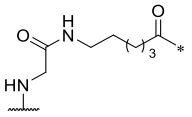 | 15.4 ± 2.6 | 973 ± 173 | 1990 ± 90 |
| **24** | 22 | 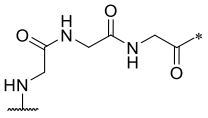 | 3.74 ± 0.20 | 129 ± 7 | 378 ± 27 |
| **25** | 23 | 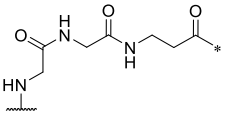 | 1.72 ± 0.03 | 68.6 ± 13.1 | 160 ± 5 |
| **26** | 23 | 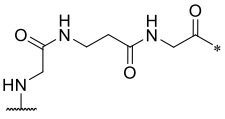 | 7.35 ±0.39 | 468 ± 3 | 815 ± 79 |
| **27** | 23 | 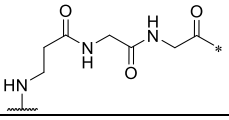 | 12.8 ± 0.5 | 974 ± 134 | 2720 ± 190 |

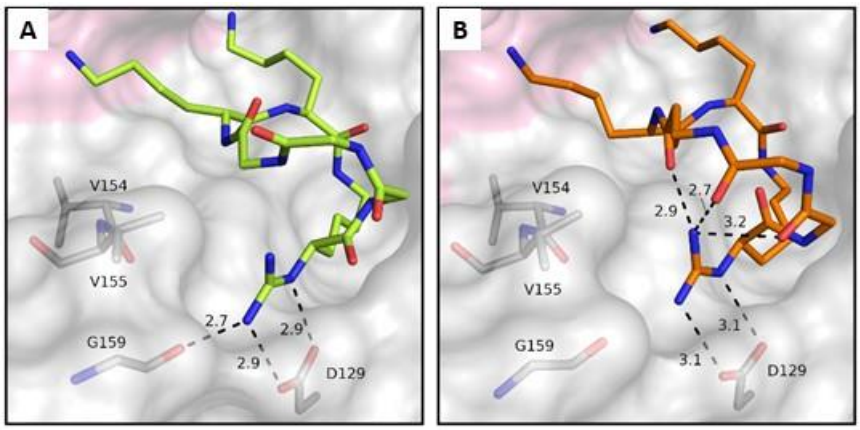


**Figure 3.3.4. Crystal structure of bZiPro in complex with P4 aliphatic amino acids inhibitors** (**A**) bZiPro in complex with inhibitor **24**. (**B**) bZiPro in complex with inhibitor **25**. bZiPro is represented in surface with NS2B in pink and NS3 in grey while the inhibitors are illustrated as green (24) and orange (25) sticks. Polar contacts of the P1 guanidines are presented as black dashed lines (distances in Å).

Four linear reference compounds were prepared to explore the effect of cyclization on inhibitory efficacy (**Table 3.3.5**). Inhibitor **28** is more than 1000-fold weaker than analogue **9** against bZiPro. The reduction in potency was hypothesized to be due to the increased conformational flexibility, but also by charged P1 carboxyl group, which is near Asp129 in the S1 site. By changing to a non-charged amide analogue **29** or acetylated compound **30**, a more than 100-fold improved potency was observed. Finally, the complete removal of the -NH-CO- segment of inhibitor **9** generated the derivative **31**. **U**pon binding to the protease, the increased flexibility of the homoagmatine group would contribute to a stronger entropic penalty resulting in reduced potency.

**Table 3.3.5. Chemical formulas and inhibition constant of linear inhibitors.** The chemical structure at the top is the generic chemical structure of the linear inhibitor series. The different P1 residues of the inhibitors are shown as a box and illustrated in the table. The inhibition constants against various viral proteases are also indicated. (The chemical synthesis and inhibition assay against WNV protease were conducted by Steinmetzer's Lab, PU.)

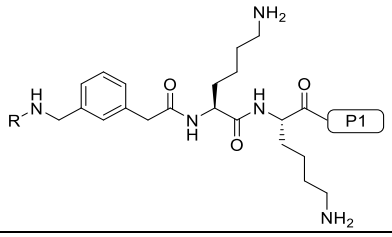


| No. | R | P1 | $K_i$ (nM) bZiPro | WNV protease | bD4Pro |
|---|---|---|---|---|---|
| **28** | H-Gly | 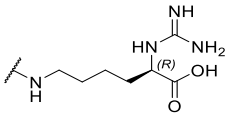 | 2040 ± 600 | 51600 ± 700 | 75000 ± 3400 |
| **29** | H-Gly | 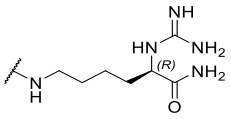 | 13.6 ± 2.6 | 1550 ± 380 | 775 ± 47 |
| **30** | Ac | 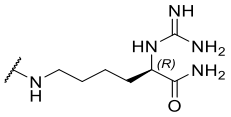 | 9.48 ± 0.61 | 1480 ± 100 | 1210 ± 90 |
| **31** | Ac | 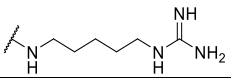 | 88.2 ± 3.8 | 4940 ± 530 | 18100 ± 1200 |

From the study, 24 inhibitors were found to have Ki values of less than 1 µM against bZiPro. Generally, these inhibitors are about 55- to 200-fold weaker against WNV protease and bD4Pro respectively. The difference in potencies could be because of the different NS2B residues at position 83; Asp83 in ZIKV, corresponding to Asn84 in WNV and Thr84 or Ser84 in DENV1-4. ZIKV Asp83 has previously been suggested to interact with P2 Lysine or Arginine of substrate-analogue inhibitors. Nevertheless, the inhibitors show a strong correlation potency ranking across the flaviviruses (**Figure 3.3.5**). This trend can be attributed to the rather conserved active site architecture across the flaviviruses protease, suggesting that the current macrocyclic inhibitor design can serve as a basis for future pan-flavivirus protease inhibitors development.

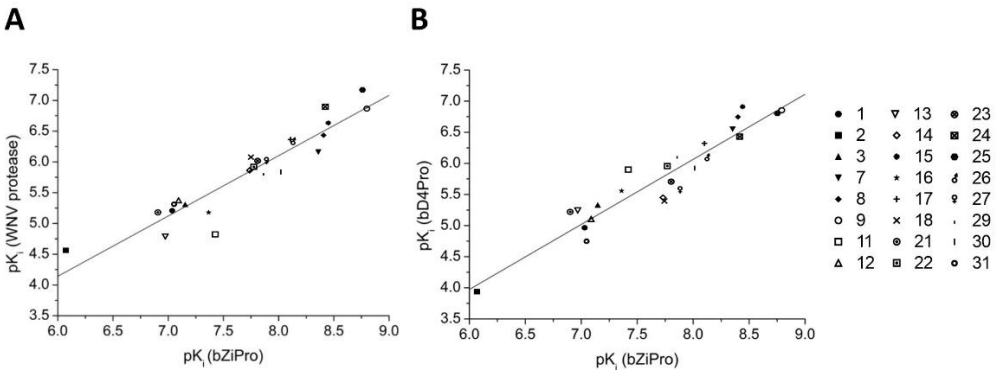


**Figure 3.3.5. Correlation of the pK$_i$ values across flaviviruses** Correlation of the pK$_i$ values for the inhibition of bZiPro and the (A) WNV protease or the (B) bD4Pro for the top 24 inhibitors with Ki values of less than 1 µM against bZiPro. The pK$_i$ against bZiPro/WNV protease and bZiPro/bD4Pro displayed a strong positive correlation of 0.98 and 1.05 respectively. The inhibitors displayed around 55-fold ($10^{1.74}$) or 200-fold ($10^{2.30}$) weaker activity against WNV protease and bD4Pro as compared to bZiPro.

Next, we seek to investigate the antiviral activity of the 2 most potent inhibitors, inhibitor **9** and **25**. For the initial screening, A549 cells were infected using ZIKV luciferase reporter virus with an initial inhibitor concentration of 20 µM. Ribavirin, a nucleoside inhibitor, was used as the positive control at a concentration of 100 µM. The luciferase activities were measured 48 hours post-infection (**Figure 3.3.6A**). A reduction in luciferase activity was only observed for inhibitor **9**. Thus, we proceed to evaluate if inhibitor **9** resulted in any cellular cytotoxic effect (**Figure 3.3.6B**). No cytotoxic effect was observed after 48 hours with inhibitor concentration up to 80 µM.

Subsequently, plaque assays were conducted to examine if inhibitor **9** resulted in any reduction in virus titers (**Figure 3.3.6C**). A549 cells were infected by the French Polynesia ZIKV strain H/PF/2013. At 24 h p.i., a slight reduction of the virus titers has been observed in the supernatants, but not with the cell lysate. However, no significant differences were observed 48 h p.i.

Lastly, the effect of inhibitor **9** on the expression of ZIKV proteins was also examined. Immunofluorescence microscopy analyses using ZIKV NS1 (green)- and E (red)-specific antibodies revealed that inhibitor **9** did not affect the number of ZIKV-infected cells as compared to the DMSO-treated control (**Figure 3.3.6D**).

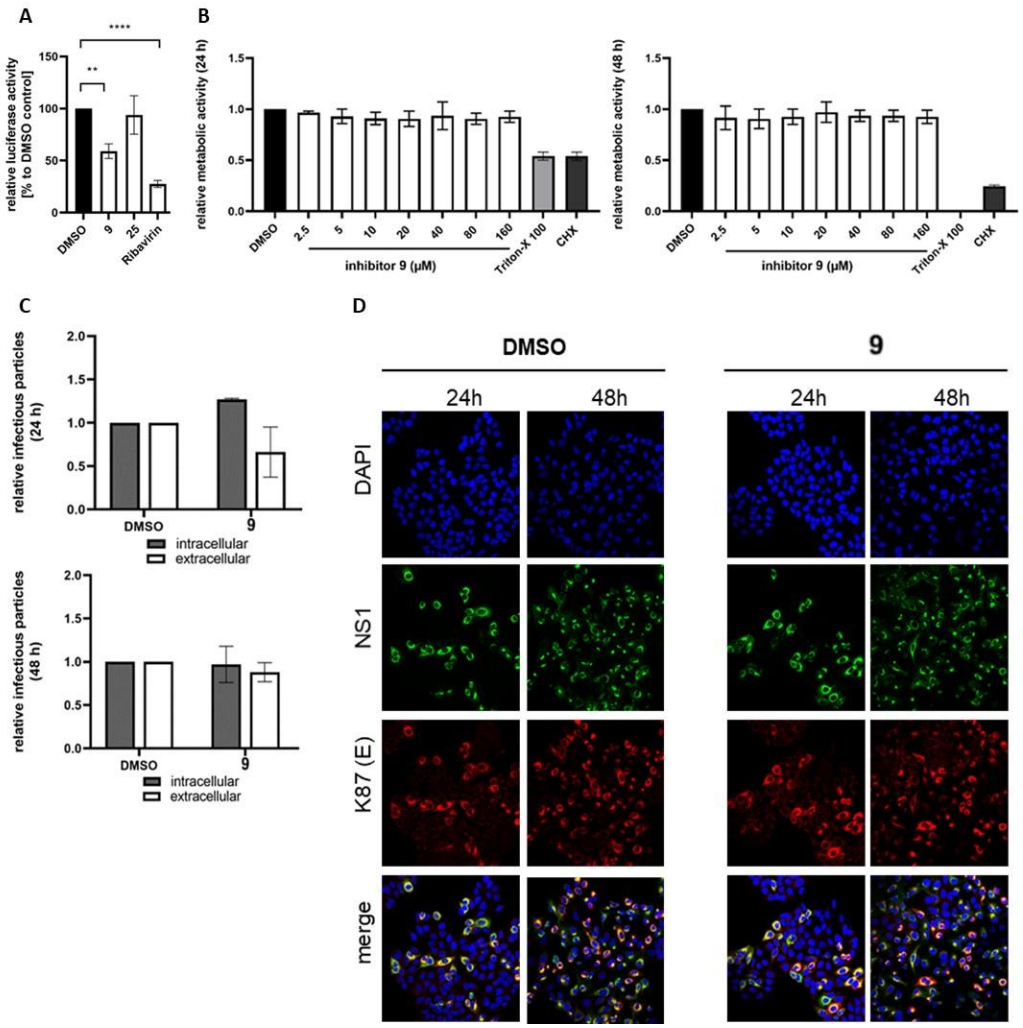


**Figure 3.3.6. In vitro antiviral activity of inhibitor 9**(**A**) Antiviral testing using a ZIKV luciferase reporter virus. A549 cells were infected with the ZIKV luciferase reporter virus in the presence of the protease inhibitors (20 µM) and ribavirin (100 µM) was as reference compound. At 48 h p.i. luciferase activity was determined. The results are described as means ± SD from at least five independent experiments. The statistical significance was compared to the DMSO control group. ** = p > 0.01; **** = p > 0.0001. (**B**) Cell cytotoxicity assay. A549 cells were treated with different inhibitor concentrations for 24 and 48 h. The relative metabolic activity was determined using the PrestoBlue™ cell viability reagent. DMSO, Triton-X 100 (1 %) and cycloheximide

(CHX, 0.1 %) served as controls. All relative values were normalized to the DMSO control. The results are presented as means ± SD from at least two independent experiments. (**C**) Inhibition of ZIKV propagation. The number of intracellular and extracellular plaque-forming infectious viruses after treatment with inhibitors 9 (80 µM) was determined 24 and 48 h p.i. by plaque assay. The results are presented as means ± SD from at least three independent experiments. All relative values were normalized to the DMSO control. (**D**) Influence on ZIKV proteins after treatment with inhibitor 9. A549 cells were infected with the ZIKV French Polynesia strain (H/PF/2013) at an MOI of 1 in the presence of the inhibitors at 80 µM or DMSO (0.8 %) as control. The cells were fixed with 4 % formaldehyde 24 and 48 h p.i. and analyzed using NS1- (green) and E (K87)- (red) specific antisera. Nuclei were visualized with DAPI (blue). The images were obtained using the Leica Stellaris 8 System at 40X Magnification. (The experiment is conducted by Steinmetzer's Lab, PU)

**Table 3.3.6. X-ray data collection and refinement statistics.**

| **Data Collection Statistics** | **1** PDB: 6KK2 | **3** PDB: 6KK3 | **7** PDB: 6KPQ | **8** PDB: 6KK4 | **9** PDB: 6Y3B | **14** PDB: 6KK5 | **15** PDB: 6KK6 |
|---|---|---|---|---|---|---|---|
| Wavelength (Å) | 0.95372 | 1 | 0.97924 | 0.95373 | 0.9184 | 0.97924 | 0.95373 |
| Beamline | ALS, MXII | TPS, 05A | SLS, PSIII | ALS, MXII | BESSY, MX 14.1 | SLS, PSIII | ALS, MXII |
| Detector | ADSC Quantum 315r Detector | MX300HS | PILATUS 2M-F | ADSC Quantum 315r Detector | PILATUS 6M | PILATUS 2M-F | ADSC Quantum 315r Detector |
| Space group | P $4_3$ 2 2 | P $4_3$ 2 2 | P $4_3$ 2 2 | P $2_1$ $2_1$ $2_1$ | P $2_1$ $2_1$ $2_1$ | P $4_3$ 2 2 | P $2_1$ $2_1$ $2_1$ |
| Unit cell a, b, c (Å) | 42.4 42.4 215.7 | 42.6 42.6 215.3 | 42.6 42.6 214.2 | 48.8 60.4 83.2 | 48.6 60.5 83.1 | 42.5 42.5 215.4 | 48.6 60.7 83.4 |
| Matthews coefficient (Å$^3$/Da) | 2.2 | 2.3 | 2.2 | 2.7 | 2.5 | 2.2 | 2.9 |
| Solvent content (%) | 44 | 45 | 45 | 55 | 50 | 45 | 57 |
| Resolution range (Å) | 42.4 - 2.02 (2.10 - 2.02) | 53.8 - 2.05 (2.12 - 2.05) | 42.6 - 2.62 (2.71 - 2.62) | 41.6 - 1.74 (1.80 - 1.74) | 48.9 – 1.59 (1.69 – 1.59) | 42.5 - 2.03 (2.10 - 2.03) | 42.0 - 1.74 (1.80 - 1.74) |
| Total reflections | 189875 (16956) | 160734 (16002) | 85505 (8791) | 289548 (27245) | 197383 (32248) | 170433 (16674) | 290724 (27264) |
| Unique reflections | 13825 (1265) | 13375 (1289) | 6571 (629) | 25939 (2483) | 33699 (5398) | 13722 (1317) | 25997 (2478) |
| Multiplicity | 13.7 (12.8) | 12.0 (12.4) | 13.0 (14.0) | 11.2 (11.0) | 5.9 (6.0) | 12.4 (12.7) | 11.2 (11.0) |
| Completeness (%) | 99.4 (95.2) | 99.9 (100.0) | 99.8 (99.8) | 99.7 (97.4) | 99.8 (99.7) | 99.8 (99.5) | 99.6 (96.2) |
| Mean I/sigma (I) | 35.1 (3.0) | 10.6 (1.8) | 12.1 (1.8) | 36.0 (7.3) | 21.2 (3.1) | 18.5 (1.8) | 21.6 (2.8) |
| Wilson B-factor (Å$^2$) | 39.7 | 32.0 | 52.3 | 20.8 | 21.1 | 39.4 | 24.2 |
| $R_{merge}$ | 0.196 (0.593) | 0.155 (1.36) | 0.192 (1.64) | 0.044 (0.336) | 0.043 (0.484) | 0.091 (1.37) | 0.073 (0.912) |
| $CC_{1/2}$ | 0.99 (0.96) | 1.00 (0.72) | 1.00 (0.84) | 1.00 (0.96) | 1.00 (0.86) | 1.0 (0.86) | 1.00 (0.83) |
| **Refinement statistics** | | | | | | | |
| Resolution range (Å) | 42.4 - 2.02 (2.09 - 2.02) | 53.8 - 2.05 (2.12 - 2.05) | 42.56 - 2.62 (2.71 - 2.62) | 41.6 - 1.74 (1.80 - 1.74) | 48.9 – 1.59 (1.64 – 1.59) | 42.5 - 2.03 (2.10 - 2.03) | 42.0 - 1.74 (1.80 - 1.74) |
| Reflections work | 13136 (1204) | 12702 (1223) | 6225 (595) | 24642 (2344) | 32014 (3146) | 13036 (1249) | 24698 (2357) |
| Reflections free | 689 (61) | 673 (66) | 346 (34) | 1297 (123) | 1685 (165) | 686 (68) | 1299 (121) |

| | | | | | | | |
|---|---|---|---|---|---|---|---|
| $R_{work}$ | 0.219 (0.235) | 0.189 (0.257) | 0.218 (0.313) | 0.162 (0.212) | 0.162 (0.203) | 0.198 (0.274) | 0.172 (0.225) |
| $R_{free}$ | 0.256 (0.298) | 0.217 (0.351) | 0.246 (0.309) | 0.184 (0.243) | 0.188 (0.263) | 0.231 (0.308) | 0.181 (0.255) |
| Protein residues (NS2B / NS3) | 39 / 156 | 38 / 154 | 38 / 153 | 39/ 161 | 38 / 159 | 38 / 153 | 38 / 152 |
| Inhibitor atoms | 47 | 47 | 47 | 46 | 45 | 46 | 46 |
| Water molecules | 38 | 76 | 4 | 143 | 129 | 51 | 99 |
| Other ligand atoms | 0 | 0 | 0 | 4 | 11 | 0 | 11 |
| RMSD (bonds) (Å) | 0.008 | 0.015 | 0.009 | 0.017 | 0.007 | 0.008 | 0.007 |
| RMSD (angles) (°) | 1.23 | 1.66 | 1.38 | 1.86 | 0.92 | 1.25 | 1.29 |
| Ramachandran favored (%) | 96.8 | 97.3 | 95.7 | 96.9 | 96.4 | 96.3 | 97.3 |
| Ramachandran allowed (%) | 3.2 | 2.7 | 4.3 | 3.1 | 3.6 | 3.7 | 2.7 |
| Ramachandran outliers (%) | 0.0 | 0.0 | 0.0 | 0.0 | 0.0 | 0.0 | 0.0 |
| Average B-factor ($Å^2$) | 49.7 | 36.9 | 62.8 | 27.5 | 30.0 | 46.9 | 32.7 |
| Protein | 49.2 | 36.0 | 62.7 | 26.5 | 29.5 | 46.7 | 32.1 |
| Inhibitor | 65.2 | 51.2 | 64.4 | 18.3 | 20.0 | 49.2 | 22.5 |
| Water molecules | 49.2 | 44.6 | 53.2 | 40.0 | 39.0 | 50.2 | 43.2 |
| Other ligands | - | - | - | 38.8 | 40.8 | - | 58.2 |

Statistics for the highest-resolution shell are shown in parentheses.

| **Data Collection Statistics** | **24**<br>7VLH | **25**<br>7VLI |
|---|---|---|
| Wavelength (Å) | 0.9537 | 1.000 |
| Beamline | ALS MX2 | SLS X06DA |
| Detector | ADSC QUANTUM 315r | PILATUS 2M-F |
| Space group | P 43 2 2 | P 43 2 2 |
| Unit cell a, b, c (Å) | 40.9, 40.9, 214.4 | 42.5, 42.5, 215.7 |
| Matthews coefficient ($Å^3$/Da) | 2.1 | 2.3 |
| Solvent content (%) | 41 | 45 |
| Resolution range (Å) | 40.26 - 2.62 (2.72 - 2.62) | 41.65 - 2.39 (2.47 - 2.39) |
| Total reflections | 74659 (7078) | 206864 (19831) |
| Unique reflections | 6110 (580) | 8604 (812) |
| Multiplicity | 12.2 (12.2) | 24.0 (24.4) |
| Completeness (%) | 99.4 (98.3) | 99.6 (98.7) |
| Mean I/sigma (I) | 16.6 (1.8) | 14.5 (1.2) |
| Wilson B-factor ($Å^2$) | 56.0 | 48.8 |
| $R_{merge}$ | 0.132 (1.26) | 0.300 (3.65) |
| $CC_{1/2}$ | 1.00 (0.95) | 1.00 (0.76) |
| **Refinement statistics** | | |
| Resolution range (Å) | 40.26 - 2.62 (2.71 - 2.62) | 41.65 - 2.39 (2.47 - 2.39) |
| Reflections work | 6087 (579) | 8579 (807) |
| Reflections free | 305 (30) | 430 (41) |
| $R_{work}$ | 0.239 (0.347) | 0.230 (0.389) |
| $R_{free}$ | 0.289 (0.362) | 0.288 (0.442) |

| | | |
|---|---|---|
| Protein residues (NS2B / NS3) | 38 / 153 | 38 / 152 |
| Inhibitor atoms | 42 | 43 |
| Water molecules | 3 | 8 |
| Other ligand atoms | 5 | 5 |
| RMSD (bonds) (Å) | 0.001 | 0.004 |
| RMSD (angles) (°) | 0.53 | 0.99 |
| Ramachandran favored (%) | 96.26 | 93.55 |
| Ramachandran allowed (%) | 3.74 | 6.45 |
| Ramachandran outliers (%) | 0.00 | 0.00 |
| Average B-factor (Å$^2$) | 67.0 | 53.9 |
| Protein | 66.7 | 53.6 |
| Inhibitor | 83.1 | 65.4 |
| Water molecules | 61.5 | 49.9 |
| Other ligands | 87.6 | 71.9 |

Statistics for the highest-resolution shell are shown in parentheses.

### 3.2.3 Discussion

In this section, we report several crystal structures of ZIKV protease in complex with both cyclic peptidomimetics inhibitors and digested derivatives. The inhibition potencies of these compounds were also evaluated. For both series of the cyclic peptidomimetics inhibitors, we demonstrated that the cyclic forms have a stronger inhibition potency as compared to their linear analogues. The inhibition constant of peptide **2c** is 78 times higher than the inhibition constant of **2b**. While for inhibitor **28** to **31** also showed 6 to 1000-fold weaker in inhibition potency than inhibitor **9**. Thus, showing that a lower entropic barrier of binding might be an important contributor to its significantly higher affinity.

Furthermore, both series of cyclic inhibitors also show relatively conserved binding mode to the S1- S3 pockets of the ZIKV protease as compared to previously solved co-crystal structures with linear peptides (Lei et al., 2016; Li et al., 2017a; Phoo et al., 2018; Zhang et al., 2016).

From the SAR analysis of both series, we have also observed the size of the cyclic backbone serves as a key factor influencing the inhibition potential. In the first series, comparing the inhibition constants of cyclic peptide **2b – 5b,** cyclic peptide **2b** displays a significantly higher potency with its smallest 24-membered backbone. Although peptide 2**b** and **3b** only differ in one methylene, **2b** is more than 20 times stronger than **3b. T**he stronger affinity to 2b can be partially attributed to the Dap used in **2b** is an isostere of serine, allowing it to fit nicely into the S1' pocket of the protease' active site.

In the second series, the inhibition constants of inhibitors **7**-**10** demonstrated that an optimal ring size of 23 atoms displayed the strongest potency against all three viral proteases. Further truncation beyond the 23-membered ring leads to a dramatic decline in potency as illustrated by inhibitor **10**. Interestingly, for the cyclic series without the aryl ring (**21** – **27**), the 23-membered inhibitor **25** also displayed the strongest potency, although further truncation of the ring was still tolerated for inhibitor **24**.

Other than the ring size, the positioning of the amide bond in the connecting linker segment also influences the inhibitory potency. A 23-membered inhibitor **12**, shows a relatively weak inhibition constant of 80 nM against bZiPro. A similar observation was also noticed between compound **25** and **27**, although the difference in inhibition potency is less significant of 8-fold differences.

Given that DENV, WNV and ZIKV proteases share similar substrate preferences for basic residues at the P1-P3 position, these macrocyclic inhibitors can serve as pan-flavivirus protease inhibitors. For the second series, the inhibitors are about 55- to 200-fold weaker against WNV protease and bD4Pro respectively as compared to bZiPro. The difference in potencies could be because of the different NS2B residues at position 83. ZIKV Asp83 was observed to interact with P2 Lysine or Arginine of substrate-analogue inhibitors. However, the residue was not conserved, corresponding to Thr84 or Ser84 in DENV1-4 and Asn84 in WNV, leading to a lower affinity towards the inhibitors. To improve the potency of the inhibitors against DENV and WNV protease, specific SAR studies can also be carried out using DENV and WNV proteases respectively.

Using peptidomimetics inhibitor designs, only two groups managed to synthesise inhibitors with antiviral activity $EC_{50}$ value within the micromolar range (Behnam et al., 2015; Stoermer et al., 2008). Phenylacetyl-Lys-Lys-Arg-aldehyde displays $EC_{50}$ value of 1.6 µM against WNV infection (Stoermer et al., 2008). While compound 104 displays $EC_{50}$ value of 3.4 µM against DENV infection (Behnam et al., 2015). Despite, inhibitor **9** displaying the strongest inhibition potency to date, with a $K_i$ value of 1.57 nM, the cyclic inhibitor was not able to inhibit ZIKV replication in a cell-based assay. Based on our understanding of the peptide inhibitors, we can only assume that, despite macrocyclization, the highly charged amino acid residues still lead to an overall weak membrane permeability, hampering their antiviral efficacy. Moving forward, parallel artificial membrane permeability assay should be incorporated into the inhibitor screening workflow, to assess membrane permeability in parallel to inhibition efficiency.

Nevertheless, these potent cyclic peptides with their well-resolved bZiPro-inhibitor complexes provide a basis for future pan-flavivirus protease inhibitors development.

# Chapter 4: Biochemical and structural characterisation of *Flavivirus*' NS5-RNA complex

The *Flavivirus* NS5 C-terminal RdRp domain plays a critical role in replicating the viral genome during both de novo initiation and elongation steps. However, the exact mechanism of nucleotide additional catalytic cycle and the proposed conformational changes from initiation to elongation phase remains to be elucidated. Structural studies on catalytically relevant polymerase-RNA complex will help to understand flavivirus RNA replication, unravel any structural changes and potential inhibitor allosteric sites formation during various steps of RNA synthesis. Furthermore, as the NS5 RdRp is highly conserved and does not have any host homologs, it is an attractive antiviral drug target. By elucidating catalytically relevant polymerase ternary complexes with their substrates, it will also aid in the discovery and development of specific competitive inhibitors.

In this chapter, two methods were explored to capture the NS5-RNA complex. The first method involves designing the RdRp priming loop deletion mutants. While the priming loop deletion mutants retain their RNA polymerisation activity, but it does not help in the formation of protein crystals for X-ray crystallography. The second method involves fusing an RNA binding domain to NS5 to improve the affinity of RNA binding, and to facilitate the capturing of RNA at the active site.

### 4.1 Crystallization of the DENV NS5 RdRp priming loop mutant-RNA complex

#### 4.1.1 Designs of RdRp priming loop deletion constructs

From the crystal structure of apo dengue NS5 and RdRp, the RNA tunnel was observed to be too narrow to accommodate dsRNA. The priming loop was mainly associated to be involved in the formation of the AG dinucleotide primer in the initiation step of RNA synthesis, the priming loop was hypothesized to retract and widen the RNA tunnel, as the enzyme transit from the initiation step to the elongation step of the RNA synthesis. Thus, the priming loop deletion mutants were conceptualised to accommodate dsRNA for structural study. Selisko and colleagues also demonstrated that a six amino acids priming loop deletion mutant has increased catalytic activity, due to the ease of accommodating dsRNA (Selisko et al., 2012). As such two different priming loop deletion constructs were generated, ΔPl6aa with deletion from residue 794 to 799 and ΔPl15aa by replacing residue 788 – 804 with two glycines, to capture the RdRp in complex with RNA during the elongation step (**Figure 4.1.1**).

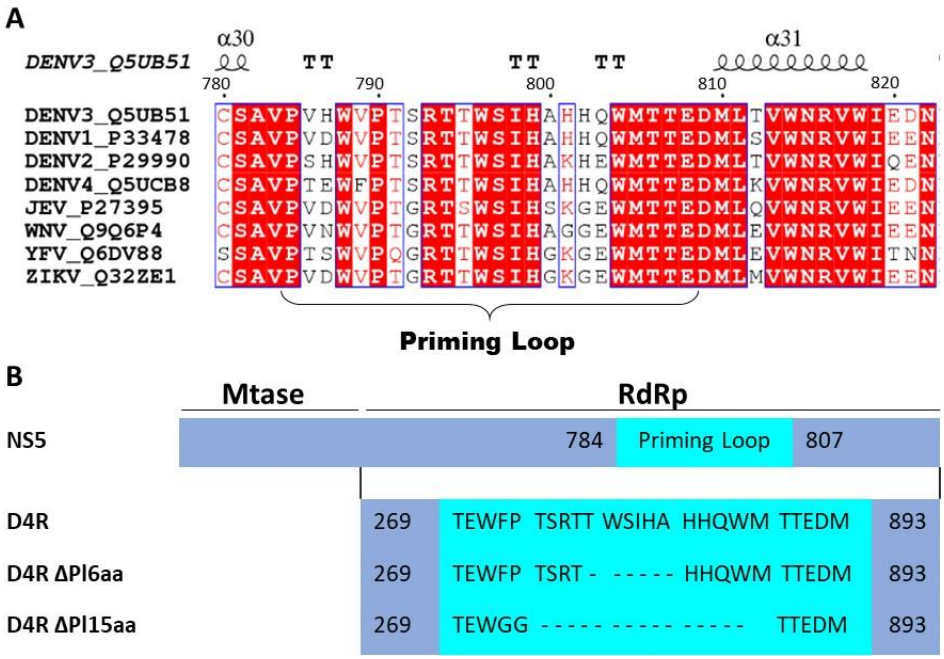

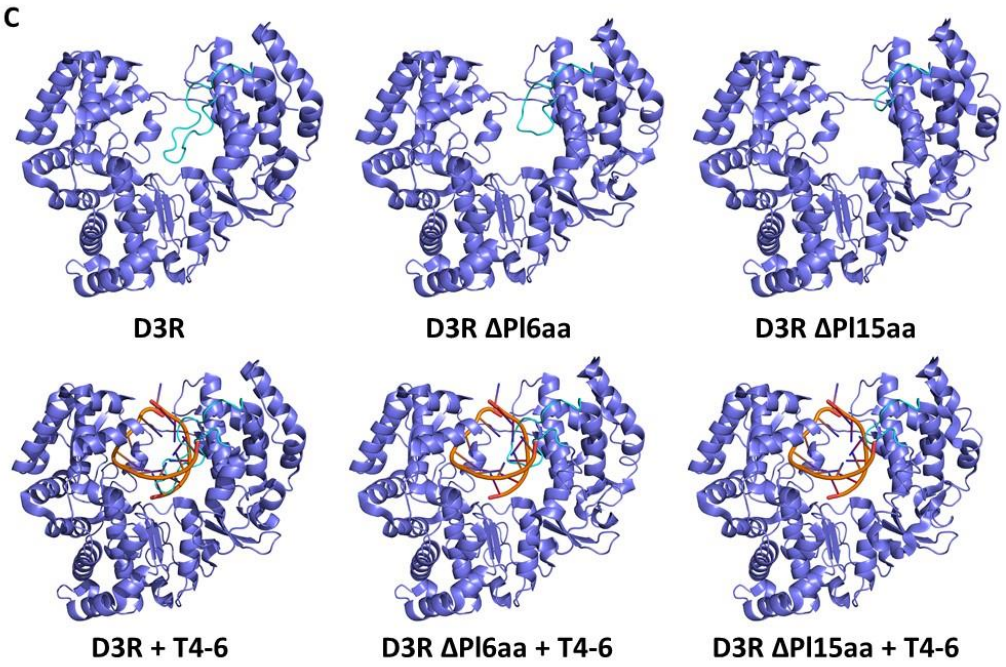


**Figure 4.1.1. Dengue RdRp priming loop deletion construct.** (**A**) The primary sequence conservation of priming loop in the Flavivirus' RdRps are presented through Espript (Gouet et al., 2003). The secondary structures are labelled on top of the alignment, spring icon and (TT) are used to represent alpha helixes and turns respectively. The amino acid residues which are highly conserved are boxed in red columns, while the amino acid residues which share similar functional groups are boxed in blue. (**B**) All the D4R constructs consist of residue 269 to 893. Residue 794 – 799 were removed in ΔPl6aa construct while residue 788 – 804 were replaced by GG in the ΔPl15aa construct. (**C**) The protein structure of D3R was obtained from PDB: 2J7U. The representative protein structures of the priming loop mutant constructs were modified from PDB: 2J7U. Structures of the RdRp with T4-6 RNA were modelled via structural superposition using Foot and Mouth Disease Virus polymerase-RNA structure (PDB: 2E9R) in Pymol (Delano, 2009). The structures are represented in the cartoon. The RdRp is coloured in blue while the priming loop is coloured in cyan.

### 4.1.2 Biochemical characterisation of RNA for suitability

Next, different RNAs were tested for their suitability in forming elongation complex with the RdRp constructs. The designs of the RNAs used in this study were modified from previously published RdRp-RNA crystal structures of Foot Mouth Disease Virus, Enterovirus-71 and Poliovirus (**Figure 4.1.2A**) (Ferrer-Orta et al., 2007; Gong and Peersen, 2010; Shi et al., 2019).

The RNAs were assessed for elongation activity by D4R ΔPl6aa (**Figure 4.1.2B**). The RNAs were able to be extended by the RdRp, showing suitability for crystal screening.

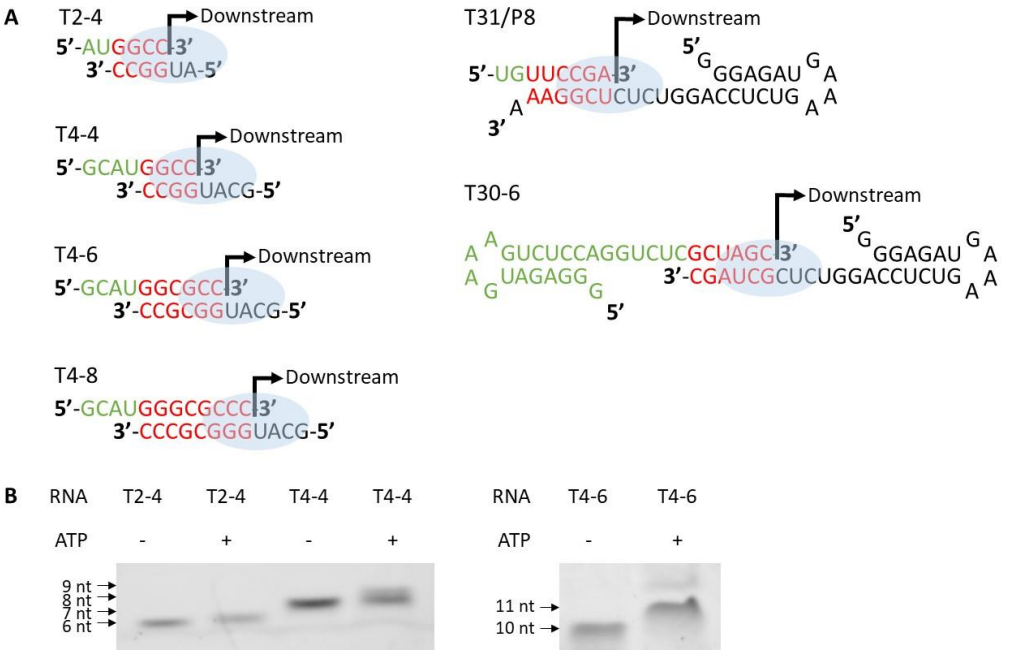


**Figure 4.1.2. Elongation activities of RdRp using different RNA substrates.** (**A**) The designs of RNA substrate were modified from previously published RdRp-RNA crystal structures of Foot Mouth Disease Virus, Enterovirus-71 and Poliovirus. The blue oval indicates the potential RdRp binding site. (**B**) 20% UREA PAGE profile to monitor nucleotide incorporation by D4R ΔPl6aa. The reactions without ATP served as negative controls.

### 4.1.3 Crystallization of DENV polymerase priming loop mutant-RNA elongation complexes

The RdRp-RNA complexes were assembled in the absence of NTPs or 1 mM ATP/GTP by incubating the various RdRp protein with the pre-annealed RNA at a 1:1.2 molar ratio on ice for 1 hour. Slight precipitation was observed and was clarified by centrifugation before being screened using commercial crystallization kits.

Out of all the screening conditions, only 1 condition, PegIon D1, manage to have plate crystal formation after 14 days in drop containing D4R-T4-6. While for several conditions, microcrystals formed after 5 days for D4R ΔPl6aa in complex T4-6 and T4-8 RNAs and 14 days for D4R in complex with T4-6 and T4-8 RNAs (**Figure 4.1.3** and **Table 4.1**). All the positive hits were illuminated with ultraviolet light and were confirmed to be protein crystals. Despite various attempts to optimise the screening conditions, the microcrystals do not increase in size to proceed for data collection. Unexpectedly, the plate crystal formed in PegIon D1 cannot be reproduced for data collection.

**Table 4.1.1. Crystallization buffer conditions that resulted in microcrystal/crystal formation.** Most of the crystallization conditions produced microcrystals while only one condition generated protein crystals.

| Buffer Condition | Crystal Form | Protein Construct | RNA |
|---|---|---|---|
| PegIon D1 | Plate | D4R | T4-6 |
| PegRx C2 | Micro-crystal | D4R | T4-6 |
| Natrix D7 | Micro-crystal | D4R | T4-6 |
| Index F1 | Micro-crystal | D4R | T4-8 |
| PegRx C2 | Micro-crystal | D4R | T4-8 |
| PegRx D6 | Micro-crystal | D4R ΔPl6aa | T4-6 |
| PegRx G2 | Micro-crystal | D4R ΔPl6aa | T4-6 |
| PegRx C3 | Micro-crystal | D4R ΔPl6aa | T4-8 |

**A** Protein Construct: D4R

RNA: T4-6

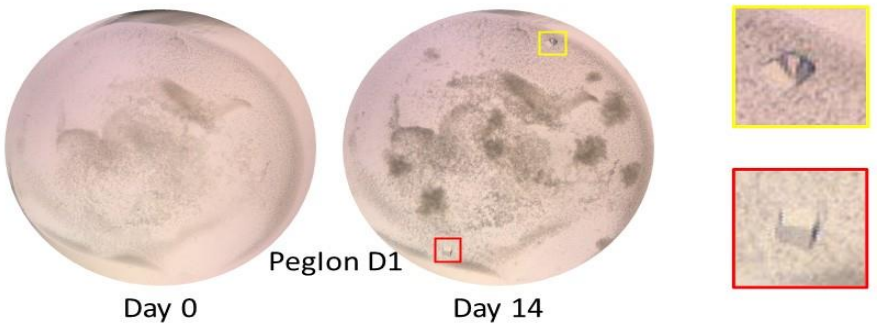


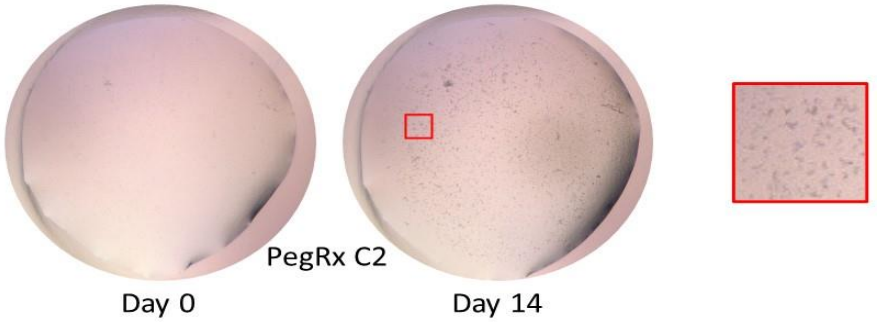


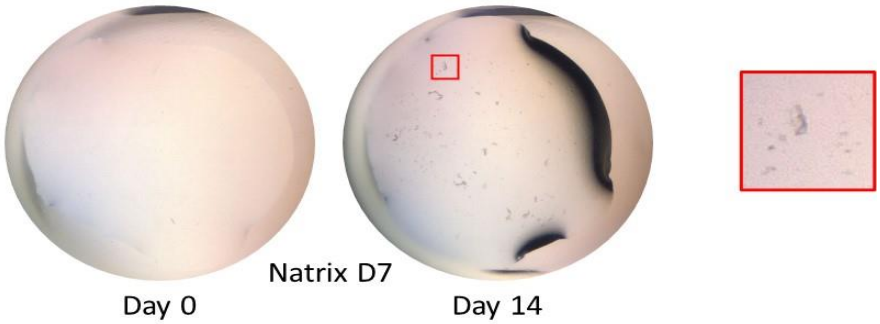


Protein Construct: D4R

RNA: T4-8

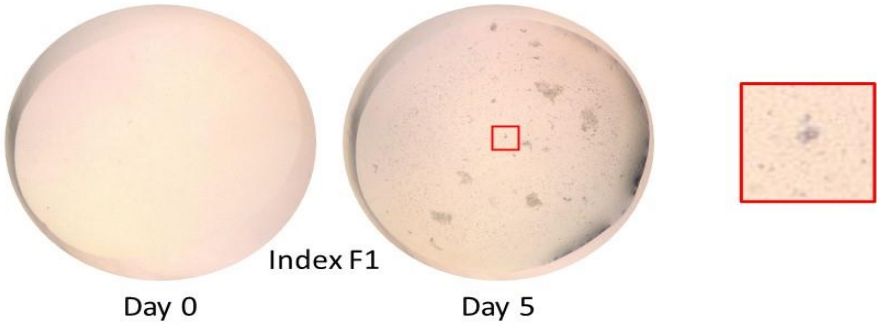


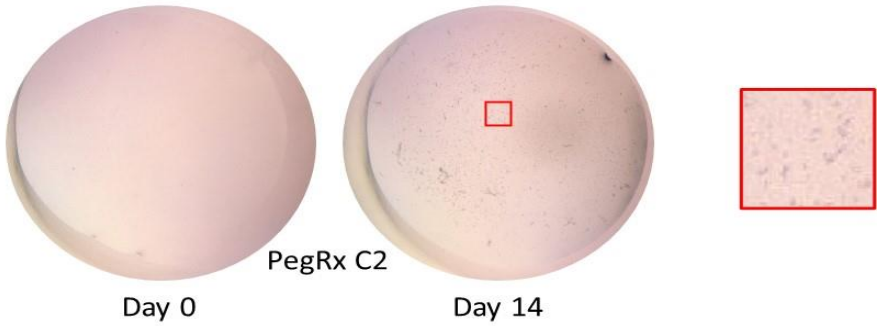

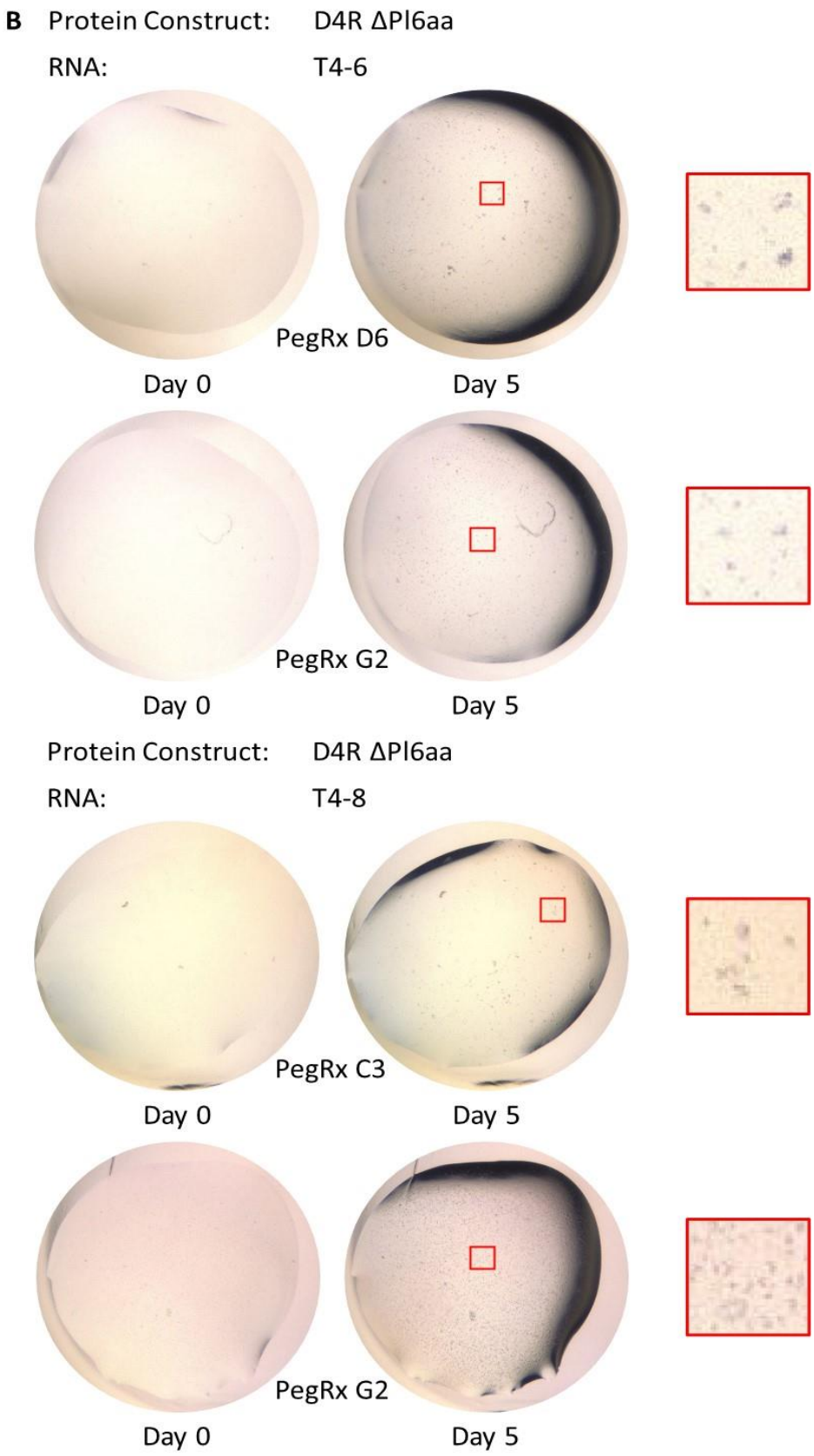


**Figure 4.1.3. Crystals obtained from the screening of DENV-4 RdRp-RNA complexes** (**A**) Images from screening D4R in complex T4-6 and T4-8 RNAs. (**B**) Images from screening D4R ΔPl6aa in complex T4-6 and T4-8 RNAs. The boxed areas were enlarged and shown on the right.

### 4.1.4 Discussion

In this section, we have designed various priming loop deletion mutants. Given that the priming loop is mainly involved in the initiation stages of RNA replication, it was expected that the mutants can still participate in the elongation of the RNA substrate. Next, different designs of RNA were assessed for their suitability in forming the elongation complex through RNA extension.

The NS5-RNA were mixed directly and used for crystal screening. While numerous crystallization buffer conditions enable the growth of protein microcrystals. Buffer optimization did not help in increasing the size of the crystal formation.

A previous study by Wu et al. shows that the elongation complex formed precipitation and can be resuspended with a reaction buffer containing 200 mM NaCl (Wu et al., 2020). This suggests that the precipitants formed during the incubation consist of an active elongation complex which was always removed before crystallization set up. This also suggests that upon RNA binding, conformational changes occur, and higher salt concentration is essential to stabilise the complex formation.

Although the priming loop is no longer obstructing the RNA tunnel, the priming loop deletion mutants might not represent the conformation of the RdRp at the elongation stage as other global conformational changes could also be expected. Thus, it might not form a proper protein-RNA complex for crystallisation.

## 4.2 Biochemical characterisation of the NS5-U1A fusion protein

To improve the binding affinity of NS5 to RNA, the fusion of an RNA recognition motif (RRM) to NS5 was hypothesised. Among the protein with known RRM, the interaction between spliceosomal U1 small nuclear ribonucleoprotein A (U1A) and the hairpin II of the U1snRNA was well characterised (Law et al., 2006). While the U1A protein contains 2 RRMs, the N-terminal RRM was enough for binding to the hairpin II with high affinity (Law et al., 2006). Hence, the fusion protein was designed with the N-terminal RRM of U1A directly fused to the C-terminal ends of the NS5 protein. The last five C-terminal residues of NS5 were restored to the NS5 protein to aid in the folding and improve the solubility of the fusion protein (**Figure 4.2.1A**).

Next, biochemical assays were conducted to check if the addition of the U1A motif affected the activity of NS5. Firstly, a polymerase assay was carried out using T8-11 hairpin RNA. Both the fusion protein and NS5 were able to fully elongate T8-11 RNA (**Figure 4.2.1B**). Subsequently, the polymerase assay was repeated using T8-11 U1A hairpin RNA, which contains a U1A recognition sequence, AUUGCAC. Interestingly, while NS5 were about to elongate the RNA from 38 bases to 46 bases, the fusion protein only manages to elongate a fraction of the RNA, with most of the T8-11 U1A remaining unchanged (**Figure 4.2.1C**).

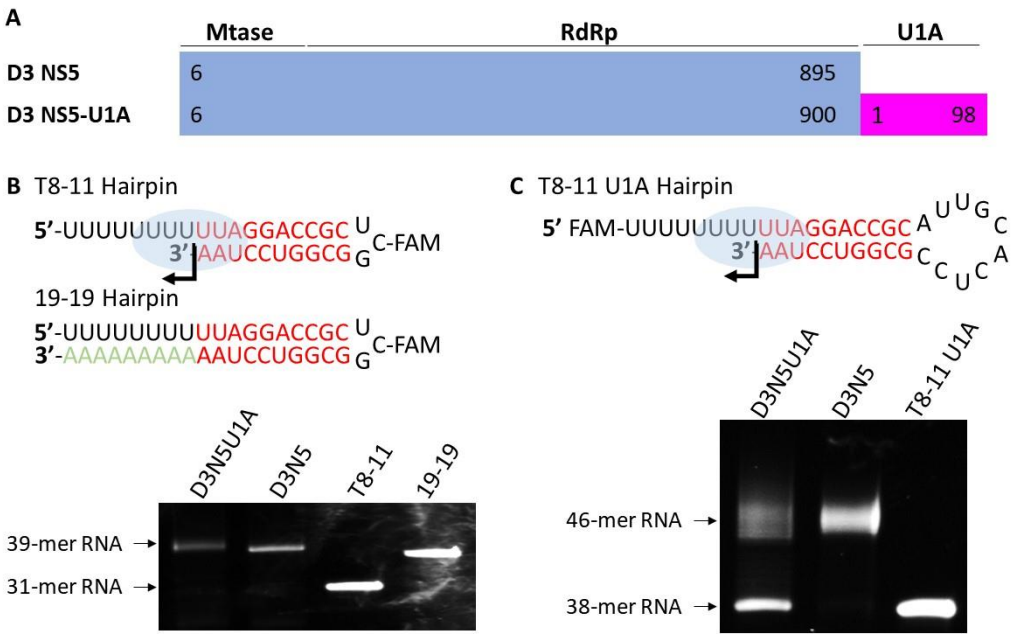


**Figure 4.2.1. Biochemical characterisation of the NS5-U1A fusion protein** (**A**) The NS5-U1A fusion protein design. The N-terminal RRM, residues 1 – 98, were linked to NS5 protein, residues 6 – 900. (**B**) The polymerisation activity of NS5 protein on T8-11 hairpin RNA. Both NS5-U1A and wild type NS5 were able to elongate T8-11 hairpin RNA from 31-mer to 39-mer with reference to the 19-19 RNA control. (**C**) The polymerisation activity of NS5 protein on T8-11 U1A hairpin RNA. Wild type NS5 can completely elongate T8-11 U1A hairpin RNA from 38-mer to 46-mer, however, the NS5-U1A only manage to elongate some of the RNA to 46-mer RNA.

Recently, an EM structure was solved for NS5 in complex with human STAT2 protein (Wang et al., 2020). Hence, instead of X-ray crystallography, we attempted to capture the EM structure of NS5-U1A fusion protein in complex with STAT2 and U1A RNA. To purify the triple complex, the NS5-U1A protein were incubated with the STAT2 and U1A hairpin RNA at a 1:1:1.2 molar ratio on ice for 1 hour. Subsequently, they were purified using the S200 gel filtration column. We managed to isolate the triple complex as shown by the shift in the peak elution volume at 12.5 ml, in contrast to the peak elution volume of 14.1 and 13.2 ml for the individual NS5-U1A and hSTAT2 respectively (**Figure 4.2.2**). Comparing the $UV_{280}$:$UV_{260}$ ratio, it also indicated a protein-RNA complex. The

eluted samples were further examined using SDS PAGE and UREA PAGE, which also shows the co-elution of NS5-U1A, hSTAT2 and T8-11 U1A RNA, indicative of the complex formation (**Figure 4.2.2**). Next, to ensure that the triple complex remains functional, a polymerase assay was also conducted by the addition of ATP to the eluted sample. The purified complex retains the polymerase activity (lane 2) as compared to the crude mixture (Lane 3) (**Figure 4.2.2C**).

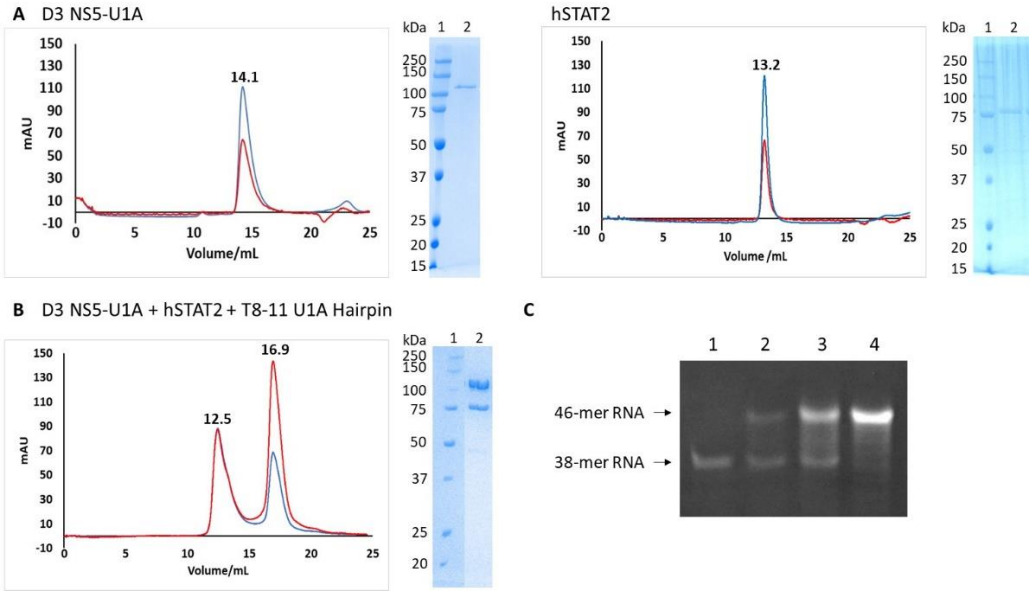


**Figure 4.2.2. Purification of NS5-U1A Fusion Protein in complex with T8-11 U1A hairpin RNA by Gel Filtration** (**A**) S200 purification profile of 0.25 mg Apo NS5-U1A fusion protein and 0.25 mg hSTAT2 protein. The absorbance at $UV_{260}$ and $UV_{280}$ are represented in red and blue curves respectively. The NS5-U1A has a peak elution volume of 14.1 ml while hSTAT2 has a peak elution volume of 13.2 ml. SDS-PAGE analysis revealed protein bands with a molecular weight of 115.4 kDa and 82.5 kDa which correspond to D3 NS5-U1A and hSTAT2 respectively. (**B**) S200 purification profile of NS5-U1A fusion protein in complex with hSTAT2 and T8-11 U1A hairpin RNA. The triple complex has a peak elution volume of 12.5 ml and the excess T8-11 U1A RNA eluted at 16.9 ml. SDS-PAGE analysis revealed the co-elution of D3 NS5-U1A and hSTAT2. (**C**) Polymerase activities of NS5-U1A protein after gel filtration. Lane 1: Purified NS5-U1A/hSTAT2/T8-11 U1A hairpin RNA triple complex. Lane 2: Purified NS5-U1A/hSTAT2/T8-11 U1A hairpin RNA triple complex with the addition of 500μM ATP. Lane 3: Crude NS5-U1A/hSTAT2/T8-11 U1A hairpin RNA with the addition of 500μM ATP. Lane 4: Crude NS5/hSTAT2/T8-11 U1A hairpin RNA with the addition of 500μM ATP.

Subsequently, cryo-EM imaging was performed on the purified triple complex. The cryo-EM dataset was only able to process and achieve the highest resolution of around 7Å. Nevertheless, using the recently solved cryo-EM structure of the ZIKV NS5–hSTAT2 complex (Wang et al., 2020), the NS5 and STAT2 could be modelled into the low-resolution density map (**Figure 4.2.3**). However, no extra density was observed to model both the U1A domain and the RNA. This result strongly suggests that the U1A domain is flexible and was likely averaged out during the data processing cycle. Furthermore, despite being able to purify an RNA bound complex, the RNA-NS5 complex remains unstable to be visualised under EM.

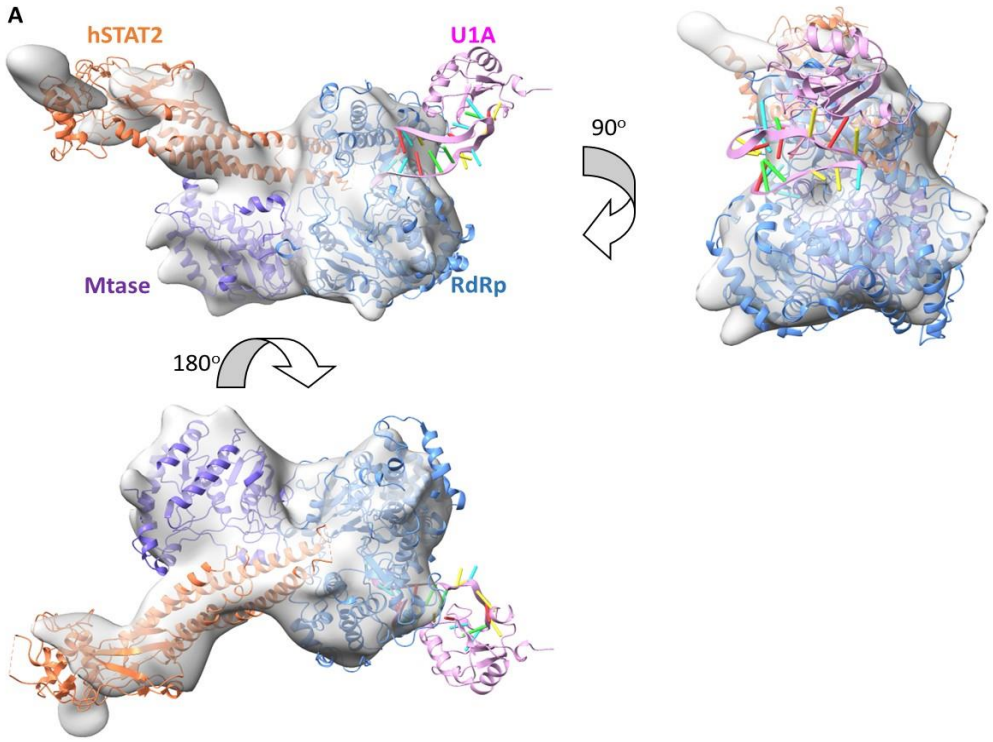


**Figure 4.2.3. Cryo-EM structure of the NS5-U1A-hSTAT2 RNA triple complex.** (A) The cryo-EM density map is represented in surface views. The cryo-EM structure of the ZIKV NS5–hSTAT2 complex (PDB: 6WCZ) was used as a reference and fitted into the cryo-EM density map. U1A-RNA structure (PDB: 1URN) was used to model an RNA-bound state for NS5. The protein structure is represented in the cartoon, with the NS5 is coloured in blue, hSTAT2 in orange and U1A in pink. (The cryo-EM data collection and processing are conducted by Dr Zhang Kuo)

### 4.2.1 Discussion

In this section, we have introduced an RRM to DENV-3 NS5 protein to improve its binding affinity to RNA. This approach was successful, and an active protein-RNA complex was isolated using liquid chromatography (**Figure 4.2.2**). Interestingly, while the NS5-U1A fusion protein remains functional with catalytic activity, it is unable to polymerise all RNA substrates with the U1A recognition sequence (**Figure 4.2.1B** & **C**). This finding may suggest that upon RNA binding to the U1A domain, the U1A domain could restrict the NS5 protein from binding and elongate the RNA in cis. However, neighbouring NS5 can still interact and elongate the RNA in trans. Future experiments to increase the linker length between NS5 and U1A domain or the use of longer RNA can be considered to promote the polymerisation of the RNA with the U1A recognition sequence. Enzyme kinetic studies can also be conducted to assess the influence of RNA binding and motility on the catalytic rate of NS5.

An article by Bronzoni et al reported that U1A protein interacts with YFV NS5 between residue 431 and 448 (Bronzoni et al., 2011). The interaction residues show sequence conservation of 71% with DENV-3 NS5, which suggests that U1A protein may also interact with DENV-3 NS5 protein and position the RNA away from the active site for polymerisation. As such, other RRMs with no known interaction with the NS5 protein can also be considered to prevent any conformation bias introduced due to protein-protein interactions.

Unfortunately, while we were able to isolate the RNA bound complex, the interaction to the RNA is still mainly contributed by the U1A domain, the binding of RNA by NS5 remains unstable for the visualisation of RNA at the RNA tunnel of the RdRp. As such, other strategies should be explored to lock the RNA into the RNA tunnel of the RdRp in addition to using RRM to improve affinity to RNA.

Nucleoside inhibitors can be explored to capture the elongation complex structure. Recently, remdesivir was used to capture the elongation complex structure of SARS-CoV-2 with double-stranded RNA (Yin et al., 2020)

Alternatively, formaldehyde crosslinking is also commonly used to study protein-nucleic acid interaction through the formation of a reversible covalent bonding to form protein-RNA complexes (Hoffman et al., 2015).

# Chapter 5: Biochemical Characterisation of the Minimal Replication Complex

Several processes of the viral genome replication occur within the replication complex. Although numerous studies have characterised the individual NS protein components of the RC as well as the protein-protein interactions between different NS proteins as discussed in Chapters **1.2.4** and **1.2.5**. However, neither the precise molecular mechanisms of the viral RNA replication nor the dynamics of these proteins in the replication complex during the replication process have yet to be fully identified. By understanding the *flavivirus* replication complex, it can provide unique insights and develop alternative target sites to manage the diseases caused by the *flavivirus,* in contrast, to directly inhibit the viral enzymatic activities. This is exemplified by the success of NS4B inhibitors which works by disrupting NS3 and NS4B interactions.

In this chapter, we developed a simple bacterial reporter assay to identify the key players involved during negative-sense RNA synthesis. C-terminal NS2B, NS3 and NS5 were identified to be sufficient for negative-sense RNA synthesis from the assay. Furthermore, we also attempt to reconstitute a minimal active replication complex for structural study. NS5 and viral RNA can be reconstituted as a complex in vitro, while NS3 binding is unstable.

## 5.1 Assay development to characterise negative-sense RNA synthesis

Currently, the conventional methods of studying the functionality of the flavivirus replication complex involved the use of replicons or infectious clones. Furthermore, these methods usually study the viral RNA replication as a whole process without detailed analysis of the different stages of RNA replication. Hence, there is a need to develop a robust in-vitro replication system that can segregate and study the various individual molecular events. In doing so, it can allow scientists to characterise the dynamic changes from one process to another as well as the molecular architectures of the replication complex during the different stages of replication.

In this section, we explored the possibility of a unique assay to study the first step of viral RNA replication, negative-sense RNA synthesis. The negative-sense RNA serves as a template for the generation of numerous strands of positive RNA, for viral translation and the genome of progeny virus. To date, there are limited studies on the negative-sense RNA synthesis, although mainly NS3 and NS5 were proposed to be involved in the process.

Hence, we developed a simple reporter assay system in a bacterial system that aims to identify the viral proteins required to form a minimal functioning replication complex that are essential for negative RNA synthesis. The bacterial system was proposed due to the lack of eukaryotic host factors. Furthermore, *E. coli* cells are fast-growing and easily manipulated. The design of the reporter assay is that the ribosome binding site (RBS), start codon and renilla luciferase gene, are encoded in a reverse complementary direction. In the absence of a

functional RC, the ribosomes are unable to recognise the RBS in reverse complementary direction, to translate the mRNA and produce the renilla luciferase proteins. Only in the presence of an active and functional RC, the negative-sense RNA will be synthesised and revert the reporter gene in 5'-3' end direction for translation. To ensure that the RC will recognise the reporter RNA, the reporter's gene is flanked by the 5' and 3' UTR of the viral genome. The design of the reporter assay is illustrated in **Figure 5.1.1**.

### 5.1.1 Proof of concept of the reporter assay

To test the concept and functionality of the reporter assay, a native Zika C-terminal NS2B-5 protein construct was used. It was observed that only *E. coli* cells that were transformed with both the reporter plasmid and protein expression vector plasmid show an increase in luciferase reading (**Figure 5.1.1E**). This demonstrated that only in the presence of viral protein, acting as a functional RC, will the negative-strand RNA encoding the reporter in the correct orientation be synthesised, allowing the translation of the luciferase protein. The result verifies that this approach can be used to detect negative-strand RNA synthesis.

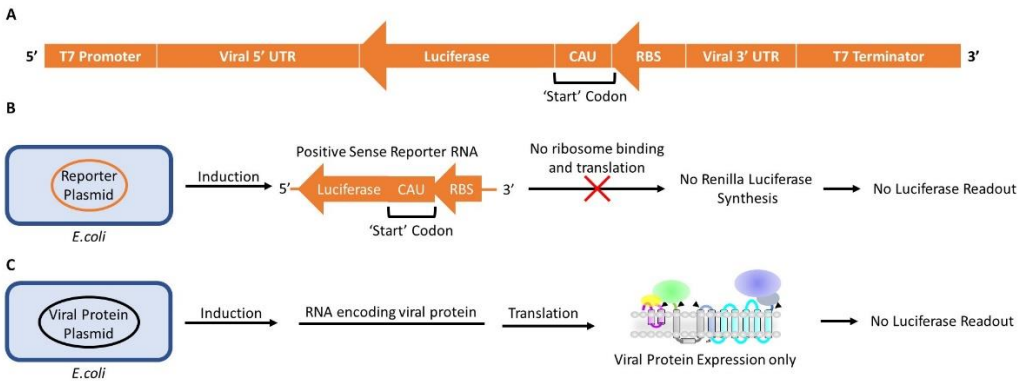

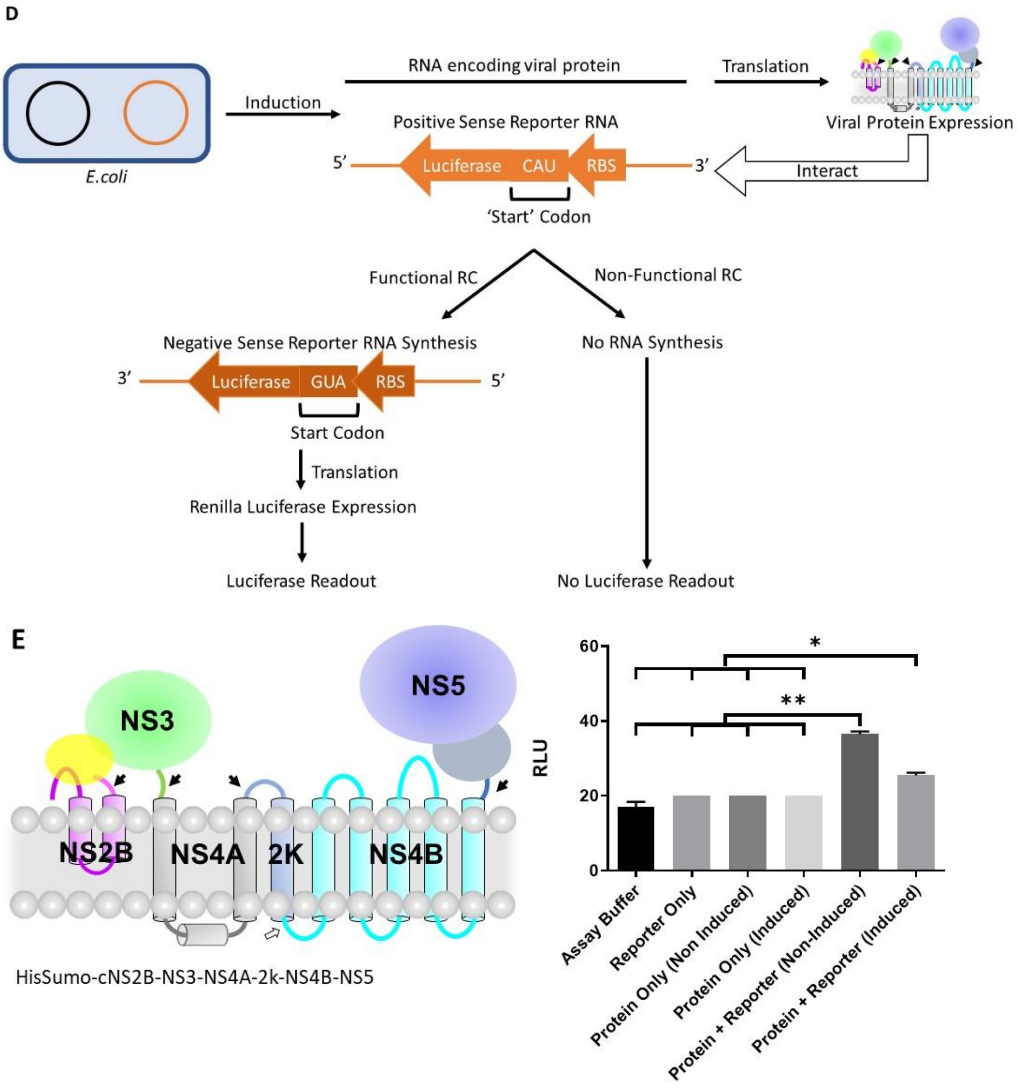


**Figure 5.1.1. Negative-sense RNA synthesis detection using a reporter assay.** (**A**) The reporter plasmid design. The reporter expression system encodes the ribosome binding site (RBS), start codon and luciferase gene in a reverse complementary direction that is flanked by the viral UTR. The whole expression system is under the control of the T7 promoter. (**B**) The design of the reporter assay with the *E. coli* cells transformed with only the reporter plasmid. Upon induction, the positive reporter RNA will be synthesised. However, as the RBS and start codon are in the reverse complementary direction, the ribosomes are unable to bind and translate the mRNA to produce the luciferase protein. (**C**) The design of the reporter assay with the *E. coli* cells transformed with only the plasmid encoding viral proteins. Upon induction, the RNA encoding the viral proteins will be synthesised. The viral proteins are unable to generate luciferase readout. (**D**) The design of the reporter assay. *E. coli* cells are transformed with plasmid encoding viral proteins and the reporter plasmid. Upon induction, RNA from both plasmids will be synthesised. If the viral proteins form a functional replication complex, it will synthesis a negative-sense RNA using the reporter RNA as a template. The negative-sense RNA, with the functional element in the 5' to 3' direction, will subsequently be translated to produce luciferase protein for luciferase assay measurement. (**E**) Native Zika C-terminal NS2B-5 protein construct and the

luminescence reading generated from 5E9 *E. coli* cells transformed with different plasmids. The results are described as means ± SD from at least three independent experiments. The statistical significance was compared independently to the buffer control, reporter plasmid only control group, protein-only control group. * = P $\leqslant$ 0.05; ** = P $\leqslant$ 0.01; non-significance ns= P > 0.05.

### 5.1.2 Characterisation of the involvement of NS protein during negative-sense RNA synthesis

Next, we seek to investigate what is the minimal functional unit required for negative RNA synthesis. 6 different protein constructs containing different combinations of NS proteins were generated (**Figure 5.1.2**).

Firstly, since NS3 and NS5 contain all the enzymatic domains of the replication complex, we wanted to investigate if just NS3 and NS5 will be sufficient to generate the negative-sense RNA However, from the luminescence reading, there was no significant increase in luminescence reading compared to the negative control, indicating that NS3 and NS5 were unable to constitute as a functional replication complex (**Figure 5.1.2A**).

Next, we hypothesised that the introduction of membrane regions can help to localise the proteins onto a membrane, to limit diffusion and promote protein and RNA interaction. The C-terminal membrane region of NS2B was introduced into the second protein construct. It was observed that there is an increase in luminescence reading, indicating the presence of a functional replication complex (**Figure 5.1.2B**). NS5 polymerase GNN mutant was also introduced into the second construct. The mutant eliminates the increase in luminescence reading, validating the functionality of protein construct 2.

To test if different membrane regions can also contribute to the formation of an active replication complex. 4 other constructs with different membrane regions were designed. Construct 3, 5 and 6 were able to generate a slight increase in luminescence reading compared to the negative control (**Figure 5.1.2C - F**). Surprisingly, construct 3 and 6 were not able to generate luminescence reading as high as construct 2 even though they contain the protein components found in construct 2.

A

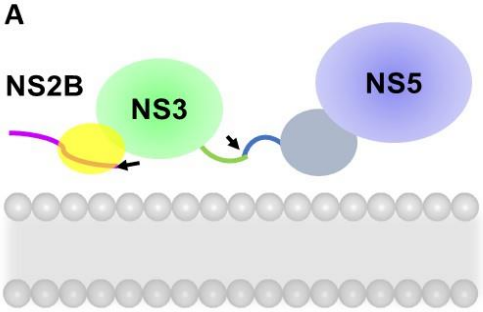


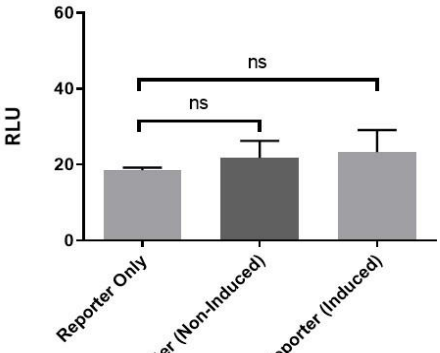


1. HisTev-eZiNS3-StrepHisSumo-NS5

B

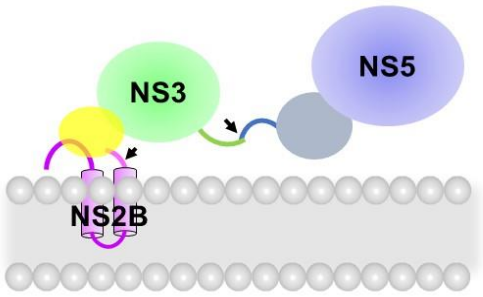


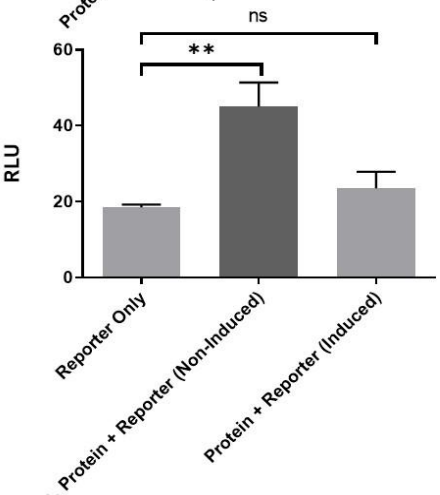


2. HisTev-cNS2B-ZiNS3-StrepHisSumo-NS5

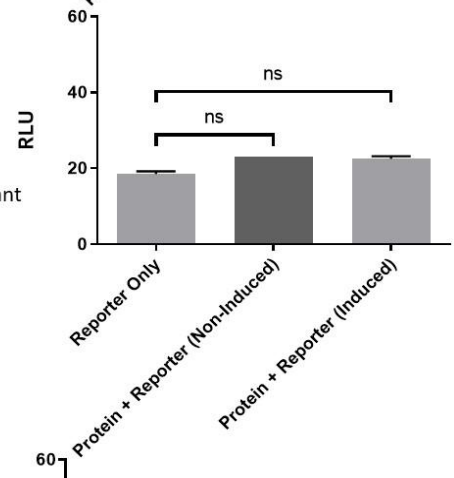


2a. HisTev-cNS2B-ZiNS3-StrepHisSumo-NS5 GNN Mutant

C

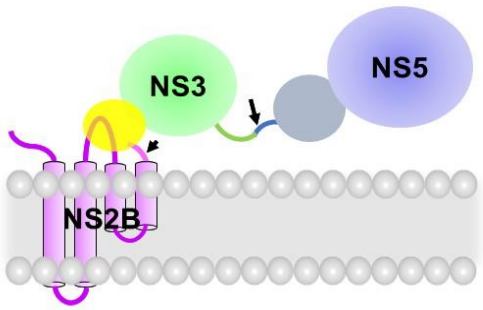


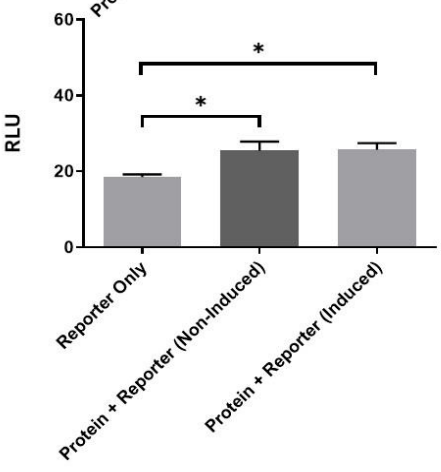


3. HisTev-NS2B-NS3-StrepHisSumo-NS5

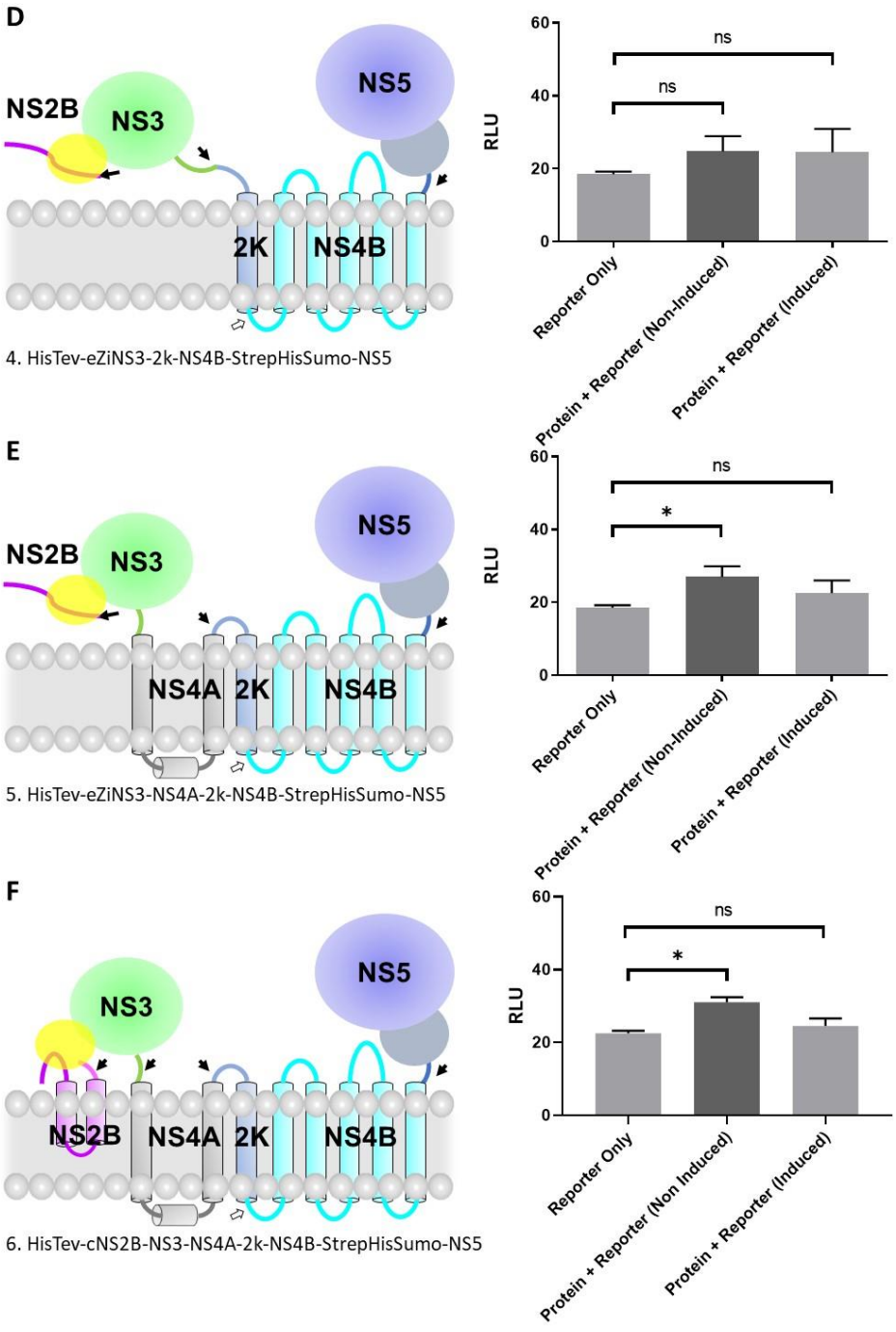


**Figure 5.1.2. Different Non-Structural Protein Constructs and negative RNA synthesis activity.** The construct design and luminescence reading from 5E9 *E. coli* cells are shown. (**A**) Construct containing only NS3 with cofactor NS2B and NS5. (**B**) Construct containing C-terminal membrane region NS2B, NS3 with cofactor NS2B and NS5. (**C**) Construct containing NS2B, NS3 and NS5. (**D**) Construct containing NS3 with cofactor NS2B, 2K-NS4B and NS5. (**E**) Construct containing NS3 with cofactor NS2B, NS4A, 2K-NS4B and NS5. (**F**) Construct containing C-terminal membrane region NS2B, NS3 with cofactor NS2B, NS4A, 2K-NS4B and NS5. The results are described as means ± SD from at least three independent experiments. The statistical significance was compared independently to the reporter plasmid only control group. * = $P \leqslant 0.05$; ** = $P \leqslant 0.01$; non-significance ns= $P > 0.05$.

### 5.1.3 Discussion

Out of the 6 constructs tested, construct 2 (**Figure 5.1.2B**) produced the highest luciferase signals, suggesting that the C-terminal membrane region of NS2B is required for the functionality of the replication complex.

However, even though construct 3 (**Figure 5.1.2C**) and construct 6 (**Figure 5.1.2F**) have similar protein components found in construct 2, it unable to generate luciferase signals as high as in construct 2. Furthermore, construct 6 is representative of the native construct used in the validation experiment (**Figure 5.1.1E**), with differences in codon usage optimisation and the addition of more affinity tags. This could be because *E. coli* is incapable of folding the extra membrane proteins component correctly, suggesting the limitation of this system.

Interestingly, non-induced samples have a higher signal luciferase signal than the induced samples. Both the protein and reporter plasmids are under the control of T7 polymerase. During the non-induced state, leaky expression of the T7 promoter provides a small amount of both reporter RNA and viral protein RNA for the reporter assay to function. However, upon IPTG induction, the reporter plasmid in a high-copy number pUC-57 vector could drive the over-production of the reporter RNA instead of viral protein RNA for translation. Thus, in contrast to the non-induced state, viral proteins are produced in a less optimal state, leading to low readout.

The reporter system can also be further expanded to detect capped RNAs, which are foreign in the bacterial system, such as using anti-7-methylguanosine cap antibody.

Even though, our bacterial reporter system can help to putatively identify the protein components involved in the negative sense RNA synthesis and allow us to assemble a minimal functioning replication complex. However, the lack of an authentic host membrane system might not fully represent the situations found in infected cells, given the essential role of remodelled ER membrane as the site of RNA replication. Furthermore, the role of host factors in viral RNA replication should also be considered. PABPC1 and CDSE1 also bind the vRNA and may be involved in its translation, synthesis or stability. While the OST complex may function as a scaffold and act to synchronise RC assembly. Thus to fully dissect the players in the negative-sense RNA synthesis, this reporter assay can be systematically carried out in other biological systems, such as cell-free systems to verify the effects on the addition of membrane and in mammalian cells to study the influence of host factors.

### 5.2 *In vitro* reconstitution of replication complex for structural study

To date, while the protein structures of some of the NS proteins were solved. We still do not have a clear understanding of the protein arrangement and stoichiometry of the replication complex. In this section, we aim to perform *in vitro* reconstitution of the replication complex, using individually expressed and purified components of the replication complex, for structural studies. In doing so, we can identify novel interaction sites for drug targeting.

A mini genomic viral RNA containing 5'UTR, 3'UTR and the functional elements, UAR and CS, of a genomic viral RNA were designed (**Figure 5.2.1A**). The RNA was synthesised by in-vitro transcription and purified. Gel electrophoresis reveals a band size of around 295 bases that correspond to the expected RNA size (**Figure 5.2.1C**).

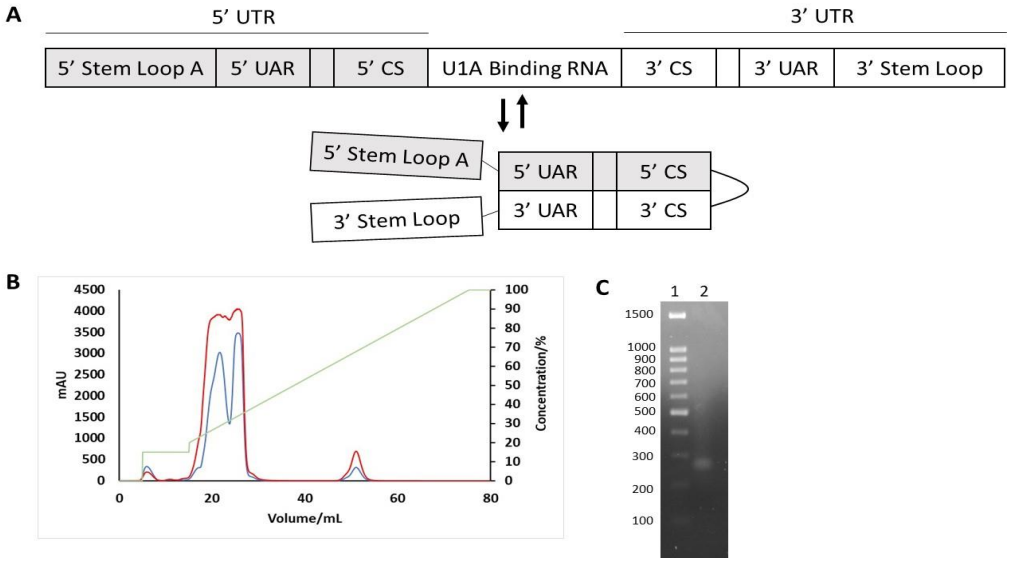


**Figure 5.2.1. In-vitro transcription of ZIKV mini-genomic viral RNA.** (**A**) The design of the ZIKV mini-genomic viral RNA. The linearised and cyclised genomes were shown on the top and bottom respectively. (**B**) Ion-exchange chromatography purification profile of in vitro transcript RNA. The absorbance at $UV_{260}$ and $UV_{280}$ are represented in red and blue curves respectively. (**C**) The purity of the eluted peak was analysed with 2% formaldehyde-agarose gel. The band corresponds to the size of the mini-genomic RNA of 295 bases.

To reconstitute the replication complex, the components were incubated on ice and purified using gel filtration chromatography. The gel filtration profiles were compared to analyse for any changes in peak elution volume to suggest complex formation. No shift in the peaks was observed for the reaction mixture containing NS3 and the viral RNA, suggesting that despite NS3 functioning as the viral helicase, it is unable to bind the mini-genomic RNA (**Figure 5.2.2D**). On the other hand, there is a clear shift in peak elution volume for the reaction mixture

containing NS5 RdRp and viral RNA as well as the mixture containing NS5 RdRp, NS3 and viral RNA from 11.0 ml to 10.6 ml and 10.7 ml respectively as compared to their individual protein constituents (**Figure 5.2.2E and 5.2.2F**). The shift in peak is indicative of a putative complex formation between NS5 RdRp and the viral RNA. Despite the addition of NS3 protein, it does not lead to any further shift in the peak, suggesting that NS3 protein might not bind strongly to the RdRp-RNA complex.

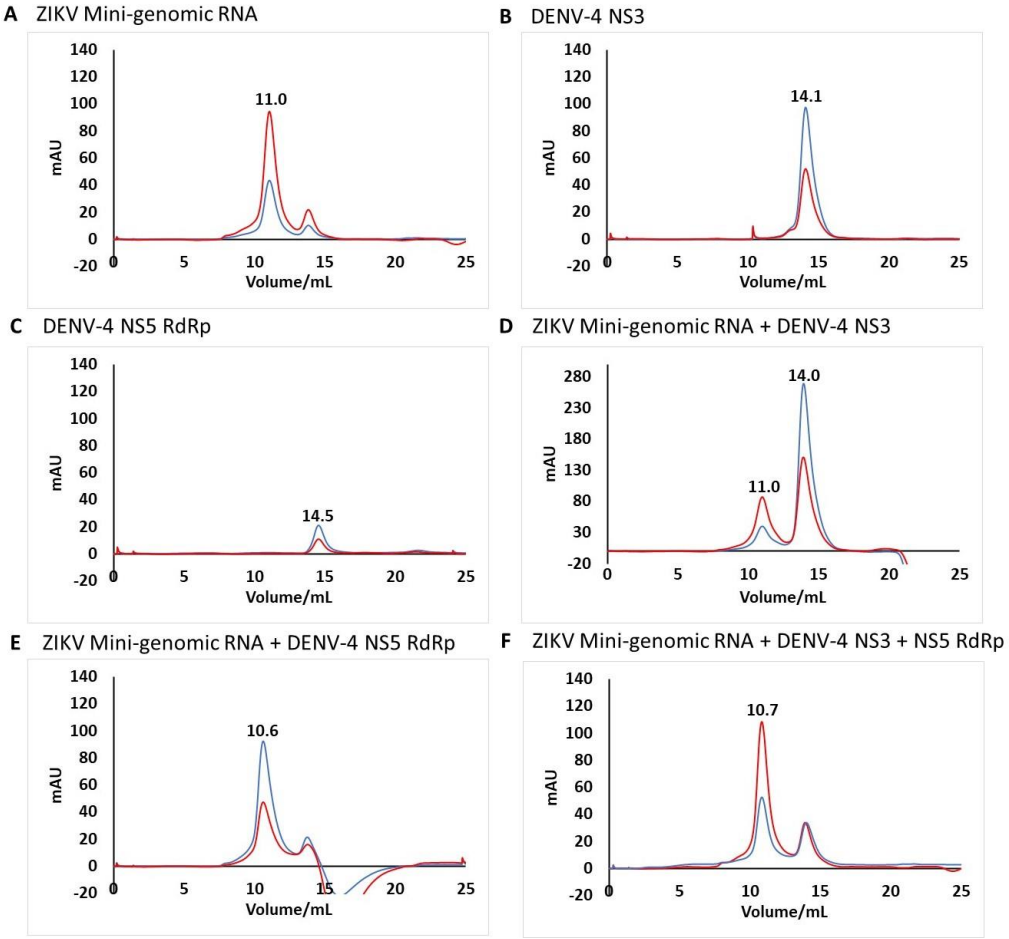


**Figure 5.2.2. In-vitro reconstitution of viral replication complex.** (**A**) Gel filtration profile of ZIKV mini-genomic RNA. (**B**) Gel filtration profile of 0.5 mg DENV-4 NS3 protein. (**C**) Gel filtration profile of 0.5 mg DENV-4 NS5 RdRp. (**D**) Gel filtration profile of DENV-4 NS3 with viral RNA. (**E**) Gel filtration profile of DENV-4 Rdrp with viral RNA. (**F**) Gel filtration profile of DENV-4 NS3, NS5 Rdrp and viral RNA. The absorbance at $UV_{260}$ and $UV_{280}$ are represented in red and blue curves respectively.

Next, to improve the binding affinity of NS3 to the complex, the NS3-NS5 fusion protein was designed. Multiple rounds of optimisations were carried out to improve the purity and yield of the full-length fusion protein. Finally, a phenylalanine mutation at the P1' residue position was introduced to prevent the viral protease from cleaving the NS3-NS5 junction. Various affinity tags pairings were also explored.

As shown in **Figure 5.2.2**, the presence of NS5 RdRp enables the association between the viral protein and RNA. The complex formation leads to the appearance of 2 additional peaks of elution volume of 9.2 ml and 10 ml (**Figure 5.2.3D**). Negative staining EM imaging was also conducted for the fusion protein with and without the viral RNA (**Figure 5.2.3C and Figure 5.2.3E**). However, both samples were not sufficiently homogenous which impedes further analysis.

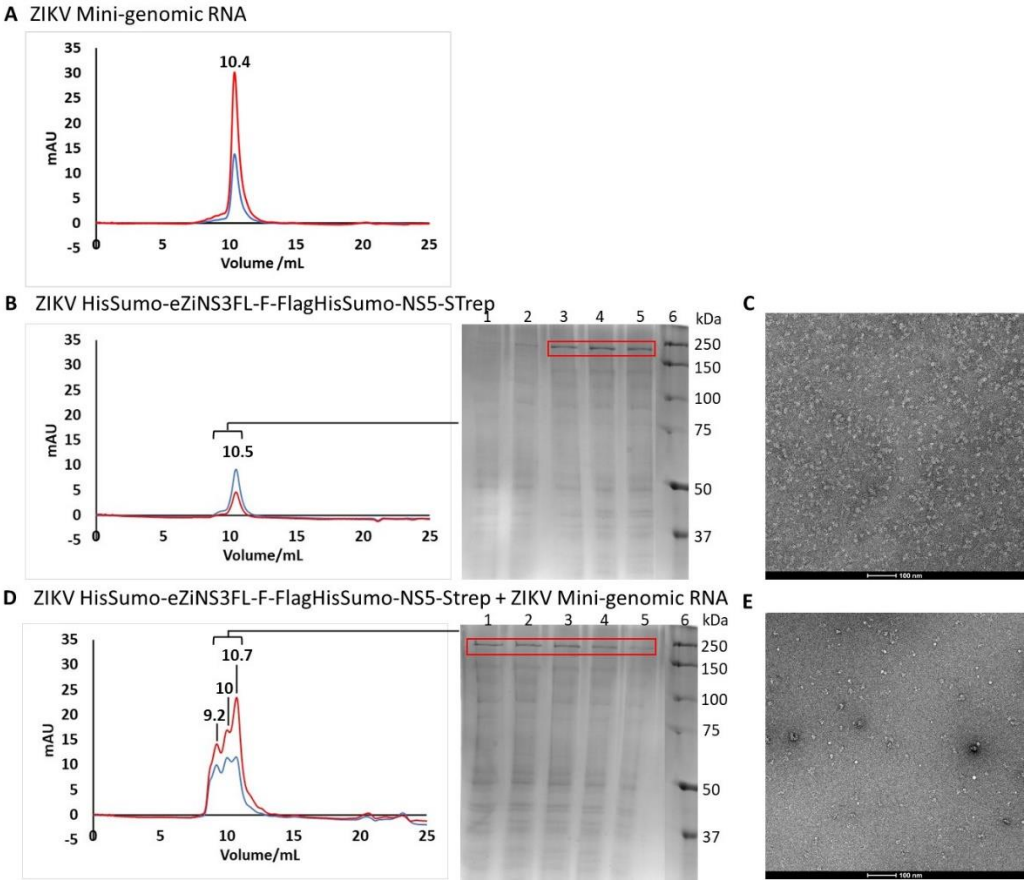


**Figure 5.2.3. In-vitro reconstitution of NS3-5-RNA viral replication complex.** (**A**) Gel filtration profile of ZIKV mini-genomic RNA. (**B**) Gel filtration profile of 0.25 mg ZIKV NS3-5 fusion protein. Sample from elution volume 9 to 11 ml were analysed with SDS-PAGE analysis. A protein band with a molecular weight of 205 kDa corresponds to ZIKV NS3-5 fusion protein. (**C**) Representative negative-staining EM image of ZIKV NS3-5 fusion protein. (**D**) Gel filtration profile of ZIKV NS3-5 fusion protein with viral RNA. Sample from elution volume 9 to 11 ml were analysed with SDS-PAGE analysis. A protein band with a molecular weight of 205 kDa corresponds to ZIKV NS3-5 fusion protein. (**F**) Representative negative-staining EM image of the peak with an elution volume of 9.2 ml for the mixture containing ZIKV NS3-5 fusion protein with viral RNA. The absorbance at $UV_{260}$ and $UV_{280}$ are represented in red and blue curves respectively.

### 5.2.1 Discussion

In contrast to the smaller RNA used in chapter 4, RNA remains bound to NS5 and the complex is purifiable using gel filtration liquid chromatography. The longer viral mini-genomic RNA can establish more charge-charge interaction with NS5 to form a stable complex. However, more analysis is required to investigate if the complex formed is of any biological significance, and if the RNA is binding at the catalytic site.

The inability of NS3 to bind to the mini-genomic RNA can also suggest that NS3 helicase unwind and acts on the double-stranded replication intermediate instead of the cyclised viral genome. The interaction between NS3 and NS5 might also be more prominent during positive sense RNA synthesis, where the RNA acts as an anchor bringing both NS3 and NS5 together, with NS3 unwinding the replication intermediate and NS5 synthesising the positive-sense RNA.

Future in-vitro reconstitution studies should consider the addition of more NS protein to stabilise the complex formation. Alternative approaches such as using a cell-free system can also be considered. Using a cell-free system can minimise the chances of disrupting the replication complex during cell lysis.

# Chapter 6: Conclusion and Future Directions

In this study, we set out to further characterise two attractive viral drug targets, NS3 and NS5. The flavivirus NS2B-NS3 protease plays an essential role in viral polyproteins processing and contributes to the host immune evasion mechanism by cleaving and inactivating host proteins. While the NS5 C-terminal RdRp domain is crucial for RNA synthesis during viral replication. Together, we hope to guide the design of antiviral compounds, to target and inhibit the different stages of the viral life cycle.

## 6.1 Conclusion

Given the limited numbers of flavivirus NS3 protease-inhibitor complex structures available as compared to HIV and HCV. We seek to study the interaction between bZiPro with other molecules to further our understanding of the substrate-binding site of viral protease. In chapter 3, we solved the crystal structures of bZiPro with two small fragments molecules, two proteolytic products of cyclic inhibitors, seven other intact peptidomimetics cyclic inhibitors. In addition, we also determined the inhibitory potency for the two different cyclic inhibitor series. The SAR study demonstrated that cyclic inhibitors provide improved inhibition activity as compared to their linear counterpart and the backbone ring size is one of the strongest determinants in influencing potency. By understanding how the different class of small types of fragment molecules and cyclic peptidomimetics inhibitors binds to the viral protease, it will be useful for future lead optimisation.

To aid in the design of specific competitive inhibitors targeting the RdRp, we attempt to capture the polymerase-RNA complex. In chapter 4, two methods were explored to capture the NS5-RNA complex, crystallisation of priming loop deletion mutants of the RdRp and EM imaging of NS5-U1A fusion protein. While the NS5-U1A RNA complex can be isolated, none of the approaches allows visualisation of the RNA-RdRp complex, and more optimisations are required to be carried out to obtain the ternary catalytic polymerase complex with short RNA.

To gain an understanding of the dynamics of the replication complex, in chapter 5, we developed a simple bacterial system to study the viral negative sense RNA replication process. Using this approach, we determined C-terminal NS2B region is integral to promote an active replication complex. In-vitro reconstitution of the viral replication complex was also carried out. Interestingly, in contrast to short RNA oligo, NS5 and viral mini-genomic RNA were able to form a stable complex. However, negative staining EM imaging revealed heterogenous particles, rendering the sample unsuitable for further structural analysis.

**6.2 Future directions and perspectives**

Although, we have determined the binding mode of a new class of inhibitors, cyclic peptidomimetics inhibitors, further optimisations are still required to improve the proteolytic stability as well as cell-penetrating activity of these inhibitors. Furthermore, ZIKV protease was used as the basis for the SAR studies, modifications should be carried on our identified inhibitors to improve their potency against other flaviviruses for the development of pan-flaviviral

inhibitors. In the meantime, structural studies of the protease in complex with other unique inhibitors should also be ongoing. For example, the binding modes of many competitive and allosteric inhibitors identified through HTS have yet to be characterised. In doing so, it will increase our structural database to be comparable to those of HCV and HIV, having more information to guide the development of successful protease inhibitors.

Extensive optimisations are needed to capture the NS5-RNA complex structures. Formaldehyde cross-linking can be explored to stabilise the complex structures for structural determination.

The bacterial reporter system provides opportunities for further optimisation and expansion to detect other steps of replication such as positive-sense RNA replication and viral RNA capping. Given that C-terminal NS2B was found to participate in negative-sense RNA synthesis, it should be included in future stepwise in vitro reconstitution of the replication complex. The understanding of the replication machinery will expand our understanding of viral replication and identify new protein-protein interactions as targets for antiviral development.

With all things considered, while DAAs is a proven antiviral therapeutic, resistance viruses towards DAAs were observed for HCV and HIV (Matthew et al., 2021). Escape mutants were also observed in the early studies of NS4B inhibitors. Hence, antiviral development targeting NS3 and NS5 remains paramount, for the development of antiviral cocktails to target the various NS proteins (NS3, NS4B and NS5) and prevent the emergence of resistant viruses.

To circumvent resistance to DAAs, understanding the host-virus interaction can also reveal potential host targets for drug development. However, drug development against host targets also faced issues such as off-targeting and unpredicted side effects. As such, drug screening and viral pathogenesis studies can be conducted in clinically representative models such as the use of induced pluripotent stem cells and differentiated organoids. Recently, brain organoids were successfully employed to study ZIKV infection (Krenn et al., 2021; Pettke et al., 2020)

## References


Acosta, E.G., Castilla, V., and Damonte, E.B. (2009). Alternative infectious entry pathways for dengue virus serotypes into mammalian cells. Cell Microbiol *11*, 1533-1549.

Adams, P.D., Afonine, P.V., Bunkoczi, G., Chen, V.B., Davis, I.W., Echols, N., Headd, J.J., Hung, L.W., Kapral, G.J., Grosse-Kunstleve, R.W.*, et al.* (2010). PHENIX: a comprehensive Python-based system for macromolecular structure solution. Acta Crystallogr D Biol Crystallogr *66*, 213-221.

Afonine, P.V., Grosse-Kunstleve, R.W., Echols, N., Headd, J.J., Moriarty, N.W., Mustyakimov, M., Terwilliger, T.C., Urzhumtsev, A., Zwart, P.H., and Adams, P.D. (2012). Towards automated crystallographic structure refinement with phenix.refine. Acta Crystallogr D Biol Crystallogr *68*, 352-367.

Aguirre, S., Luthra, P., Sanchez-Aparicio, M.T., Maestre, A.M., Patel, J., Lamothe, F., Fredericks, A.C., Tripathi, S., Zhu, T., Pintado-Silva, J.*, et al.* (2017). Dengue virus NS2B protein targets cGAS for degradation and prevents mitochondrial DNA sensing during infection. Nat Microbiol *2*, 17037.

Aguirre, S., Maestre, A.M., Pagni, S., Patel, J.R., Savage, T., Gutman, D., Maringer, K., Bernal-Rubio, D., Shabman, R.S., Simon, V.*, et al.* (2012). DENV inhibits type I IFN production in infected cells by cleaving human STING. PLoS Pathog *8*, e1002934.

Akey, D.L., Brown, W.C., Dutta, S., Konwerski, J., Jose, J., Jurkiw, T.J., DelProposto, J., Ogata, C.M., Skiniotis, G., Kuhn, R.J.*, et al.* (2014). Flavivirus NS1 structures reveal surfaces for associations with membranes and the immune system. Science *343*, 881-885.

Akiyama, B.M., Laurence, H.M., Massey, A.R., Costantino, D.A., Xie, X., Yang, Y., Shi, P.Y., Nix, J.C., Beckham, J.D., and Kieft, J.S. (2016). Zika virus produces noncoding RNAs using a multi-pseudoknot structure that confounds a cellular exonuclease. Science *354*, 1148-1152.

Aktepe, T.E., Liebscher, S., Prier, J.E., Simmons, C.P., and Mackenzie, J.M. (2017). The Host Protein Reticulon 3.1A Is Utilized by Flaviviruses to Facilitate Membrane Remodelling. Cell Rep *21*, 1639-1654.

Aktepe, T.E., and Mackenzie, J.M. (2018). Shaping the flavivirus replication complex: It is curvaceous! Cell Microbiol *20*, e12884.

Aleshin, A.E., Shiryaev, S.A., Strongin, A.Y., and Liddington, R.C. (2007). Structural evidence for regulation and specificity of flaviviral proteases and evolution of the Flaviviridae fold. Protein Sci *16*, 795-806.

Ang, L.W., Thein, T.L., Ng, Y., Boudville, I.C., Chia, P.Y., Lee, V.J.M., and Leo, Y.S. (2019). A 15-year review of dengue hospitalizations in Singapore: Reducing admissions without adverse consequences, 2003 to 2017. PLoS Negl Trop Dis *13*, e0007389.

Ang, M.J., Li, Z., Lim, H.A., Ng, F.M., Then, S.W., Wee, J.L., Joy, J., Hill, J., and Chia, C.S. (2014). A P2 and P3 substrate specificity comparison between the Murray Valley encephalitis and West Nile virus NS2B/NS3 protease using C-terminal agmatine dipeptides. Peptides *52*, 49-52.

Appleby, T.C., Perry, J.K., Murakami, E., Barauskas, O., Feng, J., Cho, A., Fox, D., 3rd, Wetmore, D.R., McGrath, M.E., Ray, A.S.*, et al.* (2015). Viral replication. Structural basis for RNA replication by the hepatitis C virus polymerase. Science *347*, 771-775.

Arroyo, J., Miller, C., Catalan, J., Myers, G.A., Ratterree, M.S., Trent, D.W., and Monath, T.P. (2004). ChimeriVax-West Nile virus live-attenuated vaccine: preclinical evaluation of safety, immunogenicity, and efficacy. J Virol *78*, 12497-12507.

Ashour, J., Laurent-Rolle, M., Shi, P.Y., and Garcia-Sastre, A. (2009). NS5 of dengue virus mediates STAT2 binding and degradation. J Virol *83*, 5408-5418.
Assenberg, R., Mastrangelo, E., Walter, T.S., Verma, A., Milani, M., Owens, R.J., Stuart, D.I., Grimes, J.M., and Mancini, E.J. (2009). Crystal structure of a novel conformational state of the flavivirus NS3 protein: implications for polyprotein processing and viral replication. J Virol *83*, 12895-12906.
Balasubramanian, A., Manzano, M., Teramoto, T., Pilankatta, R., and Padmanabhan, R. (2016). High-throughput screening for the identification of small-molecule inhibitors of the flaviviral protease. Antiviral Res *134*, 6-16.
Balinsky, C.A., Schmeisser, H., Ganesan, S., Singh, K., Pierson, T.C., and Zoon, K.C. (2013). Nucleolin interacts with the dengue virus capsid protein and plays a role in formation of infectious virus particles. J Virol *87*, 13094-13106.
Barik, S. (2002). Megaprimer PCR. Methods Mol Biol *192*, 189-196.
Barnard, T.R., Abram, Q.H., Lin, Q.F., Wang, A.B., and Sagan, S.M. (2021). Molecular Determinants of Flavivirus Virion Assembly. Trends Biochem Sci.
Barrows, N.J., Anglero-Rodriguez, Y., Kim, B., Jamison, S.F., Le Sommer, C., McGee, C.E., Pearson, J.L., Dimopoulos, G., Ascano, M., Bradrick, S.S.*, et al.* (2019). Dual roles for the ER membrane protein complex in flavivirus infection: viral entry and protein biogenesis. Sci Rep *9*, 9711.
Barrows, N.J., Campos, R.K., Liao, K.C., Prasanth, K.R., Soto-Acosta, R., Yeh, S.C., Schott-Lerner, G., Pompon, J., Sessions, O.M., Bradrick, S.S.*, et al.* (2018). Biochemistry and Molecular Biology of Flaviviruses. Chem Rev *118*, 4448-4482.
Basavannacharya, C., and Vasudevan, S.G. (2014). Suramin inhibits helicase activity of NS3 protein of dengue virus in a fluorescence-based high throughput assay format. Biochem Biophys Res Commun *453*, 539-544.
Bassetto, M., Massarotti, A., Coluccia, A., and Brancale, A. (2016). Structural biology in antiviral drug discovery. Curr Opin Pharmacol *30*, 116-130.
Bastos Lima, A., Behnam, M.A., El Sherif, Y., Nitsche, C., Vechi, S.M., and Klein, C.D. (2015). Dual inhibitors of the dengue and West Nile virus NS2B-NS3 proteases: Synthesis, biological evaluation and docking studies of novel peptide-hybrids. Bioorg Med Chem *23*, 5748-5755.
Baud, D., Gubler, D.J., Schaub, B., Lanteri, M.C., and Musso, D. (2017). An update on Zika virus infection. Lancet *390*, 2099-2109.
Beesetti, H., Tyagi, P., Medapi, B., Krishna, V.S., Sriram, D., Khanna, N., and Swaminathan, S. (2018). A quinoline compound inhibits the replication of dengue virus serotypes 1-4 in Vero cells. Antivir Ther *23*, 385-394.
Behnam, M.A., Graf, D., Bartenschlager, R., Zlotos, D.P., and Klein, C.D. (2015). Discovery of Nanomolar Dengue and West Nile Virus Protease Inhibitors Containing a 4-Benzyloxyphenylglycine Residue. J Med Chem *58*, 9354-9370.
Behnam, M.A., Nitsche, C., Vechi, S.M., and Klein, C.D. (2014). C-terminal residue optimization and fragment merging: discovery of a potent Peptide-hybrid inhibitor of dengue protease. ACS Med Chem Lett *5*, 1037-1042.
Beltramello, M., Williams, K.L., Simmons, C.P., Macagno, A., Simonelli, L., Quyen, N.T., Sukupolvi-Petty, S., Navarro-Sanchez, E., Young, P.R., de Silva, A.M.*, et al.* (2010). The human immune response to Dengue virus is dominated by highly cross-reactive antibodies endowed with neutralizing and enhancing activity. Cell Host Microbe *8*, 271-283.
Benmansour, F., Trist, I., Coutard, B., Decroly, E., Querat, G., Brancale, A., and Barral, K. (2017). Discovery of novel dengue virus NS5 methyltransferase non-nucleoside inhibitors by fragment-based drug design. Eur J Med Chem *125*, 865-880.

Best, S.M. (2017). The Many Faces of the Flavivirus NS5 Protein in Antagonism of Type I Interferon Signaling. J Virol *91*.
Blazevic, J., Rouha, H., Bradt, V., Heinz, F.X., and Stiasny, K. (2016). Membrane Anchors of the Structural Flavivirus Proteins and Their Role in Virus Assembly. J Virol *90*, 6365-6378.
Brady, O.J., Gething, P.W., Bhatt, S., Messina, J.P., Brownstein, J.S., Hoen, A.G., Moyes, C.L., Farlow, A.W., Scott, T.W., and Hay, S.I. (2012). Refining the global spatial limits of dengue virus transmission by evidence-based consensus. PLoS Negl Trop Dis *6*, e1760.
Brand, C., Bisaillon, M., and Geiss, B.J. (2017). Organization of the Flavivirus RNA replicase complex. Wiley Interdiscip Rev RNA *8*.
Brecher, M., Li, Z., Liu, B., Zhang, J., Koetzner, C.A., Alifarag, A., Jones, S.A., Lin, Q., Kramer, L.D., and Li, H. (2017). A conformational switch high-throughput screening assay and allosteric inhibition of the flavivirus NS2B-NS3 protease. PLoS Pathog *13*, e1006411.
Bronzoni, R.V., Madrid, M.C., Duarte, D.V., Pellegrini, V.O., Pacca, C.C., Carmo, A.C., Zanelli, C.F., Valentini, S.R., Santacruz-Perez, C., Barbosa, J.A*., et al.* (2011). The small nuclear ribonucleoprotein U1A interacts with NS5 from yellow fever virus. Arch Virol *156*, 931-938.
Brown, W.C., Akey, D.L., Konwerski, J.R., Tarrasch, J.T., Skiniotis, G., Kuhn, R.J., and Smith, J.L. (2016). Extended surface for membrane association in Zika virus NS1 structure. Nat Struct Mol Biol *23*, 865-867.
Buckley, A., Gaidamovich, S., Turchinskaya, A., and Gould, E.A. (1992). Monoclonal antibodies identify the NS5 yellow fever virus non-structural protein in the nuclei of infected cells. J Gen Virol *73 ( Pt 5)*, 1125-1130.
Buckton, L.K., Rahimi, M.N., and McAlpine, S.R. (2020). Cyclic Peptides as Drugs for Intracellular Targets: The Next Frontier in Peptide Therapeutic Development. Chemistry.
Bujalowski, P.J., Bujalowski, W., and Choi, K.H. (2020). Identification of the viral RNA promoter stem loop A (SLA)-binding site on Zika virus polymerase NS5. Sci Rep *10*, 13306.
Byrd, C.M., Grosenbach, D.W., Berhanu, A., Dai, D., Jones, K.F., Cardwell, K.B., Schneider, C., Yang, G., Tyavanagimatt, S., Harver, C*., et al.* (2013). Novel benzoxazole inhibitor of dengue virus replication that targets the NS3 helicase. Antimicrob Agents Chemother *57*, 1902-1912.
Cannalire, R., Ki Chan, K.W., Burali, M.S., Gwee, C.P., Wang, S., Astolfi, A., Massari, S., Sabatini, S., Tabarrini, O., Mastrangelo, E*., et al.* (2020). Pyridobenzothiazolones Exert Potent Anti-Dengue Activity by Hampering Multiple Functions of NS5 Polymerase. ACS Med Chem Lett *11*, 773-782.
Carrasco, L.R., Lee, L.K., Lee, V.J., Ooi, E.E., Shepard, D.S., Thein, T.L., Gan, V., Cook, A.R., Lye, D., Ng, L.C*., et al.* (2011). Economic impact of dengue illness and the cost-effectiveness of future vaccination programs in Singapore. PLoS Negl Trop Dis *5*, e1426.
Cary, D.R., Ohuchi, M., Reid, P.C., and Masuya, K. (2017). Constrained peptides in drug discovery and development. J Synth Org Chem, Jpn *75*, 1171-1178.
Cerikan, B., Goellner, S., Neufeldt, C.J., Haselmann, U., Mulder, K., Chatel-Chaix, L., Cortese, M., and Bartenschlager, R. (2020). A Non-Replicative Role of the 3' Terminal Sequence of the Dengue Virus Genome in Membranous Replication Organelle Formation. Cell Rep *32*, 107859.

Chan, C.Y.Y., Low, J.Z.H., Gan, E.S., Ong, E.Z., Zhang, S.L., Tan, H.C., Chai, X., Ghosh, S., Ooi, E.E., and Chan, K.R. (2019). Antibody-Dependent Dengue Virus Entry Modulates Cell Intrinsic Responses for Enhanced Infection. mSphere *4*.
Chanprapaph, S., Saparpakorn, P., Sangma, C., Niyomrattanakit, P., Hannongbua, S., Angsuthanasombat, C., and Katzenmeier, G. (2005). Competitive inhibition of the dengue virus NS3 serine protease by synthetic peptides representing polyprotein cleavage sites. Biochem Biophys Res Commun *330*, 1237-1246.
Chapman, E.G., Costantino, D.A., Rabe, J.L., Moon, S.L., Wilusz, J., Nix, J.C., and Kieft, J.S. (2014). The structural basis of pathogenic subgenomic flavivirus RNA (sfRNA) production. Science *344*, 307-310.
Chatel-Chaix, L., Fischl, W., Scaturro, P., Cortese, M., Kallis, S., Bartenschlager, M., Fischer, B., and Bartenschlager, R. (2015). A Combined Genetic-Proteomic Approach Identifies Residues within Dengue Virus NS4B Critical for Interaction with NS3 and Viral Replication. J Virol *89*, 7170-7186.
Chaudhary, V., Yuen, K.S., Chan, J.F., Chan, C.P., Wang, P.H., Cai, J.P., Zhang, S., Liang, M., Kok, K.H., Chan, C.P.*, et al.* (2017). Selective Activation of Type II Interferon Signaling by Zika Virus NS5 Protein. J Virol *91*.
Chavez, J.H., Silva, J.R., Amarilla, A.A., and Moraes Figueiredo, L.T. (2010). Domain III peptides from flavivirus envelope protein are useful antigens for serologic diagnosis and targets for immunization. Biologicals *38*, 613-618.
Chen, C.J., Kuo, M.D., Chien, L.J., Hsu, S.L., Wang, Y.M., and Lin, J.H. (1997a). RNA-protein interactions: involvement of NS3, NS5, and 3' noncoding regions of Japanese encephalitis virus genomic RNA. J Virol *71*, 3466-3473.
Chen, H., Liu, L., Jones, S.A., Banavali, N., Kass, J., Li, Z., Zhang, J., Kramer, L.D., Ghosh, A.K., and Li, H. (2013). Selective inhibition of the West Nile virus methyltransferase by nucleoside analogs. Antiviral Res *97*, 232-239.
Chen, W.N., Loscha, K.V., Nitsche, C., Graham, B., and Otting, G. (2014). The dengue virus NS2B-NS3 protease retains the closed conformation in the complex with BPTI. FEBS Lett *588*, 2206-2211.
Chen, Y., Maguire, T., Hileman, R.E., Fromm, J.R., Esko, J.D., Linhardt, R.J., and Marks, R.M. (1997b). Dengue virus infectivity depends on envelope protein binding to target cell heparan sulfate. Nat Med *3*, 866-871.
Chernov, A.V., Shiryaev, S.A., Aleshin, A.E., Ratnikov, B.I., Smith, J.W., Liddington, R.C., and Strongin, A.Y. (2008). The two-component NS2B-NS3 proteinase represses DNA unwinding activity of the West Nile virus NS3 helicase. J Biol Chem *283*, 17270-17278.
Chu, J.J., Lee, R.C., Ang, M.J., Wang, W.L., Lim, H.A., Wee, J.L., Joy, J., Hill, J., and Brian Chia, C.S. (2015). Antiviral activities of 15 dengue NS2B-NS3 protease inhibitors using a human cell-based viral quantification assay. Antiviral Res *118*, 68-74.
Ci, Y., Liu, Z.Y., Zhang, N.N., Niu, Y., Yang, Y., Xu, C., Yang, W., Qin, C.F., and Shi, L. (2020). Zika NS1-induced ER remodeling is essential for viral replication. J Cell Biol *219*.
Ci, Y., Yang, Y., Xu, C., Qin, C.F., and Shi, L. (2021). Electrostatic Interaction Between NS1 and Negatively Charged Lipids Contributes to Flavivirus Replication Organelles Formation. Front Microbiol *12*, 641059.
ClinicalTrials.gov (2020). A Study of JNJ-64281802 in Participants With Confirmed Dengue Fever (https://ClinicalTrials.gov/show/NCT04906980).
ClinicalTrials.gov (2021). A Study of JNJ-64281802 Against Dengue Serotype 1 Infection in a Dengue Human Challenge Model in Healthy Adult Participants (https://ClinicalTrials.gov/show/NCT04480736).
Clum, S., Ebner, K.E., and Padmanabhan, R. (1997). Cotranslational membrane insertion of the serine proteinase precursor NS2B-NS3(Pro) of dengue virus type 2 is

required for efficient in vitro processing and is mediated through the hydrophobic regions of NS2B. J Biol Chem *272*, 30715-30723.
Clyde, K., and Harris, E. (2006). RNA secondary structure in the coding region of dengue virus type 2 directs translation start codon selection and is required for viral replication. J Virol *80*, 2170-2182.
Collins, M.H., and Metz, S.W. (2017). Progress and Works in Progress: Update on Flavivirus Vaccine Development. Clin Ther *39*, 1519-1536.
Collins, N.D., and Barrett, A.D. (2017). Live Attenuated Yellow Fever 17D Vaccine: A Legacy Vaccine Still Controlling Outbreaks In Modern Day. Curr Infect Dis Rep *19*, 14.
Coloma, J., Jain, R., Rajashankar, K.R., Garcia-Sastre, A., and Aggarwal, A.K. (2016). Structures of NS5 Methyltransferase from Zika Virus. Cell Rep *16*, 3097-3102.
Colpitts, T.M., Barthel, S., Wang, P., and Fikrig, E. (2011). Dengue virus capsid protein binds core histones and inhibits nucleosome formation in human liver cells. PLoS One *6*, e24365.
Coutard, B., Decroly, E., Li, C., Sharff, A., Lescar, J., Bricogne, G., and Barral, K. (2014). Assessment of Dengue virus helicase and methyltransferase as targets for fragment-based drug discovery. Antiviral Res *106*, 61-70.
Cui, T., Sugrue, R.J., Xu, Q., Lee, A.K., Chan, Y.C., and Fu, J. (1998). Recombinant dengue virus type 1 NS3 protein exhibits specific viral RNA binding and NTPase activity regulated by the NS5 protein. Virology *246*, 409-417.
Daep, C.A., Munoz-Jordan, J.L., and Eugenin, E.A. (2014). Flaviviruses, an expanding threat in public health: focus on dengue, West Nile, and Japanese encephalitis virus. J Neurovirol *20*, 539-560.
Danko, J.R., Kochel, T., Teneza-Mora, N., Luke, T.C., Raviprakash, K., Sun, P., Simmons, M., Moon, J.E., De La Barrera, R., Martinez, L.J.*, et al.* (2018). Safety and Immunogenicity of a Tetravalent Dengue DNA Vaccine Administered with a Cationic Lipid-Based Adjuvant in a Phase 1 Clinical Trial. Am J Trop Med Hyg *98*, 849-856.
Davis, C.W., Nguyen, H.Y., Hanna, S.L., Sanchez, M.D., Doms, R.W., and Pierson, T.C. (2006). West Nile virus discriminates between DC-SIGN and DC-SIGNR for cellular attachment and infection. J Virol *80*, 1290-1301.
De Borba, L., Villordo, S.M., Iglesias, N.G., Filomatori, C.V., Gebhard, L.G., and Gamarnik, A.V. (2015). Overlapping local and long-range RNA-RNA interactions modulate dengue virus genome cyclization and replication. J Virol *89*, 3430-3437.
De Jesus-Gonzalez, L.A., Cervantes-Salazar, M., Reyes-Ruiz, J.M., Osuna-Ramos, J.F., Farfan-Morales, C.N., Palacios-Rapalo, S.N., Perez-Olais, J.H., Cordero-Rivera, C.D., Hurtado-Monzon, A.M., Ruiz-Jimenez, F.*, et al.* (2020). The Nuclear Pore Complex: A Target for NS3 Protease of Dengue and Zika Viruses. Viruses *12*.
de la Cruz, L., Chen, W.N., Graham, B., and Otting, G. (2014). Binding mode of the activity-modulating C-terminal segment of NS2B to NS3 in the dengue virus NS2B-NS3 protease. FEBS J *281*, 1517-1533.
de la Cruz, L., Nguyen, T.H., Ozawa, K., Shin, J., Graham, B., Huber, T., and Otting, G. (2011). Binding of low molecular weight inhibitors promotes large conformational changes in the dengue virus NS2B-NS3 protease: fold analysis by pseudocontact shifts. J Am Chem Soc *133*, 19205-19215.
De Nova-Ocampo, M., Villegas-Sepulveda, N., and del Angel, R.M. (2002). Translation elongation factor-1alpha, La, and PTB interact with the 3' untranslated region of dengue 4 virus RNA. Virology *295*, 337-347.
Delano, W.L. (2009). PyMOL Molecular Viewer: Updates and Refinements, vol. 238. Abstracts of Papers of the American Chemical Society.
Deng, S.Q., Yang, X., Wei, Y., Chen, J.T., Wang, X.J., and Peng, H.J. (2020). A Review on Dengue Vaccine Development. Vaccines (Basel) *8*.

Dethoff, E.A., Boerneke, M.A., Gokhale, N.S., Muhire, B.M., Martin, D.P., Sacco, M.T., McFadden, M.J., Weinstein, J.B., Messer, W.B., Horner, S.M.*, et al.* (2018). Pervasive tertiary structure in the dengue virus RNA genome. Proc Natl Acad Sci U S A *115*, 11513-11518.
Dokland, T., Walsh, M., Mackenzie, J.M., Khromykh, A.A., Ee, K.H., and Wang, S. (2004). West Nile virus core protein; tetramer structure and ribbon formation. Structure *12*, 1157-1163.
Dong, H., Chang, D.C., Xie, X., Toh, Y.X., Chung, K.Y., Zou, G., Lescar, J., Lim, S.P., and Shi, P.Y. (2010). Biochemical and genetic characterization of dengue virus methyltransferase. Virology *405*, 568-578.
Dong, H., Fink, K., Zust, R., Lim, S.P., Qin, C.F., and Shi, P.Y. (2014). Flavivirus RNA methylation. J Gen Virol *95*, 763-778.
Dong, H., Ren, S., Zhang, B., Zhou, Y., Puig-Basagoiti, F., Li, H., and Shi, P.Y. (2008). West Nile virus methyltransferase catalyzes two methylations of the viral RNA cap through a substrate-repositioning mechanism. J Virol *82*, 4295-4307.
Dubankova, A., and Boura, E. (2019). Structure of the yellow fever NS5 protein reveals conserved drug targets shared among flaviviruses. Antiviral Res *169*, 104536.
Durbin, A.P. (2020). Historical discourse on the development of the live attenuated tetravalent dengue vaccine candidate TV003/TV005. Curr Opin Virol *43*, 79-87.
Durbin, A.P., Kirkpatrick, B.D., Pierce, K.K., Carmolli, M.P., Tibery, C.M., Grier, P.L., Hynes, N., Opert, K., Jarvis, A.P., Sabundayo, B.P.*, et al.* (2016). A 12-Month-Interval Dosing Study in Adults Indicates That a Single Dose of the National Institute of Allergy and Infectious Diseases Tetravalent Dengue Vaccine Induces a Robust Neutralizing Antibody Response. J Infect Dis *214*, 832-835.
Dwivedi, V.D., Arya, A., Yadav, P., Kumar, R., Kumar, V., and Raghava, G.P.S. (2020). DenvInD: dengue virus inhibitors database for clinical and molecular research. Brief Bioinform.
Ebi, K.L., and Nealon, J. (2016). Dengue in a changing climate. Environ Res *151*, 115-123.
Edgil, D., Polacek, C., and Harris, E. (2006). Dengue virus utilizes a novel strategy for translation initiation when cap-dependent translation is inhibited. J Virol *80*, 2976-2986.
El Sahili, A., and Lescar, J. (2017). Dengue Virus Non-Structural Protein 5. Viruses *9*.
El Sahili, A., Soh, T.S., Schiltz, J., Gharbi-Ayachi, A., Seh, C.C., Shi, P.Y., Lim, S.P., and Lescar, J. (2019). NS5 from Dengue Virus Serotype 2 Can Adopt a Conformation Analogous to That of Its Zika Virus and Japanese Encephalitis Virus Homologues. J Virol *94*.
Emsley, P., and Cowtan, K. (2004). Coot: model-building tools for molecular graphics. Acta Crystallogr D Biol Crystallogr *60*, 2126-2132.
Erbel, P., Schiering, N., D'Arcy, A., Renatus, M., Kroemer, M., Lim, S.P., Yin, Z., Keller, T.H., Vasudevan, S.G., and Hommel, U. (2006). Structural basis for the activation of flaviviral NS3 proteases from dengue and West Nile virus. Nat Struct Mol Biol *13*, 372-373.
Ezgimen, M., Lai, H., Mueller, N.H., Lee, K., Cuny, G., Ostrov, D.A., and Padmanabhan, R. (2012). Characterization of the 8-hydroxyquinoline scaffold for inhibitors of West Nile virus serine protease. Antiviral Res *94*, 18-24.
Fajardo, T., Sanford, T.J., Mears, H.V., Jasper, A., Storrie, S., Mansur, D.S., and Sweeney, T.R. (2020). The flavivirus polymerase NS5 regulates translation of viral genomic RNA. Nucleic Acids Res *48*, 5081-5093.

Ferrer-Orta, C., Arias, A., Perez-Luque, R., Escarmis, C., Domingo, E., and Verdaguer, N. (2007). Sequential structures provide insights into the fidelity of RNA replication. Proc Natl Acad Sci U S A *104*, 9463-9468.
Filomatori, C.V., Iglesias, N.G., Villordo, S.M., Alvarez, D.E., and Gamarnik, A.V. (2011). RNA Sequences and Structures Required for the Recruitment and Activity of the Dengue Virus Polymerase. Journal of Biological Chemistry *286*, 6929-6939.
Filomatori, C.V., Lodeiro, M.F., Alvarez, D.E., Samsa, M.M., Pietrasanta, L., and Gamarnik, A.V. (2006). A 5' RNA element promotes dengue virus RNA synthesis on a circular genome. Genes Dev *20*, 2238-2249.
Fisher, D., and Cutter, J. (2016). The inevitable colonisation of Singapore by Zika virus. BMC Med *14*, 188.
Friebe, P., and Harris, E. (2010). Interplay of RNA elements in the dengue virus 5' and 3' ends required for viral RNA replication. J Virol *84*, 6103-6118.
Friedrich, S., Engelmann, S., Schmidt, T., Szczepankiewicz, G., Bergs, S., Liebert, U.G., Kummerer, B.M., Golbik, R.P., and Behrens, S.E. (2018). The Host Factor AUF1 p45 Supports Flavivirus Propagation by Triggering the RNA Switch Required for Viral Genome Cyclization. J Virol *92*.
Friedrich, S., Schmidt, T., Geissler, R., Lilie, H., Chabierski, S., Ulbert, S., Liebert, U.G., Golbik, R.P., and Behrens, S.E. (2014). AUF1 p45 promotes West Nile virus replication by an RNA chaperone activity that supports cyclization of the viral genome. J Virol *88*, 11586-11599.
Garcia-Blanco, M.A., Vasudevan, S.G., Bradrick, S.S., and Nicchitta, C. (2016). Flavivirus RNA transactions from viral entry to genome replication. Antiviral Res *134*, 244-249.
Garske, T., Van Kerkhove, M.D., Yactayo, S., Ronveaux, O., Lewis, R.F., Staples, J.E., Perea, W., Ferguson, N.M., and Yellow Fever Expert, C. (2014). Yellow Fever in Africa: estimating the burden of disease and impact of mass vaccination from outbreak and serological data. PLoS Med *11*, e1001638.
Gaudinski, M.R., Houser, K.V., Morabito, K.M., Hu, Z., Yamshchikov, G., Rothwell, R.S., Berkowitz, N., Mendoza, F., Saunders, J.G., Novik, L.*, et al.* (2018). Safety, tolerability, and immunogenicity of two Zika virus DNA vaccine candidates in healthy adults: randomised, open-label, phase 1 clinical trials. Lancet *391*, 552-562.
Gebhard, L.G., Filomatori, C.V., and Gamarnik, A.V. (2011). Functional RNA Elements in the Dengue Virus Genome. Viruses-Basel *3*, 1739-1756.
Geiss, B.J., Stahla-Beek, H.J., Hannah, A.M., Gari, H.H., Henderson, B.R., Saeedi, B.J., and Keenan, S.M. (2011). A high-throughput screening assay for the identification of flavivirus NS5 capping enzyme GTP-binding inhibitors: implications for antiviral drug development. J Biomol Screen *16*, 852-861.
George, J., Valiant, W.G., Mattapallil, M.J., Walker, M., Huang, Y.S., Vanlandingham, D.L., Misamore, J., Greenhouse, J., Weiss, D.E., Verthelyi, D.*, et al.* (2017). Prior Exposure to Zika Virus Significantly Enhances Peak Dengue-2 Viremia in Rhesus Macaques. Sci Rep *7*, 10498.
Gharbi-Ayachi, A., Santhanakrishnan, S., Wong, Y.H., Chan, K.W.K., Tan, S.T., Bates, R.W., Vasudevan, S.G., El Sahili, A., and Lescar, J. (2020). Non-nucleoside Inhibitors of Zika Virus RNA-Dependent RNA Polymerase. J Virol *94*.
Giel-Moloney, M., Goncalvez, A.P., Catalan, J., Lecouturier, V., Girerd-Chambaz, Y., Diaz, F., Maldonado-Arocho, F., Gomila, R.C., Bernard, M.C., Oomen, R.*, et al.* (2018). Chimeric yellow fever 17D-Zika virus (ChimeriVax-Zika) as a live-attenuated Zika virus vaccine. Sci Rep *8*, 13206.
Giraldo, M.I., Vargas-Cuartas, O., Gallego-Gomez, J.C., Shi, P.Y., Padilla-Sanabria, L., Castano-Osorio, J.C., and Rajsbaum, R. (2018). K48-linked polyubiquitination of

dengue virus NS1 protein inhibits its interaction with the viral partner NS4B. Virus Res *246*, 1-11.
Goertz, G.P., Abbo, S.R., Fros, J.J., and Pijlman, G.P. (2018). Functional RNA during Zika virus infection. Virus Res *254*, 41-53.
Gong, P., and Peersen, O.B. (2010). Structural basis for active site closure by the poliovirus RNA-dependent RNA polymerase. Proc Natl Acad Sci U S A *107*, 22505-22510.
Gotz, C., Hinze, G., Gellert, A., Maus, H., von Hammerstein, F., Hammerschmidt, S.J., Lauth, L.M., Hellmich, U.A., Schirmeister, T., and Basche, T. (2021). Conformational Dynamics of the Dengue Virus Protease Revealed by Fluorescence Correlation and Single-Molecule FRET Studies. J Phys Chem B.
Gouet, P., Robert, X., and Courcelle, E. (2003). ESPript/ENDscript: Extracting and rendering sequence and 3D information from atomic structures of proteins. Nucleic Acids Res *31*, 3320-3323.
Grant, A., Ponia, S.S., Tripathi, S., Balasubramaniam, V., Miorin, L., Sourisseau, M., Schwarz, M.C., Sanchez-Seco, M.P., Evans, M.J., Best, S.M*., et al.* (2016). Zika Virus Targets Human STAT2 to Inhibit Type I Interferon Signaling. Cell Host Microbe *19*, 882-890.
Green, H., and Durrant, J.D. (2021). DeepFrag: An Open-Source Browser App for Deep-Learning Lead Optimization. J Chem Inf Model.
Gruba, N., Rodriguez Martinez, J.I., Grzywa, R., Wysocka, M., Skorenski, M., Burmistrz, M., Lecka, M., Lesner, A., Sienczyk, M., and Pyrc, K. (2016). Substrate profiling of Zika virus NS2B-NS3 protease. FEBS Lett *590*, 3459-3468.
Guo, F., Wu, S., Julander, J., Ma, J., Zhang, X., Kulp, J., Cuconati, A., Block, T.M., Du, Y., Guo, J.T*., et al.* (2016). A Novel Benzodiazepine Compound Inhibits Yellow Fever Virus Infection by Specifically Targeting NS4B Protein. J Virol *90*, 10774-10788.
Guzman, M.G., and Harris, E. (2015). Dengue. Lancet *385*, 453-465.
Hackett, B.A., and Cherry, S. (2018). Flavivirus internalization is regulated by a size-dependent endocytic pathway. Proc Natl Acad Sci U S A *115*, 4246-4251.
Hackett, B.A., Yasunaga, A., Panda, D., Tartell, M.A., Hopkins, K.C., Hensley, S.E., and Cherry, S. (2015). RNASEK is required for internalization of diverse acid-dependent viruses. Proc Natl Acad Sci U S A *112*, 7797-7802.
Hammamy, M.Z., Haase, C., Hammami, M., Hilgenfeld, R., and Steinmetzer, T. (2013). Development and characterization of new peptidomimetic inhibitors of the West Nile virus NS2B-NS3 protease. ChemMedChem *8*, 231-241.
Heaton, N.S., Perera, R., Berger, K.L., Khadka, S., Lacount, D.J., Kuhn, R.J., and Randall, G. (2010). Dengue virus nonstructural protein 3 redistributes fatty acid synthase to sites of viral replication and increases cellular fatty acid synthesis. Proc Natl Acad Sci U S A *107*, 17345-17350.
Heinz, F.X., and Stiasny, K. (2012). Flaviviruses and their antigenic structure. J Clin Virol *55*, 289-295.
Hernandez-Morales, I., Geluykens, P., Clynhens, M., Strijbos, R., Goethals, O., Megens, S., Verheyen, N., Last, S., McGowan, D., Coesemans, E*., et al.* (2017). Characterization of a dengue NS4B inhibitor originating from an HCV small molecule library. Antiviral Res *147*, 149-158.
Hertzog, J., Dias Junior, A.G., Rigby, R.E., Donald, C.L., Mayer, A., Sezgin, E., Song, C., Jin, B., Hublitz, P., Eggeling, C*., et al.* (2018). Infection with a Brazilian isolate of Zika virus generates RIG-I stimulatory RNA and the viral NS5 protein blocks type I IFN induction and signaling. Eur J Immunol *48*, 1120-1136.

Hill, M.E., Kumar, A., Wells, J.A., Hobman, T.C., Julien, O., and Hardy, J.A. (2018). The Unique Cofactor Region of Zika Virus NS2B-NS3 Protease Facilitates Cleavage of Key Host Proteins. ACS Chem Biol *13*, 2398-2405.
Hill, M.E., Yildiz, M., and Hardy, J.A. (2019). Cysteine Disulfide Traps Reveal Distinct Conformational Ensembles in Dengue Virus NS2B-NS3 Protease. Biochemistry *58*, 776-787.
Hodge, K., Tunghirun, C., Kamkaew, M., Limjindaporn, T., Yenchitsomanus, P.T., and Chimnaronk, S. (2016). Identification of a Conserved RNA-dependent RNA Polymerase (RdRp)-RNA Interface Required for Flaviviral Replication. J Biol Chem *291*, 17437-17449.
Hoffman, E.A., Frey, B.L., Smith, L.M., and Auble, D.T. (2015). Formaldehyde crosslinking: a tool for the study of chromatin complexes. J Biol Chem *290*, 26404-26411.
Holbrook, M.R. (2017). Historical Perspectives on Flavivirus Research. Viruses *9*.
Huber, R.G., Lim, X.N., Ng, W.C., Sim, A.Y.L., Poh, H.X., Shen, Y., Lim, S.Y., Sundstrom, K.B., Sun, X., Aw, J.G.*, et al.* (2019). Structure mapping of dengue and Zika viruses reveals functional long-range interactions. Nat Commun *10*, 1408.
Iglesias, N.G., and Gamarnik, A.V. (2011). Dynamic RNA structures in the dengue virus genome. RNA Biol *8*, 249-257.
Issur, M., Geiss, B.J., Bougie, I., Picard-Jean, F., Despins, S., Mayette, J., Hobdey, S.E., and Bisaillon, M. (2009). The flavivirus NS5 protein is a true RNA guanylyltransferase that catalyzes a two-step reaction to form the RNA cap structure. RNA *15*, 2340-2350.
Jain, R., Coloma, J., Garcia-Sastre, A., and Aggarwal, A.K. (2016). Structure of the NS3 helicase from Zika virus. Nat Struct Mol Biol *23*, 752-754.
Johnston, P.A., Phillips, J., Shun, T.Y., Shinde, S., Lazo, J.S., Huryn, D.M., Myers, M.C., Ratnikov, B.I., Smith, J.W., Su, Y.*, et al.* (2007). HTS identifies novel and specific uncompetitive inhibitors of the two-component NS2B-NS3 proteinase of West Nile virus. Assay Drug Dev Technol *5*, 737-750.
Kabsch, W. (2010). Integration, scaling, space-group assignment and post-refinement. Acta Crystallogr D Biol Crystallogr *66*, 133-144.
Kakumani, P.K., Ponia, S.S., S, R.K., Sood, V., Chinnappan, M., Banerjea, A.C., Medigeshi, G.R., Malhotra, P., Mukherjee, S.K., and Bhatnagar, R.K. (2013). Role of RNA interference (RNAi) in dengue virus replication and identification of NS4B as an RNAi suppressor. J Virol *87*, 8870-8883.
Kang, C., Gayen, S., Wang, W., Severin, R., Chen, A.S., Lim, H.A., Chia, C.S., Schuller, A., Doan, D.N., Poulsen, A.*, et al.* (2013). Exploring the binding of peptidic West Nile virus NS2B-NS3 protease inhibitors by NMR. Antiviral Res *97*, 137-144.
Kang, C., Keller, T.H., and Luo, D. (2017). Zika Virus Protease: An Antiviral Drug Target. Trends Microbiol *25*, 797-808.
Kaptein, S.J.F., Goethals, O., Kiemel, D., Marchand, A., Kesteleyn, B., Bonfanti, J.F., Bardiot, D., Stoops, B., Jonckers, T.H.M., Dallmeier, K.*, et al.* (2021). A pan-serotype dengue virus inhibitor targeting the NS3-NS4B interaction. Nature *598*, 504-509.
Khromykh, A.A., Kondratieva, N., Sgro, J.Y., Palmenberg, A., and Westaway, E.G. (2003). Significance in replication of the terminal nucleotides of the flavivirus genome. J Virol *77*, 10623-10629.
Kim, S.Y., Zhao, J., Liu, X., Fraser, K., Lin, L., Zhang, X., Zhang, F., Dordick, J.S., and Linhardt, R.J. (2017). Interaction of Zika Virus Envelope Protein with Glycosaminoglycans. Biochemistry *56*, 1151-1162.
Kim, Y.M., Gayen, S., Kang, C., Joy, J., Huang, Q., Chen, A.S., Wee, J.L., Ang, M.J., Lim, H.A., Hung, A.W.*, et al.* (2013). NMR analysis of a novel enzymatically active unlinked dengue NS2B-NS3 protease complex. J Biol Chem *288*, 12891-12900.

Knox, J.E., Ma, N.L., Yin, Z., Patel, S.J., Wang, W.L., Chan, W.L., Ranga Rao, K.R., Wang, G., Ngew, X., Patel, V.*, et al.* (2006). Peptide inhibitors of West Nile NS3 protease: SAR study of tetrapeptide aldehyde inhibitors. J Med Chem *49*, 6585-6590.
Kostyuchenko, V.A., Lim, E.X., Zhang, S., Fibriansah, G., Ng, T.S., Ooi, J.S., Shi, J., and Lok, S.M. (2016). Structure of the thermally stable Zika virus. Nature *533*, 425-428.
Kouretova, J., Hammamy, M.Z., Epp, A., Hardes, K., Kallis, S., Zhang, L., Hilgenfeld, R., Bartenschlager, R., and Steinmetzer, T. (2017). Effects of NS2B-NS3 protease and furin inhibition on West Nile and Dengue virus replication. J Enzyme Inhib Med Chem *32*, 712-721.
Krenn, V., Bosone, C., Burkard, T.R., Spanier, J., Kalinke, U., Calistri, A., Salata, C., Rilo Christoff, R., Pestana Garcez, P., Mirazimi, A.*, et al.* (2021). Organoid modeling of Zika and herpes simplex virus 1 infections reveals virus-specific responses leading to microcephaly. Cell Stem Cell.
Kuhl, N., Graf, D., Bock, J., Behnam, M.A.M., Leuthold, M.M., and Klein, C.D. (2020). A New Class of Dengue and West Nile Virus Protease Inhibitors with Submicromolar Activity in Reporter Gene DENV-2 Protease and Viral Replication Assays. J Med Chem.
Kuhn, R.J., Zhang, W., Rossmann, M.G., Pletnev, S.V., Corver, J., Lenches, E., Jones, C.T., Mukhopadhyay, S., Chipman, P.R., Strauss, E.G.*, et al.* (2002). Structure of dengue virus: implications for flavivirus organization, maturation, and fusion. Cell *108*, 717-725.
Kuiper, B.D., Slater, K., Spellmon, N., Holcomb, J., Medapureddy, P., Muzzarelli, K.M., Yang, Z., Ovadia, R., Amblard, F., Kovari, I.A.*, et al.* (2017). Increased activity of unlinked Zika virus NS2B/NS3 protease compared to linked Zika virus protease. Biochem Biophys Res Commun *492*, 668-673.
Kumar, A., Buhler, S., Selisko, B., Davidson, A., Mulder, K., Canard, B., Miller, S., and Bartenschlager, R. (2013). Nuclear localization of dengue virus nonstructural protein 5 does not strictly correlate with efficient viral RNA replication and inhibition of type I interferon signaling. J Virol *87*, 4545-4557.
Kumar, D., Sharma, N., Aarthy, M., Singh, S.K., and Giri, R. (2020). Mechanistic Insights into Zika Virus NS3 Helicase Inhibition by Epigallocatechin-3-Gallate. ACS Omega *5*, 11217-11226.
Kummerer, B.M., and Rice, C.M. (2002). Mutations in the yellow fever virus nonstructural protein NS2A selectively block production of infectious particles. J Virol *76*, 4773-4784.
Lai, H., Dou, D., Aravapalli, S., Teramoto, T., Lushington, G.H., Mwania, T.M., Alliston, K.R., Eichhorn, D.M., Padmanabhan, R., and Groutas, W.C. (2013a). Design, synthesis and characterization of novel 1,2-benzisothiazol-3(2H)-one and 1,3,4-oxadiazole hybrid derivatives: potent inhibitors of Dengue and West Nile virus NS2B/NS3 proteases. Bioorg Med Chem *21*, 102-113.
Lai, H., Sridhar Prasad, G., and Padmanabhan, R. (2013b). Characterization of 8-hydroxyquinoline derivatives containing aminobenzothiazole as inhibitors of dengue virus type 2 protease in vitro. Antiviral Res *97*, 74-80.
Laurent-Rolle, M., Morrison, J., Rajsbaum, R., Macleod, J.M.L., Pisanelli, G., Pham, A., Ayllon, J., Miorin, L., Martinez, C., tenOever, B.R.*, et al.* (2014). The interferon signaling antagonist function of yellow fever virus NS5 protein is activated by type I interferon. Cell Host Microbe *16*, 314-327.
Law, M.J., Rice, A.J., Lin, P., and Laird-Offringa, I.A. (2006). The role of RNA structure in the interaction of U1A protein with U1 hairpin II RNA. RNA *12*, 1168-1178.
Lee, C.M., Xie, X., Zou, J., Li, S.H., Lee, M.Y., Dong, H., Qin, C.F., Kang, C., and Shi, P.Y. (2015). Determinants of Dengue Virus NS4A Protein Oligomerization. J Virol *89*, 6171-6183.

Lee, E., Bujalowski, P.J., Teramoto, T., Gottipati, K., Scott, S.D., Padmanabhan, R., and Choi, K.H. (2021). Structures of flavivirus RNA promoters suggest two binding modes with NS5 polymerase. Nat Commun *12*, 2530.
Lee, H., Ren, J., Nocadello, S., Rice, A.J., Ojeda, I., Light, S., Minasov, G., Vargas, J., Nagarathnam, D., Anderson, W.F.*, et al.* (2017). Identification of novel small molecule inhibitors against NS2B/NS3 serine protease from Zika virus. Antiviral Res *139*, 49-58.
Lee, R.A., Razaz, M., and Hayward, S. (2003). The DynDom database of protein domain motions. Bioinformatics *19*, 1290-1291.
Lee, S.H., Nam, K.W., Jeong, J.Y., Yoo, S.J., Koh, Y.S., Lee, S., Heo, S.T., Seong, S.Y., and Lee, K.H. (2013). The effects of climate change and globalization on mosquito vectors: evidence from Jeju Island, South Korea on the potential for Asian tiger mosquito (Aedes albopictus) influxes and survival from Vietnam rather than Japan. PLoS One *8*, e68512.
Lei, J., Hansen, G., Nitsche, C., Klein, C.D., Zhang, L., and Hilgenfeld, R. (2016). Crystal structure of Zika virus NS2B-NS3 protease in complex with a boronate inhibitor. Science *353*, 503-505.
Lennemann, N.J., and Coyne, C.B. (2017). Dengue and Zika viruses subvert reticulophagy by NS2B3-mediated cleavage of FAM134B. Autophagy *13*, 322-332.
Leon-Juarez, M., Martinez-Castillo, M., Shrivastava, G., Garcia-Cordero, J., Villegas-Sepulveda, N., Mondragon-Castelan, M., Mondragon-Flores, R., and Cedillo-Barron, L. (2016). Recombinant Dengue virus protein NS2B alters membrane permeability in different membrane models. Virol J *13*, 1.
Lescar, J., Soh, S., Lee, L.T., Vasudevan, S.G., Kang, C., and Lim, S.P. (2018). The Dengue Virus Replication Complex: From RNA Replication to Protein-Protein Interactions to Evasion of Innate Immunity. Adv Exp Med Biol *1062*, 115-129.
Leung, D., Schroder, K., White, H., Fang, N.X., Stoermer, M.J., Abbenante, G., Martin, J.L., Young, P.R., and Fairlie, D.P. (2001). Activity of recombinant dengue 2 virus NS3 protease in the presence of a truncated NS2B co-factor, small peptide substrates, and inhibitors. J Biol Chem *276*, 45762-45771.
Leung, J.Y., Pijlman, G.P., Kondratieva, N., Hyde, J., Mackenzie, J.M., and Khromykh, A.A. (2008). Role of nonstructural protein NS2A in flavivirus assembly. J Virol *82*, 4731-4741.
Li, G., Teleki, C., and Wang, T. (2018a). Memory T Cells in Flavivirus Vaccination. Vaccines (Basel) *6*.
Li, J., Lim, S.P., Beer, D., Patel, V., Wen, D., Tumanut, C., Tully, D.C., Williams, J.A., Jiricek, J., Priestle, J.P.*, et al.* (2005). Functional profiling of recombinant NS3 proteases from all four serotypes of dengue virus using tetrapeptide and octapeptide substrate libraries. J Biol Chem *280*, 28766-28774.
Li, L., Lok, S.M., Yu, I.M., Zhang, Y., Kuhn, R.J., Chen, J., and Rossmann, M.G. (2008). The flavivirus precursor membrane-envelope protein complex: structure and maturation. Science *319*, 1830-1834.
Li, M.I., Wong, P.S., Ng, L.C., and Tan, C.H. (2012). Oral susceptibility of Singapore Aedes (Stegomyia) aegypti (Linnaeus) to Zika virus. PLoS Negl Trop Dis *6*, e1792.
Li, P., Wei, Y., Mei, M., Tang, L., Sun, L., Huang, W., Zhou, J., Zou, C., Zhang, S., Qin, C.F.*, et al.* (2018b). Integrative Analysis of Zika Virus Genome RNA Structure Reveals Critical Determinants of Viral Infectivity. Cell Host Microbe *24*, 875-886 e875.
Li, X.D., Deng, C.L., Ye, H.Q., Zhang, H.L., Zhang, Q.Y., Chen, D.D., Zhang, P.T., Shi, P.Y., Yuan, Z.M., and Zhang, B. (2016a). Transmembrane Domains of NS2B Contribute to both Viral RNA Replication and Particle Formation in Japanese Encephalitis Virus. J Virol *90*, 5735-5749.

Li, X.D., Ye, H.Q., Deng, C.L., Liu, S.Q., Zhang, H.L., Shang, B.D., Shi, P.Y., Yuan, Z.M., and Zhang, B. (2015a). Genetic interaction between NS4A and NS4B for replication of Japanese encephalitis virus. J Gen Virol *96*, 1264-1275.
Li, Y., Kim, Y.M., Zou, J., Wang, Q.Y., Gayen, S., Wong, Y.L., Lee le, T., Xie, X., Huang, Q., Lescar, J.*, et al.* (2015b). Secondary structure and membrane topology of dengue virus NS4B N-terminal 125 amino acids. Biochim Biophys Acta *1848*, 3150-3157.
Li, Y., Lee, M.Y., Loh, Y.R., and Kang, C. (2018c). Secondary structure and membrane topology of dengue virus NS4A protein in micelles. Biochim Biophys Acta Biomembr *1860*, 442-450.
Li, Y., Li, Q., Wong, Y.L., Liew, L.S., and Kang, C. (2015c). Membrane topology of NS2B of dengue virus revealed by NMR spectroscopy. Biochim Biophys Acta *1848*, 2244-2252.
Li, Y., Wong, Y.L., Lee, M.Y., Li, Q., Wang, Q.Y., Lescar, J., Shi, P.Y., and Kang, C. (2016b). Secondary Structure and Membrane Topology of the Full-Length Dengue Virus NS4B in Micelles. Angew Chem Int Ed Engl *55*, 12068-12072.
Li, Y., Zhang, Z., Phoo, W.W., Loh, Y.R., Li, R., Yang, H.Y., Jansson, A.E., Hill, J., Keller, T.H., Nacro, K.*, et al.* (2018d). Structural Insights into the Inhibition of Zika Virus NS2B-NS3 Protease by a Small-Molecule Inhibitor. Structure *26*, 555-564 e553.
Li, Y., Zhang, Z., Phoo, W.W., Loh, Y.R., Wang, W., Liu, S., Chen, M.W., Hung, A.W., Keller, T.H., Luo, D.*, et al.* (2017a). Structural Dynamics of Zika Virus NS2B-NS3 Protease Binding to Dipeptide Inhibitors. Structure *25*, 1242-1250 e1243.
Li, Z., Brecher, M., Deng, Y.Q., Zhang, J., Sakamuru, S., Liu, B., Huang, R., Koetzner, C.A., Allen, C.A., Jones, S.A.*, et al.* (2017b). Existing drugs as broad-spectrum and potent inhibitors for Zika virus by targeting NS2B-NS3 interaction. Cell Res *27*, 1046-1064.
Li, Z., Sakamuru, S., Huang, R., Brecher, M., Koetzner, C.A., Zhang, J., Chen, H., Qin, C.F., Zhang, Q.Y., Zhou, J.*, et al.* (2018e). Erythrosin B is a potent and broad-spectrum orthosteric inhibitor of the flavivirus NS2B-NS3 protease. Antiviral Res *150*, 217-225.
Liang, Q., Luo, Z., Zeng, J., Chen, W., Foo, S.S., Lee, S.A., Ge, J., Wang, S., Goldman, S.A., Zlokovic, B.V.*, et al.* (2016). Zika Virus NS4A and NS4B Proteins Deregulate Akt-mTOR Signaling in Human Fetal Neural Stem Cells to Inhibit Neurogenesis and Induce Autophagy. Cell Stem Cell *19*, 663-671.
Lim, S.P. (2019). Dengue drug discovery: Progress, challenges and outlook. Antiviral Res *163*, 156-178.
Lim, S.P., Koh, J.H., Seh, C.C., Liew, C.W., Davidson, A.D., Chua, L.S., Chandrasekaran, R., Cornvik, T.C., Shi, P.Y., and Lescar, J. (2013a). A crystal structure of the dengue virus non-structural protein 5 (NS5) polymerase delineates interdomain amino acid residues that enhance its thermostability and de novo initiation activities. J Biol Chem *288*, 31105-31114.
Lim, S.P., Noble, C.G., Seh, C.C., Soh, T.S., El Sahili, A., Chan, G.K., Lescar, J., Arora, R., Benson, T., Nilar, S.*, et al.* (2016). Potent Allosteric Dengue Virus NS5 Polymerase Inhibitors: Mechanism of Action and Resistance Profiling. PLoS Pathog *12*, e1005737.
Lim, S.P., Sonntag, L.S., Noble, C., Nilar, S.H., Ng, R.H., Zou, G., Monaghan, P., Chung, K.Y., Dong, H., Liu, B.*, et al.* (2011). Small molecule inhibitors that selectively block dengue virus methyltransferase. J Biol Chem *286*, 6233-6240.
Lim, S.P., Wang, Q.Y., Noble, C.G., Chen, Y.L., Dong, H., Zou, B., Yokokawa, F., Nilar, S., Smith, P., Beer, D.*, et al.* (2013b). Ten years of dengue drug discovery: progress and prospects. Antiviral Res *100*, 500-519.
Lin, D.L., Inoue, T., Chen, Y.J., Chang, A., Tsai, B., and Tai, A.W. (2019a). The ER Membrane Protein Complex Promotes Biogenesis of Dengue and Zika Virus Non-

structural Multi-pass Transmembrane Proteins to Support Infection. Cell Rep *27*, 1666-1674 e1664.
Lin, S., Yang, S., He, J., Guest, J.D., Ma, Z., Yang, L., Pierce, B.G., Tang, Q., and Zhang, Y.J. (2019b). Zika virus NS5 protein antagonizes type I interferon production via blocking TBK1 activation. Virology *527*, 180-187.
Lindenbach, B.D., and Rice, C.M. (1997). trans-Complementation of yellow fever virus NS1 reveals a role in early RNA replication. J Virol *71*, 9608-9617.
Lindenbach, B.D., and Rice, C.M. (1999). Genetic interaction of flavivirus nonstructural proteins NS1 and NS4A as a determinant of replicase function. J Virol *73*, 4611-4621.
Liu-Helmersson, J., Quam, M., Wilder-Smith, A., Stenlund, H., Ebi, K., Massad, E., and Rocklov, J. (2016). Climate Change and Aedes Vectors: 21st Century Projections for Dengue Transmission in Europe. EBioMedicine *7*, 267-277.
Liu, B., Gao, X., Ma, J., Jiao, Z., Xiao, J., Hayat, M.A., and Wang, H. (2019). Modeling the present and future distribution of arbovirus vectors Aedes aegypti and Aedes albopictus under climate change scenarios in Mainland China. Sci Total Environ *664*, 203-214.
Liu, H., Wu, R., Sun, Y., Ye, Y., Chen, J., Luo, X., Shen, X., and Liu, H. (2014). Identification of novel thiadiazoloacrylamide analogues as inhibitors of dengue-2 virus NS2B/NS3 protease. Bioorg Med Chem *22*, 6344-6352.
Liu, W.J., Chen, H.B., Wang, X.J., Huang, H., and Khromykh, A.A. (2004). Analysis of adaptive mutations in Kunjin virus replicon RNA reveals a novel role for the flavivirus nonstructural protein NS2A in inhibition of beta interferon promoter-driven transcription. J Virol *78*, 12225-12235.
Liu, W.J., Wang, X.J., Clark, D.C., Lobigs, M., Hall, R.A., and Khromykh, A.A. (2006). A single amino acid substitution in the West Nile virus nonstructural protein NS2A disables its ability to inhibit alpha/beta interferon induction and attenuates virus virulence in mice. J Virol *80*, 2396-2404.
Liu, Z.Y., Li, X.F., Jiang, T., Deng, Y.Q., Ye, Q., Zhao, H., Yu, J.Y., and Qin, C.F. (2016). Viral RNA switch mediates the dynamic control of flavivirus replicase recruitment by genome cyclization. Elife *5*.
Lok, S.M. (2018). Flat-lying antibody prevents disease enhancement. Nat Immunol *19*, 1150-1152.
Lopez-Denman, A.J., Russo, A., Wagstaff, K.M., White, P.A., Jans, D.A., and Mackenzie, J.M. (2018). Nucleocytoplasmic shuttling of the West Nile virus RNA-dependent RNA polymerase NS5 is critical to infection. Cell Microbiol *20*, e12848.
Low, J.G., Ooi, E.E., and Vasudevan, S.G. (2017). Current Status of Dengue Therapeutics Research and Development. J Infect Dis *215*, S96-S102.
Low, J.G., Sung, C., Wijaya, L., Wei, Y., Rathore, A.P.S., Watanabe, S., Tan, B.H., Toh, L., Chua, L.T., Hou, Y.*, et al.* (2014). Efficacy and safety of celgosivir in patients with dengue fever (CELADEN): a phase 1b, randomised, double-blind, placebo-controlled, proof-of-concept trial. Lancet Infect Dis *14*, 706-715.
Lu, G., and Gong, P. (2013). Crystal Structure of the full-length Japanese encephalitis virus NS5 reveals a conserved methyltransferase-polymerase interface. PLoS Pathog *9*, e1003549.
Luo, D., Wei, N., Doan, D.N., Paradkar, P.N., Chong, Y., Davidson, A.D., Kotaka, M., Lescar, J., and Vasudevan, S.G. (2010). Flexibility between the protease and helicase domains of the dengue virus NS3 protein conferred by the linker region and its functional implications. J Biol Chem *285*, 18817-18827.
Luo, D., Xu, T., Hunke, C., Gruber, G., Vasudevan, S.G., and Lescar, J. (2008a). Crystal structure of the NS3 protease-helicase from dengue virus. J Virol *82*, 173-183.

Luo, D., Xu, T., Watson, R.P., Scherer-Becker, D., Sampath, A., Jahnke, W., Yeong, S.S., Wang, C.H., Lim, S.P., Strongin, A.*, et al.* (2008b). Insights into RNA unwinding and ATP hydrolysis by the flavivirus NS3 protein. EMBO J *27*, 3209-3219.
Ma, L., Jones, C.T., Groesch, T.D., Kuhn, R.J., and Post, C.B. (2004). Solution structure of dengue virus capsid protein reveals another fold. Proc Natl Acad Sci U S A *101*, 3414-3419.
Mackenzie, J.M., Jones, M.K., and Young, P.R. (1996). Immunolocalization of the dengue virus nonstructural glycoprotein NS1 suggests a role in viral RNA replication. Virology *220*, 232-240.
Mackenzie, J.M., Khromykh, A.A., Jones, M.K., and Westaway, E.G. (1998). Subcellular localization and some biochemical properties of the flavivirus Kunjin nonstructural proteins NS2A and NS4A. Virology *245*, 203-215.
Malet, H., Egloff, M.P., Selisko, B., Butcher, R.E., Wright, P.J., Roberts, M., Gruez, A., Sulzenbacher, G., Vonrhein, C., Bricogne, G.*, et al.* (2007). Crystal structure of the RNA polymerase domain of the West Nile virus non-structural protein 5. J Biol Chem *282*, 10678-10689.
Manoff, S.B., George, S.L., Bett, A.J., Yelmene, M.L., Dhanasekaran, G., Eggemeyer, L., Sausser, M.L., Dubey, S.A., Casimiro, D.R., Clements, D.E.*, et al.* (2015). Preclinical and clinical development of a dengue recombinant subunit vaccine. Vaccine *33*, 7126-7134.
Manzano, M., Reichert, E.D., Polo, S., Falgout, B., Kasprzak, W., Shapiro, B.A., and Padmanabhan, R. (2011). Identification of cis-acting elements in the 3'-untranslated region of the dengue virus type 2 RNA that modulate translation and replication. J Biol Chem *286*, 22521-22534.
Markoff, L. (2003). 5'- and 3'-noncoding regions in flavivirus RNA. Adv Virus Res *59*, 177-228.
Martin-Acebes, M.A., Blazquez, A.B., Jimenez de Oya, N., Escribano-Romero, E., and Saiz, J.C. (2011). West Nile virus replication requires fatty acid synthesis but is independent on phosphatidylinositol-4-phosphate lipids. PLoS One *6*, e24970.
Mastrangelo, E., Milani, M., Bollati, M., Selisko, B., Peyrane, F., Pandini, V., Sorrentino, G., Canard, B., Konarev, P.V., Svergun, D.I.*, et al.* (2007). Crystal structure and activity of Kunjin virus NS3 helicase; protease and helicase domain assembly in the full length NS3 protein. J Mol Biol *372*, 444-455.
Mastrangelo, E., Pezzullo, M., De Burghgraeve, T., Kaptein, S., Pastorino, B., Dallmeier, K., de Lamballerie, X., Neyts, J., Hanson, A.M., Frick, D.N.*, et al.* (2012). Ivermectin is a potent inhibitor of flavivirus replication specifically targeting NS3 helicase activity: new prospects for an old drug. J Antimicrob Chemother *67*, 1884-1894.
Matthew, A.N., Leidner, F., Lockbaum, G.J., Henes, M., Zephyr, J., Hou, S., Rao, D.N., Timm, J., Rusere, L.N., Ragland, D.A.*, et al.* (2021). Drug Design Strategies to Avoid Resistance in Direct-Acting Antivirals and Beyond. Chem Rev *121*, 3238-3270.
Maurer-Stroh, S., Mak, T.M., Ng, Y.K., Phuah, S.P., Huber, R.G., Marzinek, J.K., Holdbrook, D.A., Lee, R.T., Cui, L., and Lin, R.T. (2016). South-east Asian Zika virus strain linked to cluster of cases in Singapore, August 2016. Euro Surveill *21*.
Mazeaud, C., Freppel, W., and Chatel-Chaix, L. (2018). The Multiples Fates of the Flavivirus RNA Genome During Pathogenesis. Front Genet *9*, 595.
Mazzon, M., Jones, M., Davidson, A., Chain, B., and Jacobs, M. (2009). Dengue virus NS5 inhibits interferon-alpha signaling by blocking signal transducer and activator of transcription 2 phosphorylation. J Infect Dis *200*, 1261-1270.
McCoy, A.J. (2007). Solving structures of protein complexes by molecular replacement with Phaser. Acta Crystallogr D Biol Crystallogr *63*, 32-41.

McLean, J.E., Wudzinska, A., Datan, E., Quaglino, D., and Zakeri, Z. (2011). Flavivirus NS4A-induced autophagy protects cells against death and enhances virus replication. J Biol Chem *286*, 22147-22159.
Meertens, L., Carnec, X., Lecoin, M.P., Ramdasi, R., Guivel-Benhassine, F., Lew, E., Lemke, G., Schwartz, O., and Amara, A. (2012). The TIM and TAM families of phosphatidylserine receptors mediate dengue virus entry. Cell Host Microbe *12*, 544-557.
Messina, J.P., Brady, O.J., Scott, T.W., Zou, C., Pigott, D.M., Duda, K.A., Bhatt, S., Katzelnick, L., Howes, R.E., Battle, K.E*., et al.* (2014). Global spread of dengue virus types: mapping the 70 year history. Trends Microbiol *22*, 138-146.
Michalski, D., Ontiveros, J.G., Russo, J., Charley, P.A., Anderson, J.R., Heck, A.M., Geiss, B.J., and Wilusz, J. (2019). Zika virus noncoding sfRNAs sequester multiple host-derived RNA-binding proteins and modulate mRNA decay and splicing during infection. J Biol Chem *294*, 16282-16296.
Miller, S., Kastner, S., Krijnse-Locker, J., Buhler, S., and Bartenschlager, R. (2007). The non-structural protein 4A of dengue virus is an integral membrane protein inducing membrane alterations in a 2K-regulated manner. J Biol Chem *282*, 8873-8882.
Miller, S., Sparacio, S., and Bartenschlager, R. (2006). Subcellular localization and membrane topology of the Dengue virus type 2 Non-structural protein 4B. J Biol Chem *281*, 8854-8863.
Millies, B., von Hammerstein, F., Gellert, A., Hammerschmidt, S., Barthels, F., Goppel, U., Immerheiser, M., Elgner, F., Jung, N., Basic, M*., et al.* (2019). Proline-Based Allosteric Inhibitors of Zika and Dengue Virus NS2B/NS3 Proteases. J Med Chem *62*, 11359-11382.
Miorin, L., Laurent-Rolle, M., Pisanelli, G., Co, P.H., Albrecht, R.A., Garcia-Sastre, A., and Morrison, J. (2019). Host-Specific NS5 Ubiquitination Determines Yellow Fever Virus Tropism. J Virol *93*.
Modis, Y., Ogata, S., Clements, D., and Harrison, S.C. (2004). Structure of the dengue virus envelope protein after membrane fusion. Nature *427*, 313-319.
Monath, T.P., Guirakhoo, F., Nichols, R., Yoksan, S., Schrader, R., Murphy, C., Blum, P., Woodward, S., McCarthy, K., Mathis, D*., et al.* (2003). Chimeric live, attenuated vaccine against Japanese encephalitis (ChimeriVax-JE): phase 2 clinical trials for safety and immunogenicity, effect of vaccine dose and schedule, and memory response to challenge with inactivated Japanese encephalitis antigen. J Infect Dis *188*, 1213-1230.
Moon, S.L., Anderson, J.R., Kumagai, Y., Wilusz, C.J., Akira, S., Khromykh, A.A., and Wilusz, J. (2012). A noncoding RNA produced by arthropod-borne flaviviruses inhibits the cellular exoribonuclease XRN1 and alters host mRNA stability. RNA *18*, 2029-2040.
Moon, S.L., Dodd, B.J., Brackney, D.E., Wilusz, C.J., Ebel, G.D., and Wilusz, J. (2015). Flavivirus sfRNA suppresses antiviral RNA interference in cultured cells and mosquitoes and directly interacts with the RNAi machinery. Virology *485*, 322-329.
Moquin, S.A., Simon, O., Karuna, R., Lakshminarayana, S.B., Yokokawa, F., Wang, F., Saravanan, C., Zhang, J., Day, C.W., Chan, K*., et al.* (2021). NITD-688, a pan-serotype inhibitor of the dengue virus NS4B protein, shows favorable pharmacokinetics and efficacy in preclinical animal models. Sci Transl Med *13*.
Mori, Y., Okabayashi, T., Yamashita, T., Zhao, Z., Wakita, T., Yasui, K., Hasebe, F., Tadano, M., Konishi, E., Moriishi, K*., et al.* (2005). Nuclear localization of Japanese encephalitis virus core protein enhances viral replication. J Virol *79*, 3448-3458.
Morrison, C. (2018). Constrained peptides' time to shine? Nat Rev Drug Discov *17*, 531-533.
Morrison, J., Laurent-Rolle, M., Maestre, A.M., Rajsbaum, R., Pisanelli, G., Simon, V., Mulder, L.C., Fernandez-Sesma, A., and Garcia-Sastre, A. (2013). Dengue virus co-opts

UBR4 to degrade STAT2 and antagonize type I interferon signaling. PLoS Pathog *9*, e1003265.
Morrone, S.R., and Lok, S.M. (2019). Structural perspectives of antibody-dependent enhancement of infection of dengue virus. Curr Opin Virol *36*, 1-8.
Mueller, N.H., Pattabiraman, N., Ansarah-Sobrinho, C., Viswanathan, P., Pierson, T.C., and Padmanabhan, R. (2008). Identification and biochemical characterization of small-molecule inhibitors of west nile virus serine protease by a high-throughput screen. Antimicrob Agents Chemother *52*, 3385-3393.
Mukhopadhyay, S., Kuhn, R.J., and Rossmann, M.G. (2005). A structural perspective of the flavivirus life cycle. Nat Rev Microbiol *3*, 13-22.
Munawar, A., Beelen, S., Munawar, A., Lescrinier, E., and Strelkov, S.V. (2018). Discovery of Novel Druggable Sites on Zika Virus NS3 Helicase Using X-ray Crystallography-Based Fragment Screening. Int J Mol Sci *19*.
Munoz-Jordan, J.L., Laurent-Rolle, M., Ashour, J., Martinez-Sobrido, L., Ashok, M., Lipkin, W.I., and Garcia-Sastre, A. (2005). Inhibition of alpha/beta interferon signaling by the NS4B protein of flaviviruses. J Virol *79*, 8004-8013.
Munoz-Jordan, J.L., Sanchez-Burgos, G.G., Laurent-Rolle, M., and Garcia-Sastre, A. (2003). Inhibition of interferon signaling by dengue virus. Proc Natl Acad Sci U S A *100*, 14333-14338.
Nalam, M.N., and Schiffer, C.A. (2008). New approaches to HIV protease inhibitor drug design II: testing the substrate envelope hypothesis to avoid drug resistance and discover robust inhibitors. Curr Opin HIV AIDS *3*, 642-646.
Narayan, R., and Tripathi, S. (2020). Intrinsic ADE: The Dark Side of Antibody Dependent Enhancement During Dengue Infection. Front Cell Infect Microbiol *10*, 580096.
NEA (2020). Quarterly Dengue Surveillance Data—Q1 2019, Q2 2019, Q3 2019, Q4 2019, Q1 2020, Q2 2020, Q3 2020 and Q4 2020.
Netsawang, J., Noisakran, S., Puttikhunt, C., Kasinrerk, W., Wongwiwat, W., Malasit, P., Yenchitsomanus, P.T., and Limjindaporn, T. (2010). Nuclear localization of dengue virus capsid protein is required for DAXX interaction and apoptosis. Virus Res *147*, 275-283.
Neufeldt, C.J., Cortese, M., Scaturro, P., Cerikan, B., Wideman, J.G., Tabata, K., Moraes, T., Oleksiuk, O., Pichlmair, A., and Bartenschlager, R. (2019). ER-shaping atlastin proteins act as central hubs to promote flavivirus replication and virion assembly. Nat Microbiol *4*, 2416-2429.
Ng, E.Y., Loh, Y.R., Li, Y., Li, Q., and Kang, C. (2019a). Expression, purification of Zika virus membrane protein-NS2B in detergent micelles for NMR studies. Protein Expr Purif *154*, 1-6.
Ng, I.H.W., Chan, K.W., Tan, M.J.A., Gwee, C.P., Smith, K.M., Jeffress, S.J., Saw, W.G., Swarbrick, C.M.D., Watanabe, S., Jans, D.A*., et al.* (2019b). Zika Virus NS5 Forms Supramolecular Nuclear Bodies That Sequester Importin-alpha and Modulate the Host Immune and Pro-Inflammatory Response in Neuronal Cells. ACS Infect Dis *5*, 932-948.
Ng, W.C., Soto-Acosta, R., Bradrick, S.S., Garcia-Blanco, M.A., and Ooi, E.E. (2017). The 5' and 3' Untranslated Regions of the Flaviviral Genome. Viruses *9*.
Ngo, A.M., Shurtleff, M.J., Popova, K.D., Kulsuptrakul, J., Weissman, J.S., and Puschnik, A.S. (2019). The ER membrane protein complex is required to ensure correct topology and stable expression of flavivirus polyproteins. Elife *8*.
Nguyen, N.M., Tran, C.N., Phung, L.K., Duong, K.T., Huynh Hle, A., Farrar, J., Nguyen, Q.T., Tran, H.T., Nguyen, C.V., Merson, L*., et al.* (2013). A randomized, double-blind placebo controlled trial of balapiravir, a polymerase inhibitor, in adult dengue patients. J Infect Dis *207*, 1442-1450.

Nitsche, C., Behnam, M.A., Steuer, C., and Klein, C.D. (2012). Retro peptide-hybrids as selective inhibitors of the Dengue virus NS2B-NS3 protease. Antiviral Res *94*, 72-79.
Nitsche, C., Passioura, T., Varava, P., Mahawaththa, M.C., Leuthold, M.M., Klein, C.D., Suga, H., and Otting, G. (2019). De Novo Discovery of Nonstandard Macrocyclic Peptides as Noncompetitive Inhibitors of the Zika Virus NS2B-NS3 Protease. ACS Med Chem Lett *10*, 168-174.
Nitsche, C., Schreier, V.N., Behnam, M.A., Kumar, A., Bartenschlager, R., and Klein, C.D. (2013). Thiazolidinone-peptide hybrids as dengue virus protease inhibitors with antiviral activity in cell culture. J Med Chem *56*, 8389-8403.
Nitsche, C., Zhang, L., Weigel, L.F., Schilz, J., Graf, D., Bartenschlager, R., Hilgenfeld, R., and Klein, C.D. (2017). Peptide-Boronic Acid Inhibitors of Flaviviral Proteases: Medicinal Chemistry and Structural Biology. J Med Chem *60*, 511-516.
Noble, C.G., Lim, S.P., Arora, R., Yokokawa, F., Nilar, S., Seh, C.C., Wright, S.K., Benson, T.E., Smith, P.W., and Shi, P.Y. (2016). A Conserved Pocket in the Dengue Virus Polymerase Identified through Fragment-based Screening. J Biol Chem *291*, 8541-8548.
Noble, C.G., Seh, C.C., Chao, A.T., and Shi, P.Y. (2012). Ligand-bound structures of the dengue virus protease reveal the active conformation. J Virol *86*, 438-446.
Nybakken, G.E., Nelson, C.A., Chen, B.R., Diamond, M.S., and Fremont, D.H. (2006). Crystal structure of the West Nile virus envelope glycoprotein. J Virol *80*, 11467-11474.
Ong, J., Liu, X., Rajarethinam, J., Yap, G., Ho, D., and Ng, L.C. (2019). A novel entomological index, Aedes aegypti Breeding Percentage, reveals the geographical spread of the dengue vector in Singapore and serves as a spatial risk indicator for dengue. Parasit Vectors *12*, 17.
Osorio, J.E., Wallace, D., and Stinchcomb, D.T. (2016). A recombinant, chimeric tetravalent dengue vaccine candidate based on a dengue virus serotype 2 backbone. Expert Rev Vaccines *15*, 497-508.
Patkar, C.G., Larsen, M., Owston, M., Smith, J.L., and Kuhn, R.J. (2009). Identification of inhibitors of yellow fever virus replication using a replicon-based high-throughput assay. Antimicrob Agents Chemother *53*, 4103-4114.
Paul, D., and Bartenschlager, R. (2015). Flaviviridae Replication Organelles: Oh, What a Tangled Web We Weave. Annu Rev Virol *2*, 289-310.
Pettke, A., Tampere, M., Pronk, R., Wallner, O., Falk, A., Warpman Berglund, U., Helleday, T., Mirazimi, A., and Puumalainen, M.R. (2020). Broadly Active Antiviral Compounds Disturb Zika Virus Progeny Release Rescuing Virus-Induced Toxicity in Brain Organoids. Viruses *13*.
Phoo, W.W., El Sahili, A., Zhang, Z., Chen, M.W., Liew, C.W., Lescar, J., Vasudevan, S.G., and Luo, D. (2020). Crystal structures of full length DENV4 NS2B-NS3 reveal the dynamic interaction between NS2B and NS3. Antiviral Res *182*, 104900.
Phoo, W.W., Li, Y., Zhang, Z., Lee, M.Y., Loh, Y.R., Tan, Y.B., Ng, E.Y., Lescar, J., Kang, C., and Luo, D. (2016). Structure of the NS2B-NS3 protease from Zika virus after self-cleavage. Nat Commun *7*, 13410.
Phoo, W.W., Zhang, Z., Wirawan, M., Chew, E.J.C., Chew, A.B.L., Kouretova, J., Steinmetzer, T., and Luo, D. (2018). Structures of Zika virus NS2B-NS3 protease in complex with peptidomimetic inhibitors. Antiviral Res *160*, 17-24.
Pierson, T.C., and Diamond, M.S. (2020). The continued threat of emerging flaviviruses. Nat Microbiol.
Plaszczyca, A., Scaturro, P., Neufeldt, C.J., Cortese, M., Cerikan, B., Ferla, S., Brancale, A., Pichlmair, A., and Bartenschlager, R. (2019). A novel interaction between dengue virus nonstructural protein 1 and the NS4A-2K-4B precursor is required for viral RNA

replication but not for formation of the membranous replication organelle. PLoS Pathog *15*, e1007736.
Podvinec, M., Lim, S.P., Schmidt, T., Scarsi, M., Wen, D., Sonntag, L.S., Sanschagrin, P., Shenkin, P.S., and Schwede, T. (2010). Novel inhibitors of dengue virus methyltransferase: discovery by in vitro-driven virtual screening on a desktop computer grid. J Med Chem *53*, 1483-1495.
Polacek, C., Friebe, P., and Harris, E. (2009). Poly(A)-binding protein binds to the non-polyadenylated 3' untranslated region of dengue virus and modulates translation efficiency. J Gen Virol *90*, 687-692.
Pong, W.L., Huang, Z.S., Teoh, P.G., Wang, C.C., and Wu, H.N. (2011). RNA binding property and RNA chaperone activity of dengue virus core protein and other viral RNA-interacting proteins. FEBS Lett *585*, 2575-2581.
Poonsiri, T., Wright, G.S.A., Solomon, T., and Antonyuk, S.V. (2019). Crystal Structure of the Japanese Encephalitis Virus Capsid Protein. Viruses *11*.
Potisopon, S., Priet, S., Collet, A., Decroly, E., Canard, B., and Selisko, B. (2014). The methyltransferase domain of dengue virus protein NS5 ensures efficient RNA synthesis initiation and elongation by the polymerase domain. Nucleic Acids Res *42*, 11642-11656.
Poulsen, A., Kang, C., and Keller, T.H. (2014). Drug design for flavivirus proteases: what are we missing? Curr Pharm Des *20*, 3422-3427.
Prusis, P., Lapins, M., Yahorava, S., Petrovska, R., Niyomrattanakit, P., Katzenmeier, G., and Wikberg, J.E. (2008). Proteochemometrics analysis of substrate interactions with dengue virus NS3 proteases. Bioorg Med Chem *16*, 9369-9377.
Rajarethinam, J., Ang, L.W., Ong, J., Ycasas, J., Hapuarachchi, H.C., Yap, G., Chong, C.S., Lai, Y.L., Cutter, J., Ho, D.*, et al.* (2018). Dengue in Singapore from 2004 to 2016: Cyclical Epidemic Patterns Dominated by Serotypes 1 and 2. Am J Trop Med Hyg *99*, 204-210.
Rajarethinam, J., Ong, J., Neo, Z.W., Ng, L.C., and Aik, J. (2020). Distribution and seasonal fluctuations of Ae. aegypti and Ae. albopictus larval and pupae in residential areas in an urban landscape. PLoS Negl Trop Dis *14*, e0008209.
Raut, R., Beesetti, H., Tyagi, P., Khanna, I., Jain, S.K., Jeankumar, V.U., Yogeeswari, P., Sriram, D., and Swaminathan, S. (2015). A small molecule inhibitor of dengue virus type 2 protease inhibits the replication of all four dengue virus serotypes in cell culture. Virol J *12*, 16.
Redoni, M., Yacoub, S., Rivino, L., Giacobbe, D.R., Luzzati, R., and Di Bella, S. (2020). Dengue: Status of current and under-development vaccines. Rev Med Virol *30*, e2101.
Renner, M., Flanagan, A., Dejnirattisai, W., Puttikhunt, C., Kasinrerk, W., Supasa, P., Wongwiwat, W., Chawansuntati, K., Duangchinda, T., Cowper, A.*, et al.* (2018). Characterization of a potent and highly unusual minimally enhancing antibody directed against dengue virus. Nat Immunol *19*, 1248-1256.
Rey, F.A., Heinz, F.X., Mandl, C., Kunz, C., and Harrison, S.C. (1995). The envelope glycoprotein from tick-borne encephalitis virus at 2 A resolution. Nature *375*, 291-298.
Robin, G., Chappell, K., Stoermer, M.J., Hu, S.H., Young, P.R., Fairlie, D.P., and Martin, J.L. (2009). Structure of West Nile virus NS3 protease: ligand stabilization of the catalytic conformation. J Mol Biol *385*, 1568-1577.
Roby, J.A., Esser-Nobis, K., Dewey-Verstelle, E.C., Fairgrieve, M.R., Schwerk, J., Lu, A.Y., Soveg, F.W., Hemann, E.A., Hatfield, L.D., Keller, B.C.*, et al.* (2020). Flavivirus Nonstructural Protein NS5 Dysregulates HSP90 to Broadly Inhibit JAK/STAT Signaling. Cells *9*.

Rodriguez-Madoz, J.R., Belicha-Villanueva, A., Bernal-Rubio, D., Ashour, J., Ayllon, J., and Fernandez-Sesma, A. (2010). Inhibition of the type I interferon response in human dendritic cells by dengue virus infection requires a catalytically active NS2B3 complex. J Virol *84*, 9760-9774.
Roosendaal, J., Westaway, E.G., Khromykh, A., and Mackenzie, J.M. (2006). Regulated cleavages at the West Nile virus NS4A-2K-NS4B junctions play a major role in rearranging cytoplasmic membranes and Golgi trafficking of the NS4A protein. J Virol *80*, 4623-4632.
Rothan, H.A., and Kumar, M. (2019). Role of Endoplasmic Reticulum-Associated Proteins in Flavivirus Replication and Assembly Complexes. Pathogens *8*.
Rusanov, T., Kent, T., Saeed, M., Hoang, T.M., Thomas, C., Rice, C.M., and Pomerantz, R.T. (2018). Identification of a Small Interface between the Methyltransferase and RNA Polymerase of NS5 that is Essential for Zika Virus Replication. Sci Rep *8*, 17384.
Rut, W., Groborz, K., Zhang, L., Modrzycka, S., Poreba, M., Hilgenfeld, R., and Drag, M. (2020). Profiling of flaviviral NS2B-NS3 protease specificity provides a structural basis for the development of selective chemical tools that differentiate Dengue from Zika and West Nile viruses. Antiviral Res *175*, 104731.
Rut, W., Zhang, L., Kasperkiewicz, P., Poreba, M., Hilgenfeld, R., and Drag, M. (2017). Extended substrate specificity and first potent irreversible inhibitor/activity-based probe design for Zika virus NS2B-NS3 protease. Antiviral Res *139*, 88-94.
Saeedi, B.J., and Geiss, B.J. (2013). Regulation of flavivirus RNA synthesis and capping. Wiley Interdiscip Rev RNA *4*, 723-735.
Sanford, T.J., Mears, H.V., Fajardo, T., Locker, N., and Sweeney, T.R. (2019). Circularization of flavivirus genomic RNA inhibits de novo translation initiation. Nucleic Acids Res *47*, 9789-9802.
Saw, W.G., Tria, G., Gruber, A., Subramanian Manimekalai, M.S., Zhao, Y., Chandramohan, A., Srinivasan Anand, G., Matsui, T., Weiss, T.M., Vasudevan, S.G.*, et al.* (2015). Structural insight and flexible features of NS5 proteins from all four serotypes of Dengue virus in solution. Acta Crystallogr D Biol Crystallogr *71*, 2309-2327.
Scaturro, P., Cortese, M., Chatel-Chaix, L., Fischl, W., and Bartenschlager, R. (2015). Dengue Virus Non-structural Protein 1 Modulates Infectious Particle Production via Interaction with the Structural Proteins. PLoS Pathog *11*, e1005277.
Scherwitzl, I., Mongkolsapaja, J., and Screaton, G. (2017). Recent advances in human flavivirus vaccines. Curr Opin Virol *23*, 95-101.
Schnettler, E., Sterken, M.G., Leung, J.Y., Metz, S.W., Geertsema, C., Goldbach, R.W., Vlak, J.M., Kohl, A., Khromykh, A.A., and Pijlman, G.P. (2012). Noncoding flavivirus RNA displays RNA interference suppressor activity in insect and Mammalian cells. J Virol *86*, 13486-13500.
Schuller, A., Yin, Z., Brian Chia, C.S., Doan, D.N., Kim, H.K., Shang, L., Loh, T.P., Hill, J., and Vasudevan, S.G. (2011). Tripeptide inhibitors of dengue and West Nile virus NS2B-NS3 protease. Antiviral Res *92*, 96-101.
Selisko, B., Potisopon, S., Agred, R., Priet, S., Varlet, I., Thillier, Y., Sallamand, C., Debart, F., Vasseur, J.J., and Canard, B. (2012). Molecular basis for nucleotide conservation at the ends of the dengue virus genome. PLoS Pathog *8*, e1002912.
Shan, C., Xie, X., and Shi, P.Y. (2018). Zika Virus Vaccine: Progress and Challenges. Cell Host Microbe *24*, 12-17.
Shang, Z., Song, H., Shi, Y., Qi, J., and Gao, G.F. (2018). Crystal Structure of the Capsid Protein from Zika Virus. J Mol Biol *430*, 948-962.

Shi, W., Ye, H.Q., Deng, C.L., Li, R., Zhang, B., and Gong, P. (2019). A nucleobase-binding pocket in a viral RNA-dependent RNA polymerase contributes to elongation complex stability. Nucleic Acids Res.
Shimizu, H., Saito, A., Mikuni, J., Nakayama, E.E., Koyama, H., Honma, T., Shirouzu, M., Sekine, S.I., and Shioda, T. (2019). Discovery of a small molecule inhibitor targeting dengue virus NS5 RNA-dependent RNA polymerase. PLoS Negl Trop Dis *13*, e0007894.
Shiryaev, S.A., Chernov, A.V., Aleshin, A.E., Shiryaeva, T.N., and Strongin, A.Y. (2009). NS4A regulates the ATPase activity of the NS3 helicase: a novel cofactor role of the non-structural protein NS4A from West Nile virus. J Gen Virol *90*, 2081-2085.
Shiryaev, S.A., Kozlov, I.A., Ratnikov, B.I., Smith, J.W., Lebl, M., and Strongin, A.Y. (2007a). Cleavage preference distinguishes the two-component NS2B-NS3 serine proteinases of Dengue and West Nile viruses. Biochem J *401*, 743-752.
Shiryaev, S.A., Ratnikov, B.I., Aleshin, A.E., Kozlov, I.A., Nelson, N.A., Lebl, M., Smith, J.W., Liddington, R.C., and Strongin, A.Y. (2007b). Switching the substrate specificity of the two-component NS2B-NS3 flavivirus proteinase by structure-based mutagenesis. J Virol *81*, 4501-4509.
Shukla, R., Ramasamy, V., Shanmugam, R.K., Ahuja, R., and Khanna, N. (2020). Antibody-Dependent Enhancement: A Challenge for Developing a Safe Dengue Vaccine. Front Cell Infect Microbiol *10*, 572681.
Sim, S., Ng, L.C., Lindsay, S.W., and Wilson, A.L. (2020). A greener vision for vector control: The example of the Singapore dengue control programme. PLoS Negl Trop Dis *14*, e0008428.
Simmonds, P., Becher, P., Bukh, J., Gould, E.A., Meyers, G., Monath, T., Muerhoff, S., Pletnev, A., Rico-Hesse, R., Smith, D.B.*, et al.* (2017). ICTV Virus Taxonomy Profile: Flaviviridae. J Gen Virol *98*, 2-3.
Singapore Zika Study, G. (2017). Outbreak of Zika virus infection in Singapore: an epidemiological, entomological, virological, and clinical analysis. Lancet Infect Dis *17*, 813-821.
Sirohi, D., Chen, Z., Sun, L., Klose, T., Pierson, T.C., Rossmann, M.G., and Kuhn, R.J. (2016). The 3.8 A resolution cryo-EM structure of Zika virus. Science *352*, 467-470.
Slonchak, A., and Khromykh, A.A. (2018). Subgenomic flaviviral RNAs: What do we know after the first decade of research. Antiviral Res *159*, 13-25.
Song, H., Qi, J., Haywood, J., Shi, Y., and Gao, G.F. (2016). Zika virus NS1 structure reveals diversity of electrostatic surfaces among flaviviruses. Nat Struct Mol Biol *23*, 456-458.
Song, Y., Mugavero, J., Stauft, C.B., and Wimmer, E. (2019). Dengue and Zika Virus 5' Untranslated Regions Harbor Internal Ribosomal Entry Site Functions. mBio *10*.
Steuer, C., Gege, C., Fischl, W., Heinonen, K.H., Bartenschlager, R., and Klein, C.D. (2011). Synthesis and biological evaluation of alpha-ketoamides as inhibitors of the Dengue virus protease with antiviral activity in cell-culture. Bioorg Med Chem *19*, 4067-4074.
Stoermer, M.J., Chappell, K.J., Liebscher, S., Jensen, C.M., Gan, C.H., Gupta, P.K., Xu, W.J., Young, P.R., and Fairlie, D.P. (2008). Potent cationic inhibitors of West Nile virus NS2B/NS3 protease with serum stability, cell permeability and antiviral activity. J Med Chem *51*, 5714-5721.
Su, X.C., Ozawa, K., Qi, R., Vasudevan, S.G., Lim, S.P., and Otting, G. (2009). NMR analysis of the dynamic exchange of the NS2B cofactor between open and closed conformations of the West Nile virus NS2B-NS3 protease. PLoS Negl Trop Dis *3*, e561.
Suputtamongkol, Y., Avirutnan, P., Mairiang, D., Angkasekwinai, N., Niwattayakul, K., Yamasmith, E., Saleh-Arong, F.A., Songjaeng, A., Prommool, T., Tangthawornchaikul, N.*, et al.* (2021). Ivermectin Accelerates Circulating Nonstructural Protein 1 (NS1)

Clearance in Adult Dengue Patients: A Combined Phase 2/3 Randomized Double-blinded Placebo Controlled Trial. Clin Infect Dis *72*, e586-e593.
Suthar, M.S., Diamond, M.S., and Gale, M., Jr. (2013). West Nile virus infection and immunity. Nat Rev Microbiol *11*, 115-128.
Sweeney, N.L., Hanson, A.M., Mukherjee, S., Ndjomou, J., Geiss, B.J., Steel, J.J., Frankowski, K.J., Li, K., Schoenen, F.J., and Frick, D.N. (2015). Benzothiazole and Pyrrolone Flavivirus Inhibitors Targeting the Viral Helicase. ACS Infect Dis *1*, 140-148.
Tajima, S., Takasaki, T., and Kurane, I. (2011). Restoration of replication-defective dengue type 1 virus bearing mutations in the N-terminal cytoplasmic portion of NS4A by additional mutations in NS4B. Arch Virol *156*, 63-69.
Takagi, Y., Matsui, K., Nobori, H., Maeda, H., Sato, A., Kurosu, T., Orba, Y., Sawa, H., Hattori, K., Higashino, K.*, et al.* (2017). Discovery of novel cyclic peptide inhibitors of dengue virus NS2B-NS3 protease with antiviral activity. Bioorg Med Chem Lett *27*, 3586-3590.
Tan, M.J.A., Brown, N.G., Chan, K.W.K., Jin, J.Y., Zu Kong, S.Y., and Vasudevan, S.G. (2020a). Mutations in the cytoplasmic domain of dengue virus NS4A affect virus fitness and interactions with other non-structural proteins. J Gen Virol.
Tan, T.Y., Fibriansah, G., Kostyuchenko, V.A., Ng, T.S., Lim, X.X., Zhang, S., Lim, X.N., Wang, J., Shi, J., Morais, M.C.*, et al.* (2020b). Capsid protein structure in Zika virus reveals the flavivirus assembly process. Nat Commun *11*, 895.
Tang, W.C., Lin, R.J., Liao, C.L., and Lin, Y.L. (2014). Rab18 facilitates dengue virus infection by targeting fatty acid synthase to sites of viral replication. J Virol *88*, 6793-6804.
Tarantino, D., Cannalire, R., Mastrangelo, E., Croci, R., Querat, G., Barreca, M.L., Bolognesi, M., Manfroni, G., Cecchetti, V., and Milani, M. (2016). Targeting flavivirus RNA dependent RNA polymerase through a pyridobenzothiazole inhibitor. Antiviral Res *134*, 226-235.
Tassaneetrithep, B., Burgess, T.H., Granelli-Piperno, A., Trumpfheller, C., Finke, J., Sun, W., Eller, M.A., Pattanapanyasat, K., Sarasombath, S., Birx, D.L.*, et al.* (2003). DC-SIGN (CD209) mediates dengue virus infection of human dendritic cells. J Exp Med *197*, 823-829.
Tay, M.Y., Fraser, J.E., Chan, W.K., Moreland, N.J., Rathore, A.P., Wang, C., Vasudevan, S.G., and Jans, D.A. (2013). Nuclear localization of dengue virus (DENV) 1-4 non-structural protein 5; protection against all 4 DENV serotypes by the inhibitor Ivermectin. Antiviral Res *99*, 301-306.
Tay, M.Y., Saw, W.G., Zhao, Y., Chan, K.W., Singh, D., Chong, Y., Forwood, J.K., Ooi, E.E., Gruber, G., Lescar, J.*, et al.* (2015). The C-terminal 50 amino acid residues of dengue NS3 protein are important for NS3-NS5 interaction and viral replication. J Biol Chem *290*, 2379-2394.
Tay, M.Y., Smith, K., Ng, I.H., Chan, K.W., Zhao, Y., Ooi, E.E., Lescar, J., Luo, D., Jans, D.A., Forwood, J.K.*, et al.* (2016). The C-terminal 18 Amino Acid Region of Dengue Virus NS5 Regulates its Subcellular Localization and Contains a Conserved Arginine Residue Essential for Infectious Virus Production. PLoS Pathog *12*, e1005886.
Tay, M.Y.F., and Vasudevan, S.G. (2018). The Transactions of NS3 and NS5 in Flaviviral RNA Replication. Adv Exp Med Biol *1062*, 147-163.
Teo, C.S., and Chu, J.J. (2014). Cellular vimentin regulates construction of dengue virus replication complexes through interaction with NS4A protein. J Virol *88*, 1897-1913.
Thomas, S.J., and Yoon, I.K. (2019). A review of Dengvaxia(R): development to deployment. Hum Vaccin Immunother *15*, 2295-2314.

Tian, H., Ji, X., Yang, X., Xie, W., Yang, K., Chen, C., Wu, C., Chi, H., Mu, Z., Wang, Z*., et al.* (2016a). The crystal structure of Zika virus helicase: basis for antiviral drug design. Protein Cell *7*, 450-454.
Tian, H., Ji, X., Yang, X., Zhang, Z., Lu, Z., Yang, K., Chen, C., Zhao, Q., Chi, H., Mu, Z*., et al.* (2016b). Structural basis of Zika virus helicase in recognizing its substrates. Protein Cell *7*, 562-570.
Tomlinson, S.M., Malmstrom, R.D., Russo, A., Mueller, N., Pang, Y.P., and Watowich, S.J. (2009). Structure-based discovery of dengue virus protease inhibitors. Antiviral Res *82*, 110-114.
Tomlinson, S.M., and Watowich, S.J. (2011). Anthracene-based inhibitors of dengue virus NS2B-NS3 protease. Antiviral Res *89*, 127-135.
Tricou, V., Minh, N.N., Van, T.P., Lee, S.J., Farrar, J., Wills, B., Tran, H.T., and Simmons, C.P. (2010). A randomized controlled trial of chloroquine for the treatment of dengue in Vietnamese adults. PLoS Negl Trop Dis *4*, e785.
Ubol, S., and Halstead, S.B. (2010). How innate immune mechanisms contribute to antibody-enhanced viral infections. Clin Vaccine Immunol *17*, 1829-1835.
Uchil, P.D., and Satchidanandam, V. (2003). Architecture of the flaviviral replication complex. Protease, nuclease, and detergents reveal encasement within double-layered membrane compartments. J Biol Chem *278*, 24388-24398.
Umareddy, I., Chao, A., Sampath, A., Gu, F., and Vasudevan, S.G. (2006). Dengue virus NS4B interacts with NS3 and dissociates it from single-stranded RNA. J Gen Virol *87*, 2605-2614.
Vagin, A., and Teplyakov, A. (2010). Molecular replacement with MOLREP. Acta Crystallogr D Biol Crystallogr *66*, 22-25.
van Cleef, K.W., Overheul, G.J., Thomassen, M.C., Kaptein, S.J., Davidson, A.D., Jacobs, M., Neyts, J., van Kuppeveld, F.J., and van Rij, R.P. (2013). Identification of a new dengue virus inhibitor that targets the viral NS4B protein and restricts genomic RNA replication. Antiviral Res *99*, 165-171.
van der Schaar, H.M., Rust, M.J., Chen, C., van der Ende-Metselaar, H., Wilschut, J., Zhuang, X., and Smit, J.M. (2008). Dissecting the cell entry pathway of dengue virus by single-particle tracking in living cells. PLoS Pathog *4*, e1000244.
Vashist, S., Bhullar, D., and Vrati, S. (2011). La protein can simultaneously bind to both 3'- and 5'-noncoding regions of Japanese encephalitis virus genome. DNA Cell Biol *30*, 339-346.
Vasilakis, N., Tesh, R.B., and Weaver, S.C. (2008). Sylvatic dengue virus type 2 activity in humans, Nigeria, 1966. Emerg Infect Dis *14*, 502-504.
Vernekar, S.K., Qiu, L., Zhang, J., Kankanala, J., Li, H., Geraghty, R.J., and Wang, Z. (2015). 5'-Silylated 3'-1,2,3-triazolyl Thymidine Analogues as Inhibitors of West Nile Virus and Dengue Virus. J Med Chem *58*, 4016-4028.
Viktorovskaya, O.V., Greco, T.M., Cristea, I.M., and Thompson, S.R. (2016). Identification of RNA Binding Proteins Associated with Dengue Virus RNA in Infected Cells Reveals Temporally Distinct Host Factor Requirements. PLoS Negl Trop Dis *10*, e0004921.
Villordo, S.M., Alvarez, D.E., and Gamarnik, A.V. (2010). A balance between circular and linear forms of the dengue virus genome is crucial for viral replication. RNA *16*, 2325-2335.
Villordo, S.M., and Gamarnik, A.V. (2009). Genome cyclization as strategy for flavivirus RNA replication. Virus Res *139*, 230-239.
Vinogradov, A.A., Yin, Y., and Suga, H. (2019). Macrocyclic Peptides as Drug Candidates: Recent Progress and Remaining Challenges. J Am Chem Soc *141*, 4167-4181.

Vossmann, S., Wieseler, J., Kerber, R., and Kummerer, B.M. (2015). A basic cluster in the N terminus of yellow fever virus NS2A contributes to infectious particle production. J Virol *89*, 4951-4965.
Wang, B., Tan, X.F., Thurmond, S., Zhang, Z.M., Lin, A., Hai, R., and Song, J. (2017). The structure of Zika virus NS5 reveals a conserved domain conformation. Nat Commun *8*, 14763.
Wang, B., Thurmond, S., Zhou, K., Sanchez-Aparicio, M.T., Fang, J., Lu, J., Gao, L., Ren, W., Cui, Y., Veit, E.C*., et al.* (2020). Structural basis for STAT2 suppression by flavivirus NS5. Nat Struct Mol Biol *27*, 875-885.
Wang, Q.Y., Dong, H., Zou, B., Karuna, R., Wan, K.F., Zou, J., Susila, A., Yip, A., Shan, C., Yeo, K.L*., et al.* (2015). Discovery of Dengue Virus NS4B Inhibitors. J Virol *89*, 8233-8244.
Weigel, L.F., Nitsche, C., Graf, D., Bartenschlager, R., and Klein, C.D. (2015). Phenylalanine and Phenylglycine Analogues as Arginine Mimetics in Dengue Protease Inhibitors. J Med Chem *58*, 7719-7733.
Welsch, S., Miller, S., Romero-Brey, I., Merz, A., Bleck, C.K., Walther, P., Fuller, S.D., Antony, C., Krijnse-Locker, J., and Bartenschlager, R. (2009). Composition and three-dimensional architecture of the dengue virus replication and assembly sites. Cell Host Microbe *5*, 365-375.
Weng, Z., Shao, X., Graf, D., Wang, C., Klein, C.D., Wang, J., and Zhou, G.C. (2017). Identification of fused bicyclic derivatives of pyrrolidine and imidazolidinone as dengue virus-2 NS2B-NS3 protease inhibitors. Eur J Med Chem *125*, 751-759.
White, L.J., Young, E.F., Stoops, M.J., Henein, S.R., Adams, E.C., Baric, R.S., and de Silva, A.M. (2021). Defining levels of dengue virus serotype-specific neutralizing antibodies induced by a live attenuated tetravalent dengue vaccine (TAK-003). PLoS Negl Trop Dis *15*, e0009258.
Whitehorn, J., Nguyen, C.V.V., Khanh, L.P., Kien, D.T.H., Quyen, N.T.H., Tran, N.T.T., Hang, N.T., Truong, N.T., Hue Tai, L.T., Cam Huong, N.T*., et al.* (2016). Lovastatin for the Treatment of Adult Patients With Dengue: A Randomized, Double-Blind, Placebo-Controlled Trial. Clin Infect Dis *62*, 468-476.
WHO (2009). Dengue: Guidelines for Diagnosis, Treatment, Prevention and Control. In Dengue: Guidelines for Diagnosis, Treatment, Prevention and Control: New Edition (Geneva).
WHO (2017). Eliminate Yellow fever Epidemics (EYE): a global strategy, 2017-2026. Wkly Epidemiol Rec *92*, 193-204.
WHO (2018a). 2018 Annual review of diseases prioritized under the Research and Development Blueprint.
WHO (2018b). Fact Sheet: Zika Virus Disease.
WHO (2019). Dengue vaccine: WHO position paper, September 2018 - Recommendations. Vaccine *37*, 4848-4849.
WHO (2020). Fact Sheet: Dengue and Severe Dengue.
Wikan, N., and Smith, D.R. (2016). Zika virus: history of a newly emerging arbovirus. Lancet Infect Dis *16*, e119-e126.
Wilder-Smith, A. (2020). Dengue vaccine development by the year 2020: challenges and prospects. Curr Opin Virol *43*, 71-78.
Wilder-Smith, A., Ooi, E.E., Horstick, O., and Wills, B. (2019). Dengue. Lancet *393*, 350-363.
Wirawan, M., Fibriansah, G., Marzinek, J.K., Lim, X.X., Ng, T.S., Sim, A.Y.L., Zhang, Q., Kostyuchenko, V.A., Shi, J., Smith, S.A*., et al.* (2019). Mechanism of Enhanced Immature Dengue Virus Attachment to Endosomal Membrane Induced by prM Antibody. Structure *27*, 253-267 e258.

Wlodawer, A., and Erickson, J.W. (1993). Structure-based inhibitors of HIV-1 protease. Annu Rev Biochem *62*, 543-585.
Wojdyla, J.A., Kaminski, J.W., Panepucci, E., Ebner, S., Wang, X., Gabadinho, J., and Wang, M. (2018). DA+ data acquisition and analysis software at the Swiss Light Source macromolecular crystallography beamlines. J Synchrotron Radiat *25*, 293-303.
Wu, H., Bock, S., Snitko, M., Berger, T., Weidner, T., Holloway, S., Kanitz, M., Diederich, W.E., Steuber, H., Walter, C.*, et al.* (2015a). Novel dengue virus NS2B/NS3 protease inhibitors. Antimicrob Agents Chemother *59*, 1100-1109.
Wu, J., and Gong, P. (2018). Visualizing the Nucleotide Addition Cycle of Viral RNA-Dependent RNA Polymerase. Viruses *10*.
Wu, J., Lu, G., Zhang, B., and Gong, P. (2015b). Perturbation in the conserved methyltransferase-polymerase interface of flavivirus NS5 differentially affects polymerase initiation and elongation. J Virol *89*, 249-261.
Wu, J., Ye, H.Q., Zhang, Q.Y., Lu, G., Zhang, B., and Gong, P. (2020). A conformation-based intra-molecular initiation factor identified in the flavivirus RNA-dependent RNA polymerase. PLoS Pathog *16*, e1008484.
Wu, R.H., Tsai, M.H., Tsai, K.N., Tian, J.N., Wu, J.S., Wu, S.Y., Chern, J.H., Chen, C.H., and Yueh, A. (2017). Mutagenesis of Dengue Virus Protein NS2A Revealed a Novel Domain Responsible for Virus-Induced Cytopathic Effect and Interactions between NS2A and NS2B Transmembrane Segments. J Virol *91*.
Xie, X., Gayen, S., Kang, C., Yuan, Z., and Shi, P.Y. (2013). Membrane topology and function of dengue virus NS2A protein. J Virol *87*, 4609-4622.
Xie, X., Wang, Q.Y., Xu, H.Y., Qing, M., Kramer, L., Yuan, Z., and Shi, P.Y. (2011). Inhibition of dengue virus by targeting viral NS4B protein. J Virol *85*, 11183-11195.
Xie, X., Zou, J., Puttikhunt, C., Yuan, Z., and Shi, P.Y. (2015). Two distinct sets of NS2A molecules are responsible for dengue virus RNA synthesis and virion assembly. J Virol *89*, 1298-1313.
Xie, X., Zou, J., Zhang, X., Zhou, Y., Routh, A.L., Kang, C., Popov, V.L., Chen, X., Wang, Q.Y., Dong, H.*, et al.* (2019). Dengue NS2A Protein Orchestrates Virus Assembly. Cell Host Microbe *26*, 606-622 e608.
Xu, J., Xie, X., Ye, N., Zou, J., Chen, H., White, M.A., Shi, P.Y., and Zhou, J. (2019a). Design, Synthesis, and Biological Evaluation of Substituted 4,6-Dihydrospiro[[1,2,3]triazolo[4,5-b]pyridine-7,3'-indoline]-2',5(3H)-dione Analogues as Potent NS4B Inhibitors for the Treatment of Dengue Virus Infection. J Med Chem *62*, 7941-7960.
Xu, S., Ci, Y., Wang, L., Yang, Y., Zhang, L., Xu, C., Qin, C., and Shi, L. (2019b). Zika virus NS3 is a canonical RNA helicase stimulated by NS5 RNA polymerase. Nucleic Acids Res *47*, 8693-8707.
Xu, S., Li, H., Shao, X., Fan, C., Ericksen, B., Liu, J., Chi, C., and Wang, C. (2012). Critical effect of peptide cyclization on the potency of peptide inhibitors against Dengue virus NS2B-NS3 protease. J Med Chem *55*, 6881-6887.
Xu, T., Sampath, A., Chao, A., Wen, D., Nanao, M., Chene, P., Vasudevan, S.G., and Lescar, J. (2005). Structure of the Dengue virus helicase/nucleoside triphosphatase catalytic domain at a resolution of 2.4 A. J Virol *79*, 10278-10288.
Xu, X., Song, H., Qi, J., Liu, Y., Wang, H., Su, C., Shi, Y., and Gao, G.F. (2016). Contribution of intertwined loop to membrane association revealed by Zika virus full-length NS1 structure. EMBO J *35*, 2170-2178.
Yao, Y., Huo, T., Lin, Y.L., Nie, S., Wu, F., Hua, Y., Wu, J., Kneubehl, A.R., Vogt, M.B., Rico-Hesse, R.*, et al.* (2019). Discovery, X-ray Crystallography and Antiviral Activity of Allosteric Inhibitors of Flavivirus NS2B-NS3 Protease. J Am Chem Soc *141*, 6832-6836.

Yap, T.L., Xu, T., Chen, Y.L., Malet, H., Egloff, M.P., Canard, B., Vasudevan, S.G., and Lescar, J. (2007). Crystal structure of the dengue virus RNA-dependent RNA polymerase catalytic domain at 1.85-angstrom resolution. J Virol *81*, 4753-4765.
Yi, Z., Yuan, Z., Rice, C.M., and MacDonald, M.R. (2012). Flavivirus replication complex assembly revealed by DNAJC14 functional mapping. J Virol *86*, 11815-11832.
Yildiz, M., Ghosh, S., Bell, J.A., Sherman, W., and Hardy, J.A. (2013). Allosteric inhibition of the NS2B-NS3 protease from dengue virus. ACS Chem Biol *8*, 2744-2752.
Yin, W., Mao, C., Luan, X., Shen, D.D., Shen, Q., Su, H., Wang, X., Zhou, F., Zhao, W., Gao, M*., et al.* (2020). Structural basis for inhibition of the RNA-dependent RNA polymerase from SARS-CoV-2 by remdesivir. Science *368*, 1499-1504.
Yin, Z., Patel, S.J., Wang, W.L., Chan, W.L., Ranga Rao, K.R., Wang, G., Ngew, X., Patel, V., Beer, D., Knox, J.E*., et al.* (2006a). Peptide inhibitors of dengue virus NS3 protease. Part 2: SAR study of tetrapeptide aldehyde inhibitors. Bioorg Med Chem Lett *16*, 40-43.
Yin, Z., Patel, S.J., Wang, W.L., Wang, G., Chan, W.L., Rao, K.R., Alam, J., Jeyaraj, D.A., Ngew, X., Patel, V*., et al.* (2006b). Peptide inhibitors of Dengue virus NS3 protease. Part 1: Warhead. Bioorg Med Chem Lett *16*, 36-39.
Yokokawa, F., Nilar, S., Noble, C.G., Lim, S.P., Rao, R., Tania, S., Wang, G., Lee, G., Hunziker, J., Karuna, R*., et al.* (2016). Discovery of Potent Non-Nucleoside Inhibitors of Dengue Viral RNA-Dependent RNA Polymerase from a Fragment Hit Using Structure-Based Drug Design. J Med Chem *59*, 3935-3952.
Yon, C., Teramoto, T., Mueller, N., Phelan, J., Ganesh, V.K., Murthy, K.H., and Padmanabhan, R. (2005). Modulation of the nucleoside triphosphatase/RNA helicase and 5'-RNA triphosphatase activities of Dengue virus type 2 nonstructural protein 3 (NS3) by interaction with NS5, the RNA-dependent RNA polymerase. J Biol Chem *280*, 27412-27419.
Yoshii, K., Igarashi, M., Ichii, O., Yokozawa, K., Ito, K., Kariwa, H., and Takashima, I. (2012). A conserved region in the prM protein is a critical determinant in the assembly of flavivirus particles. J Gen Virol *93*, 27-38.
Youn, S., Ambrose, R.L., Mackenzie, J.M., and Diamond, M.S. (2013). Non-structural protein-1 is required for West Nile virus replication complex formation and viral RNA synthesis. Virol J *10*, 339.
Youn, S., Li, T., McCune, B.T., Edeling, M.A., Fremont, D.H., Cristea, I.M., and Diamond, M.S. (2012). Evidence for a genetic and physical interaction between nonstructural proteins NS1 and NS4B that modulates replication of West Nile virus. J Virol *86*, 7360-7371.
Yu, C.Y., Chang, T.H., Liang, J.J., Chiang, R.L., Lee, Y.L., Liao, C.L., and Lin, Y.L. (2012). Dengue virus targets the adaptor protein MITA to subvert host innate immunity. PLoS Pathog *8*, e1002780.
Yu, C.Y., Liang, J.J., Li, J.K., Lee, Y.L., Chang, B.L., Su, C.I., Huang, W.J., Lai, M.M., and Lin, Y.L. (2015). Dengue Virus Impairs Mitochondrial Fusion by Cleaving Mitofusins. PLoS Pathog *11*, e1005350.
Yu, I.M., Zhang, W., Holdaway, H.A., Li, L., Kostyuchenko, V.A., Chipman, P.R., Kuhn, R.J., Rossmann, M.G., and Chen, J. (2008). Structure of the immature dengue virus at low pH primes proteolytic maturation. Science *319*, 1834-1837.
Yu, L., Takeda, K., and Markoff, L. (2013). Protein-protein interactions among West Nile non-structural proteins and transmembrane complex formation in mammalian cells. Virology *446*, 365-377.
Yun, S.I., and Lee, Y.M. (2017). Zika virus: An emerging flavivirus. J Microbiol *55*, 204-219.

Zhang, K.L., YS.; Law, CY.; Tan, YB.; Wirawan, M.; Luo, D. (2021). Structural insights into viral RNA capping and plasma membrane targeting by Chikungunya virus nonstructural protein 1. Cell Host Microbe.
Zhang, X., Jia, R., Shen, H., Wang, M., Yin, Z., and Cheng, A. (2017). Structures and Functions of the Envelope Glycoprotein in Flavivirus Infections. Viruses *9*.
Zhang, X., Xie, X., Xia, H., Zou, J., Huang, L., Popov, V.L., Chen, X., and Shi, P.Y. (2019a). Zika Virus NS2A-Mediated Virion Assembly. mBio *10*.
Zhang, X., Xie, X., Zou, J., Xia, H., Shan, C., Chen, X., and Shi, P.Y. (2019b). Genetic and biochemical characterizations of Zika virus NS2A protein. Emerg Microbes Infect *8*, 585-602.
Zhang, Y., Corver, J., Chipman, P.R., Zhang, W., Pletnev, S.V., Sedlak, D., Baker, T.S., Strauss, J.H., Kuhn, R.J., and Rossmann, M.G. (2003). Structures of immature flavivirus particles. EMBO J *22*, 2604-2613.
Zhang, Z., Li, Y., Loh, Y.R., Phoo, W.W., Hung, A.W., Kang, C., and Luo, D. (2016). Crystal structure of unlinked NS2B-NS3 protease from Zika virus. Science *354*, 1597-1600.
Zhao, B., Yi, G., Du, F., Chuang, Y.C., Vaughan, R.C., Sankaran, B., Kao, C.C., and Li, P. (2017). Structure and function of the Zika virus full-length NS5 protein. Nat Commun *8*, 14762.
Zhao, Y., Soh, T.S., Chan, K.W., Fung, S.S., Swaminathan, K., Lim, S.P., Shi, P.Y., Huber, T., Lescar, J., Luo, D.*, et al.* (2015a). Flexibility of NS5 Methyltransferase-Polymerase Linker Region Is Essential for Dengue Virus Replication. J Virol *89*, 10717-10721.
Zhao, Y., Soh, T.S., Lim, S.P., Chung, K.Y., Swaminathan, K., Vasudevan, S.G., Shi, P.Y., Lescar, J., and Luo, D. (2015b). Molecular basis for specific viral RNA recognition and 2'-O-ribose methylation by the dengue virus nonstructural protein 5 (NS5). Proc Natl Acad Sci U S A *112*, 14834-14839.
Zhao, Y., Soh, T.S., Zheng, J., Chan, K.W., Phoo, W.W., Lee, C.C., Tay, M.Y., Swaminathan, K., Cornvik, T.C., Lim, S.P.*, et al.* (2015c). A crystal structure of the Dengue virus NS5 protein reveals a novel inter-domain interface essential for protein flexibility and virus replication. PLoS Pathog *11*, e1004682.
Zhou, Y., Ray, D., Zhao, Y., Dong, H., Ren, S., Li, Z., Guo, Y., Bernard, K.A., Shi, P.Y., and Li, H. (2007). Structure and function of flavivirus NS5 methyltransferase. J Virol *81*, 3891-3903.
Zou, B., Chan, W.L., Ding, M., Leong, S.Y., Nilar, S., Seah, P.G., Liu, W., Karuna, R., Blasco, F., Yip, A.*, et al.* (2015a). Lead optimization of spiropyrazolopyridones: a new and potent class of dengue virus inhibitors. ACS Med Chem Lett *6*, 344-348.
Zou, G., Chen, Y.L., Dong, H., Lim, C.C., Yap, L.J., Yau, Y.H., Shochat, S.G., Lescar, J., and Shi, P.Y. (2011). Functional analysis of two cavities in flavivirus NS5 polymerase. J Biol Chem *286*, 14362-14372.
Zou, J., Lee le, T., Wang, Q.Y., Xie, X., Lu, S., Yau, Y.H., Yuan, Z., Geifman Shochat, S., Kang, C., Lescar, J.*, et al.* (2015b). Mapping the Interactions between the NS4B and NS3 proteins of dengue virus. J Virol *89*, 3471-3483.
Zou, J., Xie, X., Lee le, T., Chandrasekaran, R., Reynaud, A., Yap, L., Wang, Q.Y., Dong, H., Kang, C., Yuan, Z.*, et al.* (2014). Dimerization of flavivirus NS4B protein. J Virol *88*, 3379-3391.
Zou, J., Xie, X., Wang, Q.Y., Dong, H., Lee, M.Y., Kang, C., Yuan, Z., and Shi, P.Y. (2015c). Characterization of dengue virus NS4A and NS4B protein interaction. J Virol *89*, 3455-3470.